A Biophysical Study of the G Protein Coupled Receptor Neurotensin Receptor 1

Thesis submitted to the Board of the Medical Sciences Division in partial fulfilment of the requirements for the Degree of Doctor of Philosophy at the University of Oxford

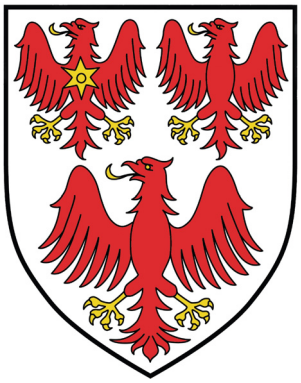

Peter James Harding

The Queen's College

Trinity Term 2007

ABSTRACT

Neurotensin (NT) is a tridecapeptide neurotransmitter found in the central nervous system and gastrointestinal tract. Neurotensin receptor 1 (NTS1), a high affinity receptor for NT, is a member of the GPCR superfamily and is a putative target for the treatment of conditions such as Schizophrenia, Parkinson's Disease and drug addiction.

Overexpression and purification are typically limiting steps in the high resolution structure determination of GPCRs. In this study, through the optimisation of the *E.coli* strain used for overexpression of rat NTS1 (NTS1) and the inclusion of phospholipids in the purification buffers to prevent delipidation, an approximate 3-fold improvement in active receptor yield was obtained relative to existing protocols. Preliminary electron microscopy (negative stain and cryo) confirmed a monodisperse receptor population. Purified NTS1 is now being produced at a sufficient level for high resolution structural studies, including 3D crystallisation and further electron microscopy studies.

The existing construct for the expression of NTS1 in *E.coli*, termed NTS1B, was modified to contain a fusion to the genes encoding either the eCFP or eYFP fluorescent proteins. These constructs were used for the *E.coli* expression of NTS1 tagged with either fluorescent protein at the C-terminus. Tagged receptor was successfully expressed at levels of up to 0.29 ± 0.03 mg per l of culture. Successful purification and proteolytic removal of the MBP and TrxA-His10 fusion partners was achieved whilst retaining both fluorescence and ligand binding capability (K_d = 0.91 ± 0.17 nM).

Purified, fluorescent receptor was reconstituted into brain polar lipid (BPL) liposomes in an active conformation which was both fluorescent and able to bind NT. Experimentation with alternative lipid compositions suggested that specific lipids are required in order to maintain ligand-binding activity. FRET between the eCFP- and eYFP-tagged receptors was observed in reconstituted samples. The FRET efficiency was comparable to that observed *in vivo* for other GPCRs, including the yeast α-factor receptor, which is believed to be dimeric. This suggests that NTS1 could also be multimeric. In contrast, no FRET was observed in detergent samples. Therefore, a functioning *in vitro* system has been developed which enables the study of NTS1 multimerisation in lipid bilayers and future studies will attempt to implement single molecule fluorescence techniques. In addition, fluorescent derivatives of NT were successfully synthesised and purified. Radioligand competition assays and fluorescence correlation spectroscopy (FCS) confirmed that the fluorescent peptides bound to purified NTS1 in specific competition with unlabelled NT.

Surface plasmon resonance (SPR) was used to confirm the ligand binding activity of purified NTS1. A novel approach was utilised which involved the measurement of the binding of detergent-solubilised NTS1 to immobilised, N-terminally biotinylated NT on the sensor surface. The use of a rigorous control, which consisted of immobilised 'scrambled sequence' NT, demonstrated a specific interaction. Analysis of the kinetics revealed a multiphasic interaction with a K_d in the nanomolar range.

In summary, improvements to the expression and purification of NTS1, the generation of fluorescent constructs as useful tools in the study of receptor multimerisation and the optimisation of lipid-reconstitution protocols have opened up several preliminary lines of study which show considerable potential for future research.

LIST OF PUBLICATIONS

Harding, P. J., Hadingham, T. C., McDonnell, J. M. and Watts, A. (2006). "Direct analysis of a GPCR-agonist interaction by surface plasmon resonance." European Biophysical Journal **35**(8): 709-12.

Harding, P. J., Attrill, H., Ross, S., Koeppe, J. R., Kapanidis, A. N. and Watts, A. (2007). "Neurotensin receptor type 1 : *Escherichia coli* expression, purification, characterisation and biophysical study." Biochemical Society Transactions **35**(4): 760-763.

Harding, P. J., Attrill, H., Ross, S., Smith, E., Wadhams, G. H., Armitage, J. P. and Watts, A. (2007). "Heterologous overexpression and purification of the GPCR NTS1 tagged with the fluorescent proteins CFP and YFP." Submitted.

ACKNOWLEDGEMENTS

I would like to express my gratitude to Professor Anthony Watts for providing the support, resources and funding which have made this project possible and for allowing me to accompany him on his tours of the Far East.

Helen Attrill was a constant source of advice during the final two years of my project, providing a rational voice in my ear when needed and for this I am indebted. She also carried out much of the time-consuming optimisation work on the NTS1 purification.

I would like to thank George Wadhams, firstly for his help with the plans for the initial cloning of the fluorescent receptor constructs, and secondly for patiently proofreading this thesis.

Jim McDonnell shared his wealth of experience of surface plasmon resonance (SPR) and was always willing to give up his valuable time at short notice for a discussion. I would also like thank Simon Davis, on whose machine much of the SPR work was carried out.

Thank you to Mike Heilemann for working with me on the FCS experiments and for his help, in combination with Achilles Kapanidis, on designing the fluorescent NT derivatives and for checking my FRET analysis.

Jon Malo and latterly Daniele Selmi carried out all of the NTS1 DNA array work. I also send my thanks to Andreas Sonnen and Robert Gilbert 'up the hill' for carrying out the recent cryo-EM study which looks to have particularly exciting prospects.

(Philip) Robin Antrobus was always on hand to (expertly) carry out mass spectrometry of my synthesised peptides when the open access machines failed to deliver and for this I am extremely grateful.

I would like to thank all of the students I have supervised over the past four years who have all made valuable contributions to the project: Eleanor Smith, Fred Brown, Olivia Berthoumieu, Jonas Boehringer. I would like to thank all other members of the Watts Lab who I have failed to mention personally for their input and I wish you all the best of luck for the future.

Thank you to all the members of OUAC and QCRFC, past and present, for providing useful distractions to labwork and for keeping me (reasonably!) fit. I would like to thank my family, Mum, Dad and David for all of their love and support and for the enjoyable sailing weekends when I needed to get away. Lastly, thank you Martine for love, support and advice.

During my DPhil project, I have been directly funded by an MRC studentship and Syngenta CASE award, and the research has also been funded by the BBSRC and the Bionanotechnology IRC and I thank all of these organisations for their support.

ABBREVIATIONS

ALEX	alternating-laser excitation spectroscopy
APDs	anti-psychotic drugs
ATP	adenosine triphosphate
BPL	brain polar lipid extract (porcine)
BRET	bioluminescence resonance energy transfer
CHAPS	3-[(3-cholamidopropyl)dimethylammonio]-1-propanesulfonate
CHO	chinese hamster ovary cell
CHS	cholesteryl hemisuccinate
CL	cardiolipin
CV	column volume
CMC	critical micellar concentration
CTC	cubic ternary complex
DA	dopaminergic
DAG	diacylglycerol
DCM	dichloromethane
DDM	dodecyl-β-D-maltoside
DMF	dimethylformamide
DOPC	dioleoylphosphatidylcholine
DOPS	dioleoylphosphatidylserine
DTT	dithiolthreitol
eCFP	enhanced cyan fluorescent protein
EDTA	ethylenediaminetetraacetate
eYFP	enhanced yellow fluorescent protein
FCS	fluorescence correlation spectroscopy
FITC	fluorescein isothiocyanate
FRET	fluorescence resonance energy transfer
GDP	guanosine diphosphate
GFP	green fluorescent protein
GIRK	G-protein-coupled inwardly rectifying potassium channel
GPCR	GTP-binding protein-coupled receptor
GTP	guanosine triphosphate
HBTU	2-(H-Benzotriazole-1-yl)-1,1,3,3-tetramethyluronium hexafluorophosphate

HEPES	4-(2-hydroxyethyl)-1-piperazineethanesulfonic acid
HOBt	N-Hydroxybenzotriazole
IMAC	immobilised metal affinity chromatography
IP_3	inositol-1,4,5-triphosphate
IPTG	Isopropyl β-D-1-thiogalactopyranoside
LDAO	lauryl-di-methyl-amino oxide
MBP	*E. coli* maltose binding protein
MPS	3-mercaptopropyltrimethoxysilane
MWCO	molecular weight cut-off
NMR	nuclear magnetic resonance
NT	neurotensin
NTS / NTR	neurotensin receptor
NTS1A	MBP-rT43NTS1-TrxA-H10
NTS1B	MBP-TeV-rT43NTS1-TeV-TrxA-H10
NTS1C	MBP-TeV-rT43NTS1-CFP-TeV-TrxA-H10
NTS1Y	MBP-TeV-rT43NTS1-YFP-TeV-TrxA-H10
	(The plasmids encoding the constructs NTS1B, NTS1C and NTS1Y are given the prefix p)
OG	octyl-glucoside
PA	phosphatidic acid
PBS	phosphate-buffered saline
PC	phosphatidylcholine
PCR	polymerase chain reaction
PE	phosphatidylethanolamine
PFO	perfluoro-octanoic acid
PG	phosphatidylglycerol
PI3Kγ	phosphoinositide 3-kinase-γ
PI	phosphatidylinositol
PIP_2	phosphatidylinositol-4,5-bisphosphate
PKA	protein kinase A
PKC	protein kinase C
PLC	phospholipase C
PMSF	phenylmethylsulphonyl fluoride
PS	phosphatidylserine

POPC	1-palmitoyl-2-oleoyl-sn-glycero-3-phosphocholine
PyBOP	benzotriazole-1-yl-oxy-tris-pyrrolidino-phosphonium hexafluorophosphate
QY	quantum yield
R_{eff}	effective detergent : lipid ratio
RGS	regulator of G-protein signalling
SDM	site-directed mutagenesis
SDS	sodium dodecyl sulphate
SM	sphingomyelin
SML	sucrose monolaurate
SPR	surface plasmon resonance
SUV	small unilamellar vesicles
T43NTS1	N-terminally truncated NTS1
TAMRA	carboxytetramethylrhodamine
TCEP	tris(2-carboxyethyl)phosphine hydrochloride
TEM	transmission electron microscopy
TES	triethylsilane
TeV	tobacco etch virus
TFA	trifluoroacetic acid
TIR	total internal reflection
TM	transmembrane
TMR	tetramethylrhodamine
Tris	2-amino-2-hydroxymethyl-1,3-propanediol
TrxA	*E.coli* thioredoxin
vvm	volume per volume per minute
WGA	wheatgerm agglutinin

CONTENTS

CHAPTER 1 - INTRODUCTION

1.1 - Biological Membranes

Biological membranes play a central role in both the structural organisation and function of all living cells. They allow the formation of discrete cellular and subcellular compartments and control the diffusion of substances into and out of these compartments.

Polar lipids comprise a major component of biological membranes, and they self-associate to form a semi-permeable barrier in aqueous environments. However, in order to achieve the multitude of functions which biological membranes must perform, including the transport of metabolites and ions, receptor-mediated signalling, ATP synthesis and cell adhesion, they must have a large protein component. Membrane proteins typically constitute 50 % of the dry mass of biological membranes although, depending on the particular source and function, a biological membrane may be composed of between 20 and 80 % protein (Jain, 1988).

Biological membranes are extremely diverse in terms of morphology, composition and function. However, the fluid-mosaic model (Singer and Nicolson, 1972) has classically been used to describe the structure of typical biological membranes and is still regarded as a broadly correct, if vastly oversimplified, description. The model comprises a polar lipid component which forms a bilayer structure, with additional protein and carbohydrate moieties that are located both within and on the surface of the bilayer (Figure 1.1).

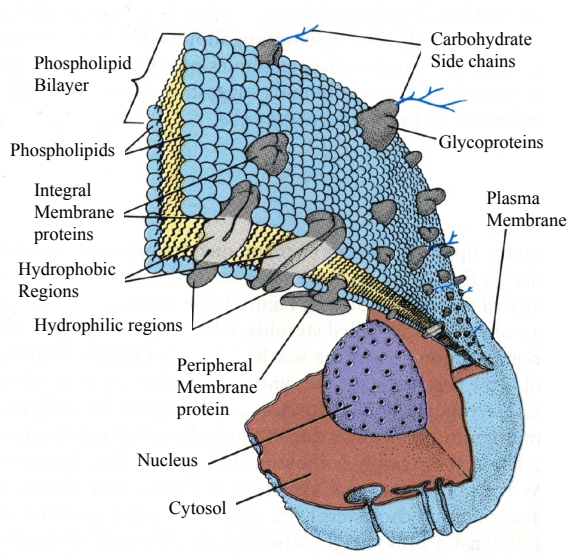

Figure 1.1 – Schematic structure of a typical cell membrane (Mathews and van Holde, 1990), drawn according to the Fluid-mosaic model (Singer and Nicolson, 1972). The membrane consists of a polar lipid component, which forms a bilayer, with proteins which are either integrated into the bilayer or peripherally attached.

1.2 - Membrane lipids

Membrane lipids are generally amphipathic molecules which associate to form a bilayer structure in an aqueous environment. Phospholipids, which have the general molecular structure described in Figure 1.2a, comprise a major lipid component. They consist of two non-polar hydrocarbon chains esterified to a glycerol, which is in turn esterified to the phosphate in the sn-3 position. The phosphate is esterified to an alcohol and the type of alcohol determines the major class of phospholipid. The chemical structure of the polar headgroup determines the overall charge and, therefore, the broad physical characterisitics of the phospholipid. For example, if the phosphate is esterified to the positively-charged alcohols such as choline (phosphatidylcholine, PC) and ethanolamine (phosphatidylethanolamine, PE), the phospholipid will be zwitterionic and will have an overall neutral charge. However, if the phosphate is esterified to alcohols with an overall neutral charge, such as serine (phosphatidylserine, PS), glycerol (phosphatidylglycerol, PG), and inositol (phosphatidylinositol, PI), the phospholipid will have an overall negative charge.

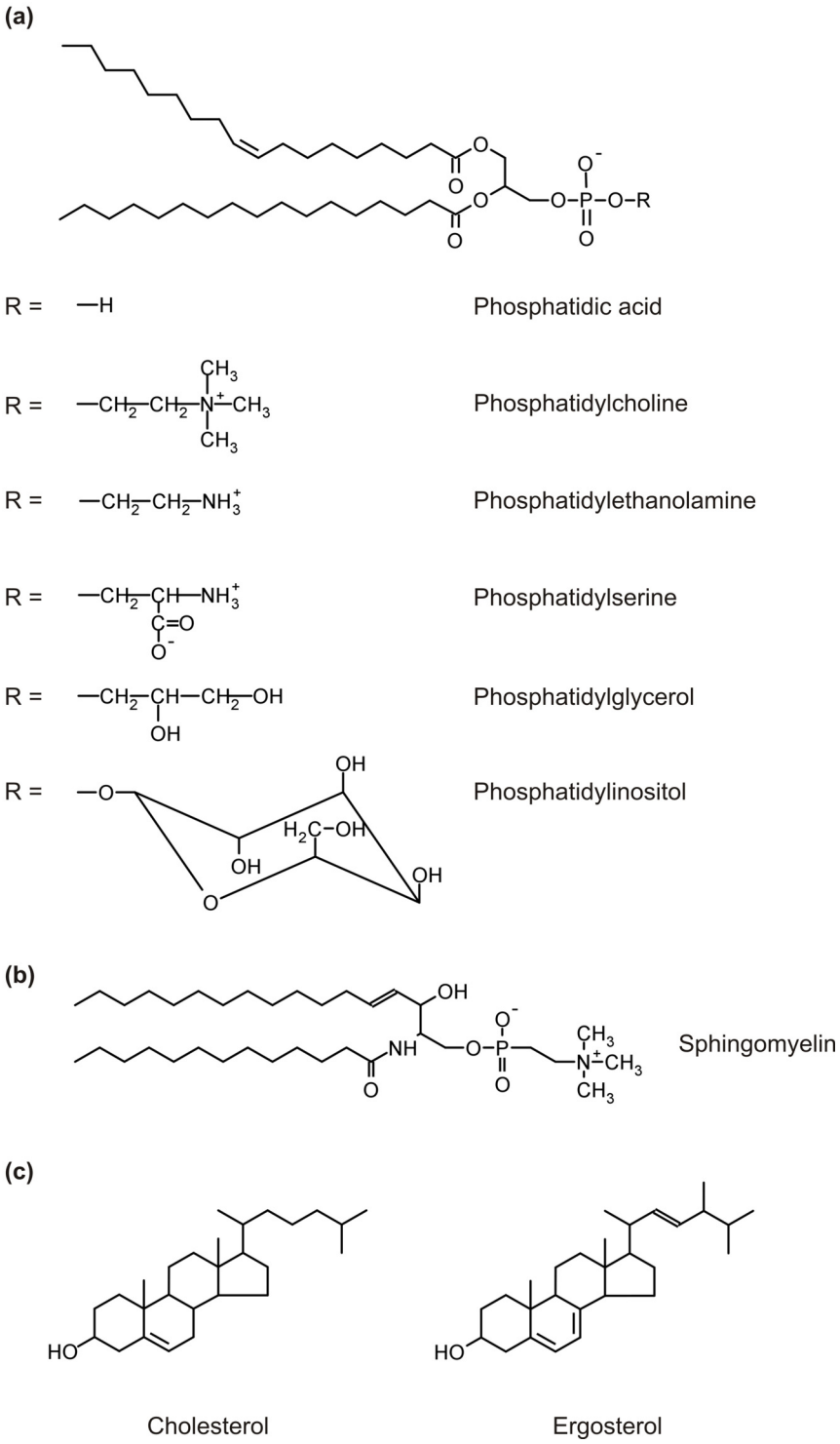

Figure 1.2 – The major lipid components of biological membranes (a) The general structure of a phospholipid. Glycerol is esterified to two fatty acid chains and a phosphate group. The phosphate is esterified to an alcohol (R). Some common alcohols are shown with the name of the resulting phospholipid. (b) Sphingomyelin, present in eukaryotic membranes (c) Sterols of eukaryotic membranes. Cholesterol is the most common, while ergosterol is the major sterol in yeasts.

Therefore, the phospholipid composition of cellular membranes with respect to head groups can be complex and individual membrane types from different classes of organism, as well as different tissue types within a single organism, can have quite distinct compositions (Table 1.1). Even greater complexity is afforded by the phospholipid hydrocarbon chain structure. The length of the carbon chain can vary in length from as few as 12 to as many as 26 carbon atoms. In addition, the hydrocarbon chains can have differing degrees of saturation, with the number of double bonds per fatty acid chain commonly ranging from zero to six (Yeagle, 1993). Given this diversity, the lipid compositions of the membranes of host organisms are likely to be a crucial factor which will determine whether successful overexpression of a particular membrane protein is possible in a heterologous system (section 1.6).

In addition, eukaryotic membranes contain two major components which are absent from prokaryotes: sphingolipids and sterols (Figure 1.2b,c). Sphingolipids have a broadly similar structure to phosphatidylcholine; a phosphatidylcholine headgroup and two hydrocarbon chains. However, they are conjugated to a sphingosine backbone, rather than to glycerol. Cholesterol is the major sterol in eukaryotic membranes, while the major sterol in yeasts is the cholesterol derivative, ergosterol.

Amphipathic molecules such as lipids typically aggregate in aqueous solutions to form a variety of macroscopic structures of differing shape and long range order (phase characteristics) including lamellar, micellar (H_I hexagonal) and inverted micellar (H_{II} hexagonal) phases (Jain, 1988) (Figure 1.3). To a first approximation, the particular phase which forms depends predominantly on the generalised shape of the lipid (Israelachvili *et al.*, 1980).

Table 1.1 – Typical lipid compositions of biological membranes from different sources.

Organism / Tissue	Phospholipid Composition (%)								Sterol Composition (mol/mol)[a]		Reference
	PC	PE	PI	PS	PG	PA	SM	CL	Cholesterol	Ergosterol	
E.coli (inner membrane	-	70-80	-	-	15-20			5	-	-	(Opekarova and Tanner, 2003)
S.cerevisiae (plasma membrane)	17	14	27.7	3.8	-	2.5	30	4.2	-	0.9	(Zinser and Daum, 1995)
P. pastoris (whole cell extract)	38	18	11	28	-	3	-	2	-	0.9	(Sakaki *et al.*, 2001)
Insect Cells (*Xenopus* oocytes, whole cells)	65	19	10	2	-	-	5	-	0.6-0.7	-	(Opekarova and Tanner, 2003)
Mammalian cells (BHK21, plasma membrane)	26	29	3	18	-	-	24	-	0.9	-	(Opekarova and Tanner, 2003)
Mammalian cells (Rat Brain)[b]	40	34	3.4	11.5	-	1	6.4	-	21.5[c]	-	(Norton *et al.*, 1975)

[a] The ratio refers to moles of sterol / moles of phospholipid. [b] 4.4 % of the membrane phospholipid composition was unidentified. [c] This ratio of cholesterol is stated as weight / weight ratio rather than mol / mol (sterol / phospolipid). **Abbreviations:** PC, phosphatidylcholine; PE, phosphatidylethanolamine; PI, phosphatidylinositol; PS, phosphatidylserine; PG, phosphatidylglycerol; PA, phosphatidic acid; SM, sphingomyelin; CL, cardiolipin

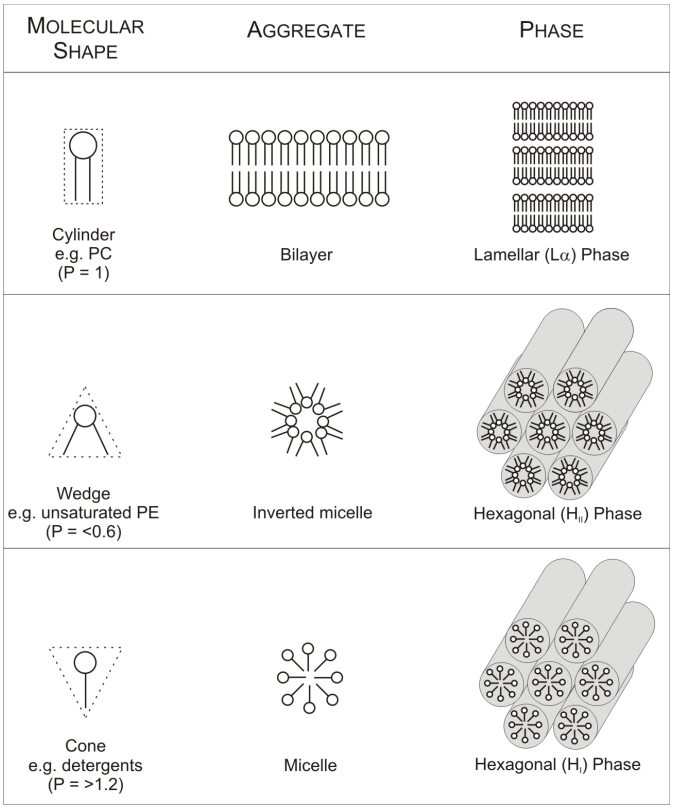

Figure 1.3 – Phases and macromolecular structures of lipids in aqueous solution. To a first approximation the 'generalised' shape (defined as P = volume / (area of the polar headgroup × length) (Israelachvili *et al.*, 1980) of the phospholipid molecule determines the shape of the aggregate and the long range order (or the phase characterisitics) in its aqueous dispersions. Cylindrical molecules organise into bilayers (lamellar phase), cone-shaped molecules into micelles (H_I hexagonal phase) and wedge-shaped molecules into inverted micelles (H_{II} hexagonal phase) (Jain, 1988).

Biological membranes typically contain a mixture of lipid types which have differing propensities to form lamellar and non-lamellar phases. It is believed that the lipids do not form a homogenous mixture but rather undergo lateral lipid phase separations (Quinn *et al.*, 2005; Yang *et al.*, 2005). In particular, there is increasing evidence to suggest that sphingomyelin and cholesterol are confined to certain discrete microdomains of the plasma membrane, termed lipid rafts, and to small indentations in the plasma membrane called caveolae. Whilst caveolae have a similar lipid composition to rafts, they also have caveolin proteins localised on the inner leaflet of the membrane bilayer (Ostrom and Insel, 2004). It is believed that the formation of these lateral compartments, which are not adequately described by the fluid-mosaic model of membrane structure, is crucial to membrane trafficking and cell signalling events.

1.3 - Membrane Proteins

Membrane proteins constitute a large proportion (50 %) of the dry weight of biological membranes (Jain, 1988). They are divided into two major classes: peripheral and integral. Peripheral membrane proteins are not integrated into the hydrophobic region of the lipid bilayer and are typically readily removed from membranes by non-disruptive techniques such as high or low ionic strength washes (Findlay, 1989). In contrast, integral membrane proteins, which are integrated into the structure of the lipid bilayer, can only be removed from the membrane by using techniques which disrupt the bilayer structure, for example detergent treatment. Such proteins may be either membrane spanning, or have only a portion of their structure buried in one side of the membrane. In order for a given amino acid sequence to pass through the centre of the bilayer, it must be structured in such a way as to limit the energetically-unfavourable exposure of charged regions to the hydrophobic environment. This is typically achieved by an α-helical secondary structure of largely hydrophobic residues (multi-spanning proteins may form a helical bundle from multiple α-helices) or, less commonly, by the formation of a β-barrel structure as is seen from the high-resolution structures of the bacterial porins (Pautsch and Schulz, 1998).

Membrane proteins are extremely diverse; 30-40 % of all genes in the human genome are believed to encode membrane proteins (Wallin and von Heijne, 1998). They are also of particular pharmacological relevance, with some 70 % of current drugs targeted towards integral membrane proteins (Lundstrom, 2007). Despite this, while the total number of protein structures deposited in the protein data bank (pdb) is currently close to 40,000 (RCSB, 2007) barely more than 100 unique high resolution structures have been published to date (Michel, 2007). This is largely due to the problems associated with the successful overexpression, purification and 3D crystallisation of membrane proteins. In addition, solution state NMR techniques are not applicable to the majority

of membrane proteins since the large molecular weight of the protein-lipid or protein-detergent complexes prevents the rapid isotropic motion required to obtain high-resolution spectra.

1.4 - G Protein-Coupled Receptors

G-protein coupled receptors (GPCRs), of which over 750 have been identified in the human genome project (Vassilatis *et al.*, 2003), are a family of integral membrane proteins with seven transmembrane helices. GPCRs are involved in a wide range of physiological processes, including cell-cell communication, sensory transduction, neuronal transmission and hormonal signalling (Ji and Ji, 1998; Iyengar *et al.*, 2002). Consequently, GPCRs are of particular pharmacological importance and are expected to comprise a large proportion of future drug targets (Terstappen and Reggiani, 2001; Vanti *et al.*, 2001). Given that the majority of GPCR-targeted drugs in clinical practice (which represent more than 30 % of all drugs) exert their actions on only 30 of the 750 identified human GPCRs, there is significant scope for further drug discovery in this field (Watts, 2005; Hill, 2006).

The multitude of GPCRs can be grouped into three distinct families, A, B, and C, on the basis of sequence similarity (Figure 1.4) (Pierce *et al.*, 2002; Jacoby *et al.*, 2006). GPCRs within each family generally share over 25 % sequence identity in the transmembrane core region, and a distinctive set of highly conserved residues and motifs. The rhodopsin-like family A is by far the largest and has been most widely studied. The other two main families are the secretin-like receptor family B, which bind several neuropeptides and other peptide hormones, and the metabotropic glutamate receptor (mGluR)-like family C, which have a characteristically large, extracellular amino terminus. In addition, a separate group termed the 'frizzled' family exists but direct coupling to heterotrimeric G-proteins is still a matter of debate (Jacoby *et al.*, 2006).

Despite this remarkable diversity, only one GPCR, wild type bovine rhodopsin, has been structurally described at high resolution (Palczewski *et al.*, 2000; Okada *et al.*, 2002; Li *et al.*, 2004; Okada *et al.*, 2004), largely because the successful expression of GPCRs for structural studies has proved so challenging (Sarramegna *et al.*, 2006) and a structure of a ligand-binding GPCR is still awaited.

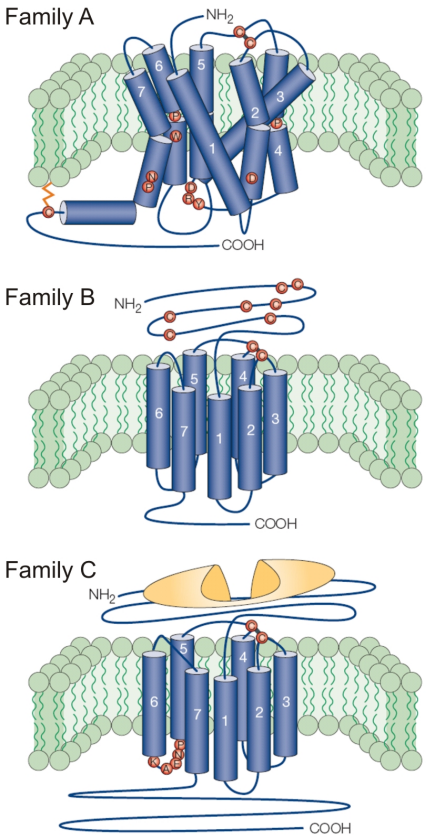

Figure 1.4 - Key structural aspects of the three main GPCR families (Ellis, 2004)**.** Family A (rhodopsin-like) is by far the largest subgroup and contains receptors for ligands including odorants, neurotransmitters (e.g. dopamine, serotonin), neuropeptides and glycoprotein hormones. Receptors of family A are characterized by several highly conserved amino acids (some of which are indicated in the diagram by red circles) and a disulphide bridge that connects the first and second extracellular loops (ECLs). Most of these receptors also have a palmitoylated cysteine in the carboxy-terminal tail, which serves as an anchor to the membrane (orange zig-zag). Family B GPCRs are characterized by a relatively long amino terminus, which contains several cysteines that form a network of disulphide bridges. Their morphology is similar to some family A receptors, but the palmitoylation site is missing and the conserved residues and motifs are different from the conserved residues in the family A receptors. Little is known about the orientation of the TM domains, but given the divergence in amino-acid sequence, they are likely to be different from family A receptors. Ligands for family B GPCRs include hormones, such as glucagon, secretin and parathyroid hormone. Family C contains the metabotropic glutamate, the Ca^{2+}-sensing and the $GABA_B$ (γ-aminobutyric acid, type B) receptors. These receptors are characterized by a long amino terminus and carboxyl tail. The ligand-binding domain (shown in yellow) is located in the amino terminus.

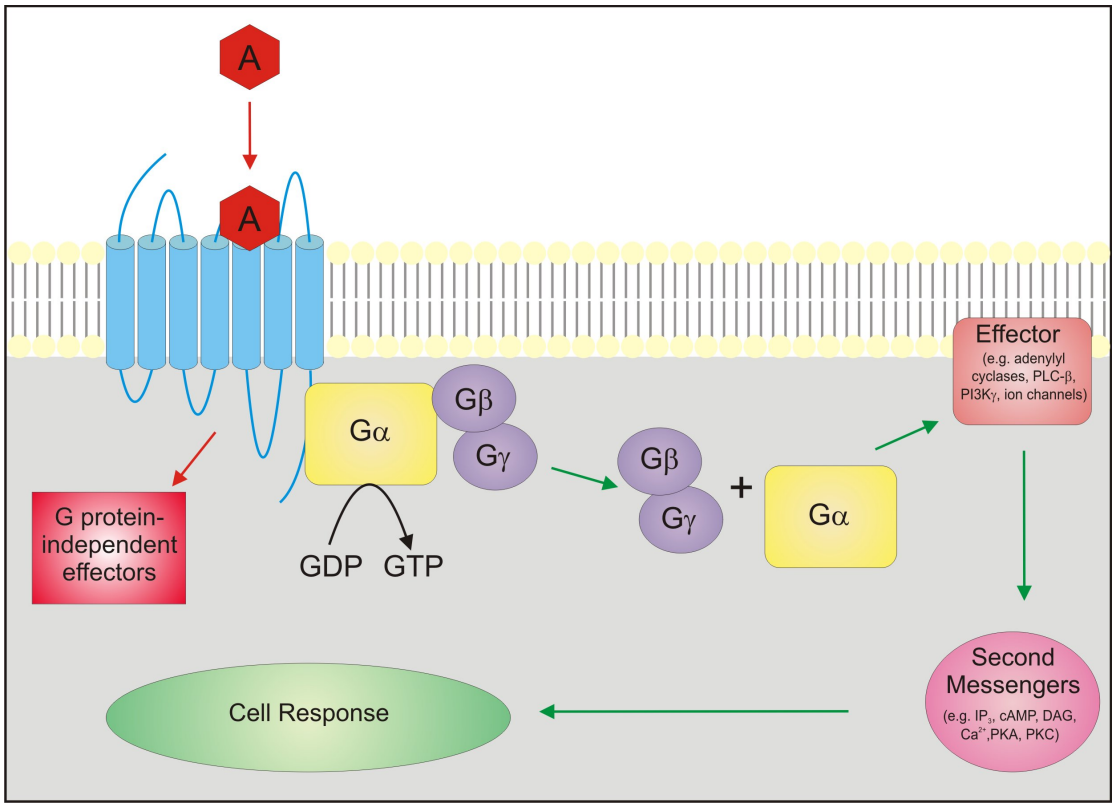

Figure 1.5 - Schematic representation of the diverse signalling mechanisms for GPCRs. Agonists (A) can, depending on the receptor type, be one of a wide range of signalling molecules including peptides (e.g. neurotensin, angiotensin, thrombin), amino acids (e.g. glutamate), lipids (e.g. leukotriene, LPA) or biogenic amines (e.g. acetylcholine, dopamine). Agonist binding to the GPCR results in a conformational change in the receptor which promotes exchange of G-protein-bound GDP to GTP. The activated heterotrimer dissociates into the Gα subunit and the Gβγ dimer, both of which can have an independent capacity to signal downstream through the activation or inhibition of effector molecules. This results in second messenger responses, which in turn triggers a cascade of cellular signal transduction events. Hydrolysis of GTP to GDP leads to signal termination and re-association of the heterotrimer. The G protein-independent effector pathway is also indicated. Abbreviations: DAG, diacylglycerol; IP_3, inositol-1,4,5-triphosphate; PI3Kγ, phosphoinositide 3-kinase-γ; PKA, protein kinase A; PKC, protein kinase C; PLC, phospholipase C.

The classical mechanism of GPCR-mediated signalling involves coupling to heterotrimeric G proteins (composed of an α-, β-, and γ-subunit) although, more recently, alternative G protein independent signalling mechanisms have been described (Brzostowski and Kimmel, 2001) (Figure 1.5). Agonist binding to the GPCR results in a conformational change in the receptor which promotes exchange of G-protein-bound GDP to GTP. The activated heterotrimer dissociates into the Gα subunit and the Gβγ dimer, both of which can have an independent capacity to signal through the activation

or inhibition of effector molecules. This results in second messenger responses, which in turn trigger a cascade of cellular signal transduction events (Pierce *et al.*, 2002).

To date, 16 α, 5 β and 12 γ proteins have been cloned which gives great scope for combinatorial complexity of heterotrimers (Pierce *et al.*, 2002). G proteins are generally referred to by their α-subunits and four distinct α-subunit subfamilies are recognised, based on their sequence and downstream signalling: G_s proteins couple to stimulation of adenylyl cyclase; G_i proteins couple to inhibition of adenylyl cyclase and activation of G-protein-coupled inwardly rectifying potassium (GIRK) channels; G_q proteins couple to the activation of phospholipase Cβ resulting in the intramembrane hydrolysis of phosphatidylinositol-4,5-bisphosphate (PIP_2) to inositol-1,4,5-triphosphate (IP_3) and diacylglycerol (DAG); and G_{12} proteins couple to the activation of Rho guanine-nucleotide exchange factors (GEFs). However, most biological responses mediated by GPCRs are not dependent on a single biochemical route, but may result from a combination of pathways involving several different G proteins, as well as G protein-independent pathways (Marinissen and Gutkind, 2001).

Hydrolysis of GTP to GDP, a process regulated by RGS (regulator of G-protein signalling) proteins, leads to re-association of the $G_{\alpha\beta\gamma}$ heterotimer and termination of the cellular signal. In addition, it has been observed that receptor signalling can be 'dampened' even in the presence of continuing agonist stimulation (Ferguson, 2001). Such 'desensitisation' is thought to be controlled by receptor phosphorylation, which is believed to be mediated either by a negative feedback loop involving second messenger kinases (PKA, PKC) or by a distinct family of G protein-coupled receptor kinases (GRKs) (Pitcher *et al.*, 1998). These kinases feedback phosphorylate GPCRs at phosphorylation consensus sites within the intracellular loops and carboxyl-terminal tails (Ferguson, 2001). GRKs can be activated allosterically by the active conformation of

the receptors themselves, by recruitment to the membrane by activated G proteins and by PKA and PKC. GRK phosphorylation of the intracellular loops and/or C-terminal tail promotes the binding of an arrestin molecule to the receptor which sterically inhibits further interactions between the receptor and the G protein (Ferguson, 2001). One form of arrestins (β) has been shown to have a central role in the coordination of receptor internalisation via endocytosis. Recently, several pathways of receptor internalisation have been described, including internalisation via clathrin-coated pits, caveolae, or uncoated vesicles (Claing *et al.*, 2002).

Most GPCRs are now believed to function not as isolated, monomeric receptors in the cell membrane, but as homo- or hetero-dimers, which form either constitutively or upon ligand binding (Milligan, 2007). GPCR multimerisation is thought to be important for the physiological function of the receptors, including ligand binding, signal transduction or receptor internalisation (for more detail see section 5.1.3).

1.5 - Neurotensin and Neurotensin Receptors

Neurotensin (NT), first isolated from calf hypothalamus (Carraway and Leeman, 1973), is a tridecapeptide neurotransmitter (N-Glu-Leu-Tyr-Glu-Asn-Lys-Pro-Arg-Arg-Pro-Tyr-Ile-Leu-C) found in mammalian gastrointestinal, cardiovascular and central nervous systems. It is synthesised as part of a large, 170 amino acid precursor which also contains neuromedin N, a six amino acid neurotensin-like peptide (Dobner *et al.*, 1987). Like many other neuropeptides, it fulfils a dual function of neurotransmitter or neuromodulator in the nervous system and of local hormone in the periphery. The biochemical and pharmacological properties of NT in the brain and in peripheral organs have been extensively reviewed (Vincent *et al.*, 1999; Dobner, 2005). Major effects of NT include analgesia, inhibition of food intake, modulation of dopaminergic (DA) systems, modulation of pituitary hormone secretion and regulation of digestive function.

The close anatomical and functional interactions between NT and the mesocorticolimbic and neostriatal DA systems, as well as marked effects of anti-psychotic drugs (APDs) on the NT system, has lead to the hypothesis that NT may act as an endogenous antipsychotic (Caceda *et al.*, 2006). In addition, NT–containing circuits have been demonstrated to mediate some of the rewarding and/or sensitising properties of drug abuse. Consequently, the NT receptors have been postulated as putative targets for the development of treatments for conditions such as Schizophrenia, Parkinson's disease and drug addiction.

The first NT receptor to be identified, neurotensin receptor 1 (NTR1 or NTS1), was initially cloned from rat brain and belongs to the family A class of GPCRs (Tanaka *et al.*, 1990). Subsequently, two new NT receptors were identified and their properties have been recently reviewed (Mazella and Vincent, 2006). One, NTS2, also belongs to the GPCR superfamily (Chalon *et al.*, 1996), whereas the other, NTS3, is structurally distinct (Mazella *et al.*, 1998).

1.5.1 - Neurotensin Receptor 1

Neurotensin receptor 1 (NTS1), the first neurotensin receptor to be cloned, is a 424 amino acid (47 kDa) protein belonging to the GPCR superfamily (Family A). The receptor has been shown to bind NT with high affinity (K_d) in various cell types, for example in *E.coli* (0.43 ± 0.11 nM) (Tucker and Grisshammer, 1996), synaptic membranes (0.9 nM) (Kitagbi *et al.*, 1977), *Xenopus* oocytes (0.19 ± 0.04 nM) (Tanaka *et al.*, 1990) and HT29 cells (0.56 ± 0.10 nM) (Vita *et al.*, 1993). Binding is sensitive to Na^+ ions and GTP but, unlike the lower affinity receptor NTS2, is insensitive to the antihistamine drug, levocabastine (Tanaka *et al.*, 1990). Northern blot analysis has revealed that NTS1 mRNAs are expressed throughout the brain and intestine of both rat (Tanaka *et al.*, 1990) and human (Vita *et al.*, 1993). In situ hybridisation experiments

have revealed high levels of NTS1 mRNA in the neurons of the diagonal band of Broca, medial septal nucleus, nucleus basalis magnocellularis, suprachiasmatic nucleus, supramammillary area, substantia nigra and ventral tegmental area (Elde *et al.*, 1990). Much of the available evidence suggests that most of the physiological functions and pharmacological effects of NT are mediated by NTS1 (Dobner, 2005).

A schematic depicting the key residues of NTS1 is shown in Figure 1.6. Early studies of NTS1 showed that only the C-terminal hexapeptide sequence of NT (NT_{8-13}, N-Arg-Arg-Pro-Tyr-Ile-Leu-C) is required for receptor binding and that it in fact binds more strongly to the receptor than the full length NT peptide (Kitagbi *et al.*, 1977). Rat / human chimeric receptor studies in HEK cells that exploited an NT_{8-13} analogue which had higher affinity for rat NTS1 than human NTS1, suggested that a region comprising residues of TM6, E3 and TM7 was involved in NT binding (Cusack *et al.*, 1996). Subsequent site directed mutagenesis and modelling studies have isolated the putative residues which are believed to be involved (summarised in Figure 1.6) (Pang *et al.*, 1996; Barroso *et al.*, 2000).

Sanofi-Aventis developed an aromatic, non-peptide antagonist, SR 48692, which binds with higher affinity to NTS1 than NTS2 (Figure 1.7). Site directed mutangensis studies revealed key residues involved in binding of the compound (summarised in Figure 1.6) (Labbe-Jullie *et al.*, 1998). The binding site for SR 48692 is situated between TM6 and TM7 and partially overlaps with the NT binding site, which explains the competitive behaviour towards NT binding. In addition, SR48692 binds to multiple residues on TM7 and, therefore, will likely act as a rigid structure that will hold together TM6 and TM7. In contrast, NT makes strong interactions with the side of the E3 loop which connects to TM7, suggesting a key role for TM7 in agonist-induced conformational changes which lead to G protein activation.

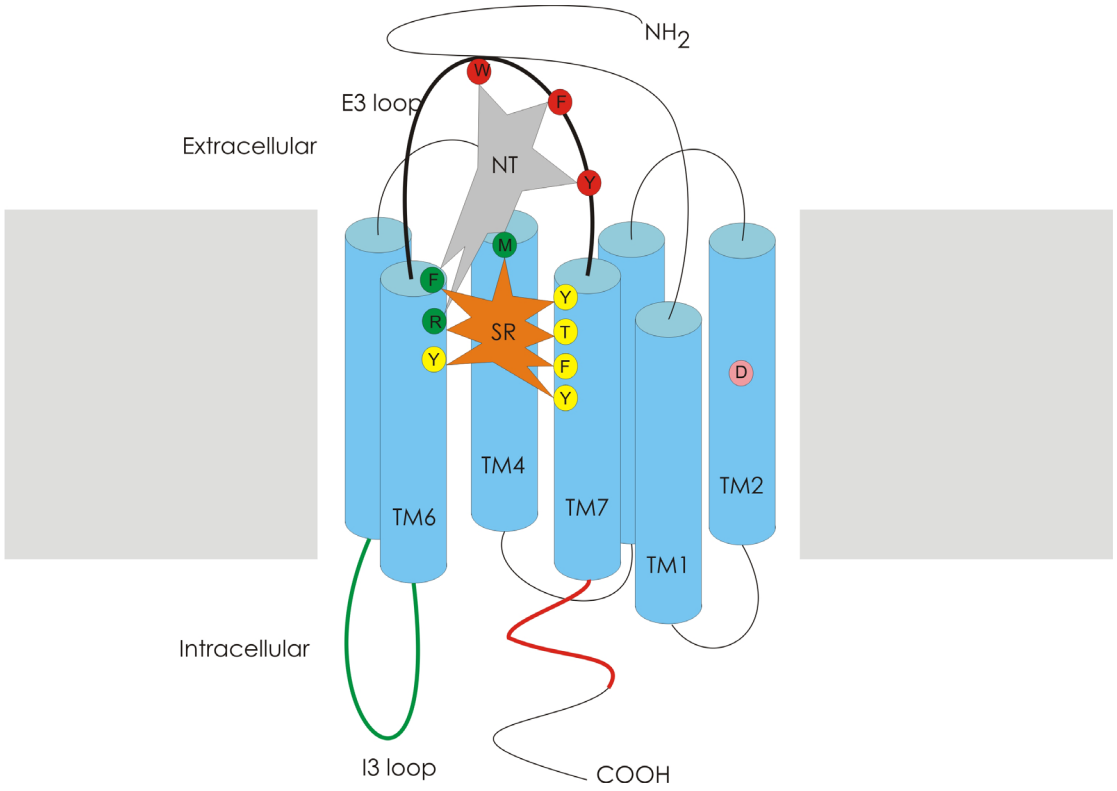

Figure 1.6 – Schematic depicting the key functional domains of rat NTS1. Residues that are involved in NT binding (Trp^{339}, Phe^{334}, Tyr^{347} (E3 loop)) are coloured red, residues that are involved with the binding of the antagonist SR 48692 (Tyr^{324} (TM6), Tyr^{351}, Thr^{354}, Phe^{358} and Tyr^{359} (TM7)) are coloured yellow, and residues that are involved in the binding of NT and SR 48692 (Met^{208} (TM4), Phe^{331}, Arg^{327} (TM6)) are coloured green. The site which confers Na^+-sensitivity (Asp^{113} (TM2)) is shown in pink. The third intracellular loop (I3), coloured green, is essential for Gq activation and coupling to phospholipase C. The first half of the C-terminal domain (red) is involved in Gs and Gi/o activation (Adapted from (Kitabgi, 2006)).

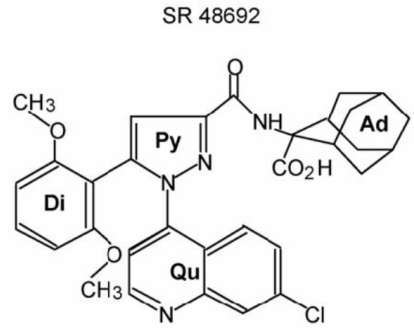

Figure 1.7 – Chemical structure of the NTS1 antagonist, SR 48692, developed by Sanofi-Aventis (Gully *et al.*, 1993). Abbreviations: Ad, adamantine; Py, pyrazole; Di, dimethoxyphenyl; Qu, quinolinyl.

Mutagenesis studies have revealed the regions of the receptor which are involved in G protein coupling. Deletion of residues in the third intracellular loop (I3) led to a loss of PLC activation by NT, without affecting stimulation of cAMP production (Yamada *et al.*, 1994). Conversely, deletion of residues in the first half of the C-terminal domain of NTS1 abolished NT-induced PLA2 and adenylyl cyclase activation, but not PLC stimulation (Skrzydelski *et al.*, 2003). Therefore, it is likely that the I3 loop is involved in receptor coupling to Gq, whereas the first half of the C-terminal domain interacts with Gs and Gi/o. Mutation of Phe^{358} in TM7 has been found to generate a form of the receptor which is constitutively active with respect to IP production, but not cAMP production (Barroso *et al.*, 2002). In addition, SR 48692 behaved as an inverse agonist at the mutant receptor, which is again consistent with TM7 being involved in the conformational changes that lead to Gq activation.

1.5.2 - Other NT Receptors

(i) Neurotensin Receptor 2 (NTS2)

NTS2 was first identified by radioligand binding studies which suggested the presence of two separate binding sites in isolated brain or gastrointestinal membranes (Kitabgi *et al.*, 1985). The high affinity, sodium sensitive sites (0.1 – 1 nM) were attributed to NTS1 while the lower affinity sites (3 – 5 nM), which were insensitive to sodium, but sensitive to the anti-histamine drug levocabastine, were attributed to a distinct NT receptor. Subsequent cloning of NTS2 showed it to be a 416 amino acid protein of the GPCR family, which shares 43 % amino acid identity and 64 % amino acid homology with NTS1 (Chalon *et al.*, 1996). However, NTS2 has a shorter N-terminal domain, which lacks putative N-glycosylation sites, and also a lack of the conserved Asp residue in TM2 which explains the absence of sensitivity to Na^+ ions.

Northern blot and in situ hybridisation studies suggest that NTS2 is mainly expressed in the brain. Its distribution in the brain is quite different to NTS1, and transcripts of both receptor subtypes are abundantly co-expressed only in the ventral mesencephalic region (Walker *et al.*, 1998). NTS2 is mainly localised to the olfactory system, the cerebral and cerebellar corticies, the hippocampal formation and selective hypothalamic nuclei. Pharmacological evidence suggests that, whilst the majority of NT functions are mediated by NTS1, two of the most prominent effects of centrally-administered NT, analgesia and hypothermia, are mediated by NTS2, since the NT-selective antagonist, SR 48692, did not antagonise these effects (Dubuc *et al.*, 1994; Mazella and Vincent, 2006). However, other studies have implicated NTS1 in NT-induced analgesia. For example, in NTS1-knockout mice, an absence of NT-induced hot plate latency was observed (Pettibone *et al.*, 2002). A current theory is that supraspinal NT-induced analgesia is mediated by both NTS1 and NTS2, whereas the spinal nociceptive properties of NT are NTS2-dependent (Mazella and Vincent, 2006).

(ii) Neurotensin Receptor 3 (NTS3)

The third neurotensin receptor, NTS3, was first identified as an NT-binding protein in detergent-solubilised brain membrane preparations and subsequent cloning revaled that it is not a member of the GPCR superfamily, but shares 100 % sequence identity with the previously identified sorting protein, sortillin (Mazella *et al.*, 1998). It belongs to a new receptor family characterised by the presence of a luminal / extracellular region containing a cysteine-rich domain homologous to that found in the yeast protein Vsp10p. The physiological function of NTS3 remains unclear, not least because it has been shown to bind several ligands in addition to NT (Mazella and Vincent, 2006), but it has been suggested that it is involved in receptor internalisation and ligand degradation (Martin *et al.*, 2002).

1.6 - Production of GPCRs in heterologous systems

Despite their clinical relevance, only a single GPCR, bovine rhodopsin, has been structurally described at high resolution (Palczewski *et al.*, 2000; Okada *et al.*, 2002; Li *et al.*, 2004; Okada *et al.*, 2004). Consequently, very little is known, at atomic resolution, about the detailed molecular mechanisms by which these membrane proteins are able to recognise their extracellular stimuli and signal across the cell membrane to the associated heterotrimeric G proteins.

The lack of high resolution structure is due, at least in part, to problems associated with obtaining sufficient purified receptor. In contrast to rhodopsin, which is endogenously expressed at high levels, most GPCRs are expressed at low levels and therefore purification from natural sources is not normally feasible. Consequently, for structural studies, most GPCRs must be overexpressed in heterologous systems. In addition, once this has been achieved, the GPCR must be extracted from the host membrane and purified (Sarramegna *et al.*, 2006).

The heterologous overexpression of GPCRs has been recently reviewed (Sarramegna *et al.*, 2003). Four main expression systems have been successfully exploited for GPCR overexpression: *E.coli*, yeast (*S.cerevisiae* and *P.pastoris*), insect cells and mammalian cells (for examples see Table 1.2). However, it is currently not possible to predict whether any given GPCR will express well in a particular expression system. It is likely that there is no universal expression system suitable for the functional production of all GPCRs and therefore the optimal expression system for a particular receptor must be empirically tested for. The difficulty of achieving overexpression of GPCRs (and its prediction) in all of these systems is likely a result of multiple factors, including the complex folding mechanism of these proteins, problems of receptor insertion into host

membranes, inappropriate lipid environment (section 1.3) and incorrect posttranslational modifications.

(i) E.coli

The expression of GPCRs in *E.coli* has the advantages of low cost, short generation and culture time, and homogeneity of the recombinant protein (no posttranslational modifications). In addition, isotopic labelling for NMR studies is relatively straightforward (Marley *et al.*, 2001). There are two strategies for the overexpression of GPCRs in *E.coli*: (a) expression of functional, membrane-inserted receptors and (b) expression of incorrectly folded, aggregate protein. The latter approach requires the isolation of the misfolded protein as 'inclusion bodies' and the subsequent refolding of the GPCR into its functional form. Relatively few GPCRs have been successfully expressed in *E.coli* in functional form. Examples include NTS1 (section 2.1.1) and the cannabinoid CB2 receptor (Yeliseev *et al.*, 2005; Krepkiy *et al.*, 2006; Yeliseev *et al.*, 2007). Both of these employed the same strategy; an N-terminal maltose binding protein (MBP) fusion and a C-terminal thioredoxin (TrxA) fusion to promote receptor folding at the cell membrane. Therefore, this is a possible general approach which could be successful with other GPCRs. A similar construct, but lacking the TrxA moiety, was also used to successfully overexpress a C-terminally truncated (protease resistant) form of the Adenosine A2 receptor at the *E.coli* membrane (Weiss and Grisshammer, 2002).

Several cases of the successful refolding of GPCRs from insoluble inclusion bodies, for example the human leukotriene B4 receptor BLT1 (Baneres *et al.*, 2003), highlight the potential to obtain large amounts of protein using this strategy. However, the formation of inclusion bodies is hard to control and refolding strategies are notoriously difficult to optimise.

Table 1.2 – Examples of the strategies used for the expression and purification of GPCRs.

Expression System	Receptor	Expression level	Detergent	Purification steps	Reference
E.coli (membrane)	Human peripheral cannabinoid receptor (CB2)	1 mg/L	DDM / CHAPS / CHS	1. IMAC 2. Strep-tag	(Yeliseev *et al.*, 2007)
E.coli (membrane)	Rat neurotensin receptor 1 (rNTS1)	0.45 mg/L	DDM / CHAPS / CHS	1. IMAC 2. Ligand Affinity	(White *et al.*, 2004)
E.coli (membrane)	Human adenosine A_{2A} receptor (hA2aR)	0.33 mg/L	DDM / CHS	1. IMAC 2. Ligand affinity 3. cation exchange	(Weiss and Grisshammer, 2002)
E.coli (inclusion bodies)	Human leukotriene B_4 (LTB_4) receptor BLT1	10 mg/L	LDAO	1. IMAC 2. cation exchange	(Baneres *et al.*, 2003)
Yeast (*S.cerevisiae*)	*S.cerevisiae* α-factor receptor (Ste2)	350 pmol/mg (approx. 0.1 mg/L †)	DDM	1. IMAC	(David *et al.*, 1997)
Yeast (*S.cerevisiae*)	Human D_{1A} dopamine receptor	1-2 pmol/mg (approx. 0.01 – 0.025 mg/L †)	DDM	1. IMAC 2. FLAG Affinity	(Andersen and Stevens, 1998)
Yeast (*P.pastoris*)	Human central cannabinoid receptor (CB2)	3.6 pmol/mg	FOS-12	1. IMAC 2. FLAG Affinity	(Kim *et al.*, 2005)
Yeast (*P.pastoris*)	Human dopamine D2S receptor	3-13 pmol/mg	DDM / CHS	1. IMAC 2. FLAG Affinity	(de Jong *et al.*, 2004)
Yeast (*P.pastoris*)	Human β_2 adrenergic receptor ($h\beta_2$)	4 mg/L	SML	1. IMAC 2. Anion exchange 3. Ligand affinity 4. Gel filtration	(Noguchi and Satow, 2006)

Mammalian (HEK293)	*S.cerevisiae* α-factor receptor (Ste2)	1-2 mg/L	DDM	1. IMAC	(Shi *et al.*, 2005)
Mammalian (CHO)	Porcine m2 muscarinic acetylcholine receptor (pM_2)	60 nmol per 30 ml of packed CHO cells	Digitonin / Na cholate	1. WGA agarose. 2. hydroxyapatite 3. ABT sepharose	(Peterson *et al.*, 1995)
Mammalian (Cos7)	Human parathyroid hormone (PTH) receptor	240 pmol/mg	DDM	1. Immunoaffinity	(Shimada *et al.*, 2002)
Insect (Sf9)	Human muscarinic acetylcholine receptor (hM_2)	4.4 nmol/L (0.15 mg/L)	Digitonin / Na cholate	1. IMAC	(Hayashi and Haga, 1996)
Insect (Sf9)	Rat neurokinin receptor 1 (rNK1)	1-2 pmol/mg	CHAPS	1. lentil lectin-agarose	(Kwatra *et al.*, 1993)
Insect (Sf9)	Human β_2 adrenergic receptor ($h\beta_2$)	20 nmol/L (0.8 mg/L)	DDM	1. IMAC 2. FLAG Affinity. 3. Ligand Affinity	(Kobilka, 1995)
Insect (Sf9)	Human pituitary adenylate cyclise-activating polypeptide (PACAP) receptor	80-150 pmol/mg (18 nmol/L or 0.85 mg/L)	Digitonin / CHAPS	1. Ligand Affinity 2. Lentil-lectin agarose 3. Hydroxyapatite	(Ohtaki *et al.*, 1998)

† Approximate yields per litre of culture were calculated from the reported total yield of receptor obtained from a 60 g (20 L) preparation of receptor.
Abbreviations used: ABT, 3-(2'-aminobenzhydryloxy) tropane; DDM, n-dodecyl-β-D-maltoside; CHAPS, 3-[(3-cholamidopropyl)dimethylammonio]-1-propanesulfonate; CHO, Chinese hamster ovary cell; CHS, cholesteryl hemisuccinate; COS, kidney african monkey green cell; HEK, human embryonic kidney cell; IMAC, immobilised metal affinity chromatography; LDAO, lauryl-di-methyl-amino oxide; Na cholate, sodium cholate; SML, sucrose monolaurate; WGA, wheatgerm agglutinin

(ii) Yeasts

GPCRs have also been expressed in various species of yeast (including *S.cerevisiae*, *S.pombe*, and *P.pastoris*). Some examples of GPCRs which have been successfully expressed and purified from yeast culture are detailed in Table 1.2. The culture of yeast using large volume fermentation is relatively straightforward and, given the short generation time (2 h) and simple media requirements, yeast expression is particularly amenable to large scale protein production. In addition, contrary to bacteria, yeasts possess endogenous GPCRs and G proteins. Consequently, they can perform most of the posttranslational modifications observed in higher eukaryotes, although N-glycans added by yeast differ from those added by mammalian cells. Methylotrophic yeasts, such as *P.pastoris*, can grow to particularly high cell densities, which maximises the cell base which can be obtained per unit volume of culture.

(iii) Mammalian Cells

Expression of GPCRs in several mammalian cell lines has been successful (Table 1.2). These cells present the environment closest to the native tissues in which GPCRs naturally occur and they are able to perform complex posttranslational modifications. However, scale-up of expression to large volumes is not straightforward. Scale-up of production from cell lines which transiently express by infection with recombinant viruses requires special attention to safety considerations. Stable cell lines which produce large amounts of receptor may also be produced and this method is preferred for the production of larger quantities of material. For example, a stably expressing Chinese hamster ovary (CHO) cell line was produced which expressed the human β_2-adrenergic receptor at up to 200 pmol per mg of membrane protein (Lohse, 1992). However, the maintenance of the cell lines in suspension culture can be problematic and their production is time-consuming. Consequently, expression of GPCRs in

mammalian cell lines has been largely limited to small scale functional studies, rather than larger scale overexpression of tagged receptors for subsequent purification (Sarramegna *et al.*, 2003).

(iv) Baculovirus / insect cells system

The *Autographa californica* baculovirus (Fraser, 1992) is able to selectively infect different insect cell types, amongst which the most frequently used are *Spodiptera frugiperda* (cell lines Sf9 and Sf21) and *Trichoplusia ni* (cell lines Hi5 and MG1). The gene of interest is placed in a plasmid between sequences of high homology for the baculovirus genome, under the control of a strong promoter (e.g. polyhedron). Co-transfection of the plasmid and viral DNA into insect cells allows the insertion of the gene of interest into the viral genome *in vivo* by homologous recombination. Post-translational modifications performed by insect cells are similar to those observed in mammalian cells. However, insect cells have relatively long generation times (24 h) and require complex growth media.

A recent study compared the expression of sixteen human GPCRs in three different baculovirus-infected insect cell lines (Sf9, Sf21, Hi5) (Akermoun *et al.*, 2005). Different GPCRs exhibited widely different expression levels, ranging from less than 1 pmol/mg membrane protein to more than 250 pmol/mg membrane protein. This study highlighted the fact that no single expression system or condition is applicable to all GPCRs. In addition, large differences were seen for expression of the same GPCR in different cell lines and closely related GPCRs did not share similar expression profiles. This emphasises the difficulty encountered in the prediction of good expression systems for any given receptor and consequently the need for empirical testing of several expression systems.

(v) Receptor Solubilisation

Once expressed, in order to begin purification the GPCR must initially be extracted from the host cell membrane. Detergents are typically employed for this task (Seddon *et al.*, 2004) and reference to Table 1.2 shows that, whilst a wide range of different detergents have been successfully used for the purification of GPCRs, a relatively small number are more generally used, for example, the non-ionic detergents DDM and digitonin, and the zwitterionic detergent, CHAPS. Non-ionic detergents contain uncharged hydrophilic head groups of either polyoxyethylene or glycosidic groups. They are generally considered to be mild and relatively non-denaturing, since they tend to break lipid-lipid interactions and lipid-protein interactions rather than protein-protein interactions. This therefore explains why they have been most widely used to extract GPCRs in their biologically relevant conformations. Zwitterionic detergents tend to have properties which combine the mild action of non-ionic detergents with the harsh solubilising (and often denaturing) properties of ionic detergent (such as sodium dodecyl sulphate (SDS)).

1.7 - Aims of the Thesis

The primary aim of the thesis is to further the knowledge of GPCR structure and function through the *in vitro* biophysical study of Neurotensin Receptor 1 (NTS1), a GPCR of the Family A subtype.

Given that high resolution structural analysis typically requires relatively large amounts of purified material, the existing expression and purification procedures of NTS1 will be optimised in order to maximise the yields of correctly folded receptor (Chapter 2). Negative stain electron microscopy will also be utilised to confirm the monodispersity of purified material and preliminary structure determination trials using cryo-EM will be carried out.

The oligomerisation characterisitics of NTS1 and many GPCRs are currently unknown. The major focus of the thesis will be the establishment of an *in vitro* system for the study of NTS1 oligomerisation state in lipid bilayers using fluorescence techniques, and achieving this goal is the focus of the following four chapters. Necessary prerequisites for such studies are firstly the overexpression and purification of NTS1 tagged with fluorescent proteins (Chapter 3) and the successful reconstitution of the fluorescent receptors into lipid vesicles in a conformation which is both fluorescent and able to bind ligand (Chapter 4). Chapter 5 will use the receptor samples produced using the protocols established in the preceding chapters to study receptor multimerisation using fluorescence resonance energy transfer (FRET) techniques and native gel electrophoresis. The labelling of the NT peptide with fluorescent dyes will be useful for the application of future single molecule fluorescence techniques. The aim of Chapter 6 is to synthesise and purify labelled NT and to investigate the effect of alternative labelling positions on the affinity of the ligand-receptor interaction using radioligand competition assays and fluorescence correlation spectroscopy (FCS).

Chapter 7 involves the use of surface plasmon resonance (SPR), a technique which to date has had only limited application to GPCRs, to study the interaction of purified, detergent-solubilised NTS1 with NT.

The overall conclusions of the thesis and likely directions for the future study of NTS1 are outlined in Chapter 8.

CHAPTER 2 - OPTIMISATION OF EXPRESSION AND PURIFICATION OF NTS1

SUMMARY

Overexpression and purification are typically limiting steps in the high resolution structure determination of GPCRs. NTS1 has previously been expressed in *E.coli* in a functional form capable of binding ligand. In this chapter, through the use of alternative *E.coli* strains (BL21(DE3), C41(DE3), C43(DE3)) an approximate 2.5-fold improvement in NTS1 expression level was obtained. Tightly bound lipids are often required for the maintenance of membrane protein functionality and they can be stripped from the protein by excess detergent and/or prolonged purification procedures. Through the inclusion of phospholipids in the NTS1 purification buffers to prevent delipidation, a 15 % improvement in active receptor yield was obtained relative to existing purification protocols. Preliminary EM (negative stain and cryo) confirmed a monodisperse receptor population. Purified NTS1 is now being produced at a sufficient level for high resolution structural studies, including 3D crystallisation and further electron microscopy studies.

2.1 - INTRODUCTION

2.1.1 - Expression and Purification of NTS1 to date

Neurotensin receptor 1 (NTS1) from rat is one of the few GPCRs which has been successfully overexpressed in a functional form capable of binding ligand at the *E.coli* plasma membrane. Functional expression was achieved by expressing the receptor as a fusion protein with N- and C-terminal fusion partners which aid targeting, membrane insertion, protein stability and purification. Several alternative fusion partners were tested for functional expression (Grisshammer *et al.*, 1993; Tucker and Grisshammer, 1996). A fusion protein, termed NTS1A (Figure 2.1), was found to yield the highest expression level of functional receptor. This consisted of T43NTS1 (NTS1 with the 43 N-terminal residues truncated) with the *E.coli* maltose binding protein (MBP), including its periplasmic targeting sequence, attached to the N-terminus, plus *E.coli* thioredoxin (TrxA) and a deca-His tag attached to the C-terminus. The N-terminally truncated form of the receptor was used since the N-terminal region, which contains 3 putative glycosylation sites, was found to be particularly sensitive to proteoyltic degradation

during preliminary expression and purification trials (Tucker and Grisshammer, 1996). The NTS1A construct was later modified to include tobacco etch virus (TeV) protease recognition sites between the MBP and T43NTS1 moieties and the T43NTS1 and TrxA moieties. This construct, termed NTS1B (Figure 2.1), allows the removal of the N- and C-terminal fusions after expression and purification, yielding the NTS1 receptor alone (White *et al.*, 2004; Grisshammer *et al.*, 2005).

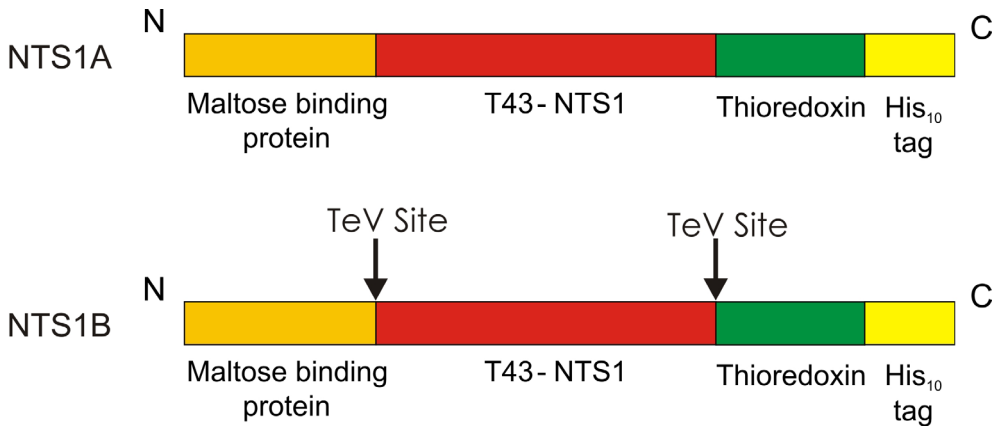

Figure 2.1 : Schematic depicting the fusion proteins used for the functional expression of NTS1 in *E.coli*. NTS1A consists of maltose-binding protein (MBP) from *E.coli*, an N-terminally truncated form of NTS1 (T43NTS1), thioredoxin A from *E.coli* (TrxA) and a deca-histidine tag (His_{10} tag). The NTS1B construct contains TeV protease cleavage sites between the MBP and T43NTS1 moieties and the T43NTS1 and TrxA moieties to facilitate proteolytic removal of the fusion partners after expression and purification.

In addition, correct folding of the receptor at the *E.coli* membrane (versus incorrect folding and targeting to inclusion bodies) was maximised by using a low copy number plasmid (pRG/III-hs-MBP (Tucker and Grisshammer, 1996)) with the weak *lac* promoter, as well as a long, low temperature induction period (20 °C, 40 h). This is thought to avoid overloading of the *E.coli* translocation machinery while allowing the sustained accumulation of functional receptor at the cell membrane (Grisshammer *et al.*, 2005). The protein has been successfully expressed in *E.coli* DH5α in culture volumes up to 200 l (White *et al.*, 2004). The receptor can be solubilised from whole cells using a combination of the detergents n-dodecyl-β-D-maltoside (DDM), 3-[(3-cholamidopropyl)dimethylammonio]-1-propanesulfonate (CHAPS) and cholesteryl

hemisuccinate (CHS) whilst maintaining a high affinity for NT (Tucker and Grisshammer, 1996). A two stage purification procedure, firstly exploiting the deca-His tag via immobilised metal affinity chromatography (IMAC), followed by a ligand affinity column, enabled the receptor to be isolated at high purity from the solubilised material (Grisshammer *et al.*, 1999; White *et al.*, 2004).

2.1.2 - Optimised expression strains

In many cases the overexpression of membrane proteins in *E.coli* produces poor levels of expression resulting from toxicity of the protein to the cell, hampered translation or incorrect protein targeting and folding (Miroux and Walker, 1996). Recently, two mutant *E.coli* strains, termed C41(DE3) and C43(DE3), have proved useful for the overexpression of several membrane and toxic proteins (Dumon-Seignovert *et al.*, 2004). These strains are adapted versions of the BL21(DE3) parental strain which were isolated from survivor colonies expressing membrane proteins that were ordinarily toxic to the BL21(DE3) strain (Miroux and Walker, 1996). Even when the toxicity of the plasmids is so high that it prevents transformation in the BL21(DE3) strain, the toxic proteins can often be expressed successfully in C41(DE3) and/or C43(DE3) (Dumon-Seignovert *et al.*, 2004).

The improved expression of membrane proteins may, at least in part, be due to the observed proliferation of intracellular membrane structures in C41(DE3) and C43(DE3) which contain the overexpressed protein (Arechaga *et al.*, 2000). Such structures are absent from the BL21(DE3) parental strain and this phenomenon could provide extra membrane area for the insertion of recombinant NTS1, resulting in improved expression level.

2.1.3 - Delipidation

Lipid-protein interactions may influence the folding, activity and stability of a membrane protein (Watts, 1989; Opekarova and Tanner, 2003; Findlay and Booth, 2006; Mandal *et al.*, 2006). Lipids are, in general, loosely associated with the protein, but some may be tightly associated, forming an integral part of the structure which is essential for functionality (Schagger *et al.*, 1990). Indeed, lipids have been observed in high resolution structures of membrane protein 3D crystals which were formed from the detergent-solubilised state, for example, the high resolution structure of the Ca^{2+} ATPase (Toyoshima *et al.*, 2000). During purification, membrane proteins are exposed to a vast excess of detergent and may become progressively delipidated. In some cases, this can lead to a loss of structure or functional activity. Supplementation of buffers with phospholipids can prevent such delipidation occurring and this can be a particularly important consideration during prolonged purification procedures. For example, purification of the Na^+, K^+-ATPase from *P.pastoris* in functional form required purification buffers to be supplemented with the lipids dioleoylphosphatidylcholine (DOPC) or dioleoylphosphatidylserine (DOPS) (Cohen *et al.*, 2005) and the exposure of purified Cytochrome b_6f complex to excess detergent caused deactivation which was attributed to delipidation (Breyton *et al.*, 1997).

2.1.4 - Aims

The primary aim of this chapter is to improve the expression of NTS1 in *E.coli* by optimising the expression strain used. To date, the *E.coli* DH5α strain has been used for NTS1 expression. The C41(DE3) and C43(DE3) strains, which have proved useful for the overexpression of other membrane proteins, are good potential expression hosts for optimised yields.

Secondly, in many cases membrane protein functionality can be lost through detergent-mediated delipidation, particularly during prolonged purification procedures. Addition of lipids to the NTS1 purification buffers will be tested in an attempt to improve yields of functional receptor.

The receptor will then be purified on a large scale using the optimised expression and purification procedure. The quality of the protein preparation will be tested using negative stain electron microscopy (EM) and the possibility of single particle cryo-EM structure determination investigated.

2.2 - MATERIALS AND METHODS

2.2.1 - Optimisation of *E.coli* expression strain

The NTS1A and NTS1B fusion constructs have been described previously (Grisshammer *et al.*, 1999; White *et al.*, 2004) (Figure 2.1). These constructs encode the rat NTS1 receptor (residues 1-43 truncated) with an N-terminal fusion of the *E.coli* maltose binding protein (MBP) (including periplasmic targeting sequence) and a C-terminal *E.coli* thioredoxin (TrxA) and deca-histidine tag (MBP-T43NTS1-TrxA-His_{10}). The NTS1B plasmid contains TeV protease sites to enable the proteolytic removal of the MBP and TrxA-His_{10} tags. The presence of the TeV cleavage sites does not influence expression levels (Grisshammer *et al.*, 2005).

NTS1A plasmid was transformed into *E.coli* DH5α, BL21(DE3), C41(DE3), or C43(DE3)pREP4 cells. For protein expression, 5 ml of an overnight culture was used to inoculate 450 ml of double strength TY media (Appendix B1) supplemented with 0.2 % (w/v) glucose, in a 2 l baffled flask and incubated at 37 °C with shaking at 140 rpm (Innova 4430 shaking incubator, New Brunswick Scientific). When an OD_{600} of 0.45 was attained, the cultures were cooled to 20 °C and, when the OD_{600} reached 0.6, protein production was induced with various concentrations of IPTG. Cells were harvested by centrifugation 42-44 h after induction, flash frozen in liquid N_2 and stored at -80 °C.

MBP-T43NTS1-TrxA-His_{10} was purified using a protocol based on that reported previously (Grisshammer *et al.*, 2005). All steps were carried out at 4 °C unless otherwise stated. Harvested cell pellet (1 g) was resuspended in 2x solubilisation buffer (100 mM Tris pH 7.4, 400 mM NaCl, 60 % glycerol (v/v), protease inhibitors (Leupeptin, Pepstatin A, Aprotinin, all 1 μg/ml). DDM, CHAPS and CHS were added to final concentrations of 1 %, 0.5 % and 0.1 % (w/v), respectively. The mixture was

diluted to a 1x concentration of solubilisation buffer with dH_2O and stirred for 1 h. Cells were further disrupted by pulsed ultrasonication (10 sec pulses, 20 sec pauses for 5 min), with samples cooled on ice to prevent localised heating effects. Insoluble material was pelleted by centifugation (4 °C, 75,000 g, 1 h) and the supernatant used for purification.

The supernatant was purified by IMAC (Ni-NTA Spin columns, Qiagen). All centrifugation steps were performed at 700 g, 4 °C. Samples were loaded by centrifugation, and the column washed with 600 µl of NiA (50 mM Tris/HCl pH7.4, 200 mM NaCl, 30 % glycerol (v/v), 0.5 % CHAPS (w/v), 0.1 % DDM (w/v), 0.1 % CHS (w/v), 50 mM Imidazole, protease inhibitors). Bound NTS1A protein was then eluted in 2 × 200 µl volumes of NiB (NiA plus 350 mM imidazole) and samples stored at -80 °C. Expression and purification were analysed by western blotting using anti-His antibody (GE Healthcare) and radioligand binding assay (Appendix A3).

2.2.2 - Phospholipid trials

NTS1B fusion protein was expressed in the *E.coli* BL21(DE3) expression strain and purified using the protocol previously described for the NTS1A construct (section 2.1.1), but with the following modifications. Cell pellet harvested from a single culture was divided into separate 1 g amounts to ensure consistency of starting material for each purification condition. Cell pellets were solubilised using either the detergents 1 % DDM / 0.1 % CHS or 1 % DDM / 0.5 % CHAPS / 0.1 % CHS (all (w/v)). For each detergent type, the solubilisation buffer was either supplemented with 0.1 mg/ml POPC (Avanti Polar Lipids) or left with no lipid supplementation as a control.

The detergent-solubilised fraction was filtered through a 0.2 µm filter (Whatman) and imidazole (BDH) was added to a final concentration of 50 mM, before loading onto a 1 ml HisTrap column (GE Healthcare) using an ÄKTA Basic purification system (GE

Healthcare). The column was washed with 30 column volumes (CV) of NiA buffer and the protein eluted in a step gradient with NiB buffer. The peak fractions were pooled and diluted five-fold in NT200 (50 mM Tris pH 7.4, 200 mM NaCl, 30 % glycerol (v/v), 0.1 % DDM (w/v), 0.5 % CHAPS (w/v), 0.1 % CHS (w/v), 1 mM EDTA). Purification buffers were supplemented with POPC (0.1 mg/ml) and/or had the detergent CHAPS omitted where appropriate for the entire process. Yields of active receptor were quantified by radioligand binding assay (Appendix A3).

2.2.3 - Large Scale Expression

Double strength TY medium (10 l) containing ampicillin (75 μg/ml) and glucose (0.2 % (w/v)) in a 14 l fermentation vessel (BioFlo 3000, New Brunswick Scientific) was inoculated with an overnight culture (100 ml) of NTS1B-transformed BL21(DE3) grown at 37 °C. Air supply was maintained at 1 vvm and the relative oxygen saturation maintained at 50 % or above by program-controlled agitation. Cells were grown at 37 °C up to an OD_{600} of 0.4. The temperature was then decreased to 20 °C and the culture induced with 0.25 mM IPTG when an OD_{600} of 0.6 was reached. Cells were harvested after 40 h by centrifugation (approximately 50 g wet weight), frozen in liquid nitrogen and stored at -80 °C.

All purification steps were carried out at 4 °C unless otherwise stated. Cell pellet (50 g wet weight) was resuspended in 100 ml of 2x solubilisation buffer. Lysozyme was added at a concentration of 1 mg/ml, followed by gentle agitation (30 min). DDM stock (10 % (w/v)) and CHAPS/CHS stock (5 % / 1 % (w/v)) were added dropwise whilst stirring on ice to a final concentration of 1 % (w/v) and 0.5 % / 0.1 % (w/v) respectively. Water was added to give a final volume of 200 ml followed by gentle stirring at 4 °C (1 h).

Insoluble material was pelleted by centrifugation at 70,000 g for 90 min, the supernatant decanted and supplemented with protease inhibitors and imidazole to a concentration of 50 mM.

The solubilised material was purified by IMAC using a 5 ml HisTrap HP column (GE Healthcare). After loading, the column was washed with 30 CV NiA (supplemented with 0.05 mg/ml POPC) and eluted using NiB (supplemented with 0.05 mg/ml POPC).

TeV-His_6 was expressed in *E.coli* BL21(DE3) and purified by nickel affinity and size exclusion chromatography (Appendix A5). Trial cleavage reactions with purified TeV-His_6 on IMAC-purified NTS1B were carried out to determine the effect of the amount of TeV-His_6 on cleavage efficiency. This was carried out individually for every batch of purified TeV (Appendix A6).

IMAC eluate was treated with TeV protease at a concentration of approximately 4 μg of TeV-His_6 per μg fusion protein (the exact concentration was dependent on the particular TeV preparation used) in a total volume of 100 ml cleavage buffer, at 4 °C overnight with gentle agitation. The cleavage mixture was concentrated to 2.5 ml using an Amicon stirred cell (Millipore, 100,000 MWCO) and loaded onto a Superdex 200 XK16/100 gel filtration column pre-equilibrated with GF buffer (50 mM Tris pH 7.4, 15 % glycerol (v/v), 500 mM NaCl, 0.1 % DDM (w/v), 0.01 % CHS (w/v), 0.05 mg/ml POPC, 1 mM EDTA, protease inhibitors). Proteins were separated at a flow rate of 0.25 ml/min and 1 ml fractions collected. A ^{3}H-NT (New England Nuclear) radioligand binding assay was used to quantify amounts of active receptor present throughout the purifications (Appendix A3). Protein identification by tryptic digestion followed by electrospray MS and MS/MS was carried out by Robin Antrobus (Biochemistry Dept., University of Oxford).

2.2.4 - Electron Microscopy

(i) Negative Stain EM

Transmission electron microscopy of negatively-stained samples was carried out by Dimitrios Fotiadis (M. E. Muller Institute for Microscopy, Biozentrum, University of Basel). T43NTS1 receptor sample was purified as described in section 2.2.3. Samples were prepared on carbon-coated copper grids (Agar Scientific) and were negatively stained using 2 % uranyl acetate. Images were recorded on Eastman Kodak Co. SO-163 sheet film with a Hitachi H-7000 electron microscope operated at 100 kV.

(ii) Cryo-EM sample preparation and microscopy

Cryo electron microscopy was carried out by Andreas Sonnen and Robert Gilbert (Division of Structural Biology (STRUBI), University of Oxford). 3 µl of purified, detergent-solubilised NTS1 (0.025 mg/ml) was applied to a negatively glow-discharged lacey carbon-coated EM grid (Agar Scientific) and plunge-frozen in liquid ethane after blotting. Several grids were prepared and all vitrified samples were imaged at liquid nitrogen temperatures with a Tecnai F30 operating at 300 kV and a magnification of 59000x. The objective lens astigmatism was corrected at 115 kx magnification. All images were recorded on Kodak S0163 electron image film (Kodak, Rochester, USA) at a one second exposure time and a defocus between 2 – 3.5 µm. All samples were stored at liquid nitrogen temperatures.

(iii) Cryo-EM data analysis

Micrographs were digitised on a Zeiss PhotoScan 2000 scanner (Carl Zeiss Jena GmbH, Jena, Germany) in 8-bit mode with a scan-step size of 7 µm, resulting in pixel size of 0.1186 nm/pixel at a magnification of 59000x. The micrographs were then imported into *boxer* (*EMAN* software package) for windowing particles. The selected 880

particles were then band-pass filtered in *IMAGIC-5*, centered and classified by multiple statistical analysis. Classums corresponding to different orientations of the particle were used to compute an initial model, which was subsequently filtered to a resolution of 30 Å (based on the 0.5 Fourier Shell correlation cut-off). This model was then used for a projection-based alignment of the unfiltered images and subsequent 3-D reconstruction in *SPIDER*.

2.3 - RESULTS AND DISCUSSION

2.3.1 - Optimisation of *E.coli* Expression Strain

In many cases the overexpression of membrane proteins in *E.coli* results in poor levels of expression arising from toxicity of the protein to the cell, hampered translation or incorrect protein targeting and folding (Miroux and Walker, 1996). Rat NTS1 has previously been expressed as a protein fusion with MBP and TrxA in the *E.coli* DH5α strain (Grisshammer *et al.*, 1993; Tucker and Grisshammer, 1996; Williamson *et al.*, 2002; White *et al.*, 2004). Expression trials of the NTS1A construct were carried out in an attempt to improve the levels of overexpression. Expression of receptor in *E.coli* DH5α was compared with BL21(DE3), as well as C41(DE3) and C43(DE3)pREP4 (the pREP4 plasmid carries the *lac* repressor gene which is also supplied in *cis* from the expression vector), two mutant strains derived from BL21(DE3) which have proved useful for the overexpression of several membrane and toxic proteins (Miroux and Walker, 1996).

The expression of NTS1A was examined in all cell lines under three different IPTG concentrations and in the absence of IPTG. The cells were harvested after 42 h of induction and NTS1A was purified from the solubilised material using IMAC. The expression levels were compared by western blot analysis (Figure 2.2). Additionally, since the overexpression of membrane proteins in *E.coli* often leads to incorrect folding, the amount of functional protein was determined by radioligand binding assay using [^{3}H]-NT (Table 2.1). In general, the relative levels of functionally active receptor mirrored the relative amounts seen in western blot analysis.

Table 2.1: Optimisation of *E.coli* expression of functional NTS1A. Cell pellets were isolated from 450 ml cultures, solubilised using the detergents CHAPS/CHS/DDM and purified by IMAC. A radioligand binding assay was used to determine expression level of functional receptor, with all measurements carried out in triplicate.

Expression Strain	IPTG concentration used for induction (mM)	Expression of functional receptor (µg/l culture)
C43(DE3)pREP4	0	21.3 ± 2.3
	0.1	27.7 ± 0.8
	0.25	33.6 ± 3.4
	0.5	40.0 ± 5.0
C41(DE3)	0	1.2 ± 1.2
	0.1	29.0 ± 2.3
	0.25	73.0 ± 3.9
	0.5	40.7 ± 3.0
BL21(DE3)	0	31.1 ± 1.2
	0.1	48.0 ± 3.3
	0.25	86.3 ± 8.8
	0.5	60.4 ± 2.3
DH5α	0	17.8 ± 1.6
	0.1	28.9 ± 4.1
	0.25	12.8 ± 2.6
	0.5	9.6 ± 0.8

With the exception of C41(DE3), all cells lines showed leaky expression in the absence of IPTG, despite the presence of the *lac* repressor in *cis*. This observation is important when considering the choice of strain in NMR isotopic labelling experiments. For example, media-swap labelling techniques (Marley *et al.*, 2001), in which cells are grown to a high density before induction of expression in the final labelling media, require the tight regulation of expression in order to avoid expression of unlabelled protein during the growth phase.

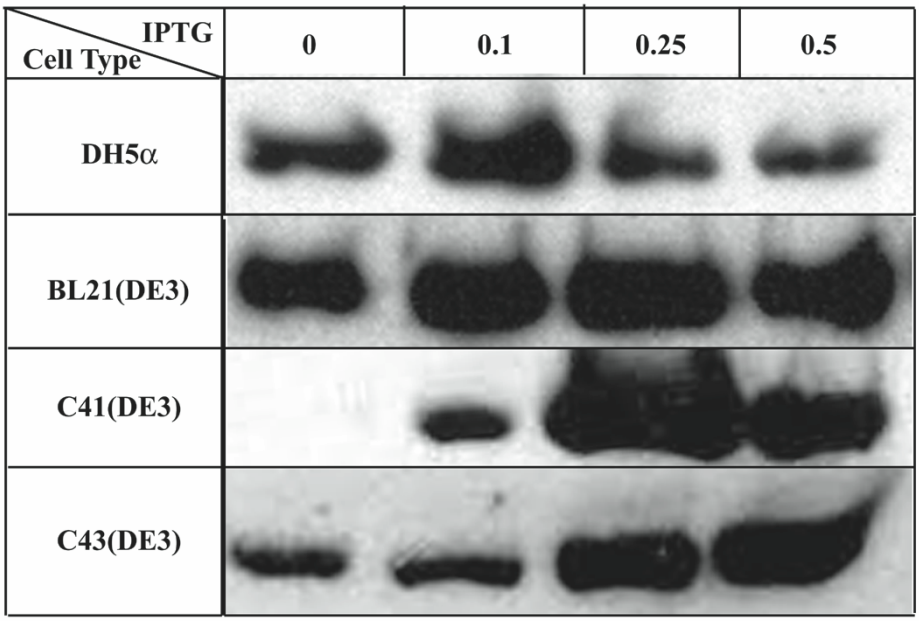

Figure 2.2 - Comparison of NTS1A expression in different *E.coli* expression strains and at different concentrations of IPTG for induction. In each case, 1 g of cell pellet was detergent-solubilised and partially purified using IMAC. Equal volumes of each sample were separated by SDS-PAGE and analysed by western blot (anti-His tag). Note that comparison of band intensity across the different strains cannot be made since they were separated and immunoblotted on separate gels.

The highest levels of NTS1A expression were seen in BL21(DE3) cells induced with 0.25 mM IPTG, closely followed by C41(DE3) using the same induction conditions (86.3 ± 8.8 and 73.0 ± 3.9 μg/l respectively); the maximum yield from DH5α cells (induced with 0.1 mM IPTG) was only 28.9 ± 4.1 μg/l. The yield of active receptor can therefore be increased approximately 2.5-fold by using the BL21(DE3) and C41(DE3) expression strains instead of DH5α. The C43(DE3)/pREP4 strain also performed better at higher levels of IPTG induction compared to DH5α cells. Expression in these cells was also tested using 1 mM IPTG for induction, but this did not yield higher levels of protein. In addition, all strains except for C43(DE3) showed decreased expression of functional receptor at higher IPTG concentrations (greater than 0.25 mM for BL21(DE3) and C41(DE3) and greater than 0.1 mM for DH5α). This could be due to a toxicity effect of NTS1A expression, or due to increased receptor misfolding or incorrect membrane insertion at higher rates of expression.

2.3.2 - The effect of phospholipids on the purification of NTS1

As discussed previously (section 2.1.3), while many lipids are loosely associated with proteins, some are integral to protein structure and function. Detergents may potentially remove such lipids from purified membrane proteins, especially during long purification procedures, leading to loss of membrane protein function. Thus, supplementing the purification media with phospholipids may help to stabilise proteins and retain their active conformation.

When NTS1B was extracted and purified using buffers containing the detergents DDM, CHS and CHAPS, the inclusion of the phospholipid POPC in the purification buffers gave a slightly improved yield of active protein compared with no lipid supplementation (Table 2.2). However, when CHAPS was omitted and only DDM/CHS was used for solubilisation, extraction and purification, no enhancement in the yield of ligand-binding NTS1 obtained was observed upon lipid supplementation. This result could be due to reduced delipidation of the receptor in the presence of lower levels of total detergent, or to the specific absence of CHAPS. Delipidation of this receptor may therefore lead to loss of protein activity, and it would be prudent to include phospholipids throughout the purification, particularly during the large volume gel filtration steps.

The result also highlights the importance of the inclusion of CHAPS in the early stages of the purification. Assay of the purification fractions after solubilisation (prior to IMAC) showed that the absence of CHAPS resulted in a 49 ± 4 % decrease in the yield of functional receptor. It therefore appears that CHAPS is particularly important during the initial extraction of NTS1A from the *E.coli* membrane. This is likely due to the relatively high solubilising capacity of CHAPS, a zwitterionic detergent, relative to DDM, a non-ionic detergent.

Table 2.2 – The effect of supplementation of purification buffers with phospholipids on the yield of active receptor obtained. Cell pellet was solubilised using the stated detergents and purified by IMAC using buffers with and without POPC supplementation (0.1 mg/ml). Active receptor was quantified by radioligand binding assay.

Detergent mix	Phospholipid supplementation	Yield (μg/l cell pellet)
DDM / CHS / CHAPS	No lipid	95.1 ± 3.8
	POPC	109.6 ± 9.5
DDM / CHS	No lipid	60.5 ± 6.3
	POPC	58.6 ± 3.8

2.3.3 - Large Scale Purification of NTS1

NTS1 fusion proteins have previously been purified via a two stage purification procedure, firstly exploiting the deca-His tag via immobilised metal affinity chromatography (IMAC), followed by ligand affinity chromatography (biotinylated NT immobilised to a tetrameric avidin resin) (White *et al.*, 2004). It became apparent that the yield of active purified receptor obtained using this protocol was low. In particular, during the ligand affinity column step, approximately 95 % of ligand-binding receptor was routinely lost. Table 2.3 shows details of an example purification using this protocol.

Table 2.3 – Purification of NTS1A fusion protein. The ligand affinity column step resulted in a loss of approximately 95 % of active receptor. [a] Amount of receptor was determined by radioligand binding assay.

Purification step	Total Receptor (pmol)[a]	Yield (%)
Solubilisation	4604 ± 310	100 ± 7
IMAC Eluate	4204 ± 257	91 ± 6
BioNT Eluate	183 ± 28	4.0 ± 0.6

Given the large loss of receptor during the ligand affinity purification step, this was omitted from the protocol. Subsequent purifications consisted of the nickel affinity

chromatography followed by gel filtration chromatography. In order to obtain T43NTS1 with the MBP and TrxA-His10 fusions removed, a proteolytic cleavage reaction was incorporated between the IMAC and the gel filtration purification steps. This was made possible by the presence of two TeV protease cleavage recognition sites in the NTS1B construct, the first situated between MBP and T43NTS1 and the second between T43NTS1 and the TrxA (Figure 2.1). The improved expression strain BL21(DE3) was also used and purification buffers were supplemented with POPC throughout. Figure 2.3 shows the elution profile of a representative NTS1 purification.

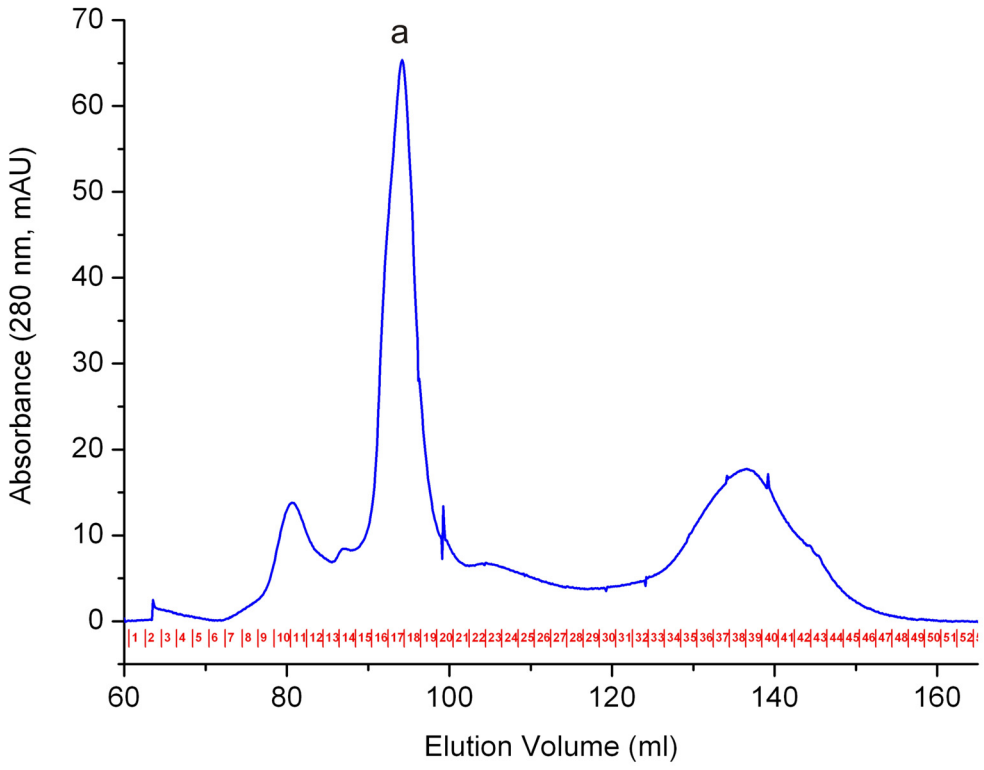

Figure 2.3 – Gel filtration elution profile for purification of TeV-cleaved NTS1B fusion protein. Nickel affinity chromatography eluate was cleaved with TeV protease to remove the MBP and TrxA-His10 fusions and the T43NTS1 cleavage product purified by gel filtration chromatography. The absorbance at 280 nm (blue) and the fraction number (red) are shown.

SDS-PAGE analysis of the major elution peak (labelled 'a', retention volume = 94 ml) showed a protein band at an apparent molecular weight (Mw) of 40 kDa. This apparent molecular weight on the SDS-PAGE is less than the theoretical Mw of NTS1 (43 kDa).

However, it is not unusual for membrane proteins to run faster on SDS-PAGE than expected. The band was excised and analysed by LC MSMS which confirmed that it was the desired T43NTS1 product. The gel filtration fractions containing T43NTS1 (14 - 20) were combined and concentrated. Analysis by SDS-PAGE showed the concentrated sample to be homogenous, with a single protein band corresponding to T43NTS1 (Figure 2.4).

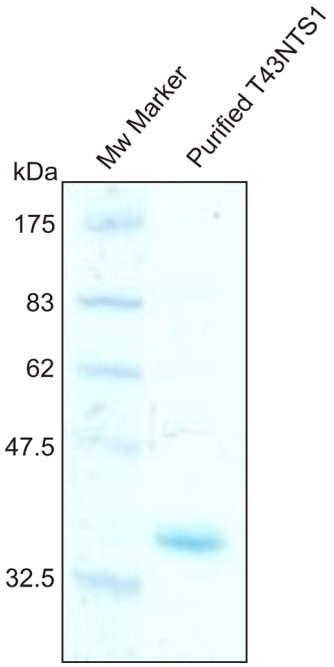

Figure 2.4 – Coomassie-stained SDS-PAGE of purified, TeV-cleaved NTS1 (T43NTS1). NTS1B was expressed in the *E.coli* BL21(DE3) strain, purified by nickel affinity chromatography, proteolytically cleaved and then further purified by gel filtration. The gel shows the T43NTS1 band (apparent Mw = 40 kDa) with no major contaminating bands.

The radioligand binding assay was used to analyse the yield of active receptor during the purification. Table 2.4 shows the yields of receptor obtained from a representative 50 g scale purification. 2.2 ± 0.3 nmol of purified, active T43NTS1 was obtained. Total protein assay measurements of the purified protein revealed a specific activity of 6.3 ± 0.6 nmol/mg for the purified receptor. This suggested that 27.1 ± 2.6 % of the purified receptor is able to bind ligand, if it is assumed that each receptor molecule has one ligand binding site. Whether this is caused by 65 – 70 % of the receptor being in an inactive form which is unable to bind ligand, or because the radioligand binding assay

underestimates the amount of functional receptor present is unclear, but this level of active protein was also observed for the fluorescent NTS1 constructs (Chapter 3).

Table 2.4 : Purification and proteolytic cleavage of NTS1B expressed in *E.coli* BL21(DE3) (50 g wet pellet weight). Progress of purification was monitored by radioligand binding assay. The percentage yield refers to the yield of active receptor relative to the detergent-solubilised fraction.

Sample	Active Receptor (nmol)	Yield (%)
Solubilised Material	12.1 ± 1.0	100 ± 5.9
Nickel Column elution	13.7 ± 0.7	113 ± 8.8
Post-TeV cleavage	8.4 ± 0.6	69.1 ± 6.0
Gel Filtration load	8.4 ± 1.2	69.1 ± 10.2
Gel Filtration eluate	2.2 ± 0.3	18.1 ± 2.3

2.3.4 - Electron Microscopy

Purified, detergent-solubilised samples of TeV-cleaved NTS1 (Figure 2.4) were initially analysed by negative stain electron microscopy (EM) in order to give further indication of the quality of the receptor preparations (Figure 2.5). The micrographs show individual particles, with no obvious sign of aggregation. The individual particles vary in diameter from 7.0 – 12.4 nm, with a mean diameter of 8.4 ± 0.2 nm (n = 50), with three main populations of particles distinguished according to size (Figure 2.5, inset). The size variation could be caused by differing profiles of the receptor particle, which is free to adopt any orientation in detergent solution. The monodisperse particle population suggests that the receptor preparations are of sufficient quality to commence cryo-electron microscopy (cryo-EM) and 3D crystallisation studies.

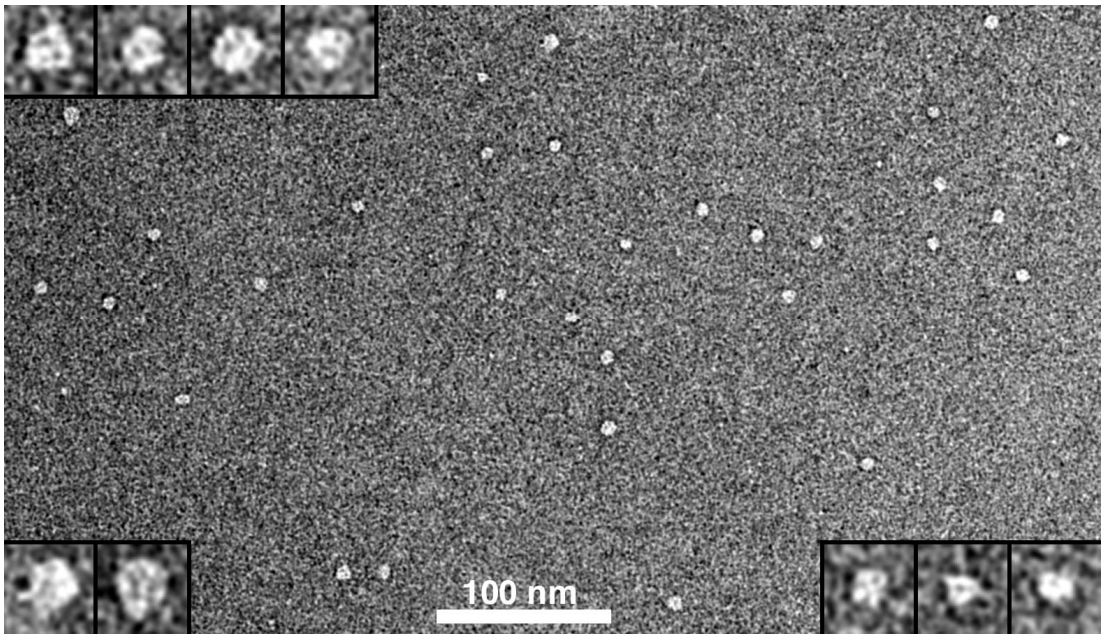

Figure 2.5 – Negative stain electron microscopy of purified, detergent-solubilised T43NTS1. The white scale bar represents a distance of 100 nm. Samples were prepared on carbon-coated copper grids and stained with 2 % uranyl acetate. Individual particles can be seen with no sign of aggregation, indicating a highly homogenous sample. There are at least 3 populations of particles, small (diameter approx. 7.6 nm, gallery bottom right), medium (diameter approx. 9.8 nm, gallery top left) and large (diameter approx. 12.0 nm, gallery bottom left). Electron microscopy was carried out by Dimitrios Fotiadis (Basel).

T43NTS1 samples were subsequently analysed using cryo-EM. In this technique, samples are cryogenically frozen in order to preserve and protect them in the electron beam. Sample preparation involves rapid freezing, usually using liquid ethane, in order to ensure vitreous water (rather than crystalline) ice formation. Cryo-EM is more amenable to high resolution structure determination than negative stain EM. Unlike negative stain EM, no staining is used to provide sample contrast. Therefore, samples can be viewed in their hydrated state and sample distortion during staining is avoided. Instead of staining, phase contrast is introduced to the images by defocusing the electron beam below the focal plane. The effect of this defocus on the images is described by a Contrast Transfer Function (CTF), an oscillating function in reciprocal space that varies between phases of +180 degrees and -180 degrees and therefore between 100 % positive and 100 % negative contrast in the real space images for different resolution zones.

Figure 2.6 shows preliminary cryo-EM results obtained from the purified T43NTS1 sample. Grouping of particle images into classes, followed by averaging and 3D reconstruction, resulted in a preliminary image of a T43NTS1 sample.

(a)

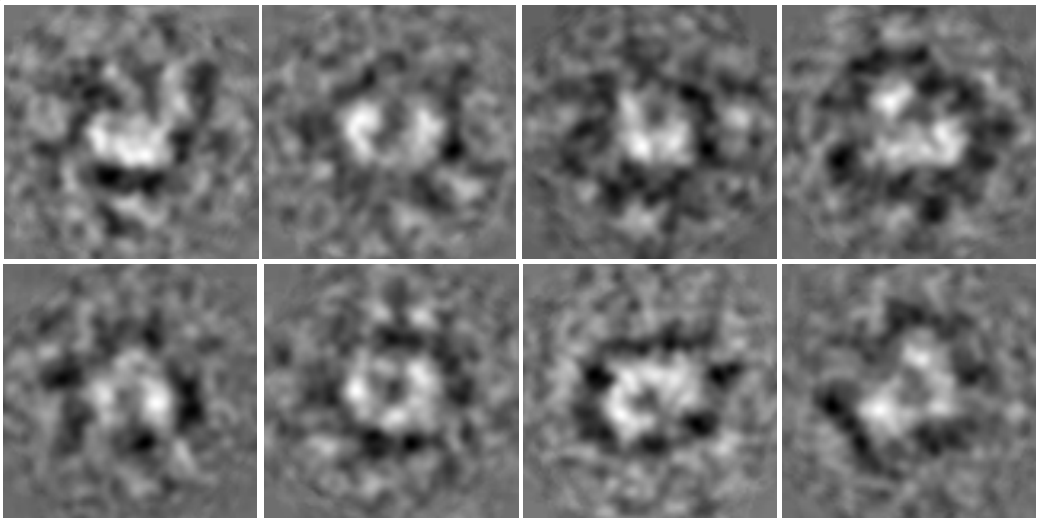

(b)

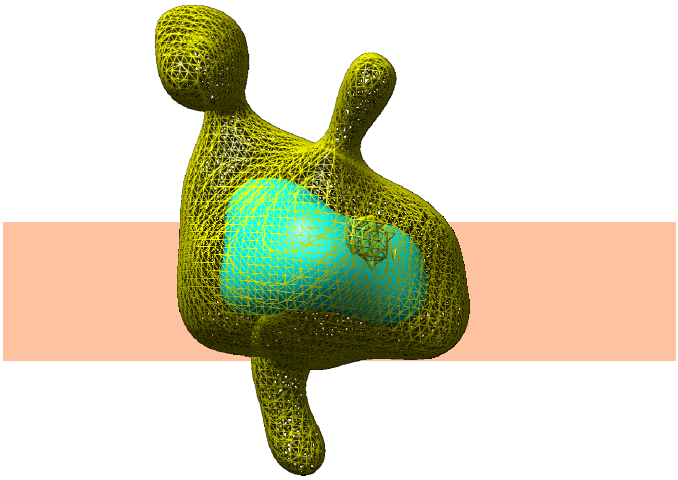

Figure 2.6 – Preliminary cryo-electron microscopy of purified, detergent-solubilised T43NTS1. (a) 8 class averages of similar views of doubly-aligned NTS1. Individual particles can be identified of a shape one would expect for a GPCR. (b) A view of an initial 3D reconstruction (25 Å resolution) at two contour levels (cyan and yellow). The putative membrane position is marked. The approximate dimensions of the reconstruction are 70 x 70 x 40 Å. The reconstruction was obtained from an average of 880 images and further images are currently being processed.

The dimensions of the reconstruction (70 x 70 x 40 Å) are similar to those previously reported for putative rhodopsin dimers which were observed using negative stain electron microscopy and atomic force microscopy (AFM) (72 ± 9 x 65 ± 8 Å) (Fotiadis *et al.*, 2006). This suggests that the NTS1 receptor could be in dimeric form. The scale of the reconstruction is also in agreement with the size of the rhodopsin monomer, as determined by x-ray crystallography (approx. 70 x 45 x 30 Å) (Palczewski *et al.*, 2000). Three protrusions from the membrane domain can be discerned, which are likely the C-termini, N-termini and/or extra-membranous loops. However, this orientation is yet to be demonstrated and cryo-EM imaging of purified, tagged receptor may enable the N- and C-termini to be assigned. This 3D reconstruction, which was obtained from only 880 images, shows real potential for further structure determination using this technique using a larger dataset and improved CTF correction.

2.4 - CONCLUSION

Structural biology studies generally require milligram amounts of purified protein for study. In addition, labelling of proteins for NMR studies requires expensive media containing NMR-visible isotopes and therefore optimal yields of protein per volume of culture is a priority. Given the problems associated with the overexpression of membrane proteins, in particular GPCRs, in an active, ligand-binding form (Sarramegna *et al.*, 2006), any optimisation of expression levels is clearly advantageous. Analysis of the levels of expression of NTS1A in alternative *E.coli* expression strains revealed a significant improvement in expression level. A 2.5-fold improvement in yield was obtained when NTS1A was expressed in the BL21(DE3) or C41(DE3) strains rather than the DH5α strain used previously (Grisshammer *et al.*, 1993; Tucker and Grisshammer, 1996; Williamson *et al.*, 2002; White *et al.*, 2004)

The reason for the improved expression levels is unclear. The NTS1 construct directs protein expression using the *lac* promoter system, therefore the increased expression observed here is not a consequence of the T7 RNA polymerase expressed in the BL21(DE3) strain and its derivatives. The increased expression may therefore be a consequence of the other expression adaptations of BL21 strains, such as deficiency in the OmpT and Lon proteases. The BL21 strains also carry a lower copy number of the plasmid, which may favour lower rates of transcription thus aiding insertion into the membrane rather than expression into inclusion bodies. Both of these factors may contribute to the higher levels of NTS1A expressed in these cell types and its derivatives. In addition, overexpression of membrane proteins in the C41(DE3) strain has been shown to be accompanied by the proliferation of intracellular membrane structures which contain the overexpressed protein (Arechaga *et al.*, 2000). This phenomenon could provide extra membrane area for the insertion of recombinant

NTS1, resulting in improved expression level. However, this hypothesis cannot be used to explain the high level of expression in the BL21(DE3) strain, which does not form such intracellular structures.

An increase in the yield of active receptor was achieved by including phospholipids during the purification process; supplementation with 0.1 mg/ml POPC gave a 15 % increase in the amount of active protein following Ni-affinity purification when compared to the omission of lipids. The enhanced effects of added lipids was not evident when CHAPS was omitted from the purification buffers, suggesting that this detergent has a particularly strong propensity to delipidate NTS1 relative to DDM / CHS alone. Receptor inactivation due to delipidation will likely worsen during the extended purification procedures involving the prolonged proteolytic cleavage and gel filtration steps. Therefore, inclusion of phospholipids in the purification would be prudent to maintain receptor stability and obtained optimal yields of purified receptor.

Large scale purification of TeV-cleaved NTS1B (T43NTS1) in an active, ligand-binding conformation was demonstrated. Negative stain EM studies revealed a monodisperse receptor population in which individual particles could be discerned with no signs of aggregation. Preliminary cryo-EM studies of the T43NTS1 receptor sample look to be highly promising. A 3D reconstruction of only 880 images revealed a single particle of comparable size to putative rhodopsin dimers reported previously (Fotiadis *et al.*, 2006). Continuation of this work has the potential to yield relatively high resolution structural details of the receptor.

Given the optimisations described, NTS1 can now be routinely expressed and purified in an active ligand binding form in sufficient quantities for high resolution structural approaches. The high purity and monodispersity of the NTS1 samples is ideal for 3D crystallisation to be attempted, and preliminary trials are underway.

CHAPTER 3 - TAGGING OF NTS1 WITH THE FLUORESCENT PROTEINS eCFP AND eYFP

SUMMARY

The expression and purification of fluorescently tagged NTS1A is a necessary prerequisite for the development of an *in vitro* system for the study of NTS1 multimerisation. Therefore, the existing construct for the expression of NTS1 in *E.coli*, termed NTS1B, was modified to contain a fusion to the genes encoding either the eCFP or eYFP fluorescent proteins. These constructs were used for the *E.coli* expression of NTS1 tagged with either of the fluorescent proteins at the C-terminus. Several *E.coli* strains (DH5α, BL21(DE3), C41(DE3) and C43(DE3)) were tested for functional expression with optimal expression observed in the C41(DE3) strain (at levels of up to 0.29 ± 0.03 mg per litre of culture). Successful purification and proteolytic removal of the MBP and TrxA-His10 fusion partners was achieved while retaining both fluorescence and ligand binding capability (K_d = 0.91 ± 0.17 nM). Analysis of the purified material using negative stain electron microscopy suggested a monodisperse receptor population with no sign of aggregation. In addition, the fluorescently tagged receptor was exploited to assay the binding of receptor to 2D DNA lattices. Imaging of NTS1 bound to DNA lattice has shown potential for high resolution structure determination.

3.1 - INTRODUCTION

3.1.1 - Tagging of GPCRs with Fluorescent Proteins

Green fluorescent protein (GFP) (see section 5.1.2 for more details) from the jellyfish *Aequorea victoria* (Tsien, 1998) has had widespread use as a genetically-encoded tag, where GFP is fused in-frame to a protein of interest and the resulting chimeric protein expressed for the examination of protein localisation, dynamics and interactions. In the case of GPCRs, GFP and its variants have been most widely used as an *in vivo* tag for the study of receptor multimerisation state. In particular, the cyan fluorescent protein (CFP) (donor) and yellow fluorescent protein (YFP) (acceptor) FRET pair has been most commonly used (see section 5.1.2), largely due to the favourable spectral and dimerisation characteristics of these proteins (Pollok and Heim, 1999).

Fluorescent proteins (FPs) have been almost exclusively fused to the end of the GPCR C-terminal domain (Overton and Blumer, 2000; Dinger *et al.*, 2003). C-terminal fusion

is less likely to interfere with the region of the receptor involved with ligand binding which, in the case of NTS1, is a region comprising the third extracellular loop and the extracellular ends of TM4, 6 and 7 (section 1.5.1). In addition, most GFP variants do not fold correctly, and are therefore not fluorescent, when fused to a membrane protein on the periplasmic face of the *E.coli* inner membrane (Feilmeier *et al.*, 2000; Thomas *et al.*, 2001). Consequently, fusion to a region of the receptor which is on the cytoplasmic side of the *E.coli* membrane is essential.

FPs have recently been used as tags to monitor overexpression, initially for soluble proteins (Waldo *et al.*, 1999), but more recently for membrane proteins. In particular, GFP was fused to the C-terminus of the μ-opioid GPCR to monitor receptor overexpression in the yeast *P. pastoris* (Sarramegna *et al.*, 2002). However, comparison of fluorescence and ligand binding measurements on whole cells revealed a 100-fold greater number of fluorescent molecules than binding sites. The reason for this result was unclear but could be due to a large amount of receptor being expressed in an inactive form, proteolytic cleavage of the fluorescent tag or binding site occlusion. In a second study, a GFP tag was used to monitor the efficiency of detergent-solubilisation of the μ-opioid receptor, although in this case, the receptor was unable to bind ligand (Sarramegna *et al.*, 2005). The use of the FP to monitor overexpression is particularly useful since GFP fusions which are targeted to inclusion bodies are not fluorescent, therefore enabling the amount of protein expressed in a correctly-folded form to be optimised (Waldo *et al.*, 1999).

3.1.2 - In-gel fluorescence

The high resolution structure of GFP (and its variants) revealed an extremely stable β-barrel fold, with the fluorophore in a well shielded position, attached to a central helix in the centre of the barrel (section 5.1.2). Consequently, the fluorescent properties are

resistant to many reagents which would typically denature globular proteins, including the detergent SDS. This feature has been exploited in the technique of in-gel fluorescence (Drew *et al.*, 2001; Drew *et al.*, 2006). Provided gel samples are not heated, the fluorescence of GFP is maintained during standard SDS-PAGE. This allows the fluorescent bands on the gel to be visualised with high sensitivity using a simple UV source and CCD camera setup, with a reported detection limit of ~5 ng GFP per protein band (Drew *et al.*, 2006). After visualisation of fluorescence, the gel can be subsequently stained with Coomassie if desired.

The technique allows the measurement, with high sensitivity, of the amount of fluorescent protein present, provided fluorescent protein standards are included on the same gel. In addition, it verifies the presence of the desired full length fluorescent fusion and problems of proteolytic degradation during either expression or purification are, therefore, immediately evident. This, and the fact that a spectrofluorimeter is not required, is a distinct advantage over fluorescence measurements in solution.

3.1.3 - DNA-Nanotechnological Approaches to Crystallisation and Biological Structure determination.

DNA self-assembly has been successfully exploited in the formation of two dimensional arrays which have a nanometre-scale repeating unit (Winfree *et al.*, 1998; Seeman, 1999). In a common approach, four oligonucleotides are designed to self-associate via complementary sequences of base pairs to form structures analogous to the naturally occurring Holliday Junction. Each arm of the Holliday Junction has a 'sticky end' which consists of six unpaired bases that are complementary to one other (Figure 3.1). Hybridisation of complementary sticky ends joins the arms of the junctions together to form an extended periodic array or pseudo-crystal. Figure 3.1 illustrates this process and details two examples of DNA lattices.

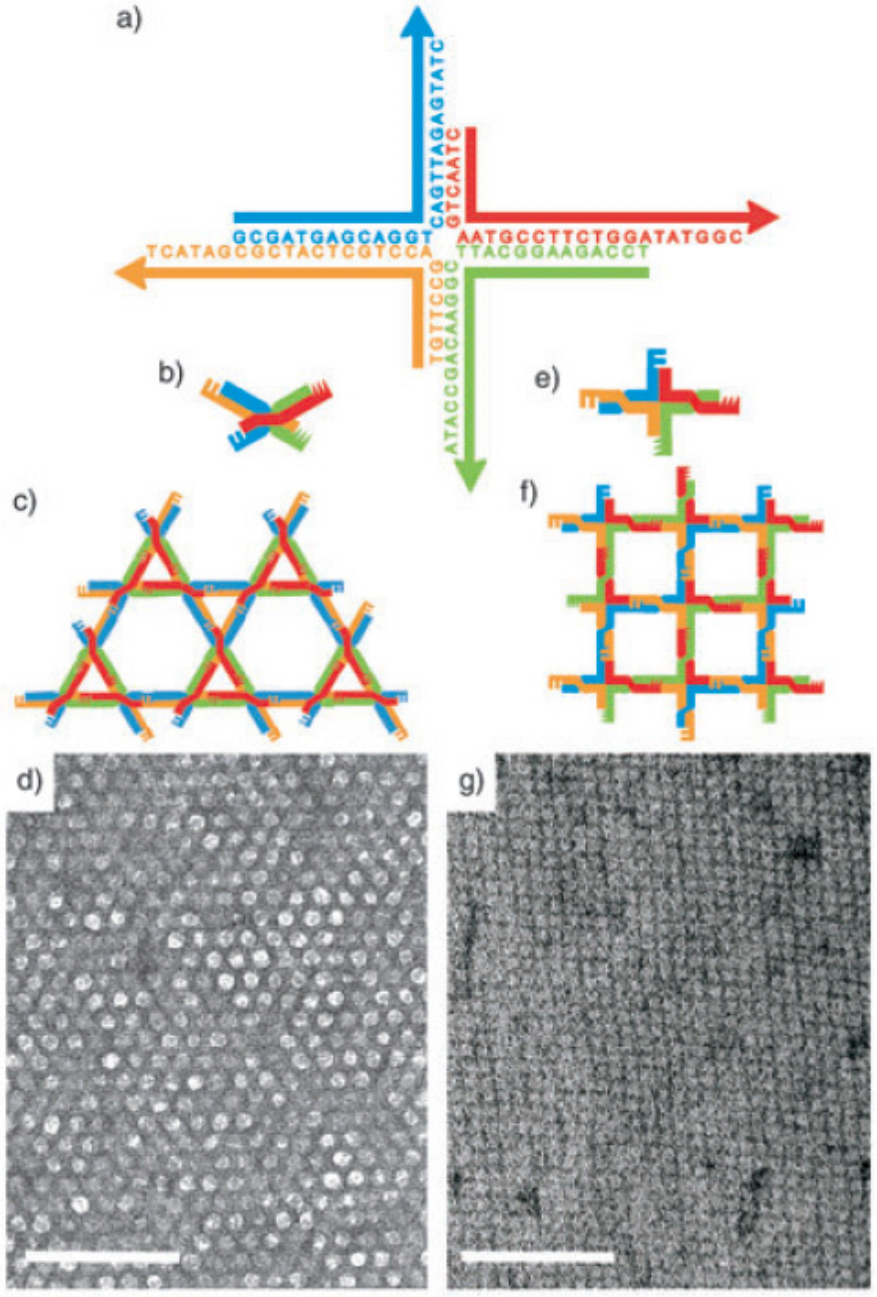

Figure 3.1 – Self-assembly of DNA oligonucleotides to form 2D arrays (taken from (Malo *et al.*, 2005)) a) The common structural unit—four oligonucleotides hybridize to form a Holliday junction (HJ) with two pairs of complementary "sticky ends". b) c-stacked junction showing the positions of complementary sticky ends. c) Kagome lattice formed by assembly of c-stacked junctions (for clarity, half a helical turn is shown between junctions that are, in fact, separated by 2.5 turns). d) TEM (transmission electron microscopy) image of the Kagome lattice (DNA is positively stained (dark); scale bar: 100 nm). e) Square-planar junction. f) Square lattice formed from HJs held in a square-planar configuration by protein RuvA. g) TEM image of the RuvA lattice (negatively stained: protein is lighter than background; scale bar: 100 nm).

The structure of the DNA-binding protein, RuvA, bound to a 2D DNA lattice has been determined to a resolution of 25 Å using cryo-electron microscopy (EM) (Malo *et al.*, 2005). This technique could potentially be applied to proteins which do not directly bind to the DNA of the pseudo-crystal, provided a suitable affinity group, which binds to the protein of interest, could be covalently attached to the DNA oligonucleotides. Such a group could either have a relatively broad specificity, for example Ni-NTA, to allow interaction with poly-histidine-tagged proteins or be highly specific, such as a protein ligand. The technique could therefore be of particular application to proteins for which classical crystallisation methods for high resolution structure determination are problematic. Membrane proteins, and GPCRs in particular, fall into this category.

Application of this technique to the structure determination of NTS1 has yielded some preliminary results. Negative stain EM of NT-functionalised DNA arrays pre-incubated with purified NTS1A revealed some electron density which was postulated to be bound NTS1A (Meier and Turberfield, 2003). In addition, negative stain EM of purified NTS1B bound to Ni-NTA-functionalised DNA lattices via the C-terminal His_{10} tag has yielded some promising preliminary results (Malo, J., unpublished data). Areas of electron density could be observed which coincided with the position of NTA-functionalisation and were absent from identical arrays which had not been incubated with NTS1B receptor (Figure 3.2).

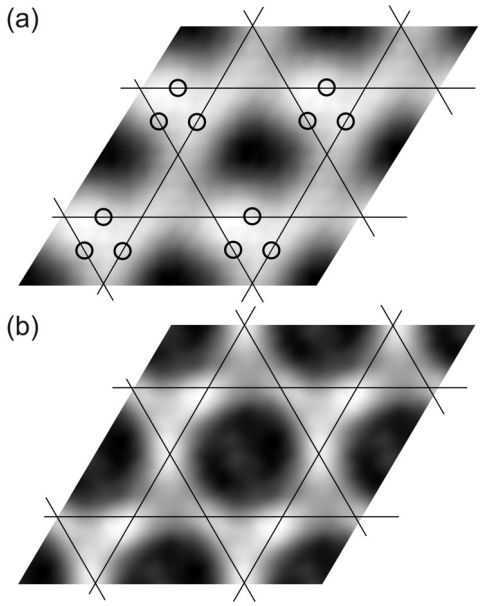

Figure 3.2 – Negative stain electron microscopy image of NTS1B bound to Ni-NTA-functionalised DNA arrays (Malo, J., unpublished data). (a) DNA arrays which were pre-incubated with NTS1B prior to staining. (b) Control DNA arrays which were not incubated with NTS1B. Extra areas of electron density can be observed (circled) which are absent from the control and are postulated to arise from bound NTS1B.

However, verification that the NTS1 protein was actually bound to the DNA array was difficult in both cases. The only method available for confirmation of binding was to carry out EM on the sample, perform preliminary image processing and identify areas of electron density arising from protein in the areas expected. In addition to being extremely time consuming, this made the screening for optimal receptor-array binding conditions impractical and did not unambiguously demonstrate that observed electron density was due to the NTS1 protein itself.

3.1.4 - Aims

The aim is to modify the existing NTS1 *E.coli* expression construct to contain the fluorescent proteins eCFP and eYFP fused to the C-terminus of the receptor. The fluorescent receptors will then be expressed and purified in an active conformation.

Also, in-gel fluorescence, which has yet to be applied to GPCR systems, will be exploited to monitor the fluorescence-tagged receptor during the purification. In combination with radioligand binding data, this technique has the potential to monitor the proportion of the total receptor present which is able to bind ligand and, therefore, gives a measure of the amount of receptor which is in native conformation.

The binding of NTS1 to two-dimensional DNA lattices to form two dimensional arrays has the potential to yield high resolution structural information. Given the lack of a simple method to verify NTS1 binding to DNA lattices in preliminary studies to date, the fluorescent tag will be exploited in the development of an assay for NTS1-lattice binding.

3.2 - MATERIALS AND METHODS

3.2.1 - Cloning of Fluorescent Constructs

The existing NTS1B construct (MBP-TeV-T43NTS1-TeV-TrxA-His10) (White *et al.*, 2004) was altered to contain a gene encoding a fluorescent protein, either eCFP or eYFP, between the T43NTS1 and the C-terminal TeV protease recognition site. In the NTS1B construct, the first four residues of the C-terminal TeV site (ETLY) were integrated into the C-terminus of the T43NTS1 protein. In addition, the C-terminal sequence of T43NTS1 has been identified as a cryptic TeV protease recognition site (White *et al.*, 2004). Therefore, an overlap extension PCR strategy was employed to allow both the inactivation of the cryptic TeV site and the introduction of the fluorescent protein followed by a new TeV site. This yielded two new constructs, NTS1C (MBP-TeV-T43NTS1-eCFP-TeV-TrxA-His_{10}) and NTS1Y (MBP-TeV-T43NTS1-eYFP-TeV-TrxA-His_{10}) (Figure 3.5).

The following primers were used in the cloning procedure (summarised in Figure 3.3):

1. 5'-GCCCTGAAAGACGCGCAG-3'
2. 5'-CTCGCCCTTGCTCACTGCGGCCGCGAACAGGGTC-3'
3. 5'-CTGTTCGCGGCCGCAGTGAGCAAGGGCGAG-3'
4. 5'-CGTACTCCGGACCTTGTACAGCTCGTCCATG-3'
5. 5'-CGGCCGCGAACAGGGTCTCC-3'
6. 5'-CGTACTCCGGACCTTGTACAG-3'

(The *BspEI* restriction sites are highlighted in green, the sequence corresponding to the 5' sequence of the *ecfp* / *eyfp* genes is highlighted in red, and the sequence corresponding to the 3' region of *T43NTS1* is highlighted in blue).

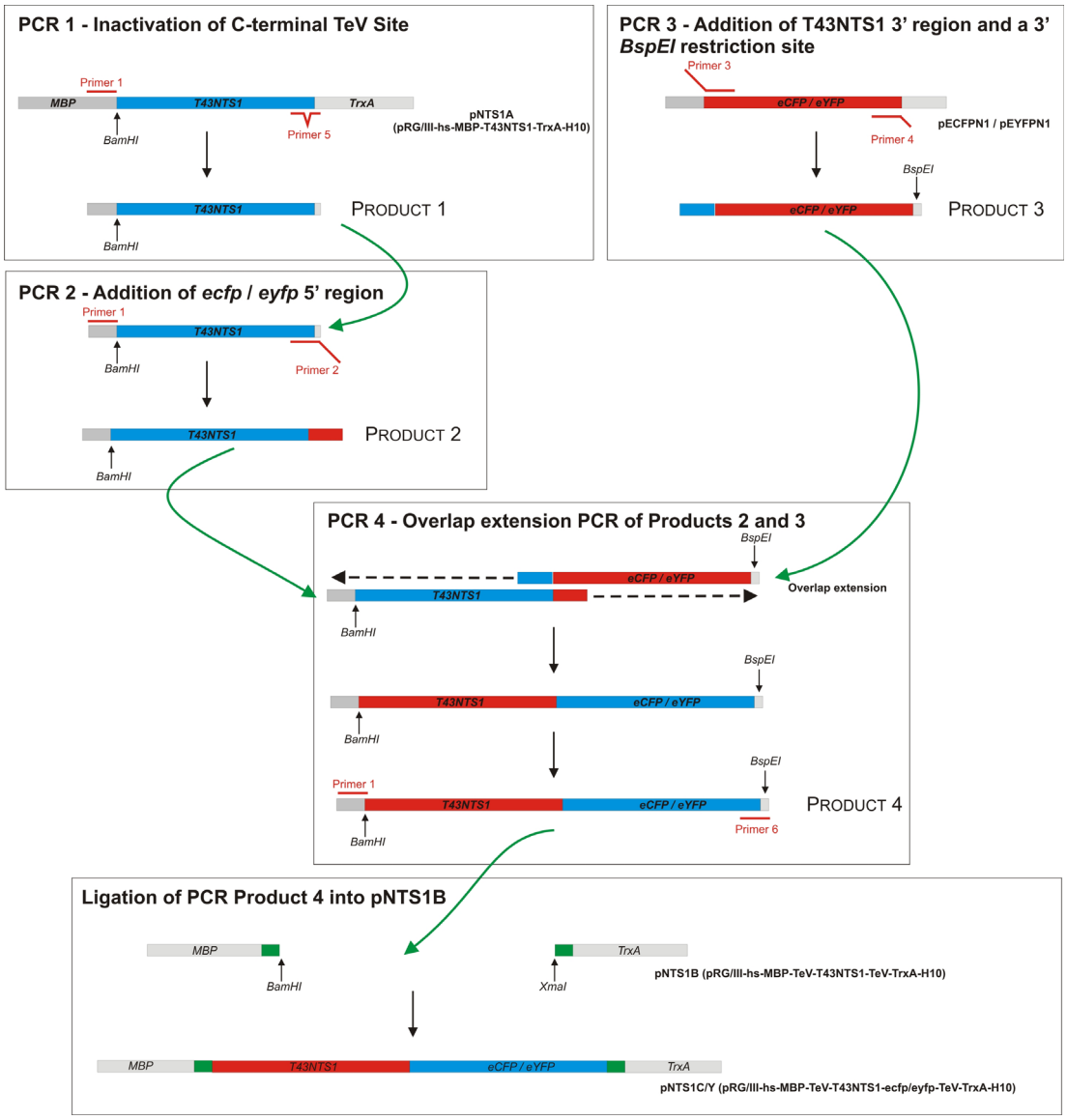

Figure 3.3 – Overview of the overlap extension PCR strategy employed to generate the constructs encoding the fluorescent NTS1 fusion proteins (pNTS1C and pNTS1Y). The cryptic TeV site at the C-terminus of T43NTS1 was inactivated and the genes encoding the fluorescent proteins (*ecfp* / *eyfp*) were introduced, followed by a new TeV recognition site.

The gene encoding T43NTS1 was amplified from the pRG/III-hs-MBP-T43NTS1-TrxA-H10 plasmid (Tucker and Grisshammer, 1996; Grisshammer *et al.*, 1999; Williamson *et al.*, 2002) with primers 1 and 5 by PCR, generating product 1, using a high fidelity DNA polymerase enzyme mix (Applied Biosciences). Primers 1 and 5 were designed to inactivate the cryptic TeV site by mutation of the C-terminal residue, Tyr^{424}

to Phe^{424}. Product 1 was subsequently amplified using primers 1 and 2 in order to add the sequence corresponding to the N-terminus of the fluorescent proteins on to the 3' end of the T43NTS1 gene (product 2). *ecfp* and *eyfp* genes were amplified from pECFPN1 and pEYFPN1 vectors (Living Colours, BD Biosciences) by PCR, using primers 3 and 4, which added a sequence corresponding to the C-terminus of the T43NTS1 gene on to the 5' end and a *Bsp*EI restriction enzyme site on to the 3' end (product 3). Overlap extension PCR was then performed on PCR products 2 and 3 with primers 1 and 6 to yield the full T43NTS1-*ecfp*/*eyfp* fragment (product 4).

PCR product 4 was cloned into *E.coli* TOP10F' (pCRT7 TOPO TA Expression Kit, Invitrogen). The T43NTS1-*ecfp*/*eyfp* fragment was then liberated by *Bam*HI/*Bsp*EI digestion and cloned into *Bam*HI/*Xma*I-digested pNTS1B, in place of the T43NTS1 fragment using standard cloning techniques. Correct amplification and insertion were confirmed by DNA sequencing and the plasmids designated pNTS1C and pNTS1Y.

3.2.2 - Optimisation of Expression Strain

A double strength TY starter culture (5 ml) containing ampicillin (75 μg/ml) and glucose (0.2 % (w/v)) was inoculated with a single colony of pNTS1Y-transformed DH5α and incubated overnight (16 h, 37 °C). Double strength TY (450 ml, 75 μg/ml ampicillin, glucose 0.2 % (w/v)) in a 2 l baffled conical flask was inoculated with starter culture (5 ml) and incubated (37 °C, 200 rpm) until the cells reached an OD_{600} of 0.45. The temperature was reduced to 20 °C and expression induced by adding IPTG when and OD_{600} of 0.6 was reached. The cells were harvested after 40 h of induction, frozen in liquid nitrogen and stored at -80 °C. The procedure was repeated using pNTS1Y-transformed BL21(DE3), C41(DE3) and C43(DE3)pREP4. In the case of C43(DE3)pREP4, kanamycin was added to both starter and 2 l cultures to a final concentration of 50 μg/ml.

All purification steps were carried out at 4 °C unless otherwise stated. Cell pellets were resuspended in a volume of 2x solubilisation buffer (100 mM Tris/HCl, pH 7.4, 400 mM NaCl, 60 % glycerol (v/v), protease inhibitors (Leupeptin, Pepstatin A, Aprotinin, all 1 μg/ml)) equal to double the pellet weight (i.e. 2.5 g pellet resuspended in 5 ml). DDM stock (10 % (w/v)) and CHAPS/CHS stock (5 % / 1 % (w/v)) were added dropwise whilst stirring, to final concentrations of 1 % (w/v) and 0.5 % / 0.1 % (w/v) respectively. Water was added to give a final volume of 10 ml followed by gentle stirring for 1 h at 4 °C. The cells were disrupted by ultrasonication at 4 °C and cell debris removed by centrifugation (70,000 g, 4 °C, 90 min). Imidazole (final concentration 50 mM) and protease inhibitors were added to the supernatant.

The supernatant was purified by IMAC (Ni-NTA Spin columns, Qiagen). All centrifugation steps were performed at 700 g, 4 °C. Samples were loaded by centrifugation, and the column washed with 600 μl of NiA (50 mM Tris/HCl, pH7.4, 200 mM NaCl, 30 % glycerol (v/v), 0.5 % CHAPS (w/v), 0.1 % DDM (w/v), 0.1 % CHS (w/v), 50 mM Imidazole, protease inhibitors). Bound NTS1Y protein was then eluted in 2 × 200 μl volumes of NiB (NiA plus 350 mM imidazole) and samples stored at -80 °C. Expression and purification were analysed by western blotting using anti-His antibody (GE Healthcare) and radioligand binding assay (Appendix A3). In order to quantify the expression level per mg membrane protein, the membrane fraction from C41(DE3) cells induced with 0.25 mM IPTG was isolated (Grisshammer *et al.*, 1993) (Appendix A2) and the total protein content determined by a commercially available Lowry assay according to the manufacturers instructions (RC DC Protein Assay, Biorad).

3.2.3 - Large Scale Expression

Double strength TY medium (10 l) containing ampicillin (75 μg/ml) and glucose (0.2 % (w/v)) in a 14 l fermentation vessel (BioFlo 3000, New Brunswick Scientific) was inoculated with an overnight culture (100 ml) of NTS1Y-transformed C41(DE3) grown at 37 °C. Air supply was maintained at 1 vvm and the relative oxygen saturation maintained at 50 % or above by program-controlled agitation. Cells were grown at 37 °C up to an OD_{600} of 0.4. The temperature was decreased to 20 °C and the culture induced with 0.25 mM IPTG when an OD_{600} of 0.6 was reached. Cells were harvested after 40 h by centrifugation (typically 50-60 g wet weight), frozen in liquid nitrogen and stored at -80 °C.

3.2.4 - Purification of full length construct

All purification steps were carried out at 4 °C unless otherwise stated. Cell pellet (20 g wet weight) was resuspended in 40 ml of 2x solubilisation buffer. Lysozyme was added at a concentration of 1 mg/ml, followed by gentle agitation (30 min). DDM stock (10 % (w/v)) and CHAPS/CHS stock (5 % / 1 % (w/v)) were added dropwise whilst stirring on ice to a final concentration of 1 % (w/v) and 0.5 % / 0.1 % (w/v) respectively. Water was added to give a final volume of 80 ml followed by gentle stirring at 4 °C (1 h). Insoluble material was pelleted by centrifugation at 70,000 g for 90 min, the supernatant decanted and supplemented with protease inhibitors and imidazole to a concentration of 50 mM.

The solubilised material was purified by IMAC using a 5 ml HisTrap HP column (GE Healthcare). After loading, the column was washed with 30 CV NiA (supplemented with 0.05 mg/ml POPC) and eluted using NiB (supplemented with 0.05 mg/ml POPC).

IMAC eluate was diluted 5-fold with GF buffer (50 mM Tris pH 7.4, 15 % glycerol (v/v), 500 mM NaCl, 0.1 % DDM (w/v), 0.01 % CHS (w/v), 0.05 mg/ml POPC, 1 mM

EDTA, protease inhibitors), concentrated to 2.5 ml using an Amicon stirred cell (Millipore, 100,000 MWCO) and loaded onto a Superdex 200 XK16/100 gel filtration column pre-equilibrated with GF buffer. Proteins were separated at a flow rate of 0.25 ml/min and 1 ml fractions collected.

3.2.5 - Purification of TeV-cleaved receptor

TeV-His_6 was expressed in *E.coli* BL21(DE3) and purified by nickel affinity and size exclusion chromatography (Appendix A5). Trial cleavage reactions with purified TeV-His_6 on IMAC-purified NTS1Y were carried out to determine the effect of the amount of TeV-His_6 on cleavage efficiency (Appendix A6). This was carried out individually on every batch of purified TeV.

Full length construct was purified (according to section 3.2.4) up to and including the IMAC purification step. IMAC eluate purified from a 20 g pellet weight was treated with TeV protease at a concentration of approximately 4 μg TeV-His_6 per μg fusion protein (the exact concentration was dependent on the particular TeV preparation used) in a total volume of 100 ml cleavage buffer, at 4 °C overnight with gentle agitation. The cleavage mixture was concentrated to 2.5 ml using an Amicon stirred cell (Millipore, 100,000 MWCO) and loaded onto a Superdex 200 XK16/100 gel filtration column pre-equilibrated with GF buffer (50 mM Tris pH 7.4, 15 % glycerol (v/v), 500 mM NaCl, 0.1 % DDM (w/v), 0.01 % CHS (w/v), 0.05 mg/ml POPC, 1 mM EDTA, protease inhibitors). Proteins were separated at a flow rate of 0.25 ml/min and 1 ml fractions collected. A ^{3}H-NT (New England Nuclear) radioligand binding assay was used to quantify amounts of active receptor present throughout the purifications (Appendix A3).

3.2.6 - In-Gel Fluorescence

The fluorescence of eCFP and eYFP moieties was monitored by in-gel fluorescence using the method of Drew *et al* (Drew *et al.*, 2001; Drew *et al.*, 2006) using standard Tris-Glycine SDS-PAGE (Invitrogen). eCFP-His_6 / eYFP-His_6 standards (Appendix A9) were loaded onto the same gel to allow quantification of the amount of fluorescent protein present in the receptor samples. To detect fluorescent bands, the gel was illuminated with UV light and images captured with a CCD camera system (Gel Doc, BioRad). Fluorescence intensities were quantified using ImageJ software v.1.36b (NIH) and the gels were subsequently stained with Coomassie Brilliant Blue.

3.2.7 - Electron Microscopy

Electron microscopy (EM) was carried out by Dimitrios Fotiadis (M. E. Muller Institute for Microscopy, Biozentrum, University of Basel). NTS1Y and T43NTS1-eCFP receptor samples were purified as described in the previous sections. Samples were prepared on carbon-coated copper grids (Agar Scientific) and were negatively stained using 2 % uranyl acetate. Images were recorded on Eastman Kodak Co. SO-163 sheet film with a Hitachi H-7000 electron microscope operated at 100 kV.

3.2.8 - DNA array binding assay

The DNA array binding assay was carried out by Jonathan Malo (Physics Dept., University of Oxford). A ~5 μl tunnel was formed between two parallel strips of double-sided sticky tape, a glass coverslip functionalised with a 5'-thiolated 15-mer oligonucleotide (Anchor-TWW) and a glass microscope slide (see Appendix A10 for details). TrisNTA-functionalised Kagome arrays (see Figure 3.1) were formed by cooling four oligonucleotides, at a concentration of 3 μM, from 90 to 10 °C over 65 h in Array Buffer A (20 mM Tris·HCl pH 8.8, 30 mM $MgCl_2$) using a Mastercycler PCR machine (Eppendorf). The Kagome-trisNTA oligonucleotides included LMRtrisNTA,

a 41-base strand (LMTanchor) containing a 13-base section complementary to Anchor-TWW, and three 26-base strands. Hybridisation of LMTanchor and Anchor-TWW strands allowed the Kagome-trisNTA arrays to be immobilized onto coverslip surfaces (Figure 3.4); array solutions were incubated within separate tunnel slides for ~10 min at 20 °C.

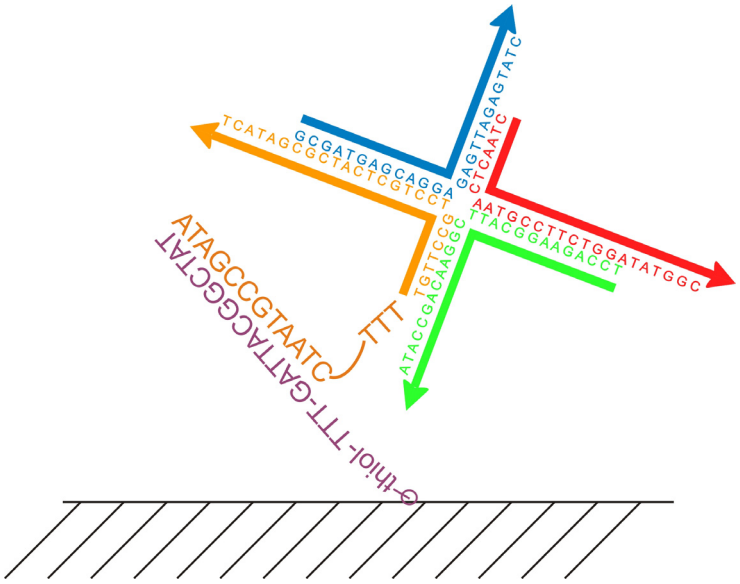

Figure 3.4 – Schematic depicting the immobilisation of the Kagome lattice to the Anchor-TWW-functionalised coverslip. This was made possible by the use of the LMRtrisNTA oligonucleotide in the formation of the lattice, a 41-base strand (yellow) containing a 13-base section complementary to Anchor-TWW (purple).

Non-immobilized arrays were washed off the coverslip surface using four 10 µl washes of Array Buffer A. The tunnel slide was then incubated for 5 min at 20 °C with ~10 µl of Array Buffer B (Array Buffer A plus 500 nM NTS1Y, BSA (1 mg/ml), 100 mM NaCl). Following four 10 µl washes with Array Buffer A, fluorescence images were captured as a control for non-specific binding. The slide was then washed with four further 10 µl volumes of Array buffer A and nickel (II) ions applied to the slide by washing with two 10 µl volumes of Array Buffer C (Array Buffer A plus 10 mM $NiCl_2$) followed by incubation with Array Buffer C for ~ 5 min at 20 °C. Excess Ni^{2+} was

removed by flushing with four 10 µl volumes of Array Buffer A and NTS1Y applied by incubation with ~10 µl of Array Buffer B for 5 min at 20 °C. Following removal of excess NTS1Y by four 10 µl washes with Array Buffer A, fluorescent images were captured. The tunnel slide was illuminated with a mercury source lamp (Olympus) and imaged using an Andor Ixon CCD (Andor) on an inverted X71 Olympus optical microscope.

3.3 - RESULTS AND DISCUSSION

3.3.1 - The Fluorescent Constructs

The genes encoding eCFP and eYFP were introduced into the NTS1B construct between the T43NTS1 and TrxA moieties by overlap extension PCR (Figure 3.5). The C-terminal TeV recognition site, which encompassed the previously identified cryptic TeV site at the C-terminus of T43NTS1 (White *et al.*, 2004), was removed and a new TeV site introduced between the fluorescent protein and the TrxA. Proteolytic cleavage of the resulting NTS1C and NTS1Y constructs after expression and purification will therefore yield T43NTS1-eCFP and T43NTS1-eYFP respectively for use as tools for the study of NTS1 multimerisation.

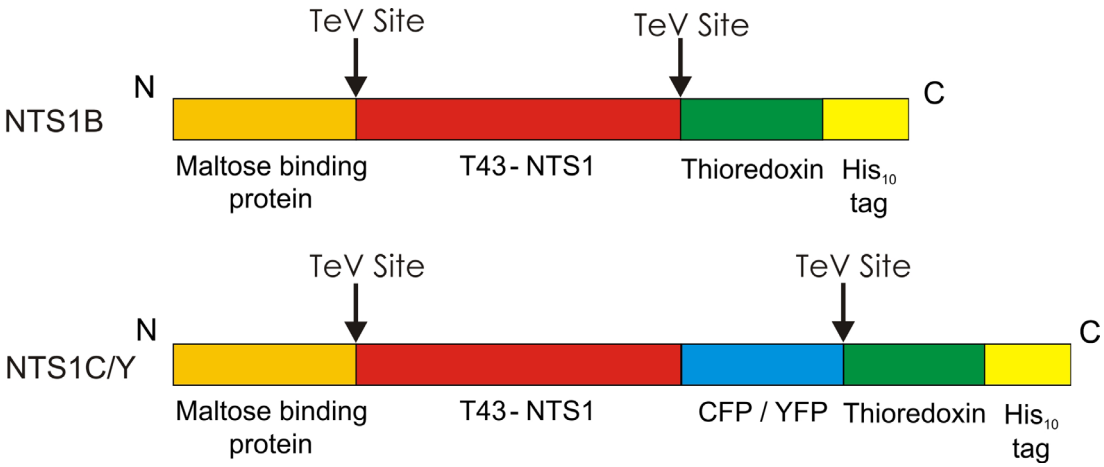

Figure 3.5 : Schematic depicting the untagged NTS1B construct (White *et al.*, 2004) and the fluorescence-tagged NTS1C and NTS1Y constructs. NTS1B consists of maltose-binding protein (MBP) from *E.coli*, an N-terminally truncated form of NTS1 (T43NTS1), thioredoxin A from *E.coli* (TrxA) and a deca-histidine tag (His_{10} tag). TeV protease cleavage sites are present between the MBP and T43NTS1 moieties and the T43NTS1 and TrxA moieties to facilitate proteolytic removal of the fusion partners. The genes for eCFP and eYFP were introduced into the NTS1B construct by overlap extension PCR, to yield the NTS1C and NTS1Y constructs. The C-terminal TeV site was moved to a position C-terminal of the fluorescent protein gene.

3.3.2 - Optimisation of Expression Strain

Rat NTS1 has previously been expressed as a protein fusion with MBP and TrxA in the *E.coli* DH5α strain (Grisshammer *et al.*, 1993; Tucker and Grisshammer, 1996; Williamson *et al.*, 2002; White *et al.*, 2004) (section 2.1.1). Expression trials of the NTS1Y construct were carried out in the same manner as for NTS1B (Chapter 2) using the *E.coli* strains DH5α and BL21(DE3) as well as C41(DE3) and C43(DE3)pREP4, two mutant strains derived from BL21(DE3) which have proved useful for the overexpression of several membrane and toxic proteins (Miroux and Walker, 1996). Cell pellet was detergent-solubilised, purified by IMAC and assayed by radioligand binding assay (Table 3.1).

Table 3.1: Optimisation of *E.coli* expression for NTS1Y. Cell pellets were isolated from 450 ml cultures, solubilised using the detergents CHAPS/CHS/DDM and purified by IMAC. A radioligand binding assay was used to determine expression level of functional receptor, with all measurements carried out in triplicate. NTS1C was found to express at a comparable level to NTS1Y.

Expression Strain	IPTG concentration used for induction (mM)	Expression of functional receptor (µg/l culture)
C43(DE3)pREP4	0.1	3.1 ± 1.1
	0.25	21.5 ± 1.4
	0.5	5.1 ± 0.8
C41(DE3)	0.1	16.1 ± 3.1
	0.25	33.0 ± 1.5
	0.5	17.5 ± 1.5
BL21(DE3)	0.1	ND
	0.25	21.0 ± 1.3
	0.5	4.3 ± 0.6
DH5α	0.1	15.7 ± 1.4
	0.25	8.7 ± 3.3
	0.5	2.3 ± 0.4

The C41(DE3) strain, induced with an IPTG concentration of 0.25 mM, proved to produce the highest level of functional protein per litre of culture and was therefore chosen as the expression host of choice. Functional expression was also observed in

the other strains, but at a lower level, with observed expression levels in BL21(DE3), C43(DE3)pREP4 and DH5α of 64 %, 65 % and 48 % respectively of those observed in C41(DE3). Increasing the IPTG concentration above 0.25 mM resulted in a decreased receptor yield in all cell types. This lower functional expression level at IPTG concentrations higher than 0.25 mM was also observed for the NTS1B construct (Chapter 2) and suggests that expression of the construct at higher rates has a toxic effect. However, it is clear that the functional expression level of the fluorescently tagged receptor can be significantly improved by using optimised *E.coli* expression strains instead of DH5α, as was also the case for the non-fluorescent NTS1B construct.

Subsequent isolation and activity assay of the C41(DE3) membrane fraction revealed an expression level of 12.7 ± 0.9 pmol/mg membrane protein. This compares favourably with the level of 10 - 15 pmol/mg observed previously for the NTS1A construct (Tucker and Grisshammer, 1996) and suggests that the addition of the extra eCFP and eYFP C-terminal tag does not adversely affect functional expression. However, yields of active receptor per mass of cell base were significantly higher when whole cells were directly solubilised. A mean yield of receptor, solubilised directly from C41(DE3) cell pellet (20 g cell pellet, n = 5), of 2.3 ± 0.2 nmol/l culture (294 ± 31 μg/l culture) was obtained, whilst the yield of receptor, solubilised from C41(DE3) membrane fractions (20 g cell pellet, n=3) was only 0.33 ± 0.14 nmol/l culture (37 ± 12 μg/l culture). In addition, since isolation of membrane fractions prior to solubilisation is a time consuming process, all subsequent purifications were carried out by direct solubilisation of whole cells.

3.3.3 - Purification of full length construct (NTS1C/NTS1Y)

NTS1Y fusion protein was subsequently expressed in the C41(DE3) strain on a 10 l scale (BioFlo 3000, NBS). Cell pellet was solubilised, purified by nickel affinity

chromatography and subsequently further purified using gel filtration chromatography. Figure 3.6 shows the elution profiles of a representative purification. A step gradient from wash buffer, which contained 50 mM imidazole, to elution buffer, which contained 350 mM imidazole, resulted in the elution of a single peak which absorbed at a wavelength of 280 nm and was observed to be fluorescent by eye. Fractions containing receptor (2 – 6) were combined and further purified by gel filtration chromatography.

Gel filtration elution fractions were separated using SDS-PAGE and visualised by both in-gel fluorescence (Drew *et al.*, 2001; Drew *et al.*, 2006) and Coomassie Brilliant Blue staining (Figure 3.7). NTS1Y (MBP-TeV-T43NTS1-TeV-eYFP-TrxA-His_{10}) can be seen in the fractions which correspond to the major peak (labelled 'a', retention volume of 82 ml, fractions 4 - 12) in both the in-gel fluorescence and the Coomassie staining. Some lower molecular weight fluorescent bands can also be seen in these fractions. These are likely cleavage products which are co-purifying with the full length receptor. However, these are totally undetectable on the Coomassie-stained gel and are, therefore, at extremely low level, and are only evident because of the high sensitivity of the in-gel fluorescence technique. Another fluorescent protein can be seen in fraction 26. This fraction is part of the peak which eluted at a retention volume of 118 ml (labelled 'b'). This protein has a molecular weight of approximately 30 kDa and is therefore likely to be a small cleavage product which comprises the fluorescent protein.

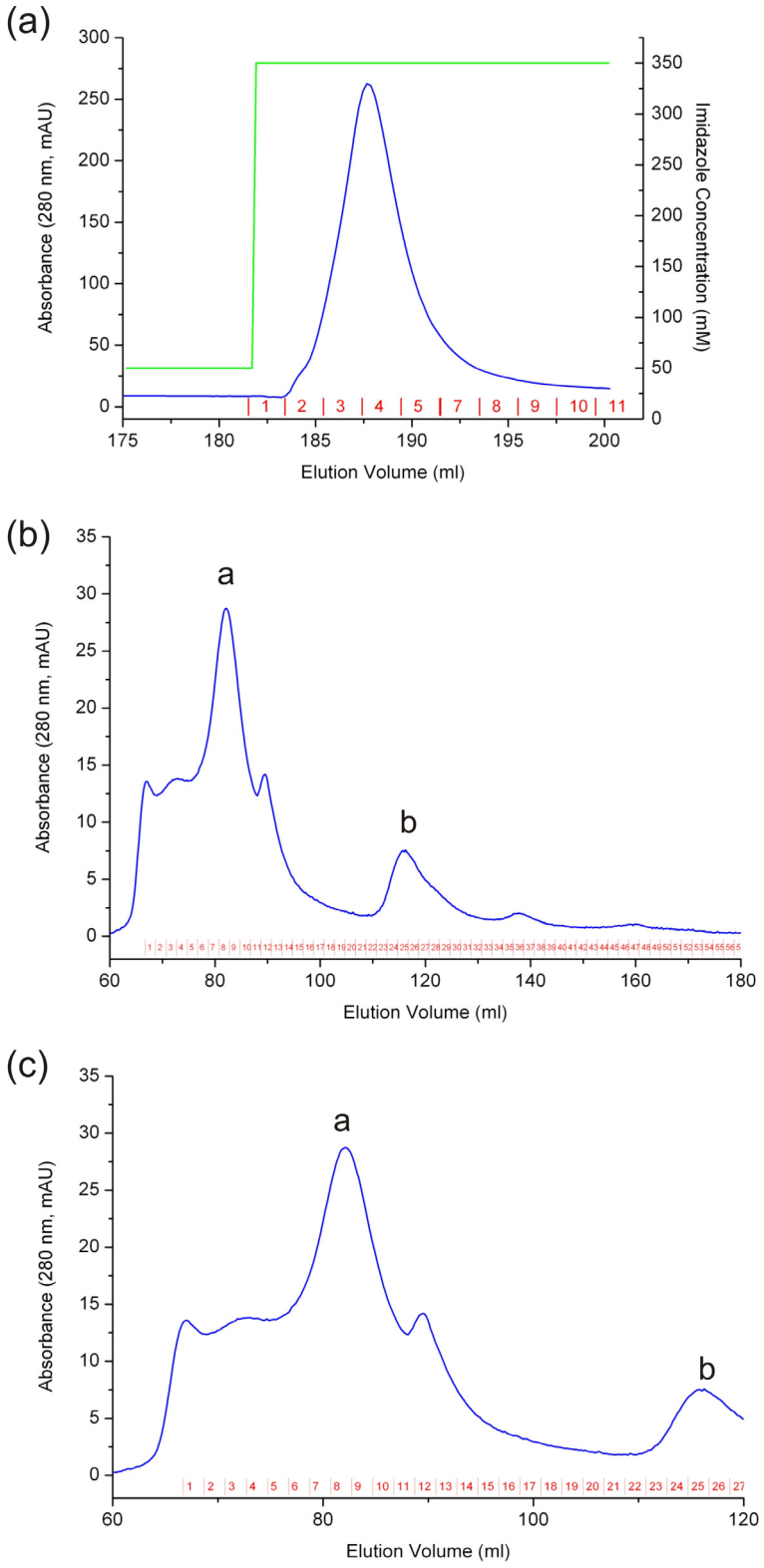

Figure 3.6 – Elution profiles for purification of NTS1Y fusion protein. The protein was purified by nickel affinity chromatography (a), and gel filtration chromatography (b). Part (c) shows the gel filtration elution profile in more detail around the receptor peak. In each case the absorbance at 280 nm (blue) and the fraction number (red) are shown. In addition, the step gradient from wash buffer (50 mM Imidazole) to elution buffer (350 mM Imidazole) is shown in green for the nickel affinity elution profile.

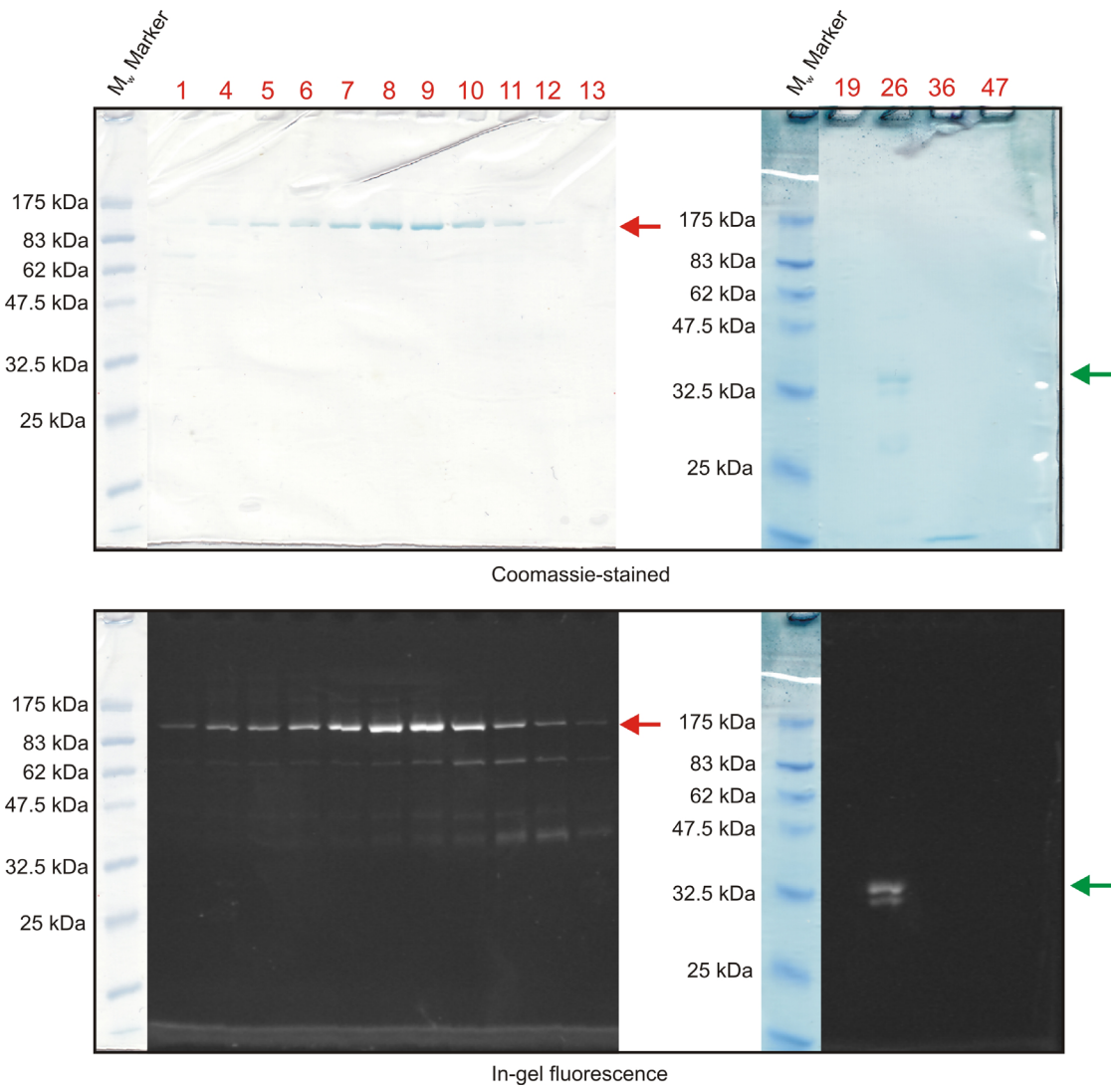

Figure 3.7 – SDS-PAGE analysis of gel filtration chromatography elution fractions from the NTS1Y purification (Figure 3.6b). Samples of each fraction (fraction number labelled in red) were separated by SDS-PAGE (12 % Tris-Glycine gel) and visualised by in-gel fluorescence and Coomassie Brilliant Blue staining. NTS1Y (molecular weight (Mw) approx. 130 kDa, red arrow) can be seen to elute between fractions 4 - 12. A lower molecular weight fluorescent band (Mw approx 30 kDa, green arrow) can be seen in fraction 26.

Gel filtration fractions 5 – 10, which contain the majority of the NTS1Y, were combined and concentrated. The progress of the purification was monitored by analysing the major purification samples by radioligand binding assay and in-gel fluorescence (Table 3.2 and Figure 3.8). In combination with radioligand binding data, in-gel fluorescence provides a useful measure of the proportion of the total receptor present which is able to bind ligand. After in-gel fluorescence analysis the gel was subsequently stained with Coomassie.

Table 3.2 : Purification of NTS1Y expressed in *E.coli* C41(DE3) (20 g wet pellet weight). Progress of purification was monitored by both in-gel fluorescence and radioligand binding assay. Percentage activity = (yield of active receptor / yield of fluorescent receptor) × 100. The percentage yield refers to the yield of fluorescent receptor relative to the detergent-solubilised fraction.

Purification Stage	Yield of NTS1Y receptor (nmol)		% Active	% Yield
	In-gel fluorescence	Radioligand binding assay		
Solubilised Material	14.2 ± 1.3	5.9 ± 0.9	41.2 ± 6.7	100
Nickel Column elution	9.4 ± 1.0	5.0 ± 0.6	53.7 ± 6.9	65.8 ± 9.2
Gel Filtration load	9.4 ± 1.0	4.7 ± 0.4	50.0 ± 5.1	65.9 ± 9.2
Gel Filtration eluate	5.0 ± 0.5	1.7 ± 0.3	33.1 ± 5.6	35.3 ± 5.0

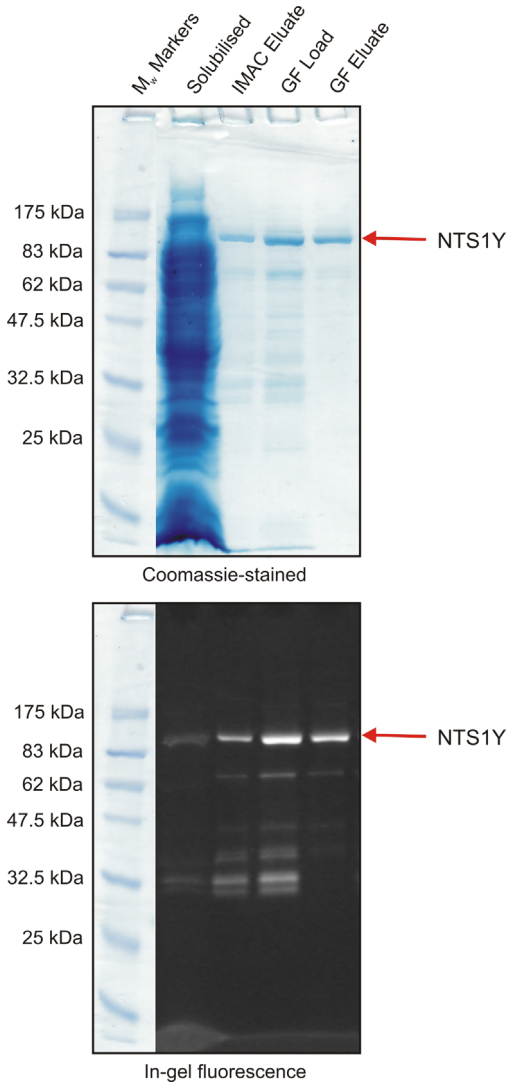

Figure 3.8 : SDS-PAGE analysis of the NTS1Y (MBP-TeV-T43NTS1-eYFP-TrxA-His$_{10}$) purification showing how overexpression and purification of NTS1Y was monitored using in-gel fluorescence. Indicated fractions from an NTS1Y purification from an *E.coli* C41(DE3) culture were separated on a 12 % SDS PAGE gel. In-gel fluorescence was monitored and the gel was subsequently stained with Coomassie. The NTS1Y protein can be seen between the 175 kDa and 83 kDa Mw markers (theoretical molecular weight = 130 kDa). Varying amounts of eYFP-His$_6$ were loaded onto the same gel (not shown) to enable quantification of the amount of fluorescent receptor present at each stage of purification using gel densitometry (Drew *et al.*, 2001; Drew *et al.*, 2006). Comparison of the Coomassie-staining and in-gel fluorescence of the solubilised fraction highlights the sensitivity and selectivity of this technique.

The results (Table 3.2 and Figure 3.8) indicate that the receptor is both fluorescent and able to bind ligand with high affinity throughout the purification. Given that GFP and its variants are not fluorescent when either expressed on the periplasmic face of the membrane, or in inclusion bodies (Waldo *et al.*, 1999), the expression of fluorescent protein confirms that the protein is being correctly targeted to the plasma membrane and is folding with the C-terminus of the receptor on the cytoplasmic side. The SDS-PAGE analysis (Figure 3.8) shows the NTS1Y protein (Mw = 130 kDa, MBP-TeV-T43NTS1-eYFP-TeV-TrxA-His_{10}) by both Coomassie-staining and in-gel fluorescence. Lower molecular weight protein bands, some of which are fluorescent, are evident in the IMAC elution and GF load lanes. However, these are effectively removed by the gel filtration step and are largely absent in the gel filtration eluate lane. Therefore, NTS1Y was effectively purified to near homogeneity, with a 20 g cell pellet yielding 5.0 ± 0.5 nmol (0.7 ± 0.1 mg) of fluorescence-tagged receptor. There is a good correlation between receptor fluorescence and ligand-binding activity during the purification, suggesting that approximately 40 % of the purified receptor is able to bind ligand if it is assumed that each receptor molecule has one ligand binding site. Whether this is caused by 60 % of the receptor being in an inactive form which is unable to bind ligand, or because the radioligand binding assay underestimates the amount of functional receptor present is unclear, but this correlation between fluorescence and activity is maintained throughout the purification.

3.3.4 - Purification of TeV-cleaved receptor

Fluorescence–tagged receptor, T43NTS1-FP (i.e. with the MBP and TrxA-His10 fusions removed), was obtained by incorporating a proteolytic cleavage reaction between the nickel affinity chromatography and the gel filtration purification steps. This was made possible by the incorporation of two TeV protease cleavage recognition

sites between MBP and T43NTS1 and the FP and TrxA respectively. Nickel column eluate was cleaved with TeV protease overnight and the resulting T43NTS1-FP product was purified by gel filtration chromatography. Figure 3.9 shows the elution profiles of a representative purification of T43NTS1-eCFP.

Gel filtration elution fractions were separated using SDS-PAGE and visualised by both in-gel fluorescence and Coomassie Brilliant Blue staining (Figure 3.10). T43NTS1-eCFP (molecular weight = 69.9 kDa, red arrow) can be seen in the fractions which correspond to the major peak (labelled 'a', retention volume of 85 ml, fractions 7 - 11) in both the in-gel fluorescence and the Coomassie staining. However, on the gel it has run between the 63 kDa and 47.5 kDa molecular weight markers. Membrane proteins typically run faster on SDS-PAGE than expected, and GFP and its variants will also run at a lower apparent molecular weigh than expected since they remain properly folded during electrophoresis (Drew *et al.*, 2006). Some lower molecular weight fluorescent bands can also be seen in these fractions, but these are present at much lower intensity than for the uncleaved preparation (Figure 3.8) and are totally undetectable on the Coomassie-stained gel. Another fluorescent protein (green arrow) can be seen in fractions 29 and 31 which correspond to the peak which eluted at a retention volume of 120 ml (labelled 'b'). This protein has a molecular weight of approximately 30 kDa and is therefore likely to be a small cleavage product comprising the fluorescent protein. These fractions also contain a non-fluorescent protein (blue arrow) which is only evident on the Coomassie-stained gel. The main receptor peak is well resolved from both of these impurities.

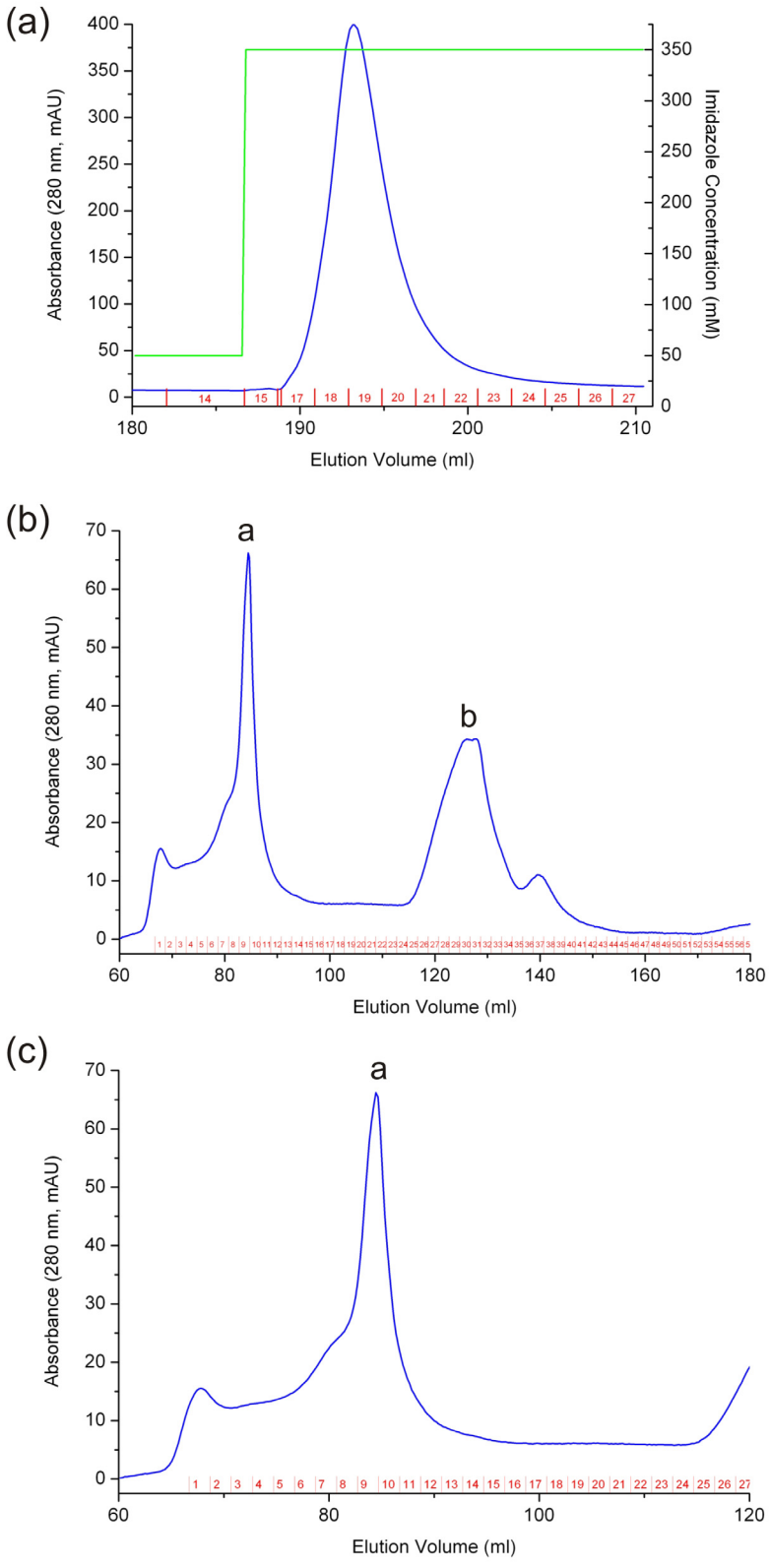

Figure 3.9 – Elution profiles for purification of TeV-cleaved NTS1C fusion protein. The protein was purified by nickel affinity chromatography (a) and, following proteolytic cleavage to remove the MBP and TrxA-His10 fusions, gel filtration chromatography (b). Part (c) shows the gel filtration elution profile in more detail around the receptor peak. In each case the absorbance at 280 nm (blue) and the fraction number (red) are shown. In addition, the step gradient from wash buffer (50 mM Imidazole) to elution buffer (350 mM Imidazole) is shown in green for the nickel affinity elution profile.

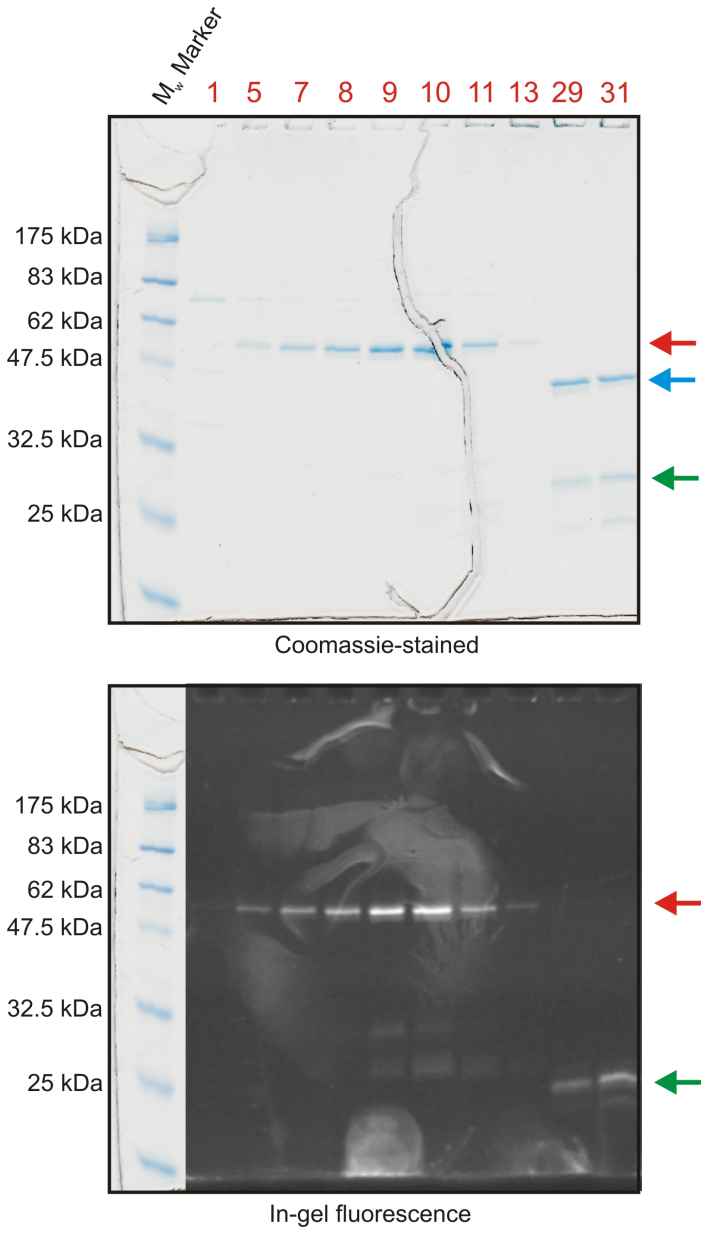

Figure 3.10 – SDS-PAGE analysis of gel filtration chromatography elution fractions from the T43NTS1-eCFP (TeV-cleaved) purification (see Figure 3.9b). Samples of each fraction (fraction number labelled in red) were separated by SDS-PAGE (12 % Tris-Glycine gel) and visualised by in-gel fluorescence and Coomassie Brilliant Blue staining. T43NTS1-eCFP (molecular weight approx 69.9 kDa, red arrow) can be seen to elute between fractions 7-11. A lower molecular weight fluorescent band (molecular weight approx 30 kDa, green arrow) can be seen in fractions 29 and 31. These fractions also contain a non-fluorescent lower molecular weight band (molecular weight approx. 42 kDa) which is only evident on the Coomassie-stained gel (blue arrow).

The progress of the purification was monitored by analysing the major purification samples using radioligand binding assay and in-gel fluorescence (Table 3.3, Figure 3.11) in the same manner as was carried out for the uncleaved receptor preparation (section 3.3.3).

Table 3.3 : Purification and proteolytic cleavage of NTS1C expressed in *E.coli* C41(DE3) (20 g wet pellet weight). Progress of purification was monitored by both in-gel fluorescence and radioligand binding assay. Percentage activity = (yield of active receptor / yield of fluorescent receptor) × 100. The percentage yield refers to the yield of fluorescent receptor relative to the detergent-solubilised fraction.

Purification Stage	Yield of NTS1Y receptor (nmol)		% Active	% Yield
	In-gel fluorescence	Radioligand binding assay		
Solubilised Material	34.2 ± 1.3	10.6 ± 0.3	31.0 ± 1.5	100
Nickel Column elution	28.1 ± 2.2	9.8 ± 0.5	34.8 ± 2.8	82.2 ± 7.1
Post-TeV cleavage	20.6 ± 2.7	7.1 ± 0.2	34.5 ± 4.6	60.3 ± 8.2
Gel Filtration load	17.5 ± 1.0	6.6 ± 0.2	37.6 ± 2.4	51.3 ± 3.5
Gel Filtration eluate	8.6 ± 0.5	2.2 ± 0.1	25.8 ± 2.0	25.2 ± 1.7

The introduction of the TeV-cleavage does not seem to significantly alter the percentage activity of the receptor (radioligand binding compared with in-gel fluorescence) or the yield of the receptor after the gel filtration (Table 3.3). There is a small decrease (approximately 10 %) in both ligand binding activity and fluorescence during the cleavage step. In addition, the majority of impurities were successfully separated from the T43NTS1-eCFP cleavage product during the final gel filtration purification, as shown by both in-gel fluorescence and Coomassie-staining (Figure 3.11), with a 20 g cell pellet yielding 8.6 ± 0.5 nmol (0.6 ± 0.1 mg) of cleaved, fluorescence-tagged receptor.

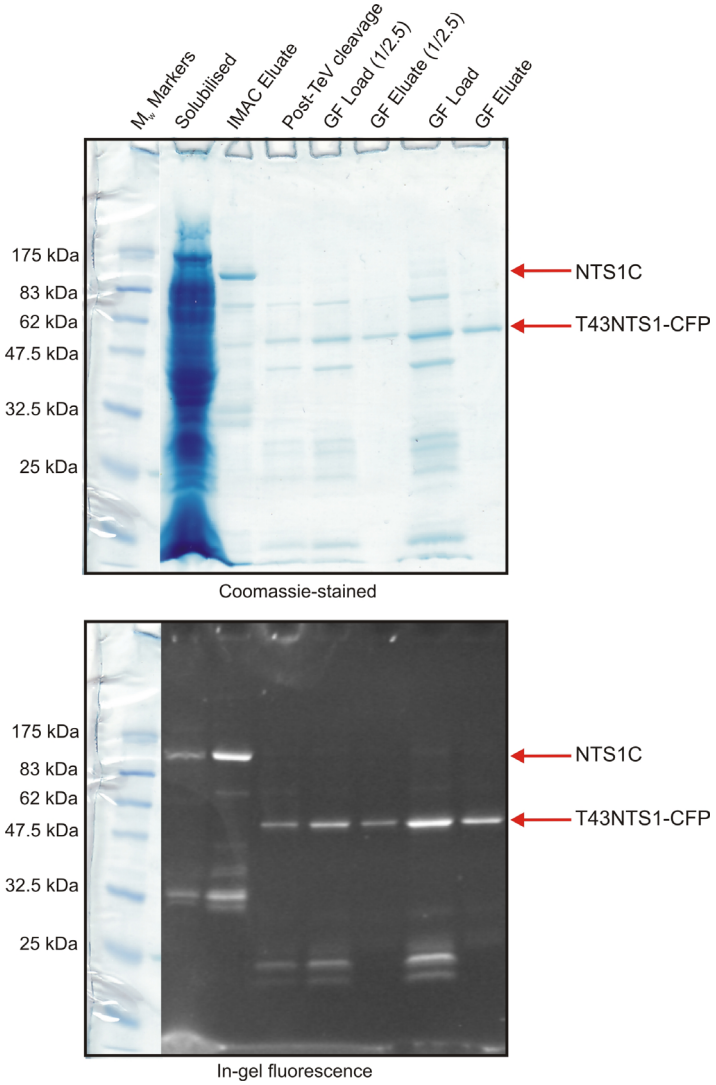

Figure 3.11 : SDS-PAGE analysis of the T43NTS1-eCFP purification showing how overexpression and purification were monitored using in-gel fluorescence. Indicated fractions from a T43NTS1-eCFP purification from an *E.coli* C41(DE3) culture were separated on a 12 % SDS PAGE gel. In-gel fluorescence was monitored and the gel was subsequently stained with Coomassie. The NTS1C protein can be seen between the 175 kDa and 83 kDa Mw markers in the solubilised and IMAC elution samples (theoretical molecular weight = 130 kDa). In the post-TeV cleavage, GF load and GF eluate lanes, the T43NTS1-eCFP cleavage product (theoretical molecular weight = 69.9 kDa) can be seen. Varying amounts of eCFP-His_6 were loaded onto the same gel (not shown) to enable quantification of the amount of fluorescent receptor present at each stage of purification using gel densitometry (Drew *et al.*, 2001; Drew *et al.*, 2006).

3.3.5 - Ligand Binding Affinity

Further radioligand binding analysis confirmed the high affinity of purified, fluorescence-tagged NTS1 for NT, both before (K_d = 0.91 ± 0.17 nM) and after (K_d = 0.84 ± 0.12 nM) proteolytic cleavage (Figure 3.12). These affinities compare well with affinities for the NT-NTS1 interaction reported previously, both for receptor expressed in *E.coli* (0.43 ± 0.11 nM) (Tucker and Grisshammer, 1996) and other systems, including synaptic membranes (0.9 nM) (Kitagbi *et al.*, 1977), *Xenopus* oocytes (0.19 ± 0.04 nM) (Tanaka *et al.*, 1990) and HT29 cells (0.56 ± 0.10 nM) (Vita *et al.*, 1993). In addition, the affinity of the non-fluorescent NTS1B construct (1.14 ± 0.15 nM) also indicates that the fusion with fluorescent protein does not alter

the affinity of the receptor for NT. Therefore the detergent environment and the addition of the fluorescent tag do not alter the ligand binding affinity of NTS1 for NT.

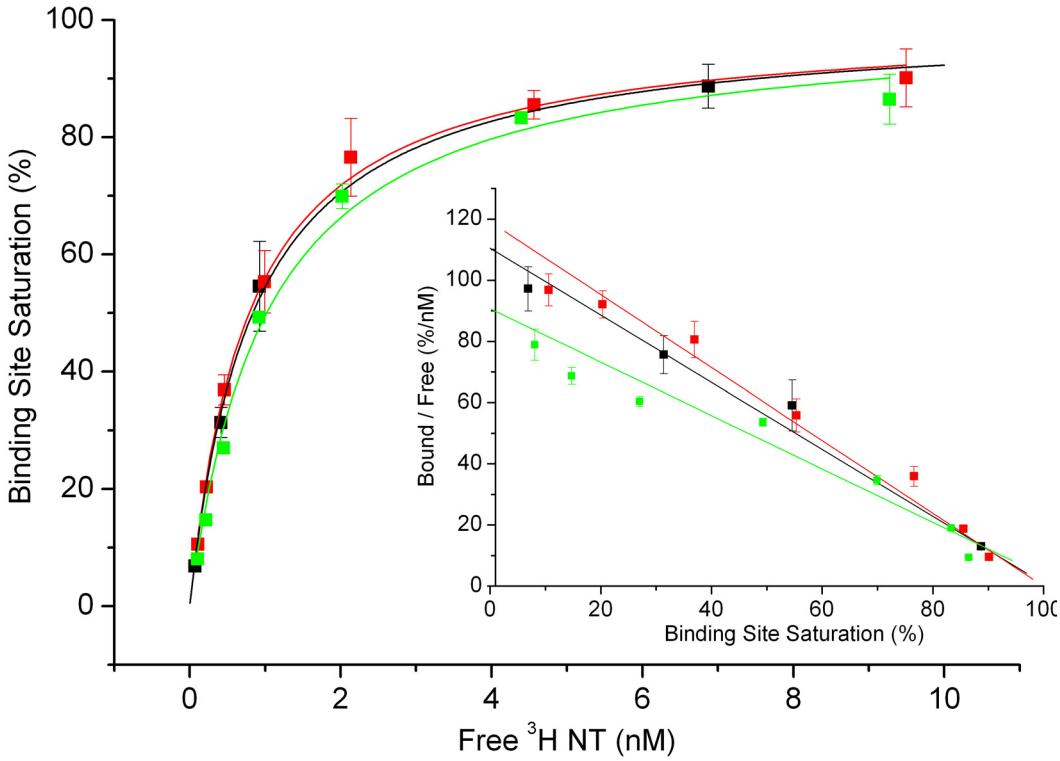

Figure 3.12 : Saturation radioligand binding data for purified, detergent-solubilised NTS1Y (■, black line), cleaved T43NTS1-eCFP (■, red line) and NTS1B (■, green line). Fitting of Langmuir isotherms to the data and Scatchard transformations (inset) shows that the affinity of the fluorescence-tagged receptor for NT (uncleaved NTS1Y, K_d = 0.91 ± 0.17 nM, cleaved T43NTS1-eCFP, K_d = 0.84 ± 0.12 nM) is very close to that for the untagged receptor (K_d = 1.14 ± 0.15 nM).

3.3.6 - Electron microscopy analysis of fluorescence-tagged NTS1

Purified, detergent-solubilised samples of fluorescence-tagged NTS1, were analysed by negative stain electron microscopy, both before and after cleavage with TeV protease (Figure 3.13). The micrographs show individual particles, with no obvious sign of aggregation. The individual particles vary in diameter from 7 – 13 nm, with a mean diameter of 9.4 ± 0.5 nm. The size variation could be caused by differing profiles of the receptor particle, which is free to adopt any orientation in detergent solution. For example, several particularly long particles (approx. length = 16.3 ± 0.4 nm) can be seen

in the uncleaved receptor sample which could be a side profile of the whole fusion protein including the MBP and TrxA fusions at either end of the receptor. Such long particles are absent from the micrograph of the cleaved sample and from the negative stain image of the non-fluorescently tagged receptor (T43NTS1, Chapter 2). A lack of distinguishing features prevents further image reconstruction to verify this suggestion. However, these preliminary micrographs are useful for the verification of the quality of the receptor preparation and indicate that further electron microscopy studies using either negative stain or cryo-EM have the potential to yield structural information for the NTS1 receptor.

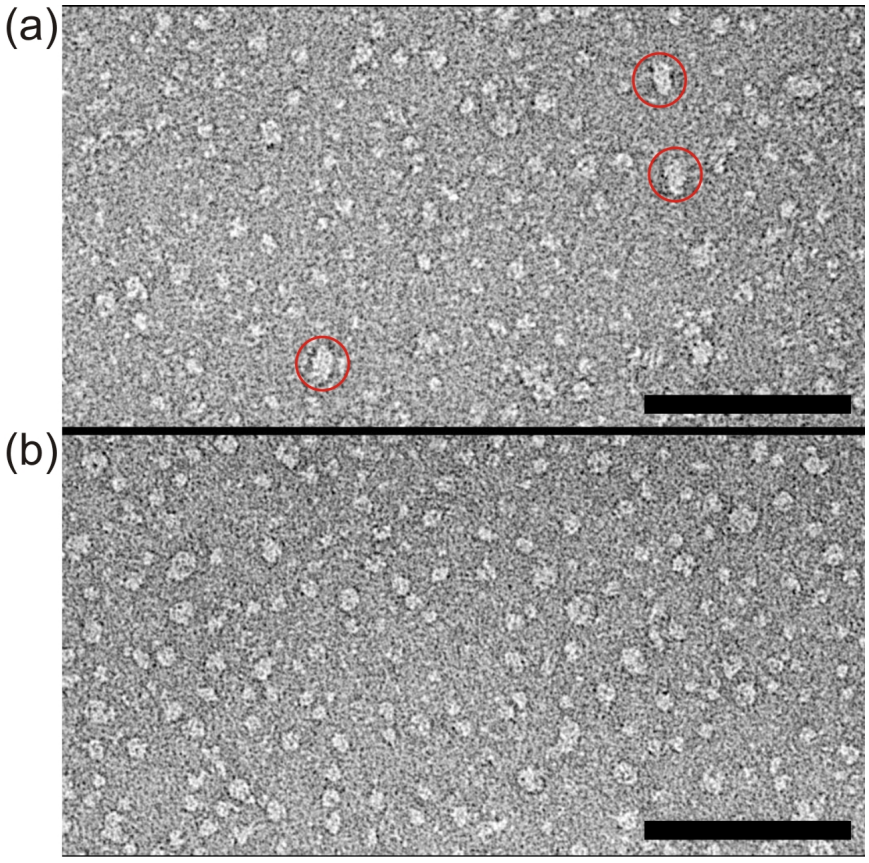

Figure 3.13 – Negative stain electron microscopy of purified, detergent-solubilised NTS1Y (a) and T43NTS1-eCFP (b). The black scale bar represents a distance of 100 nm. Samples were prepared on carbon-coated copper grids and stained with 2 % uranyl acetate. Individual particles can be seen in each case with no sign of aggregation. Particularly long particles can be seen in figure (a) (circled in red) which are not present in the TeV-cleaved sample and likely represent a side profile of the fusion protein, including the MBP and TrxA fusions. Electron microscopy was carried out by Dimitrios Fotiadis (Basel).

3.3.7 - Optimisation of Two-Dimensional DNA array decoration

DNA oligonucleotides can be designed to self associate and form extended two dimensional arrays. Immobilisation of a protein of interest to the array can form a 2D protein crystal which can be imaged using EM to potentially yield a high resolution protein structure. The approach is particularly applicable to proteins, such as GPCRs, which have proven difficult to crystallise using classical techniques.

Preliminary studies using NTS1 have been carried out (Meier and Turberfield, 2003; Selmi *et al.*, 2003). However, as discussed in section 3.1.3, verification that the NTS1 protein was actually bound to the DNA array was problematic. The only method available to confirm binding was to carry out EM on the sample, perform preliminary image processing and identify electron density arising from protein in the vicinity of the functionalised regions of the lattice. Therefore, the fluorescent constructs were exploited to develop an assay to verify receptor binding to arrays prior to electron microscopy. A Kagome lattice which was functionalised with NTA groups was immobilised on a glass coverslip. The lattice was charged with nickel and incubated with purified, detergent-solubilised NTS1Y, followed by extensive washing to remove non-specifically bound material. Imaging using a fluorescent microscope revealed fluorescent receptor bound to the lattices (Figure 3.14a). Control experiments, in which the NTA-lattice was not charged with nickel revealed no receptor binding (Figure 3.14b), which suggested that the binding observed was a specific interaction of the receptor His_{10} tag with the lattice Ni-NTA group, rather than a non-specific interaction of the receptor with the glass coverslip, or the lattice structural components.

This application of the NTS1 fluorescent fusion protein appears to have useful potential as a binding assay for the verification of receptor binding to DNA lattices. The technique will also facilitate the optimisation of receptor binding conditions and the

method is currently being extended for the imaging of NTS1Y bound to DNA lattices on EM grids to allow verification of sample quality directly prior to electron microscopy.

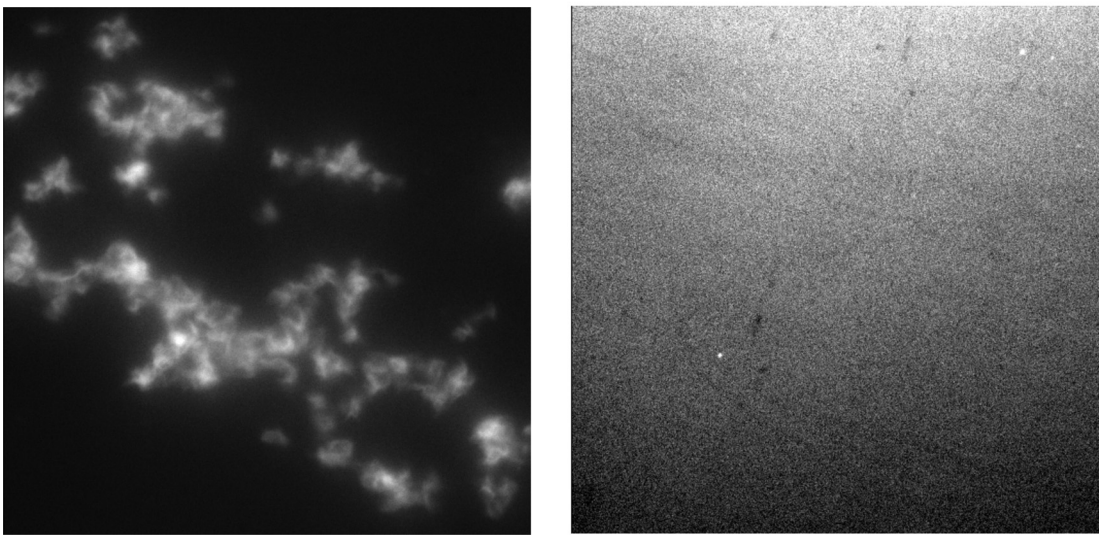

Figure 3.14 – Use of the NTS1 fluorescent constructs to assay receptor binding to DNA lattices. (a) Fluorescence microscopy image of NTS1Y bound to Ni-NTA-functionalised DNA arrays. (b) Control experiment in which arrays were not pre-charged with nickel ions. In both cases, the samples were excited using a mercury lamp and the size of each image is 128 μm square.

3.4 - CONCLUSIONS

Proteins of the GPCR family are predicted to comprise a large proportion of future drug targets. Consequently, further knowledge of how ligand binding at the cell surface is transformed into an intracellular signal is required. The application of fluorescence studies to GPCRs in lipid-reconstituted systems, in particular the study of NTS1 multimerisation, has the potential to be extremely useful in this area. The expression and purification of active, fluorescent receptor, a necessary prerequisite for such work, has been successfully demonstrated. Addition of the C-terminal eCFP and eYFP fluorescent tags does not have any significant adverse affect on the expression of ligand-binding NTS1 receptor in *E.coli*. 1 - 2 nmol of fluorescent receptor, either with or without the MBP and TrxA-His_{10} fusions on the N- and C-terminus respectively, can be effectively purified from 20 g of *E.coli* C41(DE3) cell pellet using a two stage purification involving nickel affinity chromatography followed by gel filtration chromatography. Radioligand binding analysis showed that the purified, fluorescence-tagged receptor bound NT with high affinity which was similar to the non-fluorescently tagged receptor and previously published examples of NTS1 expressed in other systems.

Negative stain electron micrographs of the purified receptor, both before and after TeV protease cleavage, suggest a monodisperse receptor population with no obvious sign of aggregation. Further electron microscopy study using both negative stain and cryo-EM will be carried out in an attempt to elucidate finer structural details. Preliminary negative stain EM of NTS1 incubated with 2D DNA lattices suggest that it may be possible to self assemble 2D crystals of NTS1. This technique has the potential to yield high resolution structural information. A binding assay exploiting the fluorescent receptor constructs has been developed and will be a useful tool in the verification of

sample quality prior to imaging and in the optimisation of receptor-array binding conditions.

In addition, given that high resolution structural techniques require milligram amounts of purified receptor in an active, ligand-binding form, and the challenges associated with the overexpression of GPCRs, any optimisation of expression levels is clearly advantageous. The labelling of the receptor with a fluorescent tag has the potential to facilitate the optimisation of protein expression and purification; further optimisation of the expression and purification of NTS1, as well as other GPCRs, will likely be possible. As demonstrated, in-gel fluorescence measurements can be readily applied to GPCRs and, in combination with radioligand binding assays, allow the direct comparison of the total receptor present with the proportion of receptor which is able to bind ligand. The in-gel fluorescence technique has the added advantage of selectively measuring the presence of full length fluorescent receptor fusion. Consequently, any truncation or cleavage, either during expression or purification, is easily monitored. Incorporation of an alternative protease site between the T43NTS1 and fluorescent moieties would allow removal of the fluorescent tag after expression and purification for structural analysis, if required.

CHAPTER 4 - RECONSTITUTION OF FLUORESCENCE-TAGGED NTS1

SUMMARY

The reconstitution of fluorescent NTS1 into phospholipid vesicles will enable the multimerisation state of the receptor to be assayed in a membrane environment. Purified, fluorescent receptor was successfully reconstituted into brain polar lipid (BPL) liposomes using a strategy based on partial vesicle solubilisation. The receptor was reconstituted in an active conformation which was both fluorescent and able to bind NT. Experimentation with alternative lipid compositions suggested that specific lipids are required in order to maintain ligand-binding activity. Variation of the detergent : lipid ratio used for liposome disruption had no effect on reconstitution yields. Tryptic digestion of reconstituted material suggested that the receptor was inserted into the membrane in a random orientation, as has been observed previously for the DDM-mediated reconstitution of other membrane proteins.

4.1 - INTRODUCTION

4.1.1 - Lipid Reconstitution Strategies

The reconstitution of purified, detergent-solubilised protein into lipid bilayers is fundamental to the study of the structure and function of membrane proteins in the lipid environment. Five basic strategies have been outlined for the insertion of membrane protein into liposomes: mechanical means, direct incorporation, organic solvents, detergent-mediated and partial vesicle solubilisation (Rigaud *et al.*, 1995).

(i) Mechanical means

Exposure of a phospholipid / protein mixed dispersion to mechanical disruption, for example sonication, can catalyse the insertion of the protein into vesicles. However, this technique is of limited use due to the inactivation of many membrane proteins by sonication and the small size of the resulting proteoliposomes (20-40 nm). The problem of small proteoliposome size was overcome by the combination of sonication with freeze-thaw and this technique was used for the reconstitution of the D-glucose carrier from red blood cells (Kasahara and Hinkle, 1977).

(ii) Direct Incorporation

Some membrane proteins are capable of spontaneously inserting into lipid bilayers of well-defined composition with a strict requirement for acidic phospholipids (Eytan and Broza, 1978). Protein incorporation was found to preferentially occur into a small proportion of the liposomes, which are of small diameter (~20 nm) followed by fusion of the proteoliposomes with the remaining liposomes. This results in proteoliposomes of heterogeneous size and protein content.

(iii) Organic solvent-mediated reconstitution

Organic solvents are widely used to prepare liposomes with large internal aqueous space, for example by using reverse-phase evaporation (Szoka *et al.*, 1980). The method has been applied to the reconstitution of bacteriorhodopsin (Rigaud *et al.*, 1983) where large unilamellar proteoliposomes were formed by the slow evaporation of organic solvent from a water-in-oil emulsion containing both lipid and protein. However, the usefulness of such strategies for the study of membrane proteins has been limited because they require exposure of the protein to organic solvents which often denature the membrane protein.

(iv) Detergent-mediated reconstitutions

The most successful and frequently used strategy for proteoliposome preparation involves the use of detergents since, for most membrane proteins, detergents are required to maintain membrane protein structure outside the lipid environment of the membrane. Detergents are therefore normally present during membrane protein isolation and purification. Protein and lipid are typically co-solubilised to form a mixture of lipid-protein-detergent and lipid-detergent micelles. The detergent is subsequently removed resulting in the formation of unilamellar vesicles with incorporated protein. There are various methods of detergent removal, depending on

the physical properties of the detergent in question, such as the micelle size and the critical micelle concentration (cmc) (Levitzki, 1985; Rigaud *et al.*, 1995). When a detergent with a high cmc is used (e.g. octyl-glucoside (OG), cmc = 10-24 mM) the protein-detergent solution can simply be diluted after the addition of phospholipids. The dilution lowers the detergent concentration below its cmc and the proteoliposomes form spontaneously. Alternatively, dialysis or gel filtration can be used for removal of such detergents. However, if the detergent has a low cmc and/or a large micelle size (e.g. dodecyl-β-D-maltoside (DDM), cmc = 0.1 - 0.2 mM, micelle size ~ 70 kDa), dialysis, dilution and gel filtration are impractical. In this case, active detergent adsorption onto hydrophobic resins such as polystyrene beads (Biobeads SM-2 (Biorad)) has been shown to be effective (Rigaud *et al.*, 1997). Hydrophobic adsorption can also be used for removal of many types of detergent, including those with high cmc.

(v) Partial Vesicle Solubilisation

This method is a variant of detergent-mediated reconstitution where pre-formed lipid vesicles are saturated with detergent at a detergent/lipid ratio experimentally determined to give optimal reconstitution conditions. The physical state of liposomes during the titration with detergent can be followed with turbidity measurements. Figure 4.1 illustrates the phase transitions from liposome to micelle caused by detergent partitioning into bilayers, based on the three stage model proposed previously (Lichtenberg, 1985). During stage I, detergents added to the pre-formed vesicle solution are partitioned into the vesicle membrane until a saturation point is reached. This partitioning leads to an increase in the turbidity of the solution. Further addition of detergent to the saturated vesicles leads to solubilisation of the vesicles and the formation of detergent-lipid mixed micelles (stage II). This stage is combined with a decrease in the turbidity. The start of stage III is characterised by the complete

solubilisation of the lipids and further addition of detergent leads to no change in the turbidity of the solution.

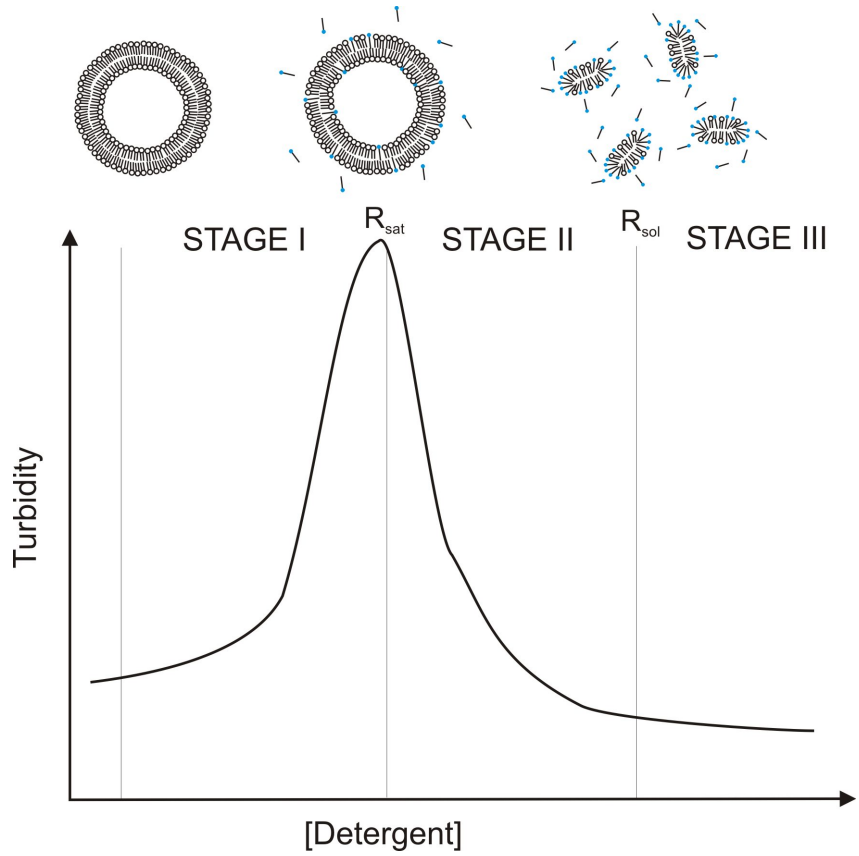

Figure 4.1 – Schematic showing the phase transition from liposome to micelle caused by detergent partitioning into bilayers (three stage model (Lichtenberg, 1985)) and the corresponding turbidity change. In the first stage, detergent begins to partition into the bilayers until the saturation point is reached (R_{sat}). During stage II the liposomes are increasingly solubilised into detergent / lipid mixed micelles, eventually reaching total solubilisation (R_{sol}). Further increase in detergent (stage III) does not change the turbidity of the solution. The turbidity profile is difficult to interpret in terms of liposome morphological changes because it can be related to many parameters, such as changes in the average diameter, the number of particles, viscosity and/or refractive index (Lambert et al., 1998). In addition, electron microscopy studies have shown that intermediate lipid morphologies are highly dependent on the particular detergent used for liposome disruption (Knol et al., 1998) (see below).

The detergent-saturated liposomes appear to favour the partitioning of membrane proteins from solution. The excess detergent can then be removed using the methods already mentioned for detergent-mediated reconstitutions. This approach has been exploited in the reconstitution of several membrane proteins. For example, the reconstitution of the lactose symporter from *S.thermophilus* (LacS) into liposomes

destabilised by DDM or Triton X-100 has been investigated (Knol *et al.*, 1998). DDM was found to markedly disrupt the membrane structure of liposomes (egg yolk phosphatidylcholine / *E.coli* lipids mixture), even at the beginning of the solubilisation process and long, thread-like structures were observed at high DDM : lipid ratios. LacS was found to incorporate with random orientation into the DDM-disrupted vesicles. In contrast, Triton X-100 was found to be far less disruptive to the vesicular bilayer structure and allowed the protein to be inserted in an oriented manner, with the hydrophilic surfaces exposed to the outside of the liposome (Figure 4.2).

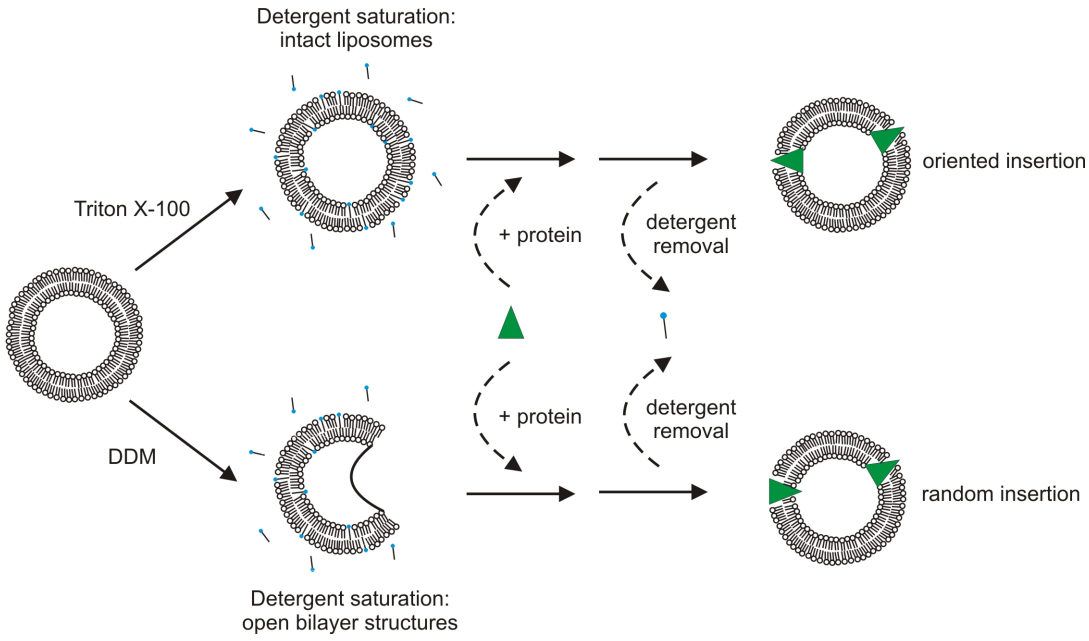

Figure 4.2 – Model for membrane protein reconstitution mediated by DDM or Triton X-100 (Knol *et al.*, 1998). Saturation of unilamellar lipsomes by Triton X-100 maintained closed bilayer structures whilst saturation with DDM caused large perturbations to the lipsomes, with open bilayer structures observed (Knol *et al.*, 1998; Lambert *et al.*, 1998). It has been proposed that membrane proteins will insert unidirectionally into the closed bilayer structures, preferentially penetrating the bilayer with the most hydrophobic surface of the protein. Conversely, membrane proteins could insert into the open structures from both surfaces without the need for the more hydrophilic surfaces to cross the bilayer.

Bacteriorhodopsin has also been successfully reconstituted into detergent-disrupted liposomes (Rigaud *et al.*, 1988; Lambert *et al.*, 1998). In the study by Lambert *et al* (1998), a viscous 'gel-like' phase was found to form during the solubilisation of

liposomes by DDM, which was found to be composed of thread-like multilamellar structures similar to those observed by Knol *et al* (1998). Crucially, rapid detergent removal was found to give optimal protein incorporation and unilamellar lipid morphology, while slow detergent removal was found to give poor incorporation and predominantly multilamellar structures. This was attributed to fast and slow transitions through the gel-like phase respectively and is likely to be an important consideration when reconstituting membrane proteins from DDM-containing buffers.

4.1.2 - Reconstitution of GPCRs

There are numerous examples of successful reconstitutions of purified GPCRs into lipid bilayers and a summary is displayed in Table 4.1. Clearly, the experimental conditions such as detergent type, lipid type, and mode of detergent removal are wide-ranging and specific conditions are likely to be protein-specific. However, general trends can be seen in the literature. With regard to the mode of detergent removal, the majority of the reconstitutions which require removal of the detergent DDM have used the adsorptive polystyrene beads (Biobeads SM-2), likely because the properties of DDM (low cmc, large micelle size) make other forms of detergent removal ineffective (see section 4.1.1). Therefore, this would appear to be the method of choice, especially since it was used for the only other previously reported successful reconstitution of NTS1 (Luca *et al.*, 2003).

Table 4.1 – Examples of the methods used for the lipid-reconstitution of recombinantly expressed GPCRs.

Receptor	Expression System	Detergents	Detergent removal	Lipids	Reference
α-Factor receptor (yeast)	*S.cerevisiae*	DDM	Biobeads SM-2	POPC / POPG (3:2)	(David *et al.*, 1997)
β-adrenergic receptor (turkey)	Sf9	Digitonin, Na cholate	Gel filtration	POPE / bovine PS (3:2)	(Parker *et al.*, 1991)
β_2-adrenergic receptor (human)	*E.coli*	Dodecanoyl sucrose	Biobeads SM-2	POPC	(Hampe *et al.*, 2000)
Muscarinic cholinergic receptor m1 (human)	Sf9	Digitonin, Na cholate	Gel filtration	POPE / bovine PS (3:2)	(Parker *et al.*, 1991)
Muscarinic cholinergic receptor m2 (human)	Sf9	Digitonin, Na cholate	Gel filtration	POPE / bovine PS (3:2)	(Parker *et al.*, 1991)
Neurotensin Receptor 1 (rat)	*E.coli*	DDM, CHAPS, CHS	Biobeads SM-2	Porcine brain polar extract	(Luca *et al.*, 2003)
PACAP receptor (Human)	Sf9	Digitonin	Dialysis	Bovine brain extract	(Ohtaki *et al.*, 1998)
Parathyroid hormone receptor (human)	COS-7	DDM	Sucrose gradient (dilution)	POPC / PE / DMPG (6:3:1)	(Shimada *et al.*, 2002)
Substance P receptor (rat)	Sf9	CHAPS	Gel filtration	PC (soybean)	(Kwatra *et al.*, 1993)

Abbreviations: COS = kidney african green monkey cell, DMPG = dimyristoyl phosphatidylglycerol, PACAP = pituitary adenylate cyclase-activating polypeptide, PC = phosphatidylcholine, PE = phosphatidylethanolamine, PS = phosphatidylserine, POPC = palmitoyl-oleoyl-phosphatidylcholine, POPE = palmitoyl-oleoyl-phosphatidylethanolamine, POPG = palmitoyl-oleoyl-phosphatidylglycerol, Sf = Spodoptera frugiperda,

The choice of lipid composition for reconstitution is highly varied. Successful reconstitution into simple POPC or PC bilayers has been reported (Kwatra *et al.*, 1993; Hampe *et al.*, 2000), while more complex mixtures which include charged and non-lamellar phase (Hexagonal H_{II} phase) forming lipids, or natural extracts, are used in the remaining cases. Indeed, other studies have suggested that specific lipid types can play a key role in receptor activity and function. For example, the non-lamellar-forming lipid phosphatidylethanolamine (PE) was found to enhance rhodopsin photoactivation and transducin binding in model bilayers (Botelho *et al.*, 2002; Alves *et al.*, 2005). In addition, G proteins themselves have been found to have preferential affinity for certain lipid compositions. Heterotrimeric G_i protein and $G_{\beta\gamma}$ dimers were found to bind markedly more strongly to model membranes in the presence of non-lamellar phases of PE. Conversely, activated G protein α subunits showed an opposite membrane binding behaviour, with a marked preference for lamellar membranes (Vogler *et al.*, 2004). Lipid composition could therefore play a crucial role in both receptor activity and downstream signalling. The previous reported reconstitution of NTS1 used porcine brain polar lipid extract, which is a complex mixture of lamellar-forming, non-lamellar-forming and charged phospholipids (Table 4.2) and this would therefore be a good a starting point for reconstitution attempts with the fluorescently tagged protein.

Table 4.2 : Lipid composition of the Brain Polar Lipid Extract (Porcine). Data supplied by Avanti Polar Lipids inc.

Component	Percent (weight)
Phosphatidylethanolamine	33.1
Phosphatidylserine	18.5
Phosphatidylcholine	12.6
Phosphatidic Acid	0.8
Phosphatidylinositol	4.1
Other	30.9

4.1.3 - Aims

The aim of this study is to reconstitute purified, detergent-solubilised, fluorescence-tagged NTS1 into phospholipid liposomes. This is a necessary prerequisite for the study of receptor multimerisation in *in vitro* lipid systems (Chapter 5). Parameters such as the detergent : lipid ratio used for liposome disruption and lipsome phospholipid composition will be optimised and the success of the reconstitutions will be assessed using receptor fluorescence, which gives a measure of total fluorescent receptor reconstituted, and radioligand binding activity, which gives a measure of the amount of reconstituted receptor that is in a conformation capable of binding ligand.

4.2 - MATERIALS AND METHODS

4.2.1 - Lipid Preparation

Porcine brain polar lipid extract and POPC (Avanti Polar Lipids) were dissolved in chloroform : methanol (50 : 50 (v/v)) at a concentration of 5 mg/ml and dried to a lipid film under a stream of nitrogen gas. Remaining trace solvent was removed by dessication under vacuum for 3 h. Lipids were resuspended at 5 mg/ml in buffer A (50 mM Tris pH 7.4, 200 mM NaCl, 1 mM EDTA) by pipetting. Small unilamellar vesicles (SUV) were formed by bath sonication (three 2 minute bursts). Large multilamellar vesicles were then formed by 10 freeze-thaw cycles. Unilamellar vesicles of uniform size were generated by extrusion of the freeze-thawed material through 0.4 μm and 0.1 μm polycarbonate membranes (Whatman) using a mini-extruder (Avanti Polar Lipids). 11 passes through each membrane pore size has been previously found to yield unilamellar vesicles of uniform size distribution (MacDonald *et al.*, 1991).

4.2.2 - Vesicle Disruption by DDM

Vesicles were prepared as above and sufficient DDM stock solution (10 % (w/v)) added to give a final concentration of DDM between 0 and 20 mM. Lipid solutions were allowed to equilibrate at room temperature for 6 h before measuring the turbidity at a wavelength of 500 nm.

4.2.3 - Reconstitution of Neurotensin Receptor 1

All steps were carried out at 4 °C unless otherwise stated. Lipid solutions were prepared as above. DDM stock solution was added to give the desired DDM : lipid effective molar ratio (R_{eff}) as calculated using equation 4.1:

$$R_{eff} = \left(\frac{[\text{detergent}] - [\text{cmc}]}{[\text{L}]} \right) \qquad \text{Equation 4.1}$$

Where [L] is the lipid concentration and the effective detergent concentration is defined as ([detergent] – [cmc]), since the cmc is the concentration of monomeric detergent unable to participate in solubilisation.

Solutions were allowed to equilibrate for 3 h at room temperature, cooled to 4 °C and sufficient volume added to aliquots of purified NTS1 (2 μM) to yield the desired protein : lipid ratio. After incubation for 1 h, pre-washed Biobeads SM-2 (Biorad) were added to the protein / lipid mixture to a final concentration of 120 mg/ml and the sample incubated overnight with gentle agitation to mediate detergent removal.

Biobeads were removed and the reconstituted samples layered on top of a discontinuous sucrose gradient (5 % steps, 0-35 % sucrose (w/v) in 50 mM Tris pH 7.4, 200 mM NaCl, 1 mM EDTA) and centrifuged overnight at 100,000 g, 4 °C (Beckman SW41 Ti rotor). Fractions from the gradient were collected and analysed by SDS-PAGE. This usually confirmed the formation of a tight band on the gradient which contained reconstituted receptor. Fractions containing receptor were pooled and stored at 4 °C.

Proteoliposome density was estimated from the position of the reconstituted bands on the sucrose gradient using the equation for the density of sucrose between 0 °C and 30 °C (Barber, 1966) (Equation 4.2):

$$\rho(T) = (B_1 + B_2T + B_3T^2) + (B_4 + B_5T + B_6T^2)Y + (B_7 + B_8T + B_9T^2)Y^2 \qquad \text{Equation 4.2}$$

Where ρ = density of the sucrose solution (kg/dm^3), T = Temperature (°C), Y = weight of sucrose in solution (w/v) and $B_{1\text{-}9}$ = constants (B_1 = 1.00037, $B_2 = 3.96805 \times 10^{-5}$, $B_3 = -5.85133 \times 10^{-6}$, B_4 = 0.389824, $B_5 = -1.05789 \times 10^{-3}$, $B_6 = 1.23928 \times 10^{-5}$, B_7 = 0.170976, $B_8 = 4.75301 \times 10^{-4}$, $B_9 = -8.92397 \times 10^{-6}$). An estimation of the

lipid : protein (w/w) ratio was calculated given that the calculated partial specific volume (vbar) has contributions from vbar(lipid) and vbar(protein), where vbar(lipid) was estimated from sucrose density gradient centrifugation of BPL-only samples to be 0.986 ± 0.003 ml/g and vbar(protein) was calculated as 0.734 ml/g from the amino acid composition of NTS1-eCFP/eYFP using the method of Cohn and Edsall (Cohn and Edsall, 1943):

$$vbar_{25} = \frac{\sum n_i M_i vbar_i}{\sum n_i M_i}$$

Equation 4.3

Where n is the number of moles of the *i*th component (each amino acid), M is its molecular weight and $vbar_{25}$ is the partial specific volume at a temperature of 25 °C. This value for vbar was then adjusted for the temperature of 4 °C, which was the temparature at which the sucrose density gradient centrifugation took place (Durchschlag, 1986):

$$vbar_T = vbar_{25} + 4.25 \times 10^{-4} \left(T - 25\right)$$

Equation 4.4

Where T is the temperature (°C) and $vbar_T$ is the partial specific volume at temperature, T.

4.2.4 - Resolubilisation

Aliquots of reconstituted samples were resolubilised to expose any binding sites which could have been occluded after reconstitution. 150 µl of 2 x solubilisation buffer and 50 µl of DDM / CHS (10 % / 1 % (w/v)) were added to 200 µl of reconstituted sample and incubated for 1 h at 4 °C to mediate solubilisation of reconstituted receptor.

4.2.5 - Ligand Binding Assay

A ^{3}H-NT (New England Nuclear) radioligand binding assay was used to quantify amounts of active receptor in reconstituted and resolubilised samples (Appendix A3).

4.2.6 - In-gel fluorescence

Reconstituted samples were separated by SDS-PAGE and visualised using in-gel fluorescence (section 3.2.6). Bands were quantified using gel densitometry (ImageJ, NIH) with reference to fluorescent protein standards.

4.2.7 - Tryptic Digestion

Reconstituted samples were subjected to trypsin digestion to determine receptor orientation. Digestion reactions were carried out at 4 °C. Trypsin (Sigma Aldrich) was added to reconstituted samples to a final concentration of 40 μg/ml. Aliquots of cleavage reaction were removed at t = 1, 5, 15, 25 min, added to soybean trypsin inhibitor (400 μg/ml) and incubated on ice in order to quench the cleavage reaction. As a positive control, a detergent-solubilised sample was digested in the same manner. As a negative control, trypsin was denatured by heating to 95 °C for 15 min, added to a separate reconstituted sample to a concentration of 40 μg/ml and incubated for 25 min before quenching. Cleavage reactions were analysed by SDS-PAGE and visualised by in-gel fluorescence.

4.3 - RESULTS AND DISCUSSION

4.3.1 - Detergent disruption of brain polar lipid liposomes.

Recent successful reconstitution of integral membrane proteins, including GPCRs, has exploited the method of protein insertion into detergent-destabilised liposomes (Paternostre *et al.*, 1988; Knol *et al.*, 1998). This method exploits the observation that detergent-saturated liposomes favour the partitioning of membrane proteins from solution, and is the technique that was used to successfully reconstitute the non-fluorescently tagged NTS1B construct into brain polar lipid vesicles (Luca *et al.*, 2003). The established approach for the optimisation of membrane protein reconstitution into detergent-destabilised liposomes involves the stepwise addition of detergent to preformed liposomes and the measurement of protein incorporation at each stage of the solubilisation process (Rigaud *et al.*, 1988; Rigaud *et al.*, 1995; Knol *et al.*, 1998). The profile of vesicle disruption by DDM was monitored in order to determine the lipid saturation and solubilisation characteristics, using a method similar to that employed by Lambert *et al* (1998). The disruption of porcine brain polar lipid (BPL) vesicles by DDM was followed by monitoring of the optical density at 500 nm after incubation with various concentrations of DDM (Figure 4.3).

The solubilisation of BPL by DDM appears to broadly follow the three stage model proposed previously (Lichtenberg, 1985) (Figure 4.1). During stage I, detergent molecules partition between the aqueous buffer and the bilayer. This stage is usually combined with an increase in optical density, which reaches a peak where the lipids are saturated with detergent (R_{sat}). At this point, stage II begins, where a further increase in detergent induces gradual liposome solubilisation and a corresponding decrease in optical density. Stage III is characterised by complete solubilisation of the lipid, at

which point the optical density has reached a minimum value (R_{sol}) due to an optically transparent solution of mixed micelles.

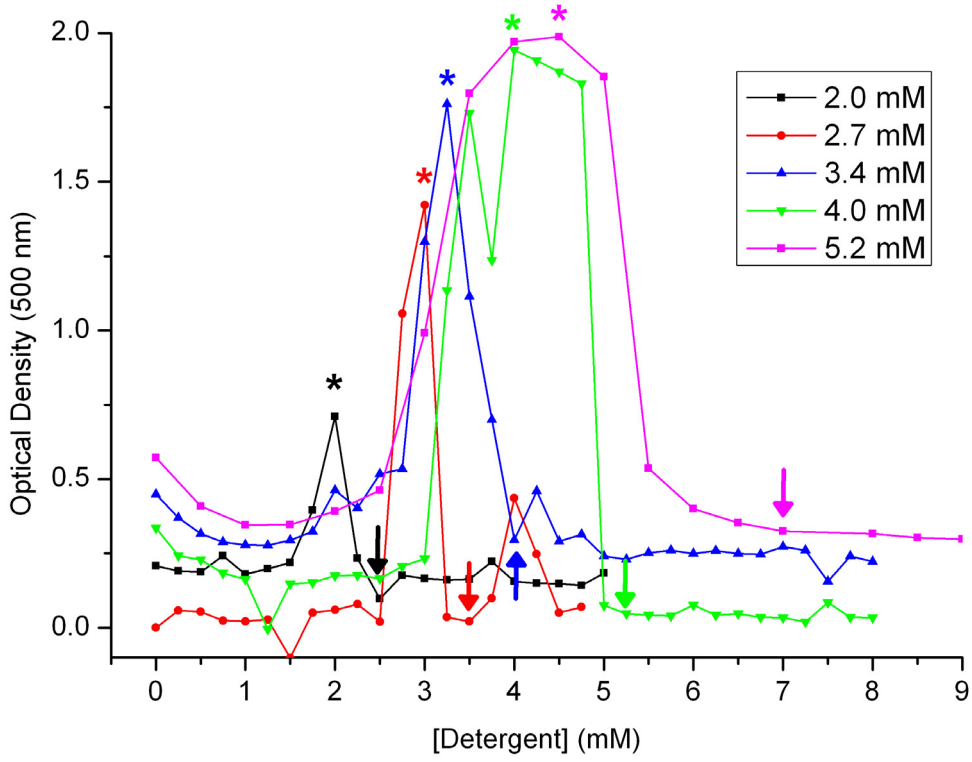

Figure 4.3: Changes in the turbidity of liposome suspensions upon addition of increasing amounts of DDM. Liposomes of uniform size were generated by extrusion through 0.4 µm and 0.1 µm nucleopore filter membranes. They were diluted to the stated concentrations and treated with different amounts of DDM. Optical densities were measured at 500 nm after equilibration at room temperature for 6 h. The onset of solubilisation (R_{sat}, labelled *) and total solubilisation (R_{sol}, arrows) are marked for each lipid concentration.

The solubilisation process can be further analysed quantitatively. Rearrangement of equation 4.1 enables a linear relationship between detergent and lipid concentration to be derived (Equation 4.5):

$$[\text{detergent}] = R_{eff}[L] + [\text{cmc}] \qquad \text{Equation 4.5}$$

Therefore, in order to calculate the effective molar ratios for R_{sat} and R_{sol}, the detergent concentrations corresponding to the onset of solubilisation (maximum turbidity) and total solubilisation were plotted against the molar concentration of lipid (Figure 4.4).

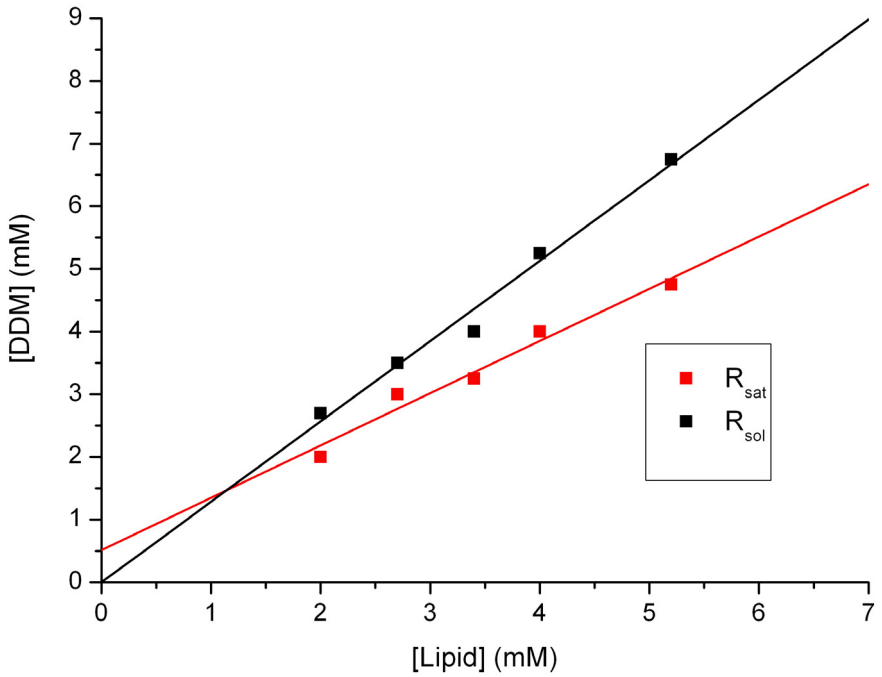

Figure 4.4 : Determination of the R_{sat} and R_{sol} effective molar ratios. The values for onset of solubilisation and total solubilisation were obtained from Figure 4.3 according to Equation 4.5. Values obtained from linear fits to the data were $R_{sat} = 0.9 \pm 0.1$ and $R_{sol} = 1.3 \pm 0.1$.

The values obtained from this analysis for R_{sat} and R_{sol} were 0.9 ± 0.1 and 1.3 ± 0.1 respectively. There is no data in the literature for disruption of BPL liposomes with DDM; existing data for disruption of POPC liposomes has shown values for R_{sat} and R_{sol} of ~1 and ~1.6 respectively (Lambert *et al.*, 1998). Therefore it appears that the relatively complex brain polar lipid mixture does not alter the value for R_{sat} significantly, but that R_{sol} is decreased. A rationale for this observation could be the destabilising effect caused by the large proportion of non-lamellar forming lipids present in the BPL mixture (Table 4.2). However, for this hypothesis to be confirmed, a more rigorous experiment involving the supplementation of POPC lipid with non-lamellar forming lipids would need to be carried out.

In addition, it can be seen that DDM has a particularly high solubilising capacity as illustrated by the relatively low R_{sol} and small difference between the R_{sat} and R_{sol} effective concentrations. This characteristic, relative to other non-ionic detergents such

as OG (R_{sat} = 1.3, R_{sol} = 3.8) and Triton X-100 (R_{sat} = 0.64, R_{sol} = 2.5) (Paternostre *et al.*, 1988), has previously been observed for disruptions of POPC by DDM (de la Masa and Parra, 1997).

4.3.2 - Optimisation of NTS1Y Reconstitution

(i) Detergent : lipid ratio

The efficiency of reconstitution into destabilised, pre-formed lipid vesicles has previously been shown to be dependent on the effective concentration of detergent used for destabilisation (Rigaud *et al.*, 1988; Knol *et al.*, 1998), with optimal incorporation into detergent-saturated liposomes observed. Reconstitution of non-fluorescent NTS1B into detergent-destabilised lipid vesicles has been reported using a BPL extract followed by detergent removal using biobeads (Luca *et al.*, 2003). This approach was therefore used as a starting point for the reconstitution of purified, detergent-solubilised NTS1Y and the concentration of detergent used for destabilisation of the lipid vesicles was varied in order to determine the optimal condition.

Proteoliposomes were isolated from the reconstitution samples using a sucrose density gradient (Figure 4.5a). The presence of a single, relatively tight band on the gradients suggested that the receptor was incorporated into the liposomes and that the resulting proteoliposome population for each of the reconstitutions was relatively homogenous with respect to lipid : protein ratio. In addition, the position on the gradient, and consequently the lipid : protein ratio, seemed to be unaffected by the DDM : lipid ratio used for the liposome disruption. In-gel fluorescence of samples from the gradients confirmed the presence of NTS1Y in the proteoliposome band (Figure 4.5b).

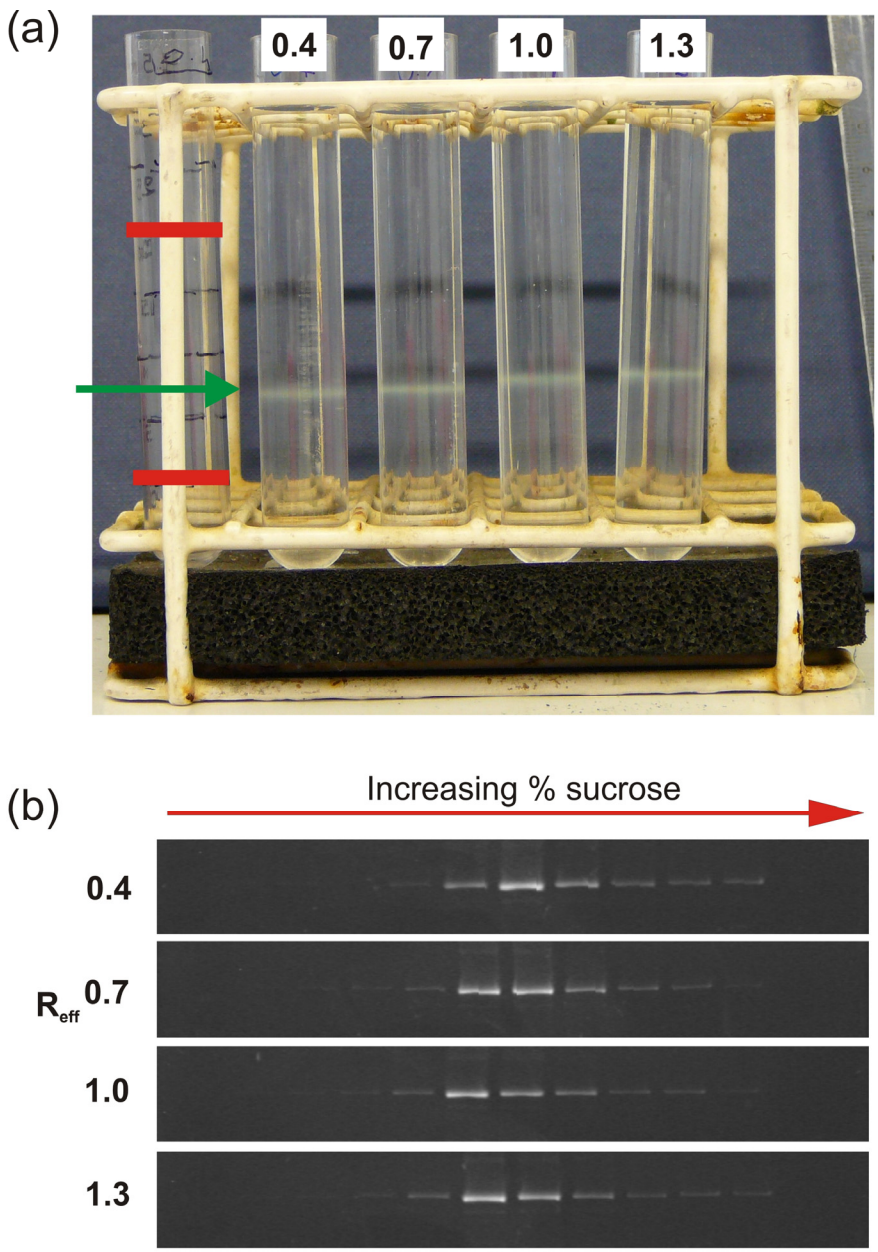

Figure 4.5 – Isolation of reconstituted NTS1Y using sucrose density gradient centrifugation. NTS1Y was reconstituted into BPL liposomes at a lipid : protein ratio of 2000 : 1. (a) The reconstitutions were layered on top of sucrose gradients (0 – 35 %) and centrifuged at 100,000 g for 16 h. The tubes are shown post-centrifugation, labelled with the effective DDM : lipid ratios (R_{eff}) used for liposome disruption (prior to the addition of protein). Discrete proteoliposome bands can be seen in each tube at a sucrose concentration of 21.6 ± 0.4 % (green arrow). 0.5 ml fractions were taken (between the red lines) which were analysed by in-gel fluorescence. (b) In-gel fluorescence of the sucrose gradient samples. Equal volumes of each gradient fraction were loaded into each lane. The fluorescent receptor is present in each tube at the location of the proteoliposome band.

The fractions from the sucrose gradient which contained NTS1Y were pooled. The efficiency of NTS1Y reconstitution was assessed using densitometry of SDS PAGE gels visualised by in-gel fluorescence, which gives a measure of total fluorescent protein

incorporation, and radioligand binding assay, which gives a measure of the amount of reconstituted protein which is able to bind NT ligand (Table 4.3).

Table 4.3 – Reconstitution of NTS1Y into BPL lipid vesicles. Reconstitutions were carried out using different effective DDM : lipid ratios for disruption of the lipid vesicles prior to addition of protein (512.7 pmol (fluorescence), 121.2 pmol (ligand binding assay)). Fractions from the sucrose gradients which contained receptor were pooled and analysed by in-gel fluorescence and radioligand binding assay.

	In-gel fluorescence		Activity Assay	
DDM : Lipid Ratio (R_{eff})	pmol	% recovery†	pmol	% recovery†
0.4	185.6 ± 12.9	36.2 ± 6.9	27.7 ± 0.3	19.1 ± 2.5
0.7	177.3 ± 10.1	34.6 ± 5.7	33.0 ± 0.6	22.7 ± 3.0
1.0	181.1 ± 8.3	35.3 ± 4.6	34.9 ± 1.2	24.0 ± 3.2
1.3	205.7 ± 8.0	40.1 ± 4.4	38.4 ± 0.6	26.4 ± 3.5

† The percentage recovery for in-gel fluorescence and activity are relative to the total fluorescence and activity measured in the detergent sample which was used for the reconstitution as determined by in-gel fluorescence and radioligand binding assay respectively.

The results in Table 4.3 confirm the successful reconstitution of NTS1Y which retained both fluorescence and ligand-binding activity. The percentage recoveries, relative to the starting detergent-solubilised samples which were added to the reconstitutions, show an approximate recovery of fluorescence of 35 – 40 % and an approximate recovery of activity of 20 – 25 %. Most other published examples of GPCR reconstitution fail to report the amount of receptor lost during the reconstitution process. However, the value of approximately 50 % reported for the human PACAP receptor (Ohtaki *et al.*, 1998) (see Table 4.1) suggests the level of incorporation for NTS1Y is reasonable.

The variation of the effective DDM : lipid ratio used for lipid disruption appears to have no significant affect on the efficiency of incorporation of NTS1Y, as measured by both fluorescence and ligand binding activity. A similar result was observed by Knol *et al* (1998) for the reconstitution of a lactose symporter from *S. thermophilus* (LacS) into DDM-disrupted vesicles, where variation of the DDM : lipid ratio between R_{sat} and R_{sol} caused only a small decrease in the incorporation of protein from 85 – 80 %. Interestingly, as discussed in section 4.1.1, the same authors reported that there was no oriented protein incorporation when reconstituting using DDM-disrupted vesicles (as opposed to Triton X-100) which was attributed to the solubilising properties of DDM, which has been found to be highly disruptive to the bilayer structure relative to other detergents. This could explain the discrepancy between the recovery of NTS1Y fluorescence (35 – 40 %) and the recovery of NTS1Y ligand binding activity (20 – 25 %). The in-gel fluorescence measures the total receptor present, whilst the radioligand binding assay only measures the number of receptor molecules oriented with ligand binding sites exposed to the outside of the vesicle. Therefore, if random orientation of NTS1Y in the membrane is assumed (see section 4.3.4), the amount of receptor measured by fluorescence should be double that measured by ligand-binding.

(ii) Lipid specificity

Whilst reconstitution of NTS1Y into the BPL extract was successful, other GPCRs have been reconstituted into far simpler lipid compositions including bilayers comprising the phospholipid phosphatidylcholine (PC) only (Table 4.1). Reconstitution into a simple lipid mixture might be advantageous for the analysis of the receptor in *in vitro* systems since it would give finer control over the lipid composition when used in place of the natural lipid extracts such as BPL, which have an element of variability and 'unknown' components in their composition (Table 4.2). Therefore, reconstitution of NTS1Y into

POPC-only bilayers and POPC supplemented with BPL (50 : 50 (w/w)) was attempted using the same protocol as used in the previous section. Proteoliposomes were isolated from the reconstitution samples using a sucrose density gradient and samples from the gradient were analysed for the presence of receptor using in-gel fluorescence (Figures 4.6 and 4.7).

Both lipid types showed evidence of proteoliposome bands on the sucrose gradient, and the presence of reconstituted receptor was confirmed by the in-gel fluorescence of the sucrose gradient fractions. However, the POPC-only band was relatively diffuse across the gradient, indicating that the protoliposome population had a relatively heterogenous lipid : protein ratio. The proteoliposome band for the BPL/POPC 50 : 50 reconstitution was far tighter and similar to that observed for BPL only (Figure 4.5). However, a distinct faint band was visible in each tube immediately above the main proteoliposome band, perhaps indicating some heterogeneity.

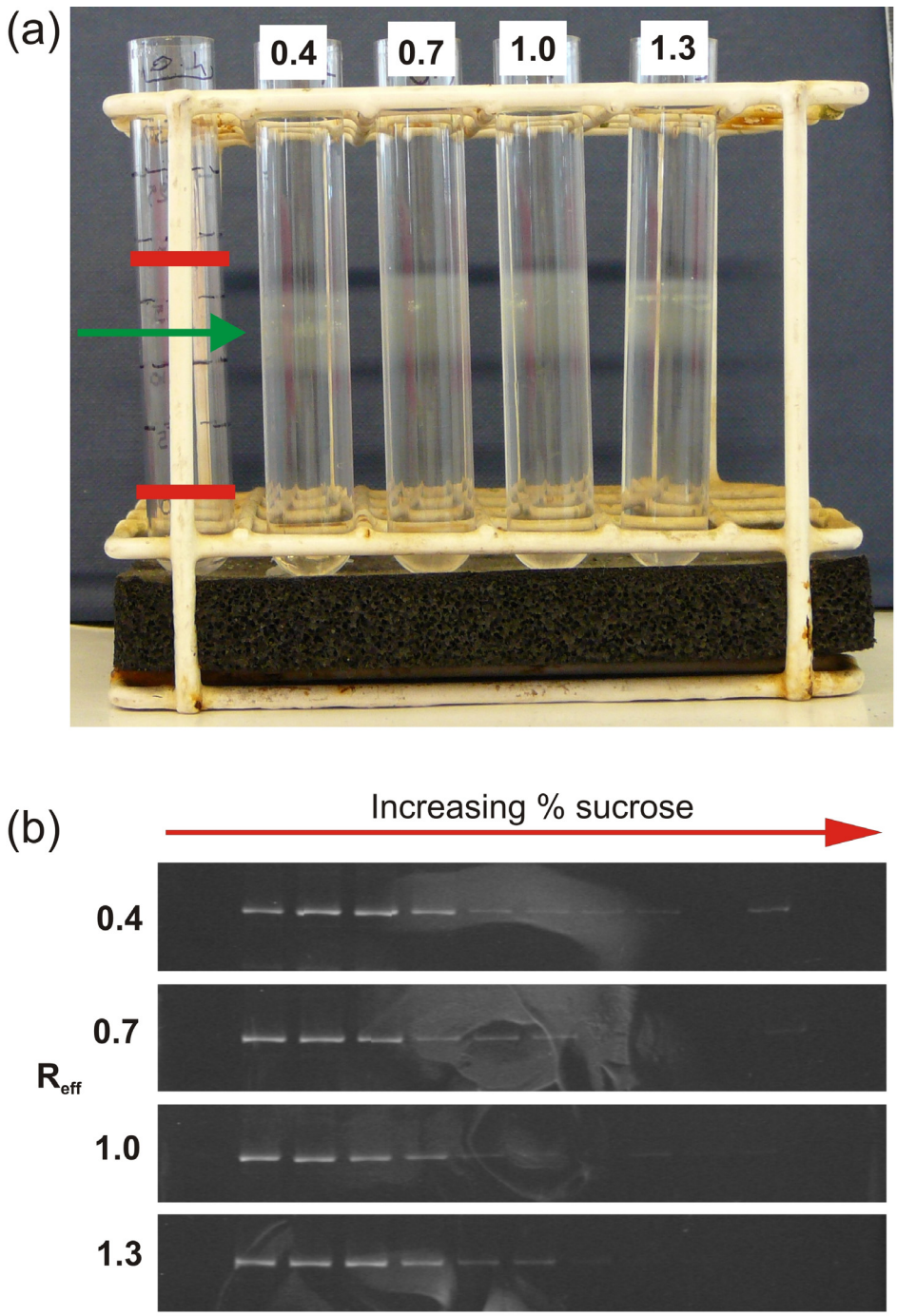

Figure 4.6 – Reconstitution of NTS1Y into POPC liposomes at a lipid : protein ratio of 2000 : 1. (a) The reconstitutions were layered on top of sucrose gradients (0 – 35 %) and centrifuged at 100,000 g for 16 h. The tubes are shown post-centrifugation, labelled with the effective DDM : lipid ratios (R_{eff}) values used for liposome disruption (prior to the addition of protein). A diffuse proteoliposome band can be seen in each tube between sucrose concentrations of 13 – 19 % (green arrow). Between the red lines, 0.5 ml fractions were taken which were analysed by in-gel fluorescence. (b) In-gel fluorescence of the sucrose gradient samples. Equal volumes of each gradient fraction were loaded into each lane. The fluorescent receptor is present in each tube at the location of the proteoliposome band.

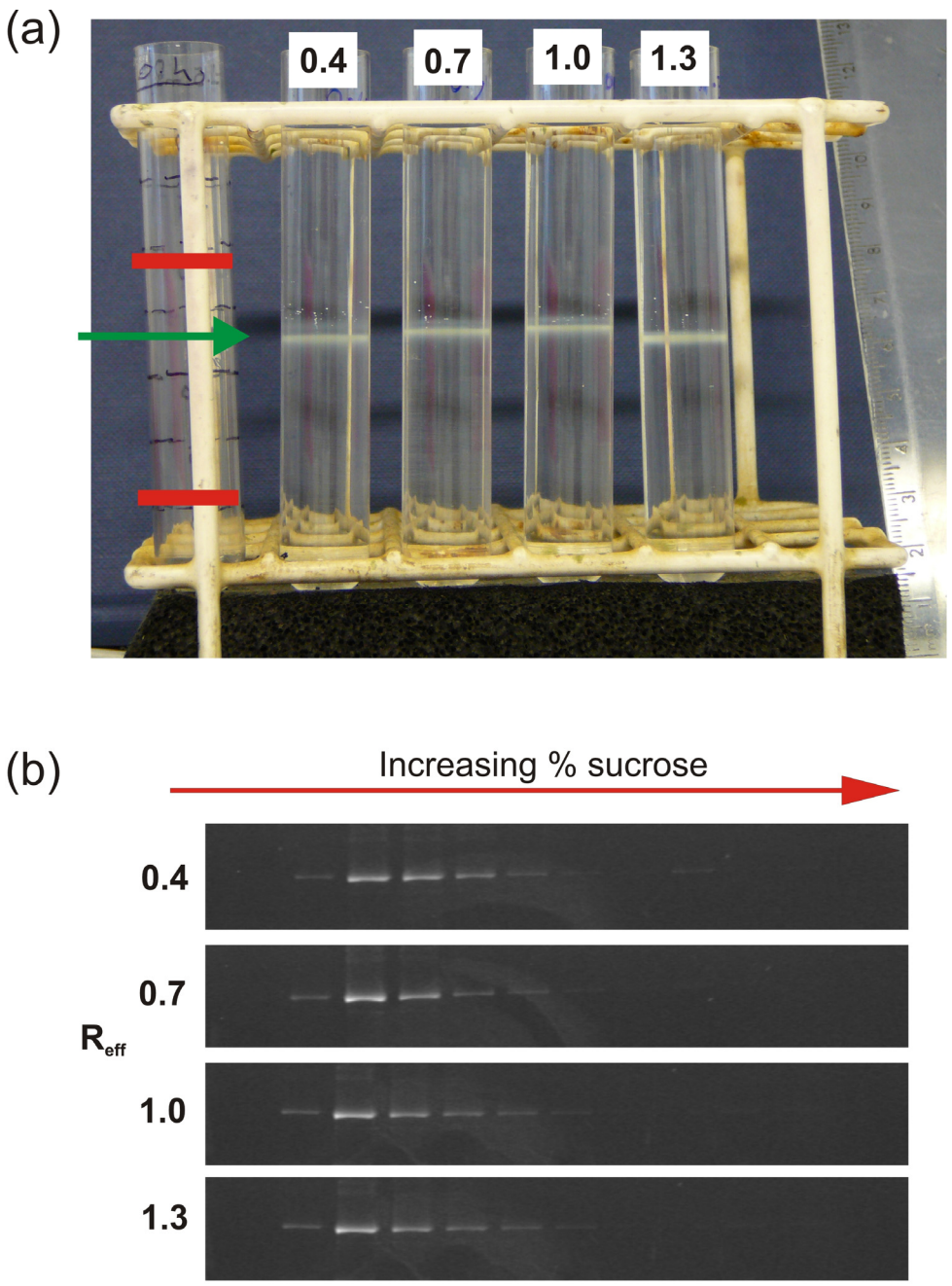

Figure 4.7 – Reconstitution of NTS1Y into POPC/BPL liposomes (50 : 50 w/w) at a lipid : protein ratio of 2000 : 1. (a) The reconstitutions were layered on top of sucrose gradients (0 - 35 %) and centrifuged at 100,000 g for 16 h. The tubes are shown post-centrifugation, labelled with the effective DDM : lipid ratios (R_{eff}) values used for liposome disruption (prior to the addition of protein). A proteoliposome band can be seen in each tube at a sucrose concentration of 16.3 ± 0.4 % (green arrow). Between the red lines, 0.5 ml fractions were taken which were analysed by in-gel fluorescence. (b) In-gel fluorescence of the sucrose gradient samples. Equal volumes of each gradient fraction were loaded into each lane. The fluorescent receptor is present in each tube at the location of the proteoliposome band.

Fractions from the gradients which contained receptor were combined and analysed by in-gel fluorescence and radioligand binding assay using the same protocol as previously

used for the BPL-only reconstitutions. The results, including the data for BPL only as a comparison, are shown in Table 4.4.

Table 4.4 – Summary of the reconstitution of NTS1Y into different lipid compositions. Reconstitutions were carried out using different DDM : lipid effective molar ratios for disruption of the lipid vesicles prior to addition of protein (512.7 pmol (fluorescence), 121.2 pmol (ligand binding assay)) [c]. Fractions from the sucrose gradients which contained receptor were pooled and analysed by in-gel fluorescence and radioligand binding assay.

		In-gel fluorescence		Activity Assay	
Lipid Composition	**DDM : Lipid Ratio (R_{eff})**	**pmol**	**% recovery[†]**	**pmol**	**% recovery[†]**
BPL	0.4	185.6 ± 12.9	36.2 ± 6.9	27.7 ± 0.3	19.1 ± 2.5
	0.7	177.3 ± 10.1	34.6 ± 5.7	33.0 ± 0.6	22.7 ± 3.0
	1.0	181.1 ± 8.3	35.3 ± 4.6	34.9 ± 1.2	24.0 ± 3.2
	1.3	205.7 ± 5.0	40.1 ± 3.1	38.4 ± 0.6	26.4 ± 3.5
POPC	0.4	210.9 ± 14.2	41.1 ± 6.8	ND[b]	ND[b]
	0.7	175.8 ± 12.0	34.3 ± 6.4	ND[b]	ND[b]
	1.0	198.9 ± 13.3	38.8 ± 6.7	ND[b]	ND[b]
	1.3	209.5 ± 14.1	40.9 ± 6.7	ND[b]	ND[b]
BPL/POPC	0.4	233.7 ± 14.2	45.6 ± 2.8	23.1 ± 1.0	15.9 ± 2.2
	0.7	245.1 ± 22.7	47.8± 4.4	15.0 ± 2.0	10.3 ± 2.0
	1.0	243.4 ± 22.5	47.5 ± 4.4	15.4 ± 0.8	10.6 ± 1.5
	1.3	312.2 ± 28.7	60.9 ± 5.6	4.8 ± 1.1	3.3 ± 0.9

[†] The percentage recovery for in-gel fluorescence and activity are relative to the total fluorescence and activity measured in the detergent sample which was used for the reconstitution as determined by in-gel fluorescence and radioligand binding assay respectively.

[b] ND = not detectable

[c] Each reconstitution used an equal volume of purified receptor from a single NTS1Y protein preparation.

The efficiency of recovery of receptor fluorescence appears to be relatively independent of the lipid composition used, with the 50 : 50 BPL/POPC mix giving a slightly higher yield. However, this is in marked contrast to the ligand-binding assay results. The reconstitution using POPC showed absolutely no ligand binding activity. When the

50 : 50 BPL/POPC mix was used, approximately 40 % of the ligand binding activity was recovered relative to the BPL-only reconstitution. Further experiments revealed that the lack of binding activity could not be attributed to binding site occlusion. The reconstitutions were resolubilised in buffer containing the detergents DDM (1 % (w/v)) and CHS (0.1 % (w/v)) and the ligand binding activity subsequently measured. Whilst the BPL and BPL/POPC samples showed ligand binding which was comparable with that observed prior to resolubilisation (in fact slightly increased, mean recovery after resolubilisation = 111.8 ± 4.6 %), the POPC sample still showed no ligand-binding activity. If the lack of ligand binding activity in the POPC-reconstituted sample was due to binding site occlusion on the inside of the proteoliposome, it would be expected that detergent solubilisation would make such sites accessible to ligand. Given that the recovery of fluorescence in the POPC samples is comparable to the BPL samples, it can be concluded that the change in lipid composition is not adversely affecting insertion of the receptor into the bilayer. Rather, it seems that the receptor is being irreversibly denatured by reconstitution into the POPC only liposomes and that components in the BPL mix are required to maintain receptor stability. For example, the high proportion of PE, a non-lamellar forming phospholipid, contained in the BPL extract, could be required by NTS1. As discussed in section 4.1.2, the GPCR rhodopsin (Botelho *et al.*, 2002; Alves *et al.*, 2005) and heterotrimeric G proteins (Vogler *et al.*, 2004) have been shown to have a non-lamellar forming lipid-specificity.

Therefore, the BPL extract appears to be the optimal lipid composition of those studied in terms of efficiency of incorporation of active, ligand-binding NTS1Y.

4.3.3 - Reconstitution of TeV-cleaved receptor

Functional studies will ideally be carried out using the TeV-cleaved receptor, which lacks the MBP and TrxA-His10 fusions. Therefore, reconstitution of purified, TeV-cleaved

receptor (T43NTS1-eCFP) into DDM-disrupted BPL liposomes was carried out using the same protocol. Proteoliposomes were isolated from the reconstitution reactions using sucrose density gradient centrifugation (Figure 4.8).

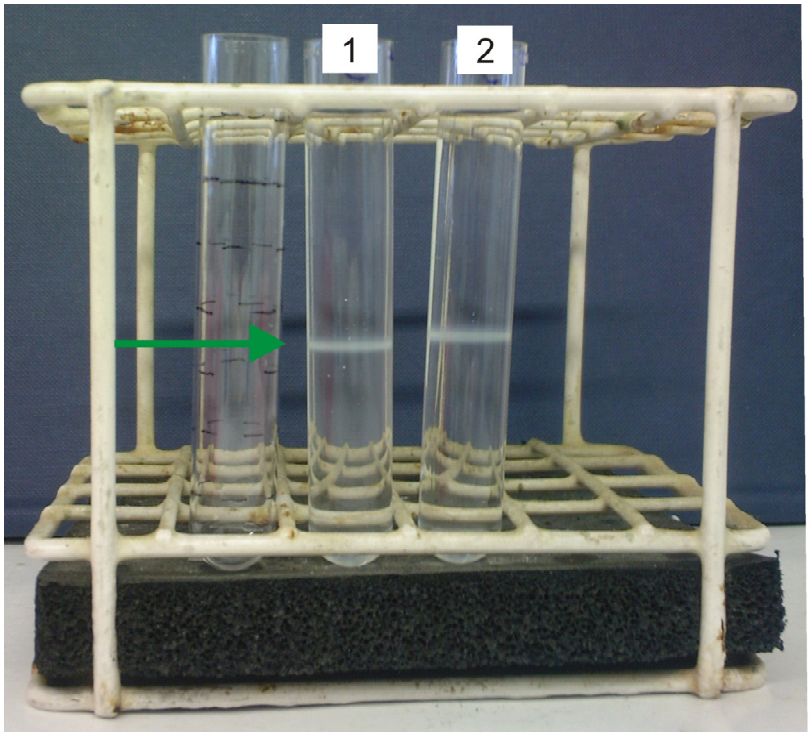

Figure 4.8 – Reconstitution of T43NTS1-eCFP into BPL liposomes at a lipid : protein ratio of 2000 : 1. The reconstitutions were layered on top of sucrose gradients (0 – 35 %) and centrifuged at 100,000 g for 16 h. The tubes from two separate reconstitutions (labelled 1 and 2), carried out using the same conditions, are shown post- centrifugation. An effective DDM : lipid ratio (R_{eff}) of 0.7 was used for liposome disruption (prior to the addition of protein). A proteoliposome band can be seen in each tube at a sucrose concentration of 17.6 ± 0.6 % (green arrow).

The presence of the discrete proteoliposome band on the gradient suggested that the reconstitution of the cleaved protein was successful. The position on the gradient (17.6 ± 0.6 %) corresponded to a lipid : protein molar ratio of 489 ± 34. The area of the gradient containing the band was pooled and analysed by in-gel fluorescence and radioligand binding assay, confirming the presence of TeV-cleaved receptor in the proteoliposome samples which was both fluorescent and ligand binding (Table 4.5).

Table 4.5 – Summary of the reconstitution of T43NTS1-eCFP into BPL liposomes. Reconstitutions were carried out using a DDM : lipid effective molar ratio of 0.7 for disruption of the lipid vesicles prior to addition of protein (693.9 pmol (fluorescence), 142.3 pmol (ligand binding assay)). Fractions from the sucrose gradients which contained receptor were pooled and analysed by in-gel fluorescence and radioligand binding assay. The sample number corresponds to the tube number in Figure 4.8.

		In-gel fluorescence		Activity Assay	
Lipid Composition	Sample	pmol	% recovery†	pmol	% recovery†
BPL	1	394.4 ± 52.0	52.3 ± 7.1	42.0 ± 1.4	24.4 ± 2.8
	2	353.2 ± 94.6	46.9 ± 12.6	43.2 ± 0.6	25.1 ± 2.8

† The percentage recovery for in-gel fluorescence and activity are relative to the total fluorescence and activity measured in the detergent sample which was used for the reconstitution as determined by in-gel fluorescence and radioligand binding assay respectively.

The percentage recoveries of both fluorescence and activity are similar to those obtained for the reconstitution of the uncleaved receptor (which contained the MBP and TrxA-His10 fusions) into BPL liposomes (Table 4.4). This suggests that the extra fusions are not required for either protein insertion into the lipsome during reconstitution or the maintenance of ligand-binding activity. As was seen for the uncleaved receptor, recovery of fluorescence is approximately 2-fold greater than the recovery of ligand binding activity which might be attributed to receptor orientation, with ~ 50 % of ligand binding sites facing towards the inside of the liposome and hence inaccessible to ligand (section 4.3.4).

4.3.4 - Receptor Orientation

As discussed in the previous sections, a discrepancy between the recovery of NTS1 fluorescence and the recovery of NTS1 ligand binding activity in the reconstitutions was observed for both the uncleaved and TeV-cleaved receptors. The observed recovery of fluorescence was approximately double the observed recovery of ligand binding activity in both cases. The in-gel fluorescence measures the total receptor present, while the radioligand binding assay only measures the number of receptor molecules oriented with

ligand binding sites exposed to the outside of the vesicle. A distribution of reconstituted receptor, with 50 % of the binding sites facing the outside of the vesicle and 50 % of the binding sites facing the inside of the vesicle, could explain these observations.

Reconstituted T43NTS1-eCFP samples, and a detergent-solubilised sample, were subjected to tryptic cleavage and the cleavage products analysed by SDS-PAGE which was visualised by in-gel fluorescence (Figure 4.9). GFP and its variants are relatively resistant to cleavage by trypsin, which allows the molecular weight of the fluorescent fragments produced to be easily and sensitively measured by in-gel fluorescence.

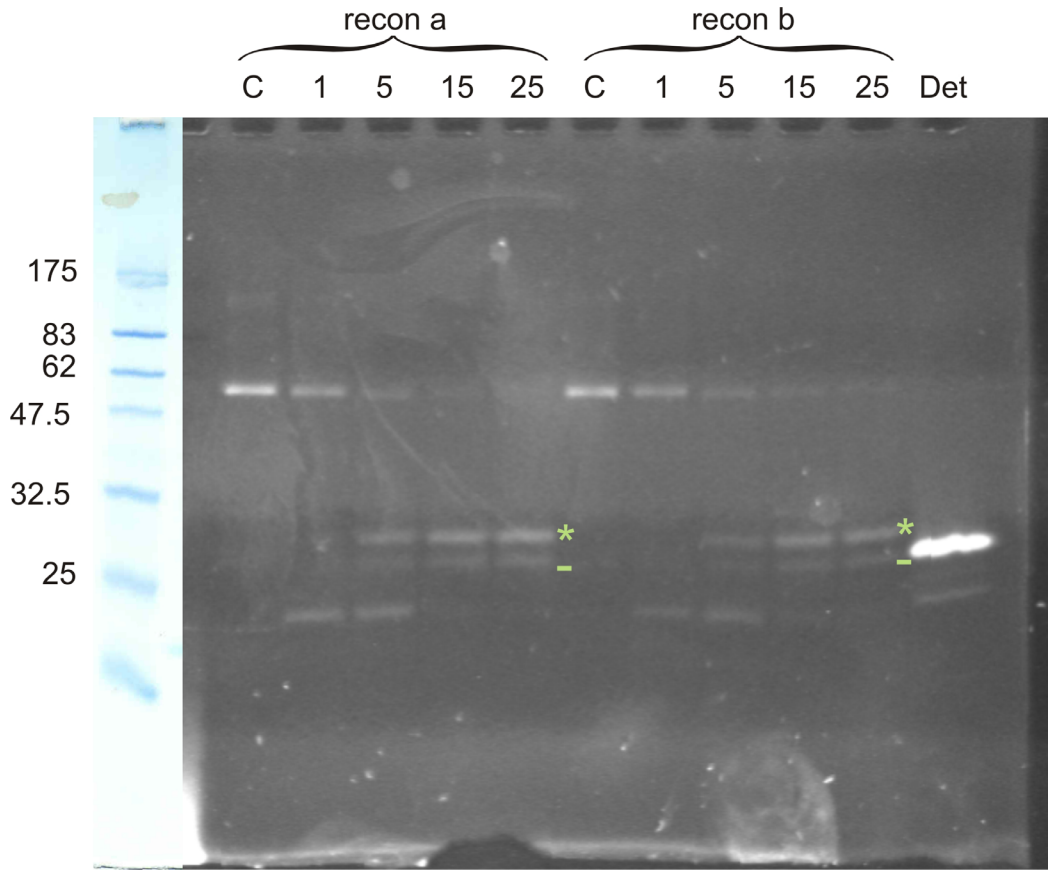

Figure 4.9 – Tryptic digestion of T43NTS1-eCFP reconstituted into BPL liposomes. Trypsin was added to reconsitituted samples at a concentration of 40 µg/ml and the samples incubated at 4 ^{o}C. Samples were taken at t = 1, 5, 15 and 25 mins (labelled 1, 5, 15 and 25 respectively) and analysed by SDS-PAGE followed by in-gel fluorescence. The negative control (denatured trypsin) is labelled C, and the positive control (detergent-solubilised sample) is labelled Det. Two reconstituted samples are shown on the gel (a and b) which are representative of the total of four separate reconstitutions which were tested. Equal volumes of the cleavage reactions were loaded for each time point.

The detergent-solubilised sample was included as a positive control since the trypsin should have access to both N- and C-terminal faces of the receptor. However, in the case of the reconstituted samples, since the trypsin is excluded from the proteoliposome interior, it will only have access to the N-terminal or C-terminal side of the protein depending on the orientation of receptor insertion into the liposome. The positive control produced a single fluorescent band (labelled -) at an approximate molecular weight of 24 kDa. The reconstituted samples produced the same band, as well as a band at a higher molecular weight (approximately 29 kDa, labelled *). There is a trypsin cleavage recognition site at position 420 in the C-terminus of NTS1, four residues N-terminal to the beginning of the fluorescent protein fusion (Figure 4.10). It is likely that the larger molecular weight band is formed due to the protection of this C-terminal cleavage site on the inside of the vesicle. In this case, the next accessible trypsin recognition site is at position 328 (between TM6 and the third extracellular loop (E3)) which will result in the larger fragment observed.

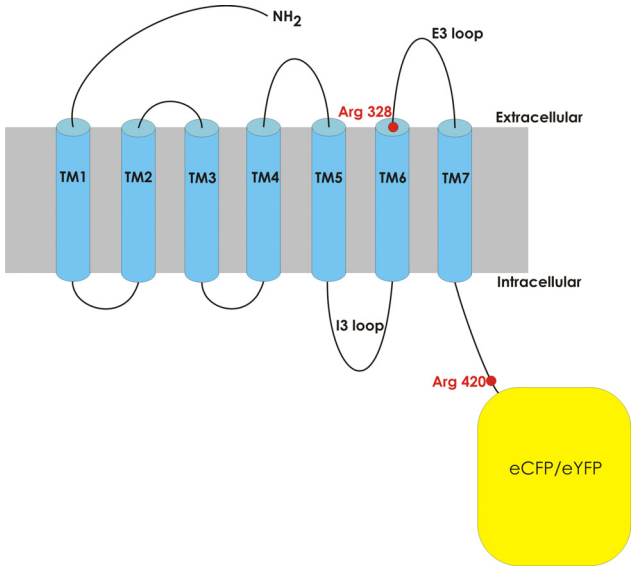

Figure 4.10 – Schematic of NTS1 depicting the key trypsin cleavage recognition sites (shown in red). If the C-terminus of the protein is exposed to the exterior, cleavage at Arg420 will yield a low molecular weight fluorescent cleavage product (27.6 kDa). If the protein is inserted into the membrane in the opposite orientation, the site at Arg420 will be protected on the inside of the vesicle. In this case, the next accessible cleavage site is Arg328 on the extracellular side of TM6. Cleavage at this site would yield a larger molecular weight fluorescent fragment (38.5 kDa).

Gel densitometry was used to compare the relative intensities of the full length receptor band (Lane 'C') with the protected cleavage band (labelled *) (Figure 4.9). Direct comparison of the two cleavage bands was not carried out because of the possibility of a loss of some fluorescence intensity if the fluorescent protein is subjected to prolonged incubation with trypsin. Therefore, the larger fragment (where the eCFP was protected from trypsin by being on the inside of the proteolipsome) was compared to the control ('C') which was only incubated with denatured trypsin. The cleaved band had an intensity of 47 ± 2 % relative to the uncleaved control (mean of four separate reconstitutions). This therefore suggests that there is a random orientation of receptor in the liposomes, with 50 % of the ligand binding sites occluded on the inside. This was observed for the DDM-mediated reconstitution of LacS into POPC liposomes (Knol *et al.*, 1998) and was attributed to the solubilising properties of DDM, which has been found to be highly disruptive to the bilayer structure relative to other detergents (de la Masa and Parra, 1997). Attempts to confirm the identity of the cleavage bands after Coomassie staining by band excision followed by LC MSMS were not possible due to the small amount of protein present.

4.4 - CONCLUSIONS

Lipid reconstitution of purified, detergent-solubilised, fluorescently-tagged NTS1 into detergent-disrupted liposomes was successful and appears to be relatively independent of the DDM : lipid effective molar ratio used for the disruption over the concentration range tested. In contrast, the lipid composition of the liposomes, while seemingly having no affect on protein insertion into the liposomes (as measured by fluorescence recovery), was crucial for the maintenance of ligand-binding activity. Reconstitution into the BPL extract maintained the ligand binding activity and was the optimal lipid composition tested. However, reconstitution into POPC-only liposomes led to a total loss of activity, which was partially recovered by supplementation of the POPC with an addition of the BPL extract (50 : 50 (w/w)). Therefore, a component of the BPL extract, for example the non-lamellar-forming lipid phosphatidylethanolamine (PE), or the charged lipid phosphatidylserine (PS), appears to be essential for the maintenance of ligand-binding activity. This hypothesis is quite reasonable given the previous observations that both the GPCR rhodopsin (Botelho *et al.*, 2002; Alves *et al.*, 2005), and heterotrimeric G proteins (Vogler *et al.*, 2004), have a specificity for non-lamellar forming lipids. In addition, *E.coli* membranes contain a large proportion of PE (~57 %) and the charged lipid PG (~15 %). Further work, involving a systematic study of the lipid composition required for maintenance of NTS1 ligand-binding activity, could confirm this hypothesis.

The TeV-cleaved fluorescently-tagged receptor, which lacks the MBP and TrxA-His10 fusions, was found to be successfully reconstituted with similar efficiency using the same protocol that was devised for the uncleaved receptor. Tryptic digestion of the reconstituted samples, followed by in-gel fluorescence analysis suggested that the receptor was inserting into the lipid bilayer in a random orientation (a 50 : 50 ratio of

inside-in and inside-out orientations). This provides an explanation for the relative recoveries after reconstitution of receptor fluorescence and ligand-binding activity for both the cleaved and uncleaved receptors. The fluorescence recovery was consistently double that of the recovered activity, suggesting that half of the ligand binding sites were being occluded on the inside of the liposome. This random insertion appears to be a property of DDM-mediated reconstitutions, since a previous study revealed that the protein LacS could be reconstituted into Triton X-100-saturated POPC liposomes asymmetrically, whereas the same protein reconstituted into DDM-saturated POPC liposomes inserted randomly (Knol *et al.*, 1998). However, Triton X-100 detergent cannot solubilise NTS1 in a native, ligand-binding confirmation (Tucker and Grisshammer, 1996), which precludes the use of this detergent for lipid reconstitutions.

The optimised reconstitution protocol allows the reproducible reconstitution of fluorescently-tagged NTS1 into liposomes, which provides a useful tool for the study of the multimerisation state of the receptor in *in vitro* lipid systems (Chapter 5). In addition, the relatively low lipid : protein molar ratio of the proteoliposomes obtained for the TeV-cleaved protein (489 ± 34) is ideal for solid state NMR studies using reconstituted receptor, provided successful scale-up of the reconstitutions can be achieved. By labelling the NT ligand with NMR-visible isotopes (which can easily be introduced during solid phase peptide synthesis) the structure of the peptide bound to the receptor can be elucidated (Williamson *et al.*, 2001; Luca *et al.*, 2003; Watts, 2005). The structure of the NT ligand at its binding site will provide a useful starting point for structure-based drug design.

CHAPTER 5 - ANALYSIS OF THE OLIGOMERISATION STATE OF NTS1

SUMMARY

The multimerisation state of fluorescently tagged NTS1 was analysed using fluorescence resonance energy transfer (FRET), both in detergent and in lipid-reconstituted systems. No FRET was observed between eCFP- and eYFP-tagged receptors in purified detergent samples, suggesting the receptor is monomeric in this environment. However, FRET was observed in lipid-reconstituted samples. The FRET efficiency was comparable to that observed *in vivo* for other GPCRs, including the yeast α-factor receptor, which is believed to be dimeric. Addition of NT to the samples had no effect on the FRET efficiency, suggesting that NTS1 could be a constitutive multimer in the lipid membrane. Variation of the receptor density of the reconstituted samples also had no effect on the FRET efficiency, suggesting that the observed FRET signal is due to a true receptor-receptor interaction, rather than random collisions of receptors in the membrane. Therefore, a functioning *in vitro* system has been developed which facilitates the study of NTS1 multimerisation in lipid bilayers and future studies will attempt to implement single molecule fluorescence techniques. Results obtained from PFO native gel electrophoresis also suggested that the T43NTS1-eCFP/eYFP receptor has a tendency to dimerise once the MBP and TrxA-His10 fusions have been proteolytically removed.

5.1 - INTRODUCTION

5.1.1 - Fluorescence

Fluorescence, a term coined in the mid-nineteenth century by Sir George Stokes (Stokes, 1852), is a form of luminescence in which light is emitted from excited singlet electron states of a molecule (fluorophore). The electronic transitions which occur during fluorophore absorption and emission can be illustrated using a Jablonski diagram (Figure 5.1) (Lakowicz, 1999). The absorption of light typically excites an electron from the singlet ground state (S_0) to a higher vibrational energy level of the first (S_1) or second (S_2) singlet excited states. Electrons then relax rapidly to the lowest vibrational level of S_1, via a process called internal conversion, which generally occurs in less than 10^{-12} s (Lakowicz, 1999). Since fluorescence lifetimes are typically between 10^{-8} - 10^{-9} s, fluorescence emission generally results from a thermally equilibrated excited state (i.e. the lowest-energy vibrational state of S_1).

The electron can then return to the singlet ground state via fluorescence emission, or via non-radiative processes, including collisional quenching. Molecules in the S_1 state can also undergo spin conversion to the first triplet state (T_1) in a process called intersystem crossing. Emission from T_1 is termed phosphorescence and is generally shifted to longer wavelengths relative to fluorescence (Lakowicz, 1999).

As the Jablonski diagram (Figure 5.1) shows, the energy of emission is typically less than that of absorption, due to the energy dissipated via vibrational relaxation and internal conversion. Therefore, the light emitted by fluorescence emission is of a longer wavelength than the light absorbed for excitation. This phenomenon, termed the Stokes Shift, was first observed by Sir George Stokes in 1852 (Stokes, 1852).

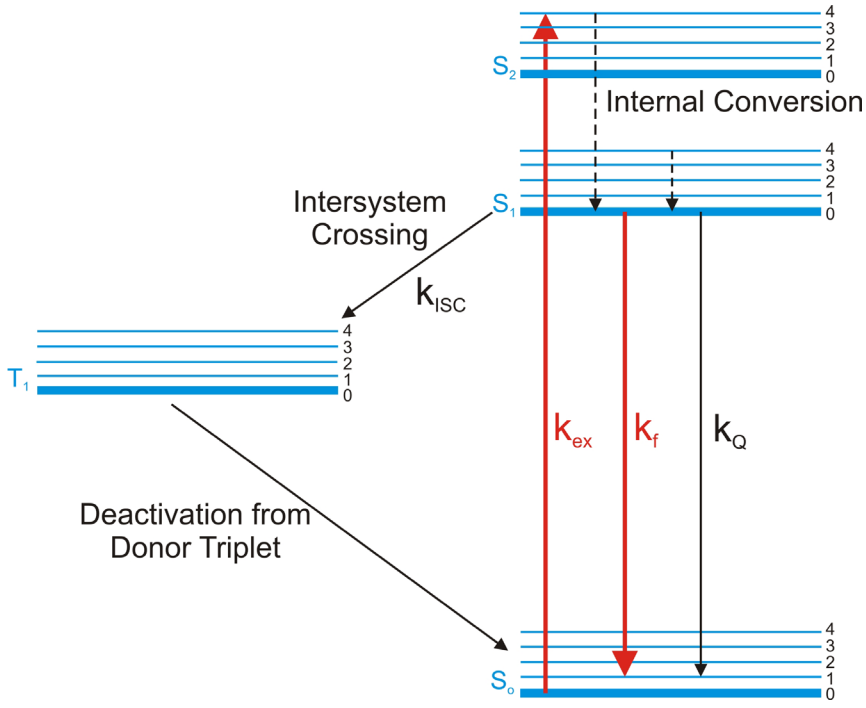

Figure 5.1 – Jablonski diagram showing the possible transitions which occur following the absorption of light by a fluorophore. The singlet ground, first and second electronic states are labelled S_o, S_1 and S_2 respectively. At each of these electronic energy levels the electrons can populate a number of vibrational energy levels, denoted by 0, 1, 2, etc. Radiative transitions between energy levels are shown in red and non-radiative transitions in black. The absorption of a photon excites an electron from the electronic ground state to a higher vibrational level of either S_1 or S_2 (k_{ex}). The electron then relaxes via internal conversion to the lowest vibrational energy level of S_1. The energy is then dissipated through fluorescent emission of the donor (k_f) or internal non-radiative processes (k_{nr}), which can include intersystem crossing to a first triplet state (T_1) (k_{ISC}) and collisional quenching reactions with an external quencher (k_Q).

5.1.2 - Fluorescence Resonance Energy Transfer

Fluorescence resonance energy transfer (FRET), a spectroscopic process by which energy is passed non-radiatively between molecules over distances between 10 and 100 Å, was first reported by Förster (hence the process is sometimes called Förster resonance energy transfer) (Förster, 1948). The principle of FRET has been reviewed (Clegg, 1992; Takanishi *et al.*, 2006). Two molecules of interest are labelled with different fluorophores (donor fluorophore and acceptor fluorophore) where the acceptor absorption spectrum overlaps with the donor emission spectrum (Figure 5.2).

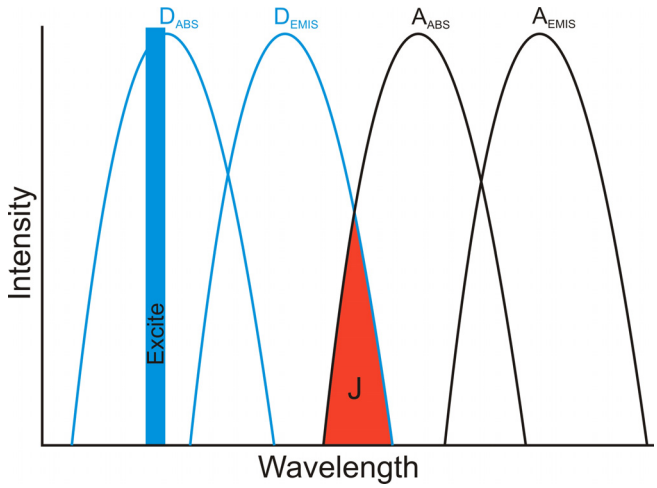

Figure 5.2 – Donor (D) and acceptor (A) absorption spectra (ABS) and emission spectra (EMIS). For FRET to occur, the emission spectrum of the donor must overlap with the excitation spectrum of the acceptor (spectral overlap (J), red shaded region). In the above example, if the donor is excited as indicated, FRET can occur (resulting in fluorescent emission from the acceptor) provided the donor and acceptor are in close enough proximity (typically 10-100 Å).

Energy transfer through the FRET mechanism decreases the donor fluorescence and increases the acceptor fluorescence. The efficiency of transfer is inversely proportional to the sixth power of the distance between the donor and acceptor fluorophores (Förster, 1948). Given this strong distance dependency and the fact that FRET takes place in a size range comparable to the size of many biological molecules, FRET has become an extremely useful reporter for molecular proximity in biological studies (dos

Remedios and Moens, 1995), including the study of GPCR multimerisation (Milligan and Bouvier, 2005).

In addition to distance dependency, the efficiency of transfer is also dependent on other factors. As mentioned above, spectral overlap (J) between the emission spectrum of the donor fluorophore and the excitation spectrum of the acceptor fluorophore is required for FRET to occur (Figure 5.2). Another major factor which influences energy transfer is the relative orientations of the fluorophores. The donor-acceptor dipole orientation factor (κ^2) makes a significant contribution to the uncertainty of FRET calculations and is generally assigned a value of 2/3, which assumes isotropic distribution of donor and acceptor molecules (dos Remedios and Moens, 1995). A more detailed description of the factors influencing FRET and their effect on FRET efficiency is discussed later (section 5.2.2)

The FRET process, the first stages of which are identical to the transitions which occur for an isolated fluorophore, can be illustrated using a Jablonski diagram (Figure 5.3). The absorption of a photon by the donor fluorophore excites its electrons from the singlet ground state (S_o) to a higher singlet state (S_1, S_2 etc). Once excited, the electrons then decay via internal conversion, on the picosecond timescale, to the lowest vibrational energy level of S_1. The donor fluorophore can then return to the ground state via the radiative and non-radiative pathways previously described for an isolated fluorophore (section 5.1.1). In addition, the energy can be dissipated via non-radiative dipole-dipole coupling to a nearby acceptor (k_T) i.e. FRET (Figure 5.3).

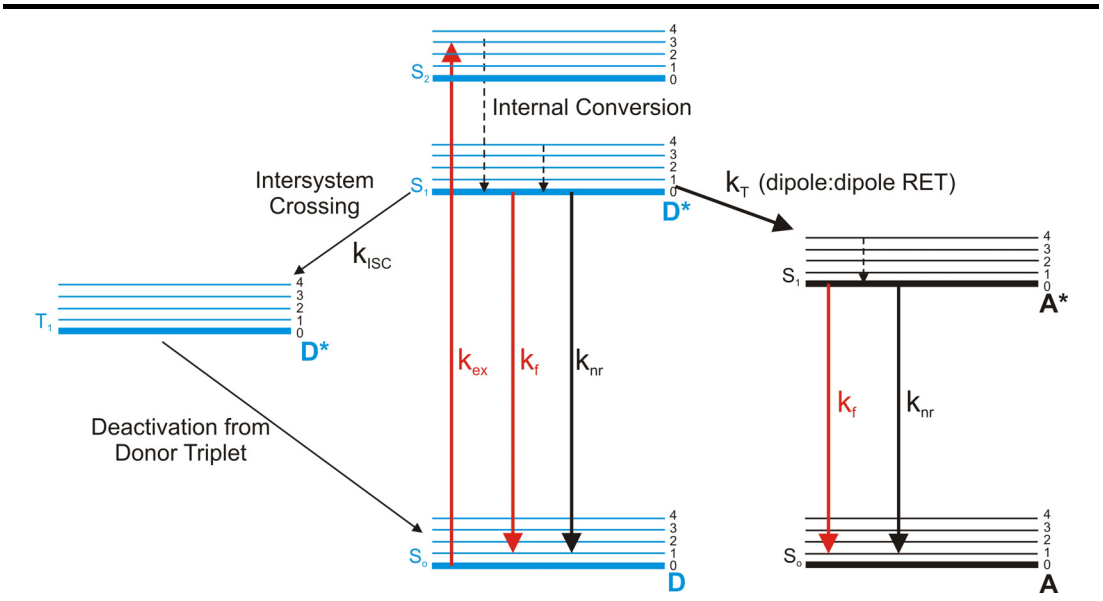

Figure 5.3 – Jablonski diagram showing the possible transitions between donor and acceptor energy levels during FRET (adapted from Clegg (1992)). The blue area of the diagram shows the electronic transitions for a donor fluorophore, which are identical to those described for the isolated fluorophore (Figure 5.1). However, when the donor is in close proximity to a suitable acceptor fluorophore (black), the donor electron can return to the singlet ground state by dissipation of energy via long-range non-radiative transfer to an acceptor molecule (k_T). The acceptor fluorophore can then relax via both radiative (k_f) and non-radiative (k_{nr}) processes.

5.1.3 - Green Fluorescent Proteins

Green fluorescent protein (GFP), a 238 amino acid fluorescent protein from the jellyfish *Aequorea victoria*, was first discovered by Shimomura (Shimomura *et al.*, 1962) as a partner to the chemiluminscent protein aequorin and has been the subject of detailed reviews (Tsien, 1998). High resolution crystal structures (Ormo *et al.*, 1996; Yang *et al.*, 1996) revealed an 11-stranded β-barrel structure threaded by an α-helix running up the axis of the cylinder (Figure 5.4). The chromophore, which comprises a p-hydroxybenzylideneimidazolinone formed by autocatalysed biosynthesis from residues Ser_{65}-Tyr_{66}-Gly_{67} during protein folding, is attached to the α-helix and is buried almost perfectly in the centre of the cylinder, which has been termed the β-can. In the Yang *et al* (1996) structure for GFP, the GFP is dimeric. However, others have reported that GFP can crystallise as a monomer (Brejc *et al.*, 1997) suggesting relatively weak dimerisation which is not an obligatory feature of GFP function. The dissociation

constant (K_d) for homodimerisation of wildtype GFP has been estimated as 100 μM using analytical ultracentrifugation (Phillips, 1997). The protein fluorescence is maximally excited at 395 nm and emits maximally at 504 nm.

The β-barrel fold of GFP and its variants is structurally highly stable and when the fluorescent protein is expressed as a fusion protein, the fluorescent properties tend to be unaffected. In addition, it is relatively inert and therefore often does not perturb the native function of proteins of interest to which it is fused. This has led to the widespread use of GFP as a genetically-encoded tag, where GFP is fused in-frame to a protein of interest, and the resulting chimeric protein expressed for the examination of protein function (Tsien, 1998). In addition, some GFP mutants have been used as environmental sensors (e.g. pH) and, since GFP is not fluorescent when targeted to inclusion bodies, GFP fluorescence has been used as a reporter to enable optimisation of folded protein expression in *E.coli* for both soluble (Waldo *et al.*, 1999) and membrane proteins (Drew *et al.*, 2006).

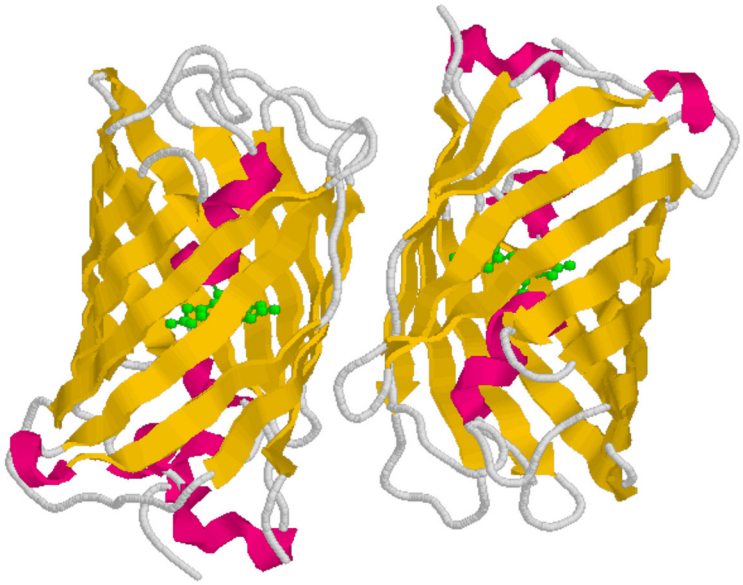

Figure 5.4 – Three-dimensional structure of GFP (Yang *et al.*, 1996), showing 11 β-strands forming a hollow cylinder, through which is threaded an α-helix bearing the chromophore (shown in ball and stick representation, highlighted in green). In this example, GFP crystallised as a dimer, but the same protein can also crystallise as a monomer (Brejc *et al.*, 1997).

The most powerful method for constructing GFP sensors has been to exploit FRET between two GFP molecules or between one GFP molecule and a secondary fluorophore. Mutagenesis of the wildtype *Aequorea* GFP has yielded variants which fluoresce from blue to yellowish green, and the gene encoding an unrelated red fluorescent protein (dsRed) from the Indo-Pacific sea anemone *Discosoma striata* has also been cloned (Matz *et al.*, 1999). Therefore fluorescent proteins with a wide range of different fluorescent properties are available (Patterson *et al.*, 2001; Shaner *et al.*, 2005). In particular, the GFP variants cyan fluorescent protein (eCFP, FRET donor) and yellow fluorescent protein (eYFP, FRET acceptor) have been widely exploited as the most popular GFP-based FRET pair (Pollok and Heim, 1999). The major properties of eCFP and eYFP are summarised in Table 5.1. eCFP contains the mutations F64L, S65A, Y66W, N1461I, M153T and V163A, while eYFP contains the mutations S65G, V68L, S72A and T203Y (Patterson *et al.*, 2001).

Table 5.1 – Properties of the GFP mutants, eCFP and eYFP. λ_{max}^{ex} = major excitation peak, λ_{max}^{em} = major emission peak, QY = fluorescence quantum yield, EC = molar extinction coefficient.

Protein	λ_{max}^{ex} (nm)	λ_{max}^{em} (nm)	EC ($M^{-1}cm^{-1}$)	QY	Brightness (EC*QY) ($mM^{-1}cm^{-1}$)	Dimerisation	References
eCFP	434	475	32500	0.4	13	Weak dimer	(Cubitt *et al.*, 1999; Patterson *et al.*, 2001; Rizzo *et al.*, 2004)
eYFP	514	527	84000	0.61	51	Weak dimer	(Tsien, 1998; Patterson *et al.*, 2001)

5.1.4 - GPCR Multimerisation

In recent years, the idea that G-protein coupled receptors (GPCRs) function as isolated monomeric receptors in the cell membrane has been challenged by results consistent with GPCRs functioning as dimers or higher-order oligomers. Indeed, evidence accumulated over the past three decades suggests that many GPCRs can exist as dimers

and/or higher-order oligomers and the hypothesis that homo- or heterodimerisation of GPCRs is a constitutive or ligand-induced property of many receptor types is widely accepted. The subject has been recently reviewed in detail (Milligan *et al.*, 2003; Milligan, 2004) and, whilst the concept of multimerisation is widely accepted, considerable variation exists between reports of the effects of agonist ligands on the multimerisation state. Whilst there are some examples of agonist-mediated multimerisation, for example as described for purified leukotriene B_4 receptor (Baneres and Parello, 2003), and agonist-mediated monomerisation, as described in an initial study of the δ-opioid receptor (Cvejic and Devi, 1997), constitutive multimerisation has been most widely reported. The contradictory nature of much of the literature on the subject is highlighted by multimerisation studies of the chemokine CXCR4 receptor. Early studies indicated that the chemokine SDF-1α induced dimerisation of the receptor (Vila-Coro *et al.*, 1999), but a more recent study combining bioluminescence resonance energy transfer (BRET) and sedimentation studies indicated that CXCR4 receptor exists as a constitutive dimer that is unaffected by the presence of agonist (Babcock *et al.*, 2003).

5.1.4.1 - Methods used to study GPCR multimerisation

GPCR multimerisation has been demonstrated for numerous receptor types using a wide range of biochemical and biophysical techniques (Milligan and Bouvier, 2005). The major approaches used are summarised below.

i) Co-immunoprecipitation

Co-immunoprecipitation, where differentially epitope-tagged GPCRs are co-expressed in the same cell and analysed by immunoblotting, has been used extensively to demonstrate association. For example, co-immunoprecipitation of c-myc- and HA-tagged forms of the β_2-adrenoceptor in insect Sf9 cells has been demonstrated (Hebert *et al.*, 1996). Rigorous controls in such studies are required in order to prevent a false

positive result caused by the non-specific aggregation of the GPCR during membrane protein solubilisation. This is generally achieved by combining detergent extracts of cells prior to immunoprecipitation, each expressing only one of the tagged GPCRs. Immunoprecipitation studies have also been criticised with regard to the incomplete solubilisation of membranes and/or the insufficient centrifugation to remove membrane fragments prior to the immunoprecipitation step, which leads to spurious immunoprecipitation. However, notwithstanding these caveats, immunoprecipitation is a useful technique for studying GPCR multimerisation *in vivo*.

ii) Functional complementation

If the co-expression of two, non-equivalent and non-functional mutants of a GPCR is both able and required to reconstitute ligand binding and/or function, then this can provide evidence in favour of direct protein-protein interactions for the active receptor. An example of such an approach used two forms of the angiotensin AT1 receptor which, individually, were unable to bind angiotensin II or related ligands due to point mutations in either TM helices III or V. Co-expression of the two mutant receptors, however, restored ligand binding (Monnot *et al.*, 1996). In a similar approach, pairs of non-functional mutants of the luteinizing hormone receptor were able to recover agonist-mediated regulation of cAMP levels following co-expression of the two mutants (Lee *et al.*, 2002). Complementation approaches have also been used to explore mechanisms of dimerisation (section 5.1.4.2).

iii) Resonance energy transfer methods

Fluorescence resonance energy transfer (FRET) (discussed in section 5.1.2) and bioluminescence resonance energy transfer (BRET), a conceptually similar technique to FRET where non-radiative transfer occurs between the bioluminescent protein *Renilla* luciferase and a GFP variant (Xu *et al.*, 1999), have been extensively used to probe the

multimerisation state of GPCRs *in vivo* (Overton and Blumer, 2002b; Milligan and Bouvier, 2005).

GFP and its variants have been widely exploited as FRET pairs, with eCFP (donor) and eYFP (acceptor) the most commonly used, given their favourable spectral characteristics and their low propensity to dimerise. FRET between eCFP and eYFP covalently fused to the GPCR C-terminus should only occur when the FRET partners are brought within 100 Å of each other. Hence a positive FRET result is interpreted as strong evidence for the existence of dimers or oligomers in living cells. However, differentiation between dimers and higher order oligomers, the quantification of the proportion of monomeric to oligomeric receptor and the interpretation of exact interfluorophore distances is challenging at present. Examples where FRET has been used to demonstrate GPCR multimerisation include the yeast α-factor receptor in *S.cerevisiae* (Overton and Blumer, 2002a), and the neuropeptide Y (NPY) receptor in BHK cells (Dinger *et al.*, 2003), both of which were found to be constitutively multimerised in the absence of agonist. For both BRET and FRET experiments, the importance of the receptor expression level on the RET efficiency observed has been raised (Mercier *et al.*, 2002). Increased apparent RET efficiency can be caused by random collisions of receptors in the membrane if the receptor density is too high (a process termed 'bystander FRET / BRET'). In the study by Mercier *et al* (2002), BRET efficiency was monitored whilst the expression level of GFP- and luciferase-tagged β_2-adrenergic receptor was varied over a 20-fold range. BRET efficiency was found to be constant up to an expression level of 26 pmol of receptor per mg of membrane protein, which is in excess of the levels commonly used for *in vivo* RET studies.

5.1.4.2 - Models of multimerisation

The mechanism of GPCR multimerisation is by no means clear, although theoretical models include both 'contact' and 'domain-swap' mechanisms (Figure 5.5) and the molecular basis for dimerisation has recently been reviewed (Milligan, 2007). The contact dimer theory suggests that dimer formation occurs through the interaction of the molecular surface of the receptor helices, largely without changing the conformation of the monomer structure. The domain-swapping mechanism involves the division of the monomer into two domains and the exchange of a domain of one monomer with the corresponding domain of a second monomer.

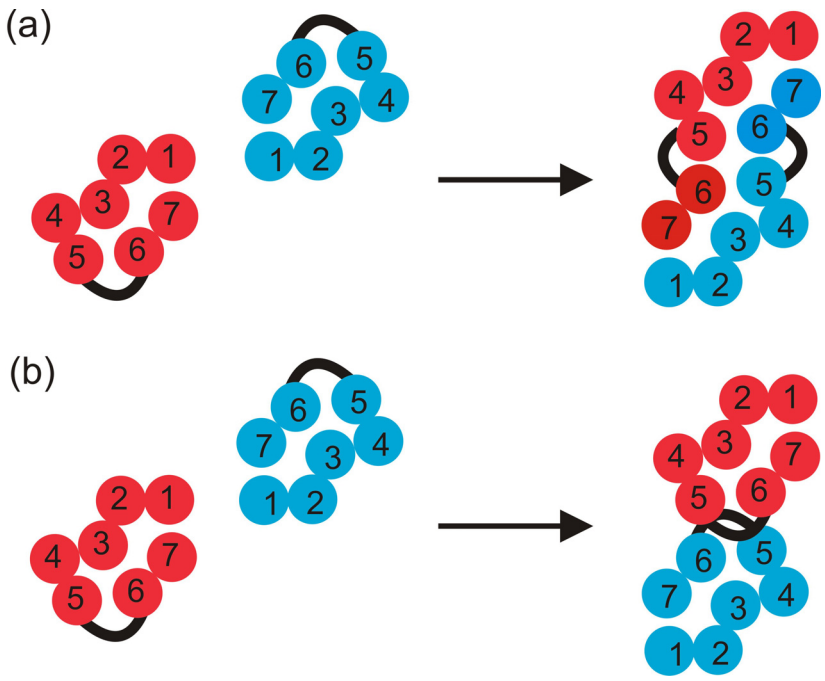

Figure 5.5 – Comparison of the proposed 'domain-swap' and 'contact' mechanisms for GPCR dimer formation. (a) domain-swapping of helices 5 and 6 between monomers (red and blue), involving a substantial conformational change compared with the monomeric structure. (b) The contact dimer model. Helices 5 and 6 associate but domain swapping does not occur. Adapted from Gouldson *et al* (2001). Note that there is no consensus regarding the particular helices involved in the intradimer contacts.

Early computational studies (Dean *et al.*, 2001; Gouldson *et al.*, 2001) pointed towards functionally important clusters of residues in TM5 and TM6 which, when modelled to the rhodopsin crystal structure (Palczewski *et al.*, 2000), were found to be on the external

faces of the helices. Thus, TM5 and TM6 were postulated to be involved in the formation of protein-protein interactions to stabilise the multimeric receptor via the domain swap model.

Experimental evidence also suggested a role for TM5 and TM6 in GPCR dimerisation. In the immunoprecipitation study of the β_2-adrenergic receptor discussed previously (Hebert *et al.*, 1996), a peptide derived from TM6 was observed to inhibit both dimerisation and activation of the receptor. In addition, chimeric receptor and point mutation studies have suggested a role for TM5 and TM6 in domain-swapping. For example, two receptor chimeras were produced: (1) helices 1-5 of the β_2-adrenergic receptor were fused with helices 6 and 7 of the muscarinic M3 receptor; (2) helices 1-5 of the muscarinic M3 receptor were fused with helices 6 and 7 of the β_2-adrenergic receptor (Maggio *et al.*, 1993). When expressed individually, the chimeric receptors were unable to bind ligand or stimulate phosphatidylinositol hydrolysis. In contrast, these functions were restored on co-expression of both chimeras, which led to the suggestion that the helices 5 and 6 of each chimera could exchange via the domain-swap mechanism in the dimeric structure to yield two functional receptors (Figure 5.5). However, an *in vivo* FRET study of the yeast α-factor receptor, in which fluorescently-tagged deletion mutants were used to find regions of the receptor required for homo-dimerisation, implicated the N-terminal extracellular domain, TM1 and TM2 in the stabilisation of α-factor oligomers (Overton and Blumer, 2002a).

In addition, recent structural studies on rhodopsin have provided direct evidence of oligomerisation interfaces. Atomic force microscopy on discs from mouse rod outer segments showed rhodopsin organised within paracrystalline arrays with densely packed, double rows of receptor (Liang *et al.*, 2003). Resulting models revealed contact dimers with intradimeric contacts involving TM4 and TM5, with contacts between rows of

dimers formed between TM1 and TM2 (Liang *et al.*, 2003; Fotiadis *et al.*, 2006). Electron density maps derived from the 2D crystals of squid rhodopsin provide evidence of contact dimers with a symmetrical TM4-TM4 interaction as the key structural intra-dimer interface (Davies *et al.*, 2001). Recent biochemical approaches have also implicated TM4 as a potential dimerisation interface. For example, cysteine cross-linking studies on the Dopamine D2 receptor showed that cross-linking occurred when cysteine residues were placed along two continguous faces of TM4 (Guo *et al.*, 2005). Interestingly, their susceptibilities to cross-linking were differentially altered by the presence of agonists and inverse agonists.

More recent computational studies have broadly supported the experimental observations (Nemoto and Toh, 2005). However, it is clear that the mechanism of dimerisation is not well understood. There is experimental evidence to support both the contact dimer and domain-swap dimer models. Indeed, it has been suggested that the two models might not be mutually exclusive and could coexist (Milligan and Bouvier, 2005). As discussed, there is by no means a consensus view on the position of the dimerisation interface. However, it has been suggested that homo-dimerisation interfaces of even closely related GPCRs that respond to similar ligands may be markedly distinct (Nemoto and Toh, 2005). If dimerisation interfaces are receptor-specific, this could go some way to explaining the alternative dimerisation interfaces reported from biochemical studies of different receptor types.

5.1.4.3 - Multimerisation of Neurotensin Receptors

Very little work has been published regarding the multimerisation of any of the neurotensin receptors. A recent immunoprecipitation study has demonstrated that NTS1 can form heterodimers with the structurally distinct NTS3/sortillin receptor in the HT29 cell line (Martin *et al.*, 2002). No change in affinity of NTS1 for NT was

reported but the NTS1/NTS3 interaction was shown to modulate both NTS1-mediated ERK1/2 MAPK signalling and phosphoinositide turnover.

In a second immunoprecipitation study, NTS1 was found to form constitutive heterodimers with NTS2 in transfected COS-7 cells (Perron *et al.*, 2006). In addition, the cell surface NTS1 receptors were more resistant to down-regulation in cells which co-expressed both receptor types, suggesting that this might represent a mode of regulation of NT-triggered responses by altering the intracellular distribution and trafficking of NTS1. However, there is currently no published information regarding the multimerisation state of NTS1.

5.1.5 - PFO Native Gel Electrophoresis

SDS-PAGE, the electrophoresis method typically used to resolve the molecular mass of a protein sample, is incompatible with the analysis of multimeric complexes, since the SDS can dissociate the inter-subunit interactions which are often relatively weak.

An alternative detergent system, perfluoro-octanoic acid (PFO), has recently been used to assess the multimerisation state of membrane protein complexes (Ramjeesingh *et al.*, 1999; Ramjeesingh *et al.*, 2003). In common with SDS-PAGE, PFO-PAGE is compatible with pre-cast gel systems, which is a distinct advantage over other native gel techniques such as blue native PAGE (Schagger and von Jagow, 1991). In PFO-PAGE, replacement of SDS with PFO in the sample and running buffers has been found to preserve physiological protein oligomeric interactions during electrophoresis, thereby allowing molecular mass determination of multimeric protein complexes.

5.1.6 - Aims

The aim is to study the oligomerisation state of NTS1, both in detergent solution and in lipid-reconstituted systems. The majority of the study of GPCR multimerisation to date has been carried out in transfected cell lines (Milligan, 2004). The development of an *in vitro*, lipid-reconstituted system will allow rigorous study of NTS1 multimerisation and fine control over the system conditions and components. Therefore, purified NTS1 fused to the fluorescent tags eCFP and eYFP, will be used for FRET studies using detergent solution and lipid-reconstituted samples (see Chapter 4 for development of the reconstitution protocol). In addition, the fluorescent tag will be exploited for the sensitive in-gel fluorescence analysis of PFO-PAGE gels.

5.2 - MATERIALS AND METHODS

5.2.1 - Sample Preparation

NTS1C and NTS1Y (Figure 5.6) were expressed in *E.coli* C41(DE3) in separate cultures and purified according to the protocol described in Chapter 3. For the sample containing both eCFP- and eYFP-tagged receptors, equal masses of the NTS1C and NTS1Y pellets were combined at the homogenisation stage of the purification to ensure homogenous dispersion of the eCFP- and eYFP-tagged receptor. The progress of the purifications was monitored by in-gel fluorescence SDS-PAGE (section 3.2.6) and radioligand binding assay (Appendix A3).

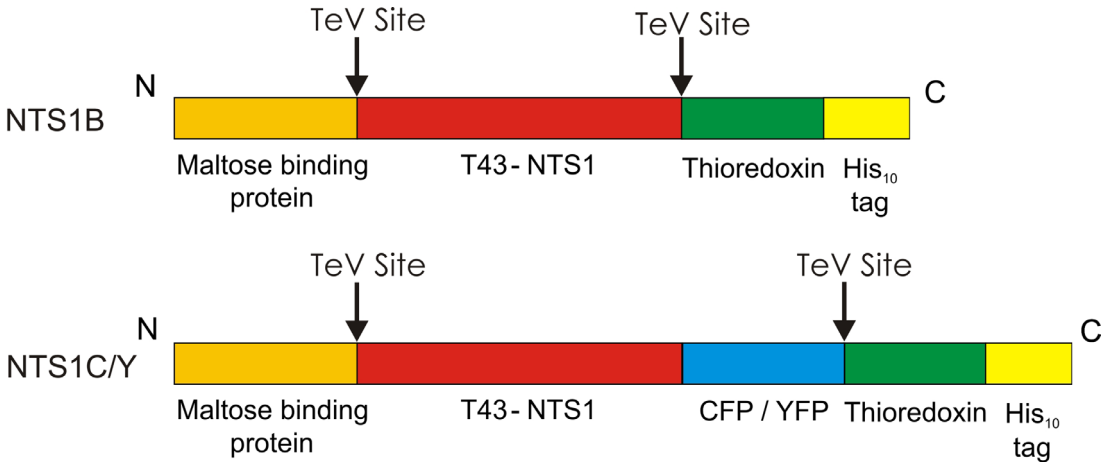

Figure 5.6 : Schematic depicting the untagged NTS1B construct (White *et al.*, 2004) and the fluorescence-tagged NTS1C and NTS1Y constructs. NTS1B consists of maltose-binding protein (MBP) from *E.coli*, an N-terminally truncated form of NTS1 (T43NTS1), thioredoxin A from *E.coli* (TrxA) and a deca-histidine tag (His_{10} tag). TeV protease cleavage sites are present between the MBP and T43NTS1 moieties and the T43NTS1 and TrxA moieties to facilitate proteolytic removal of the fusion partners. The genes for eCFP and eYFP were introduced into the NTS1B construct by overlap extension PCR, to yield the NTS1C and NTS1Y constructs (Chapter 3). The C-terminal TeV site was moved to a position C-terminal of the fluorescent protein gene.

Purified receptor was reconstituted into detergent-disrupted brain polar lipid vesicles (see section 4.2.3 for a full description). In brief, BPL vesicles of uniform size were generated by extrusion through 0.4 μm and 0.1 μm polycarbonate membranes (Whatman) and disrupted by adding DDM to an effective DDM : lipid molar ratio of 0.7, followed by incubation for 3 h at 4 °C. Disrupted vesicles were added to purified

protein to give the desired lipid : protein ratio and the samples incubated for 1 h at 4 °C. Pre-washed Biobeads SM-2 (Biorad) were added to a concentration of 120 mg/ml and the samples incubated at 4 °C overnight with gentle agitation. Finally, proteoliposomes were isolated by sucrose density gradient centrifugation (0 – 35 % sucrose in 50 mM Tris pH 7.4, 200 mM NaCl, 1 mM EDTA; 100,000 g; 4 °C; 15 h). Successful reconstitution of active, fluorescent receptor was confirmed by in-gel fluorescence SDS-PAGE and radioligand binding assay.

5.2.2 - Fluorescence Measurements

All fluorescence resonance energy transfer (FRET) experiments were carried out using a Perkin Elmer LS-55 Spectrofluorimeter and a 1.5 ml quartz microcuvette (Hellma) with magnetic stir bar. The cuvette was maintained at a constant temperature of 4 °C throughout. Excitation and emission slits were both set to 2.5 nm bandpass. Prior to fluorescence measurements, receptor samples were diluted to the stated receptor concentrations using 50 mM Tris pH 7.4, 15 % glycerol (v/v), 200 mM NaCl, 0.1 % DDM (w/v), 0.01 % CHS (w/v), 1 mM EDTA for detergent samples and 50 mM Tris pH 7.4, 200 mM NaCl, 1 mM EDTA for reconstituted samples. For samples containing neurotensin peptide (NT), an appropriate volume of NT stock solution (3.5 mM) was added and the samples allowed to equilibrate for 15 min before measurement. All fluorescence spectra were recorded in triplicate and an average taken.

The FRET protocol was a variation of that proposed previously (Overton and Blumer, 2002b) where FRET is quantified by monitoring enhanced acceptor emission (also known as sensitized emission). In each FRET experiment, fluorescence emission spectra are recorded from 4 separate samples: (1) Buffer only blank; (2) Sample containing only eCFP-tagged NTS1; (3) Sample containing only eYFP-tagged NTS1; (4) Sample containing both eCFP- and eYFP-tagged NTS1. Fluorescence emission due to

FRET between eCFP- and eYFP-tagged receptors was detected by employing a procedure to remove contributions of background signal, eCFP emission (also called 'bleed-through') and direct eYFP emission (also called 'cross talk') from the eCFP- and eYFP-tagged sample emission spectrum. This was achieved as follows:

a. Subtraction of background fluorescence

Emission spectra for all samples were recorded between 450 nm and 600 nm using an excitation wavelength of 440 nm (λ_{max}^{CFP}), and between 520 nm and 600 nm using an excitation wavelength of 510 nm (λ_{max}^{YFP}). The background emission obtained from sample (1) was then subtracted from samples (2)-(4) for both emission spectra.

b. Subtraction of 'bleed-through'

The emission spectrum obtained from the excitation of sample (2) at λ_{max}^{CFP} was normalised to give an eCFP emission peak value identical to the eCFP emission peak value of sample (4). After normalisation, the eCFP spectrum of sample (2) was subtracted from the emission spectrum of sample (4). This resulted in an eYFP emission spectrum composed of a FRET component and a 'cross talk' component due to direct excitation of eYFP, which can also be termed the extracted acceptor spectrum.

c. Subtraction of 'cross talk'

The emission spectra yielded from excitation of samples (3) and (4) at λ_{max}^{YFP} were used to quantify the amount of eYFP-tagged receptor present in each sample. This is possible because eCFP is not excited at this wavelength. The ratio of the eYFP emission peak heights of these two spectra were used as a scaling factor to normalise the emission spectrum obtained when sample (3) was irradiated at λ_{max}^{CFP}. This normalised spectrum, which corresponds to the 'cross talk', was then subtracted from the extracted acceptor spectrum obtained in the previous section. This results in an eYFP emission spectrum due solely to FRET.

5.2.3 - Measurement of donor : acceptor ratio

The donor : acceptor ratios of the T43NTS1-eCFP/eYFP detergent samples were calculated by comparing the fluorescence intensity of the maximal eCFP and eYFP emissions (when excited at λ_{max}^{CFP} and λ_{max}^{YFP} respectively). The fluorescence intensities (F) of eCFP and eYFP were corrected using the fluorophore quantum yields (Φ) and the fluorophore molar extinction coefficients (ε) using Equation 5.1 (Values of Φ and ε for eCFP and eYFP are given in Table 5.1)

$$F = c\,\Phi_D \varepsilon \qquad \text{Equation 5.1}$$

The donor : acceptor ratios of the reconstituted samples were calculated in a similar manner. However, the calculated donor fluorescence intensity was corrected using the known FRET efficiency of the sample to take into account the decrease in donor emission due to FRET (section 5.2.3).

5.2.3 - Calculation of FRET efficiency

i) Apparent FRET efficiency

In order to allow direct comparison with other multimerisation studies on GPCRs *in vivo*, a parameter termed the 'apparent FRET efficiency' was calculated (Overton and Blumer, 2002b). This does not measure the precise efficiency of FRET and is therefore not useful for interfluorophore distance measurements. However, it is a rapid method for comparison of the relative ability of GPCRs to engage in FRET. Apparent FRET efficiency was calculated as follows:

$$E^{app} = \frac{F_{DA}^{FRET}}{F_{DA}^{A}} \times 100 \qquad \text{Equation 5.2}$$

Where E^{app} is the apparent FRET efficiency, F_{DA}^{FRET} is the fluorescence intensity due to FRET and F_{DA}^{A} is the fluorescence intensity of the acceptor when excited at λ_{max}^{YFP}.

ii) Corrected FRET Efficiency

The corrected FRET efficiency was calculated as follows (Clegg, 1992; Mukhopadhyay *et al.*, 2001):

$$E = \left(\frac{\varepsilon_A}{\varepsilon_D}\right)\left(\frac{F_{DA}^{FRET}}{F_{DA}^{A}}\right)$$

Equation 5.3

Where E is the corrected FRET efficiency, ε_A is the molar extinction coefficient of eYFP at λ_{max}^{YFP} (75768 $M^{-1}cm^{-1}$ (Patterson *et al.*, 2001)) and ε_D is the molar extinction coefficient of the donor at λ_{max}^{CFP} (29817 $M^{-1}cm^{-1}$ (Cubitt *et al.*, 1999)). The corrected FRET efficiency was used to calculate the average interfluorophore distance using equation 5.4:

$$R = R_o\left(\frac{1}{E} - 1\right)^{\frac{1}{6}}$$

Equation 5.4

Where R is the average distance between donor and acceptor and R_o is the Förster distance for the eCFP/eYFP FRET pair, which was calculated using the following formula:

$$R_o^{\,6} = (8.785\times10^{-5})\kappa^2\Phi_D n^{-4} J$$

Equation 5.5

Where κ^2 is the orientation factor between donor and acceptor molecules (for random orientations of the chromophores in space and short rotational relaxation times relative to the fluorescence lifetime, $\kappa^2 = 2/3$ (Haas *et al.*, 1975)), Φ_D is the quantum yield of donor fluorescence in the absence of acceptor (0.4 (Cubitt *et al.*, 1999)), n is the refractive index (usually taken as 1.4) and J is the overlap integral between the fluorescence spectrum of the donor and the molar absorption spectrum of the acceptor:

$$J = \int F_D(\lambda)\varepsilon(\lambda)\lambda^4 d\lambda$$

Equation 5.6

Where F_D is the fluorescence emission intensity of the donor, as a fraction of the total integrated intensity and ε is the molar absorption spectrum of the acceptor (Lakowicz, 1999).

5.2.4 - PFO Gel Electrophoresis

The method of PFO-PAGE used was a variation of that previously published (Ramjeesingh *et al.*, 1999). Perfluoro-octanoic acid (PFO) was obtained from Sigma. All steps were carried out at 4 °C. Purified, detergent-solubilised NTS1C/Y (MBP-TeV-T43NTS1-eCFP/eYFP-TeV-TrxA-His_{10}) and T43NTS1-eCFP/eYFP samples were diluted 1 : 1 (v/v) with 2x PFO sample buffer (100 mM Tris pH 8.0, 8 % PFO (w/v), 20 % glycerol (v/v), 0.005 % bromophenol blue (w/v), pH adjusted to 8.0 using NaOH) and incubated at 4 °C for 30 min. Molecular weight markers (GE Healthcare) were also diluted 1 : 1 (v/v) in 2x PFO sample buffer. A pre-cast Tris-Glycine PAGE gel (4-12 % or 12 %, Invitrogen) was pre-equilibrated with PFO-PAGE running buffer (25 mM Tris, 192 mM glycine, 0.5 % PFO (w/v), adjusted to pH 8.5 with NaOH) by electrophoresis at 50 V for 1 h. Electrophoresis of the NTS1 samples was then performed at 120 V for 2 h. Protein bands were analysed by in-gel fluorescence and Coomassie Brilliant Blue staining. As a direct comparison, the same samples were also analysed by standard SDS-PAGE using the same type of pre-cast Tris-Glycine gels.

5.3 - RESULTS AND DISCUSSION

5.3.1 - Detergent Receptor Samples

FRET experiments were initially carried out on purified, fluorescence-tagged receptors in detergent solution in order to determine whether, in such an environment, NTS1 is an oligomer. Figure 5.7 shows the emission spectra for the mixed T43NTS1-eCFP and T43NTS1-eYFP sample (eCFP : eYFP ratio of 1.2 : 1 ± 0.02) and the corresponding subtractions of 'bleed through' and 'cross talk' to yield the eYFP emission due to FRET. It can be seen by the baseline emission spectrum after subtraction that, at a concentration of 60 nM and at the higher concentration of 205 nM, no FRET occurred.

Repetition of the experiment in the presence of 10 μM agonist (NT) also failed to show any FRET between eCFP- and eYFP-tagged receptors (Figure 5.8). These results together indicate that the interflurophore distance between the eCFP and eYFP tags is too large for FRET to occur (> 100 Å) and therefore suggest that the receptor is monomeric in detergent solution. In addition, the lack of any FRET suggests that there is no significant aggregation of receptor, therefore in agreement with the negative stain electron microscopy result (section 3.3.6) which indicated a monodisperse receptor population of purified, detergent-solubilised receptor, with no signs of aggregation. The results also suggest that agonist binding does not trigger multimerisation of the detergent-solubilised receptor, certainly within the timescale of the FRET experiment.

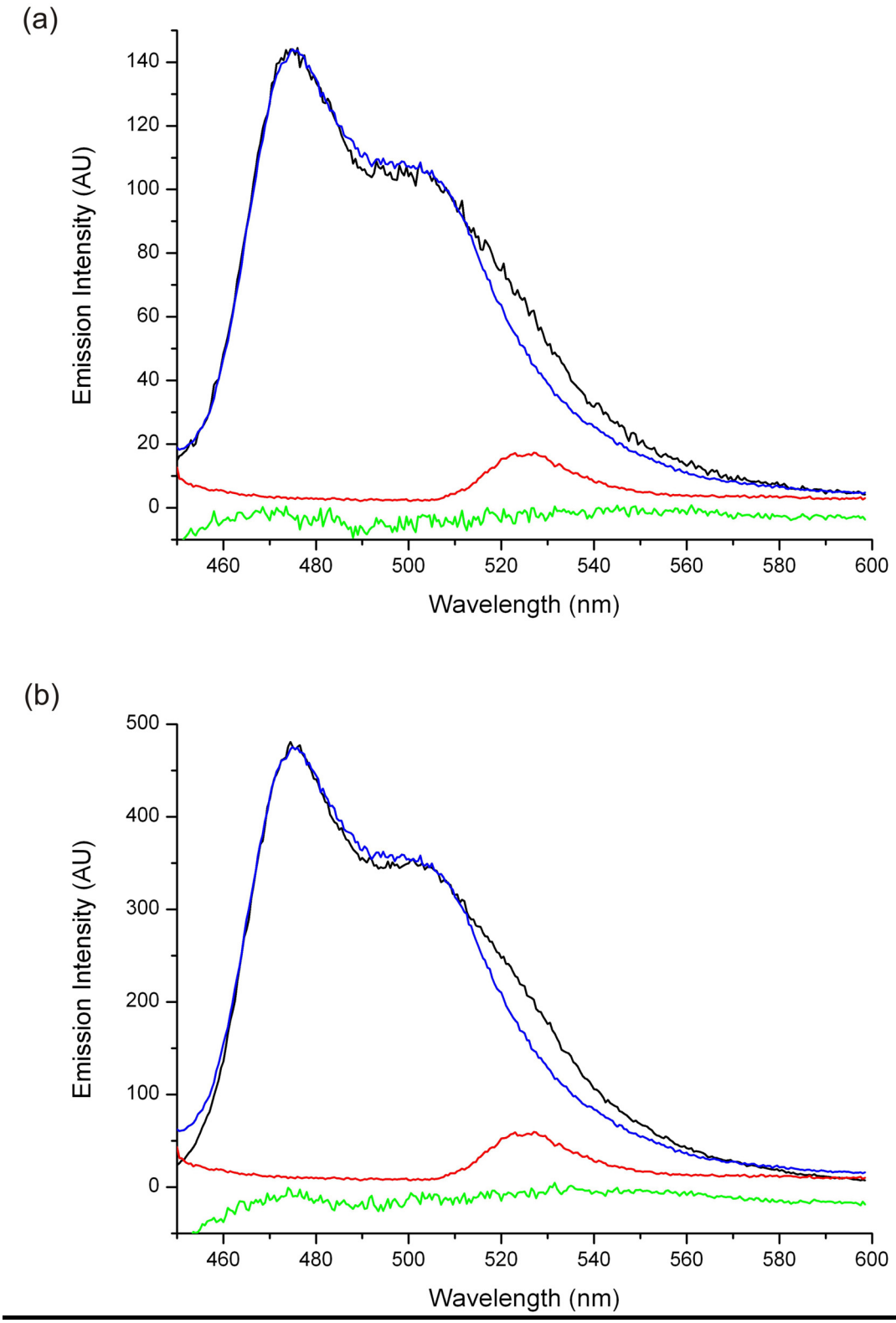

Figure 5.7 : Use of FRET to detect oligomerisation of purified T43NTS1-eCFP and T43NTS1-eYFP in detergent solution at concentrations of 60 nM (a) and 205 nM (b). Samples were excited at λ_{max}^{CFP} (440 nm) and the fluorescence emission detected by scanning fluorometry. Fluorescence emission due to FRET (green) was determined by subtracting the normalised emission spectrum of a T43NTS1-eCFP only sample (blue) and the normalised emission spectrum of a T43NTS1-eYFP only sample (red) from the emission spectrum of the mixed T43NTS1-eCFP and T43NTS1-eYFP sample (black).

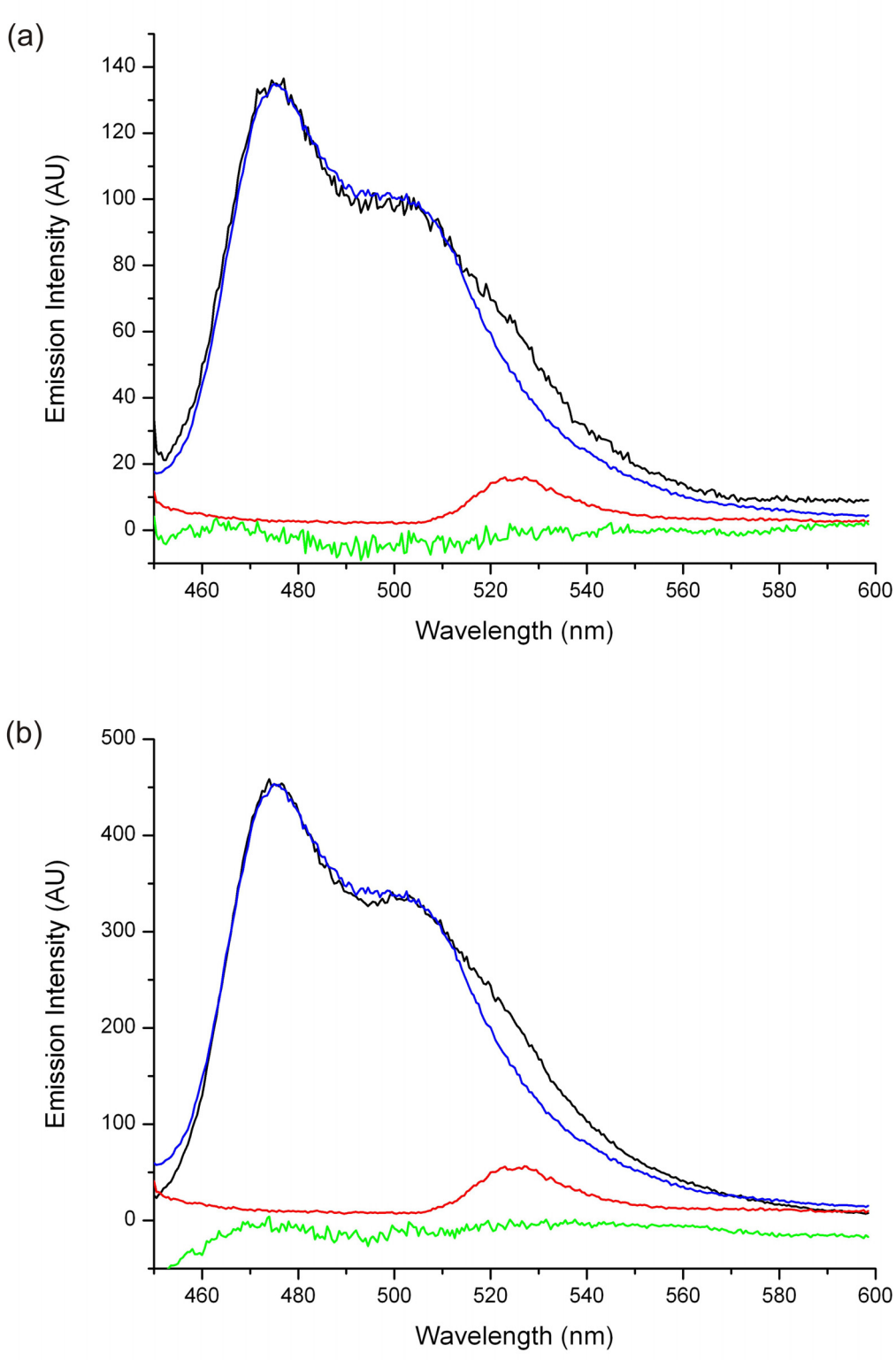

Figure 5.8 : Use of FRET to detect oligomerisation of purified T43NTS1-eCFP and T43NTS1-eYFP in detergent solution at concentrations of 60 nM (a) and 205 nM (b) in the presence of 10 µM NT. Samples were excited at λ_{max}^{CFP} (440 nm) and the fluorescence emission detected by scanning fluorometry. Fluorescence emission due to FRET (green) was determined by subtracting the normalised emission spectrum of a T43NTS1-eCFP only sample (blue) and the normalised emission spectrum of a T43NTS1-eYFP only sample (red) from the emission spectrum of the mixed T43NTS1-eCFP and T43NTS1-eYFP sample (black).

5.3.2 - Lipid-Reconstituted Receptor Samples

(i) Reconstituted Sample Preparation

The purified T43NTS1-eCFP/eYFP was subsequently reconstituted into a brain polar lipid (BPL) extract (for lipid composition see Table 4.1). The starting lipid : protein ratio was varied between 1000 : 1 and 6000 : 1 in order to vary the proteoliposome receptor density. After detergent removal using Biobeads SM-2 (BioRad), reconstitutions were isolated by sucrose density gradient centrifugation (Figure 5.9).

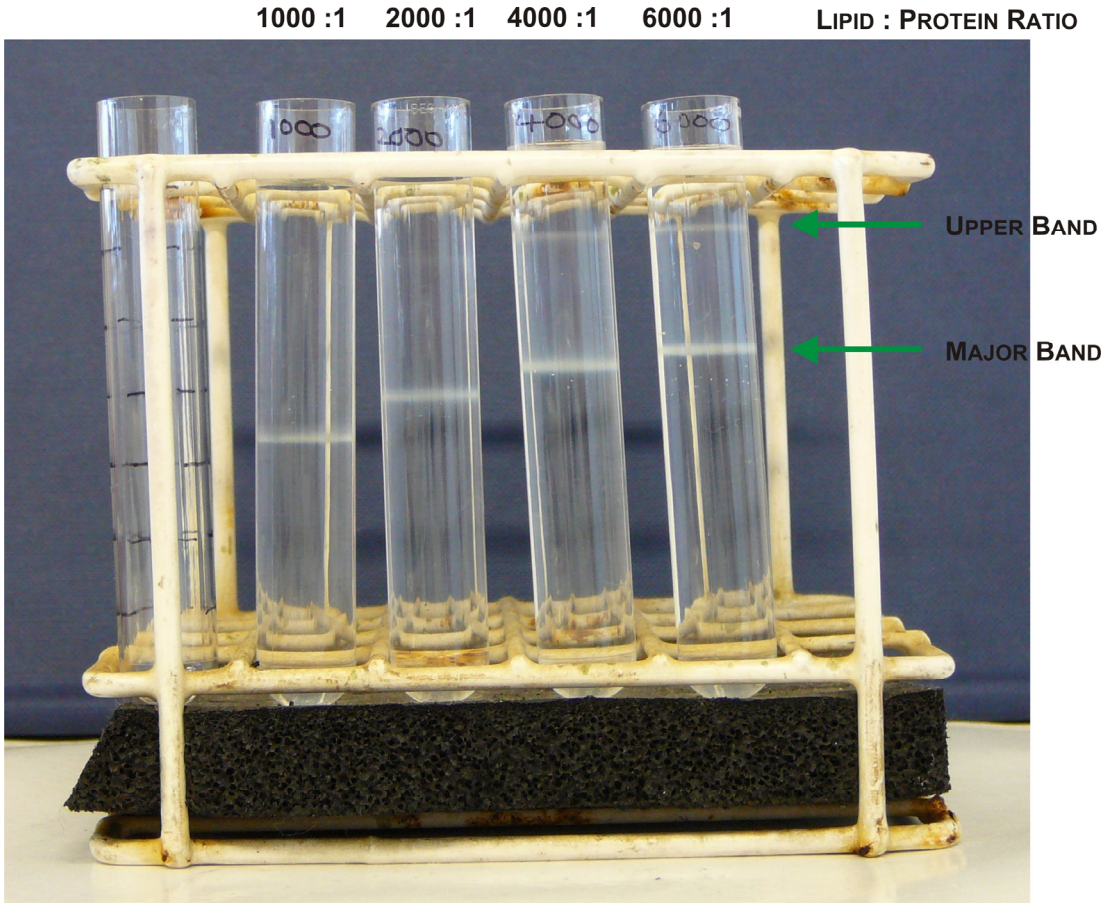

Figure 5.9 : Sucrose density gradient centrifugation of T43NTS1-eCFP/eYFP reconstitution samples at the stated initial lipid : protein ratios. The gradient was 0 - 35 % sucrose and major proteoliposome bands, which can be seen towards the centre of the gradients, were harvested and used directly for FRET measurements. An upper band, which was also visible particularly at high lipid : protein ratios, was also collected and analysed by in-gel fluorescence.

The proteoliposome bands were harvested from the sucrose gradient and the presence of reconstituted receptor confirmed by radioligand binding assay and in-gel fluorescence (Figure 5.10). A second band can be seen close to the top of the sucrose gradient which is more intense in the samples which have a higher starting lipid : protein ratio (Figure 5.9). This upper band was also collected and analysed by in-gel fluorescence and found not to contain reconstituted protein (Figure 5.10, lanes 5 – 8). It is therefore likely to be a band of pure lipid, which explains why it is more prevalent at higher lipid: protein ratios.

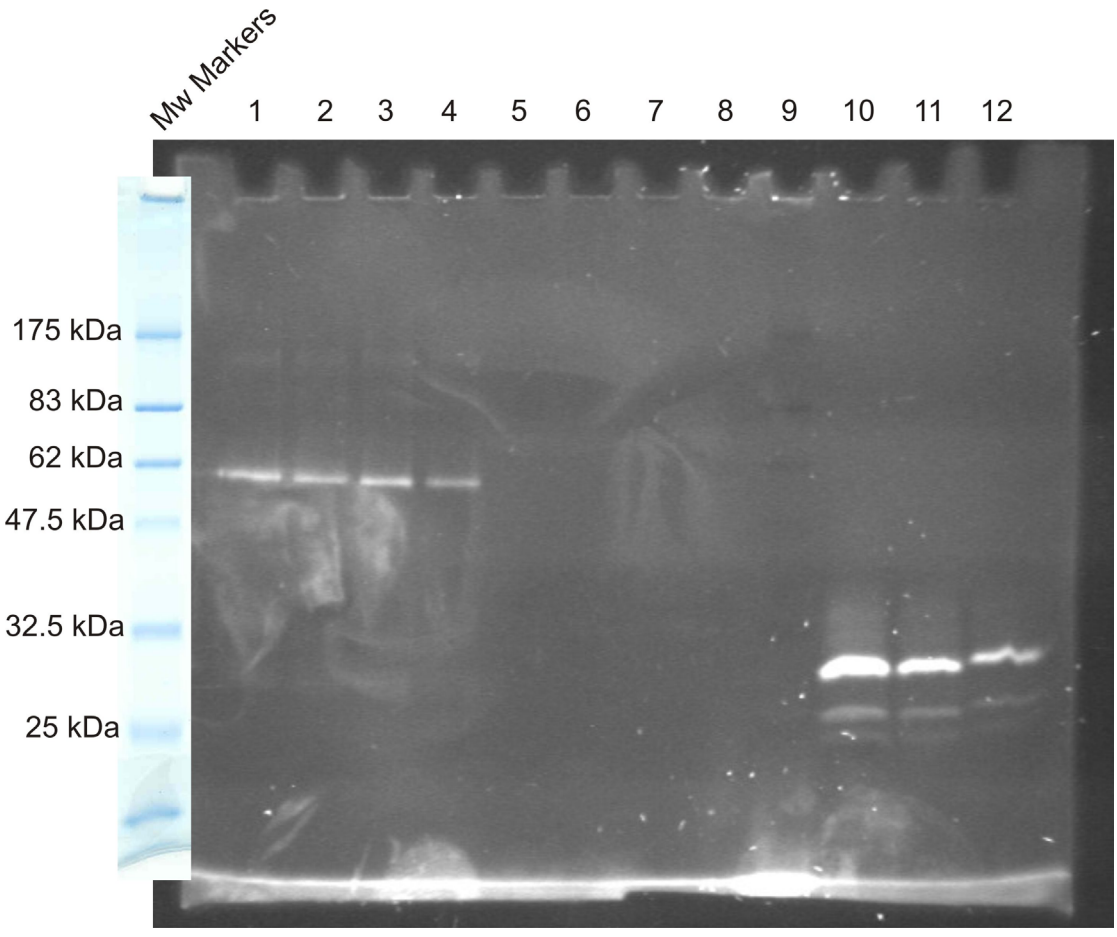

Figure 5.10 : In-gel fluorescence analysis of the proteoliposome bands harvested from the density gradient centrifugation of the T43NTS1-eCFP/eYFP reconstitutions. Samples were separated by SDS-PAGE using a 12 % Tris-Glycine gel. Lane 1 = 1000 : 1 major band; Lane 2 = 2000 : 1 major band, Lane 3 = 4000 : 1 major band; Lane 4 = 6000 : 1 major band; Lane 5 = 1000 : 1 upper band; Lane 6 = 2000 : 1 upper band; Lane 7 = 4000 : 1 upper band; Lane 8 = 6000 : 1 upper band; Lane 9 = molecular weight marker (shown pasted to the left side of the gel), Lanes 10 – 12 = eCFP / eYFP standards (14 pmol, 7 pmol and 4.7 pmol respectively).

The density of the reconstitutions can be estimated from the position of the proteoliposome bands on the sucrose gradients, assuming that the proteoliposomes have the same density as the sucrose solution at that point in the gradient, by using the following equation:

$$\rho(T) = (B_1 + B_2T + B_3T^2) + (B_4 + B_5T + B_6T^2)Y + (B_7 + B_8T + B_9T^2)Y^2$$

Equation 5.7

Where ρ = density (kg/dm^3), T = temperature (^{o}C), Y = weight fraction of sucrose in solution and $B_{1\text{-}9}$ are constants (B_1 = 1.00037, B_2 = 3.96805 × 10^{-5}, B_3 = -5.85133 × 10^{-6}, B_4 = 0.389824, B_5 = -1.05789 × 10^{-3}, B_6 = 1.23928 × 10^{-5}, B_7 = 0.170976, B_8 = 4.75301 × 10^{-4}, B_9 = -8.92397 × 10^{-6}) (Barber, 1966). The partial specific volume (vbar, ml/g) can be calculated by taking the reciprocal of the density. Hence, an estimation of the lipid : protein (w/w) ratio can be calculated given that the calculated vbar has contributions from vbar(lipid) and vbar(protein), where vbar(lipid) was estimated from sucrose density gradient centrifugation of BPL-only samples to be 0.986 ± 0.003 ml/g and vbar(protein) was calculated as 0.734 ml/g from the amino acid composition of T43NTS1-eCFP/eYFP using the method of Cohn and Edsall (Cohn and Edsall, 1943):

$$vbar_{25} = \frac{\sum n_i M_i vbar_i}{\sum n_i M_i}$$

Equation 5.8

Where n is the number of moles of the *i*th component (each particular amino acid), M is its molecular weight and $vbar_{25}$ is the partial specific volume at a temperature of 25 ^{o}C. This value for vbar was then adjusted to the temperature of 4 ^{o}C at which the sucrose density gradient centrifugation took place (Durchschlag, 1986):

$$vbar_T = vbar_{25} + 4.25 \times 10^{-4} (T - 25)$$ Equation 5.9

Where T is the temperature (°C) and $vbar_T$ is the partial specific volume at temperature T. The estimated lipid : protein ratios for each of the reconstitution samples shown in Figure 5.9 are displayed in Table 5.2. The final lipid : protein molar ratios range from 410.4 ± 16.4 (1000 : 1 initial) and 583.4 ± 32.8 (6000 : 1 initial). Therefore, variation of the final lipid : protein ratio has been achieved by varying the starting lipid : protein ratio of the reconstitution. However, the lipid : protein ratios of the reconstitutions after sucrose gradient only varied over a 1.5-fold range, despite varying the starting ratio over a 6-fold range. The reason for this is unclear but it is exemplified by the low density, lipid-only band observed at the top of the sucrose gradients at the higher lipid : protein ratios (Figure 5.9) which indicates that a significant proportion of the lipid did not contain any inserted protein.

Table 5.2 – Calculation of lipid : protein ratios of reconstituted T43NTS1-eCFP/eYFP samples using sucrose density gradient centrifugation. The proteoliposome density was calculated using the position of the proteoliposome band on the sucrose gradient and Equation 5.7. The lipid : protein (w/w) ratio was calculated using the vbar of pure BPL lipid estimated from sucrose gradient (0.986 ± 0.0024 ml/g) and the vbar of T43NTS1-eCFP/eYFP which was estimated from the amino acid composition using Equation 5.8 and Equation 5.9 (0.734 ml/g).

Starting lipid : protein ratio (mol : mol)	Proteoliposome density (kg/dm^3)	Proteoliposome vbar (ml/g)	Final lipid : protein ratio (w/w)	Final lipid : protein ratio (mol : mol)
1000	1.086 ± 0.0009	0.921 ± 0.0008	3.86 ± 0.15	410.4 ± 16.4
2000	1.075 ± 0.0011	0.931 ± 0.0009	4.52 ± 0.21	480.4 ± 22.8
4000	1.068 ± 0.0009	0.936 ± 0.0008	5.05 ± 0.26	535.9 ± 27.7
6000	1.063 ± 0.0009	0.940 ± 0.0008	5.49 ± 0.31	583.4 ± 32.8

The lipid : protein molar ratio can be used to estimate the number of receptors per vesicle and hence the receptor density (number of receptors per unit area of membrane), a useful parameter to consider when determining the validity of resonance transfer

measurements. Taking the external vesicle radius to be 500 Å (since unilamellar vesicles were generated by extrusion through 0.1 μm membranes (section 4.2.1)) and the internal vesicle radius to be 460 Å (i.e. bilayer thickness of 40 Å), the total surface area of the vesicle (SA), including both surfaces of the bilayer, is:

$$SA = 4 \times \pi \times \left(500^2 + 460^2\right) = 5.8 \times 10^6 \text{ Å}^2 \qquad \text{Equation 5.10}$$

The number of receptor molecules per vesicle is therefore given by:

$$p = \frac{SA}{r.AL + AP} \qquad \text{Equation 5.11}$$

Where p is the number of receptor molecules per vesicle; r is the lipid : protein molar ratio; AL is the surface area per lipid molecule and AP is the surface area per receptor molecule. AL was taken to be 71.7 Å^2, the surface area observed per hydrated phosphatidylcholine lipid molecule (Small, 1967), and AP was taken to be 800 Å^2 which is the approximate surface area observed from structural studies of rhodopsin (Palczewski *et al.*, 2000). The number of receptors per vesicle and the receptor density for each reconstitution are shown in Table 5.3.

Table 5.3 – Calculation of receptor molecules per vesicle and receptor density for each reconstitution using the lipid : protein molar ratio calculated in Table 5.2. The surface area per lipid molecule was taken as 71.7 Å^2 (Small, 1967) and the surface area per receptor molecule as 800 Å^2 (Palczewski *et al.*, 2000). Vesicles were assumed to be spherical structures with a 100 nm diameter and a bilayer thickness of 4 nm.

Starting lipid : protein ratio (mol : mol)	Final lipid : protein ratio (mol : mol)	Receptor molecules per vesicle	Receptor density (receptors / 10,000 Å^2)
1000	410.4 ± 16.4	191.9 ± 7.7	0.33 ± 0.013
2000	480.4 ± 22.8	164.6 ± 7.8	0.28 ± 0.014
4000	535.9 ± 27.7	147.9 ± 7.6	0.25 ± 0.013
6000	583.4 ± 32.8	136.1 ± 7.6	0.23 ± 0.013

(ii) FRET Measurements on Reconstituted Receptor Samples

FRET experiments were carried out on the major proteoliposome bands harvested from the sucrose gradients which contained reconstituted T43NTS1-eCFP/eYFP (eCFP : eYFP molar ratio of 1.2 : 1 ± 0.03). 'Bleed through' and 'cross-talk' contributions were subtracted to yield the eYFP emission spectra due to FRET for each lipid : protein ratio (Figure 5.11).

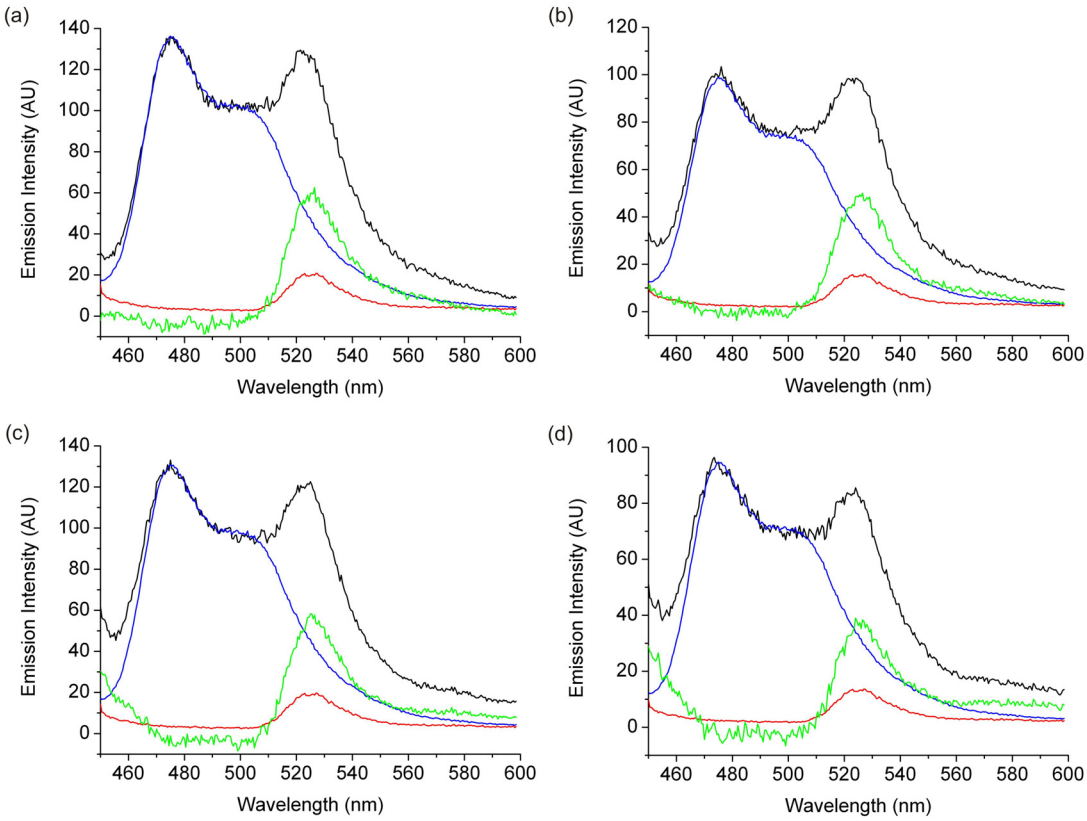

Figure 5.11 : Use of FRET to detect oligomerisation of lipid-reconstituted T43NTS1-eCFP/eYFP. Reconstitution samples had starting lipid : protein ratios of 1000 : 1 (a), 2000 : 1 (b), 4000 : 1 (c) and 6000 : 1 (d). Samples were excited at λ_{max}^{CFP} (440 nm) and the fluorescence emission detected by scanning fluorometry. Fluorescence emission due to FRET (green) was determined by subtracting the normalised emission spectrum of a T43NTS1-eCFP only sample (blue) and the normalised emission spectrum of a T43NTS1-eYFP only sample (red) from the emission spectrum of the mixed T43NTS1-eCFP and T43NTS1-eYFP sample (black).

NT stock solution was subsequently titrated into the samples to give a final NT concentration of 50 μM and the FRET experiment repeated after an equilibration time of 15 minutes (Figure 5.12). Figure 5.11 and Figure 5.12 show that there is significant FRET between eCFP- and eYFP-tagged receptors both in the absence and in the presence of NT.

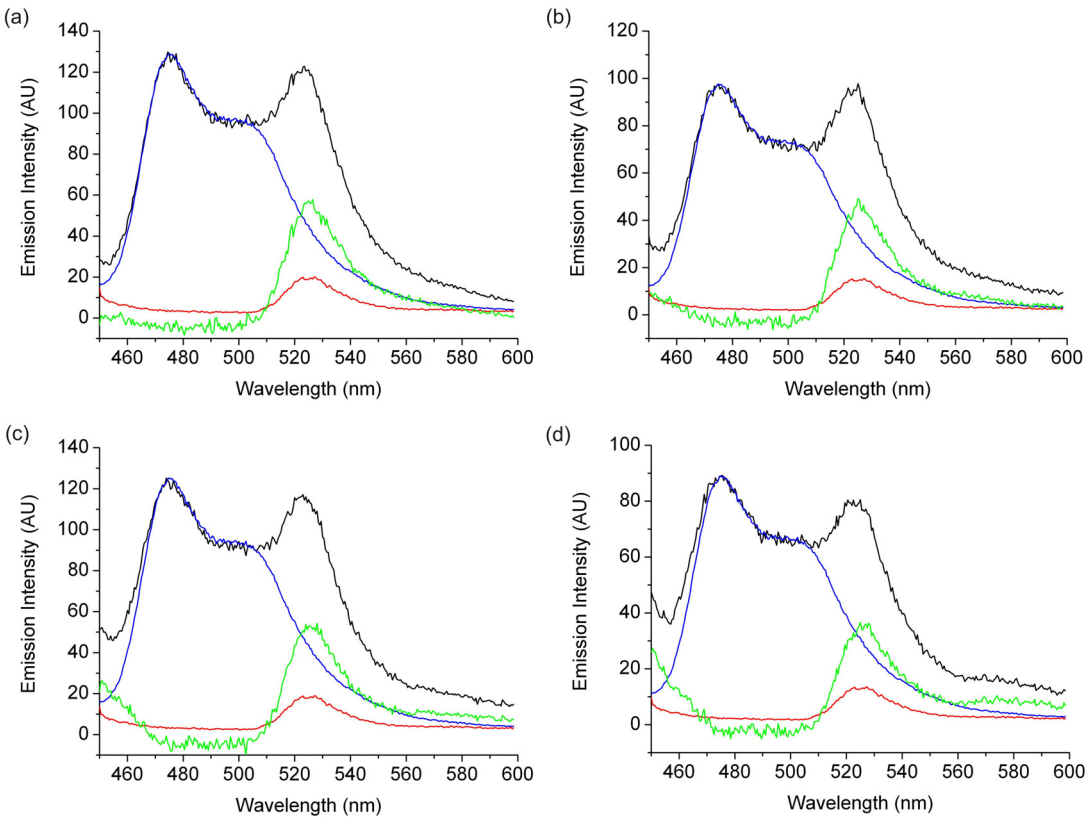

Figure 5.12 : Use of FRET to detect oligomerisation of lipid-reconstituted T43NTS1-eCFP/eYFP in the presence of 50 μM NT. Reconstitution samples had starting lipid : protein ratios of 1000 : 1 (a), 2000 : 1 (b), 4000 : 1 (c) and 6000 : 1 (d). Samples were excited at λ_{max}^{CFP} (440 nm) and the fluorescence emission detected by scanning fluorometry. Fluorescence emission due to FRET (green) was determined by subtracting the normalised emission spectrum of a T43NTS1-eCFP only sample (blue) and the normalised emission spectrum of a T43NTS1-eYFP only sample (red) from the emission spectrum of the mixed T43NTS1-eCFP and T43NTS1-eYFP sample (black).

5.3.3 - Calculation of FRET Efficiency

(i) Apparent FRET Efficiency

A number of techniques have been employed to calculate the efficiency of FRET (Clegg, 1992; Takanishi *et al.*, 2006). Previous studies of other GPCRs *in vivo* (Overton and Blumer, 2002b; Overton and Blumer, 2002a; Floyd *et al.*, 2003) have quantified FRET by calculating an 'Apparent FRET Efficiency' parameter in accordance with Equation 5.2. Whilst this term is not a measure of the precise efficiency of FRET, and is therefore not useful for interfluorophore distance measurements, it provides a rapid method for the comparison of the relative ability of GPCRs to engage in FRET, provided both the donor : acceptor ratio and the specific donor : acceptor fluorophore pair are kept constant. It is therefore a convenient approach for comparison of the FRET observed here to that observed by Overton and Blumer (2002) and Floyd *et al* (2003), where the eCFP/eYFP FRET pair, at an approximate donor : acceptor ratio of 1 : 1, was also employed.

The amount of FRET is quantified by measuring the enhancement of acceptor emission in the presence of FRET. The FRET efficiency is calculated by dividing the integrated area of the FRET spectrum by the integrated area of the YFP emission spectrum, which was obtained by irradiating the same sample at λ_{max}^{YFP}. Figure 5.13 shows the FRET emission spectra and the maximal YFP emission spectra for each sample. Both spectra are normalised to the maximal YFP emission spectrum for each sample in order to allow direct graphical comparison between the different lipid : protein ratios. The calculated apparent FRET efficiencies are given in Table 5.4.

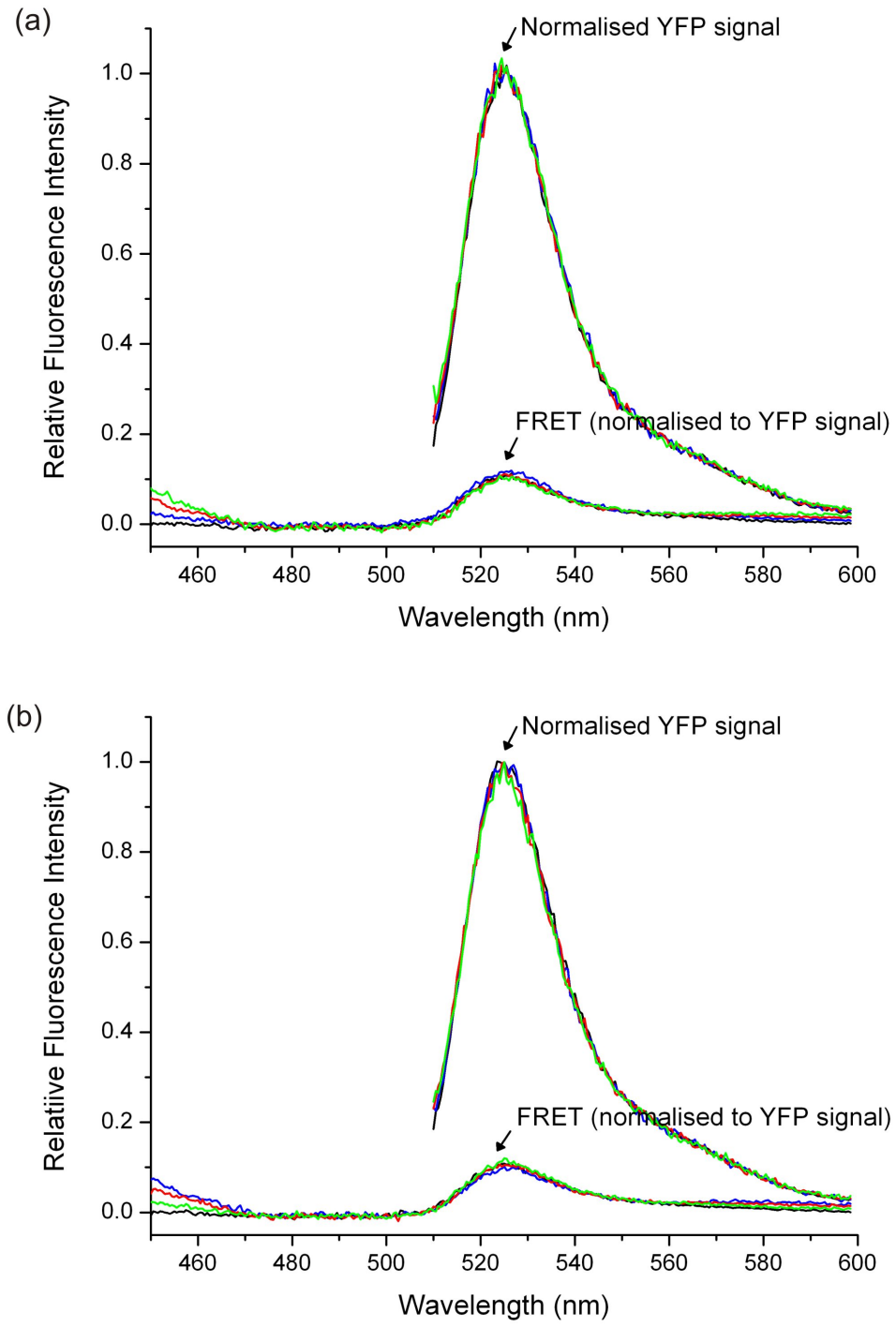

Figure 5.13 – Apparent efficiency of FRET in the absence (a) and presence (b) of 50 μM NT for T43NTS1-eCFP/eYFP lipid-reconstituted samples. eYFP emission due to FRET and YFP emission when excited at λ_{max}^{YFP} were both normalised to the YFP emission when excited at λ_{max}^{YFP} for each lipid : protein ratio (1000 : 1 = black; 2000 : 1 = blue; 4000 : 1 = red; 6000 : 1 = green).

Table 5.4 – Apparent FRET efficiency of T43NTS1-eCFP/eYFP reconstituted samples in the presence and absence of 50 μM NT. Apparent FRET efficiency was calculated from the emission spectra displayed in Figure 5.13: ((integrated FRET curve)/(integrated emission curve obtained on direct excitation of eYFP at λ_{max}^{YFP})) × 100.

Final lipid : protein ratio	Apparent FRET Efficiency (%)	
	No NT	NT (50 μM)
426	10.4	10.3
500	12.0	11.3
565	11.4	11.5
619	11.6	11.6
Mean (± error)	11.4 ± 0.3	11.2 ± 0.3

The mean apparent FRET efficiency of the reconstituted samples is 11.4 ± 0.3 % and 11.2 ± 0.3 % prior to NT addition and post NT addition respectively. This is in agreement with the apparent efficiency reported previously for *in vivo* homomultimerisation studies of eCFP- and eYFP-tagged α-factor receptors (11.5 ± 2.2 %, (Overton and Blumer, 2000)) and C5a receptors (12.6 ± 3.0 %, (Floyd *et al.*, 2003)). Yeast α-factor receptor is a GPCR which has been widely demonstrated to constitutively oligomerise. The efficiency observed for eCFP- and eYFP-tagged NTS1 is therefore of reasonable order of magnitude to support the conclusion that the receptor exists as a dimer and that the dimer is formed prior to addition of agonist. Indeed, if receptors exist as dimers, the theoretical maximum efficiency of FRET is only ~50 % since only half of the receptor dimers would be composed of an eCFP- and a eYFP-tagged receptor. In addition, the theoretical maximum efficiency in this case would be less than 50 %, since the fluorescent chromophores of eCFP and eYFP are ~15 Å from the surface of the protein (Tsien, 1998). Consequently, the minimum separation between adjacent eCFP and eYFP fluorophores is at least 30 Å. Therefore, the FRET efficiency observed suggests that the receptors are not forming higher order

oligomers or large aggregations in the reconstituted samples, since FRET efficiencies exceeding 50 % could be envisaged in such cases.

In addition, there is no significant variation in apparent FRET efficiency with receptor density. This suggests that the FRET emission observed is due to true interaction of receptor molecules, and is not a consequence of random collisions of receptors in the membrane (also called 'bystander FRET'). If FRET is caused by random collisions, a pseudo-linear increase in FRET efficiency with receptor density is expected, as has been reported in BRET studies with GPCRs (Mercier *et al.*, 2002; James *et al.*, 2006). Mercier *et al* varied the expression level of the β-adrenergic receptor GPCR fused with luciferase and GFP *in vivo*, at a donor : acceptor ratio of approximately 1 : 1, and monitored the BRET efficiency. Variation of receptor expression between 1.4 and 26 pmol/mg of membrane protein gave a constant BRET efficiency, indicating a true receptor : receptor interaction and low bystander BRET. Increase of the expression level to 47 pmol/mg and higher gave a large increase in BRET efficiency which was attributed to bystander BRET. An expression level of 47 pmol/mg corresponds to a receptor density of 2.4 receptor molecules per 10,000 $Å^2$ (Mercier *et al.*, 2002). Given that the receptor density in the T43NTS1-eCFP/eYFP reconstituted samples was varied between 0.23 and 0.33 receptors per 10,000 $Å^2$ (Table 5.3), this suggests that little contribution from bystander FRET should be expected in this case.

(ii) Corrected FRET Efficiency

In order to calculate the precise efficiency of FRET, which in turn allows the quantification of interfluorophore distance, a 'corrected FRET efficiency' term can be calculated. This is a modification of the apparent FRET efficiency to take into account the different extinction coefficients of the donor and acceptor fluorophores at their respective λ_{max} excitation (Equation 5.3). Corrected FRET efficiencies and the

corresponding interfluorophore distances for the reconstituted samples, in the presence and absence of NT, are shown in Table 5.5.

Table 5.5 – Calculation of corrected FRET efficiency and interfluorophore distance. Corrected FRET efficiency was calculated from the apparent FRET efficiency using Equation 5.3 (ε_A = 75768 $M^{-1}cm^{-1}$ (Patterson *et al.*, 2001), ε_D = 29817 $M^{-1}cm^{-1}$ (Cubitt *et al.*, 1999)). R_o was calculated as 45.6 Å for the eCFP/eYFP donor/acceptor pair.

Final lipid : protein ratio (mol : mol)	Corrected FRET Efficiency (%)		Interfluorophore distance (Å)	
	No NT	NT (50 μM)	No NT	NT (50 μM)
426	26.4	26.2	54.1	54.2
500	30.4	28.7	52.3	53.0
565	29.0	29.2	52.9	52.8
619	29.5	29.5	52.7	52.7
Mean (± error)	28.8 ± 0.9	28.4 ± 0.8	53.0 ± 0.4	53.2 ± 0.4

As might be expected, the same trends as shown for the apparent FRET efficiencies can be seen in the data, namely no significant variation in the FRET efficiency (and therefore the interfluorophore distance) with receptor density and NT addition. However, interpretation of the yielded interfluorophore distances must be approached with caution for several reasons.

Firstly, as discussed above, if the receptor is dimeric, then the maximum corrected FRET efficiency that can be attained is 50 %. Secondly, in the particular case of the eCFP and eYFP fluorescent proteins, this theoretical maximum is decreased further because of the 15 Å distance from the surface of the protein to the chromophore itself. Therefore, the approximate maximum efficiency for dimeric receptor, taking the above factors into account, is only ~46.2 %. Lastly, changes in the orientation of donor and acceptor fluorophores can also significantly affect FRET efficiency. The Förster radius is usually calculated using a value for the orientation factor (κ^2, see Equation 5.5) for dipole-dipole coupling of 2/3 which assumes an equal distribution of the fluorophores

in all orientations in the excited state. The orientation of fluorophores attached to a GPCR could be restricted in such a way that would either favour or hinder efficient FRET.

6.3.4 - PFO Native Gel Electrophoresis

PFO-PAGE, a form of native gel PAGE, was used to further assess the multimerisation state of T43NTS1-eCFP/eYFP. This technique has been previously demonstrated to maintain the physiological oligomerisation state of several other membrane proteins, by replacing the standard SDS detergent normally used in electrophoresis with the detergent perfluoro-octanoic acid (PFO) (Ramjeesingh *et al.*, 1999; Ramjeesingh *et al.*, 2003). Purified, detergent-solubilised T43NTS1-eCFP was analysed, as well as purified full length, uncleaved NTS1C (MBP-TeV-T43NTS1-eCFP-TeV-TrxA-His10) as a comparison. All gels were repeated using standard SDS-PAGE as a direct comparison of migration characteristics in the two detergent systems. Gels were analysed by in-gel fluorescence (Figure 5.14) and were subsequently stained with Coomassie Brilliant Blue (Figure 5.15).

For molecular weight determinations, the mobilities of the molecular weight standard protein bands for the Tris-Glycine 12 % PFO-PAGE gel were plotted against the logarithm of the molecular masses yielding a linear relationship (Figure 5.16).

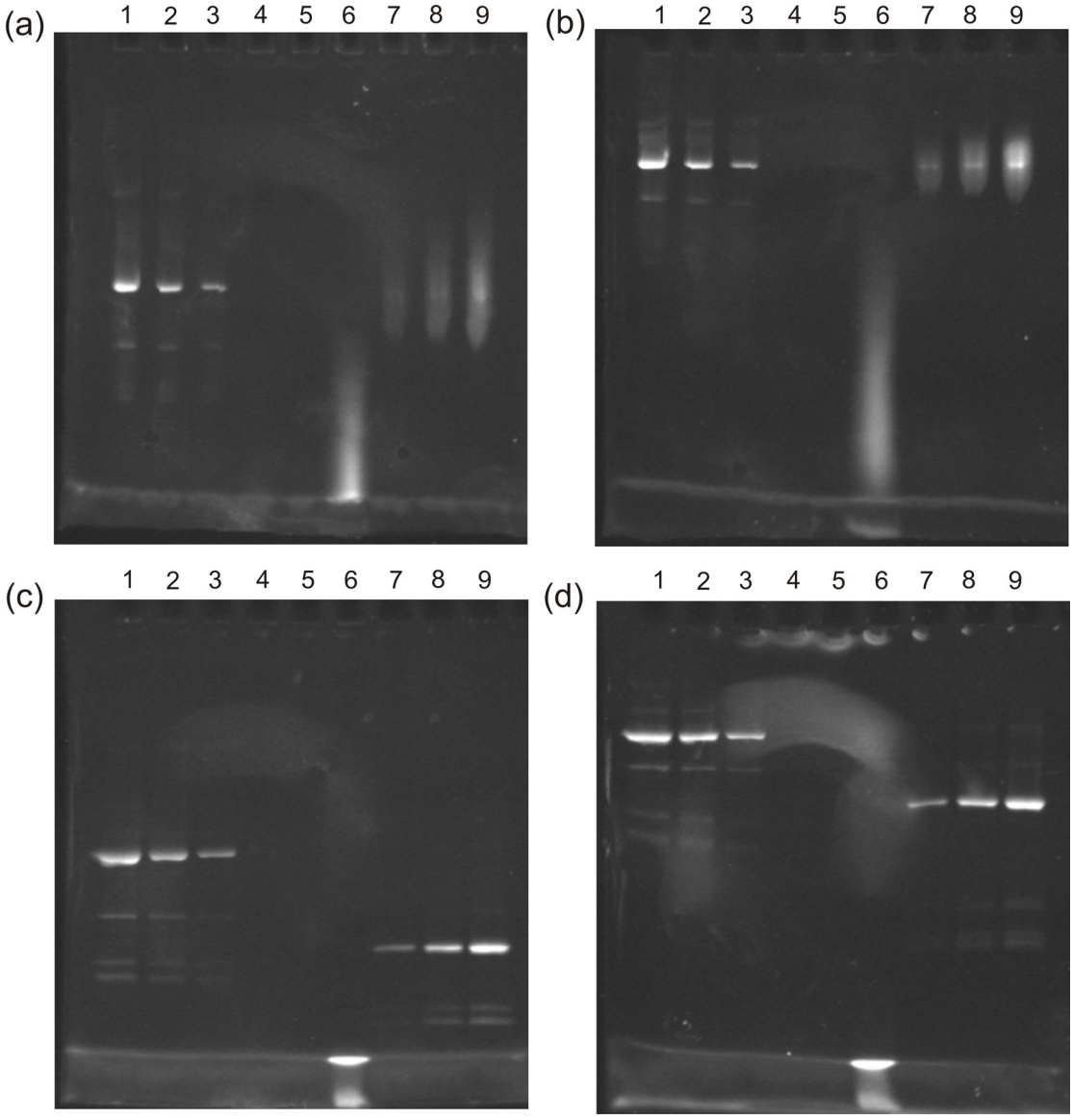

Figure 5.14 – PFO-PAGE and SDS-PAGE of purified, detergent solubilised NTS1C (uncleaved) and T43NTS1-eCFP (cleaved) receptor, visualised by in-gel fluorescence. Samples were separated by PFO-PAGE using 4-12 % (a) and 12 % (b) Tris-Glycine gels and by SDS-PAGE using 4-12 % (c) and 12 % (d) Tris-Glycine gels. For all gels, lane 1 = NTS1C (20 pmol); lane 2 = NTS1C (10 pmol); lane 3 = NTS1C (5 pmol); lanes 4-6 = molecular weight standards (not visible); lane 7 = T43NTS1-eCFP (7.5 pmol); 8 = T43NTS1-eCFP (15 pmol); 9 = T43NTS1-eCFP (30 pmol). All images were obtained with a 0.5 sec exposure.

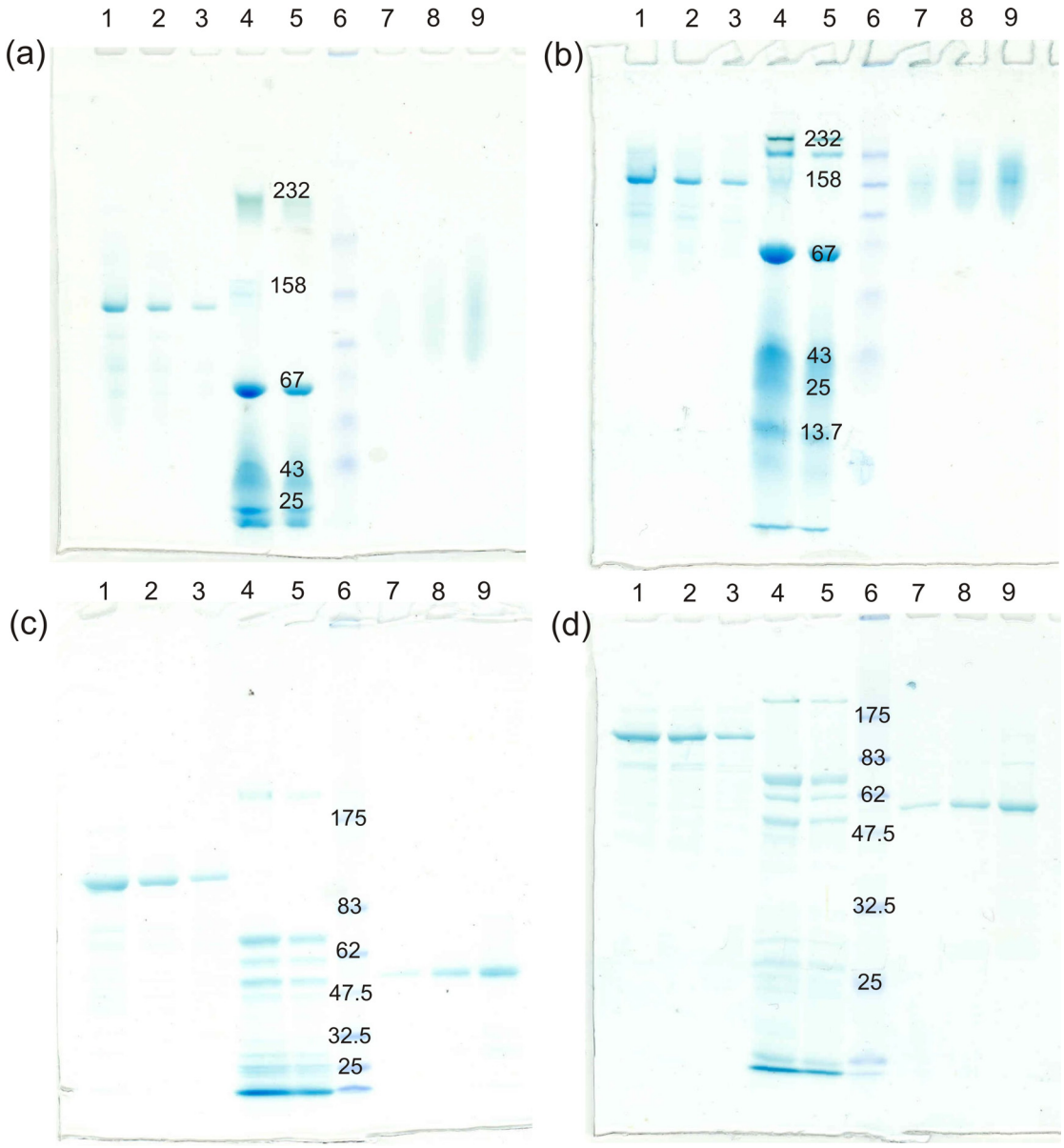

Figure 5.15 – PFO-PAGE and SDS-PAGE of purified, detergent solubilised NTS1C (uncleaved) and T43NTS1-eCFP (cleaved) receptor, visualised by Coomassie Brilliant Blue staining. Samples were separated by PFO-PAGE using 4-12 % (a) and 12 % (b) Tris-Glycine gels and by SDS-PAGE using 4-12 % (c) and 12 % (d) Tris-Glycine gels. For all gels, lane 1 = NTS1C (20 pmol); lane 2 = NTS1C (10 pmol); lane 3 = NTS1C (5 pmol); lane 4 = PFO molecular weight standards; lane 5 = PFO molecular weight standards 1 in 2 dilution; lane 6 = Prestained SDS molecular weight standards; 6 = molecular weight standards; lane 7 = T43NTS1-eCFP (7.5 pmol); 8 = T43NTS1-eCFP (15 pmol); 9 = T43NTS1-eCFP (30 pmol).

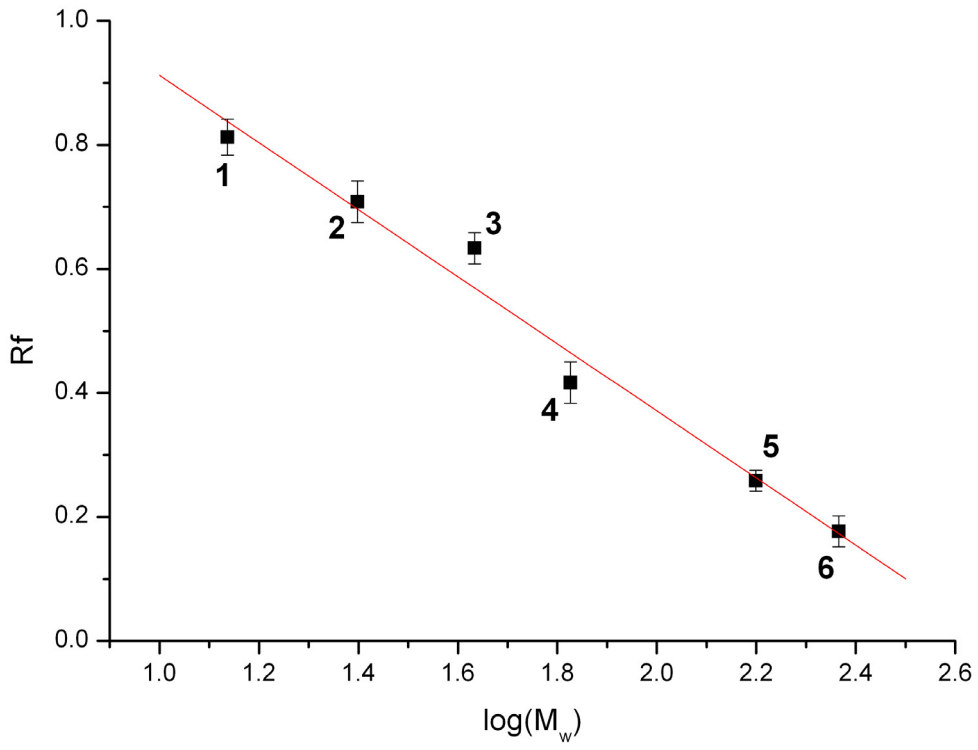

Figure 5.16 – Molecular weight determination. The mobilities of the protein bands relative to the front (Rf) for the 12 % Tris-Glycine PFO-PAGE gel were plotted against the logarithm of the molecular masses (Mw). The identities of the molecular weight standards were: 1 = Catalase (232 kDa); 2 = Aldolase (159 kDa); 3 = Albumin (67 kDa); 4 = Ovalbumin (43 kDa); 5 = Chymotrypsin (25 kDa); 6 = Ribonuclease A (13.7 kDa).

It can be seen from both in-gel fluorescence and Coomassie visualisation of the PFO gels (Figures 5.14a, 5.14b, 5.15a, 5.15b) that the T43NTS1-eCFP (expected Mw = 69.9 kDa) has approximately the same mobility as the uncleaved NTS1C protein (expected Mw = 131 kDa). This therefore suggests that the uncleaved protein migrates as a monomer and that T43NTS1-eCFP migrates as a dimer. Closer inspection of the molecular weight relative to the molecular weight standards yields apparent molecular weights of 161 kDa for NTS1C and 159 kDa for T43NTS1-eCFP. Therefore, the uncleaved NTS1C appears to be migrating at a slightly higher molecular weight than expected for the monomeric form and T43NTS1-eCFP appears to be migrating at a slightly higher molecular weight than expected for the dimeric form. The NTS1C protein also migrates as a tight, discrete band whilst the T43NTS1-eCFP band is quite

diffused around the stated molecular weight. The reason for this is not clear but could be envisaged to be an artefact of relatively weak multimerisation.

Comparison of the PFO gels with the standard SDS-PAGE confirms that the SDS-solubilised, monomeric forms of each protein migrate quite differently. The proteins migrate in bands corresponding to 115 kDa and 67 kDa for NTS1C and T43NTS1-eCFP respectively. The proteins are therefore migrating at a slightly lower molecular weight than expected on the SDS gels, a phenomenon which has been observed previously for GFP-fusions (Drew *et al.*, 2006) and is likely due to the fact that the eCFP moiety remains folded after SDS-treatment. It is of course this property which the in-gel fluorescence technique exploits.

The PFO electrophoresis results, whilst by no means a definitive demonstration of the physiological oligomerisation state of NTS1, do suggest that the T43NTS1-eCFP fusion protein does have a tendency to multimerise. In addition, the apparent molecular weight of the multimer in PFO detergent suggests that it is composed of two receptor monomers.

5.4 - CONCLUSIONS

FRET experiments were carried out with eCFP- and eYFP-tagged NTS1 both in detergent solution and in lipid-reconstituted systems. The lack of FRET between eCFP and eYFP in the detergent samples at concentrations of up to 200 nM and in the presence and absence of NT suggests that, in this case, the receptor is monomeric. A negative result caused by a lack of exchange of eCFP- and eYFP-tagged receptors between detergent micelles can be excluded, since eCFP- and eYFP-tagged samples were combined at the beginning of the purification (cell resuspension stage). However, the cryo-EM of detergent-solubilised T43NTS1 (section 2.3.4) yielded a reconstruction of comparable dimensions to the putative rhodopsin dimers observed by EM and AFM (Fotiadis *et al.*, 2006). It is therefore possible that dimerisation of T43NTS1 can occur in detergent solution but in a concentration dependent manner.

FRET was observed between eCFP and eYFP in the lipid-reconstituted samples. The apparent efficiency of FRET (11.2 ± 0.3 % and 11.4 ± 0.3 %, in the absence and presence of NT respectively) compares favourably with the efficiency observed for FRET between eCFP- and eYFP-tagged yeast α-factor receptor *in vivo* (11.5 ± 2.2 %), a GPCR which is widely believed to constitutively dimerise (Overton and Blumer, 2000; Overton and Blumer, 2002b). A comparable FRET efficiency was also observed for eCFP- and eYFP-tagged C5a receptor *in vivo* (12.6 ± 3.0 %, (Floyd *et al.*, 2003)). In addition, variation of the receptor density had no significant effect on the FRET efficiency. This is indicative of FRET which is caused by a true receptor-receptor interaction rather than by random collisions ('bystander FRET'). Comparison of the receptor density with an *in vivo* BRET study between luciferase- and GFP-tagged β-adrenergic receptor (Mercier *et al.*, 2002) also suggests that FRET due to random collisions should not be significant at the receptor densities used in this study. The

FRET efficiency also did not change significantly upon addition of NT, which suggests that multimerisation and the relative orientations of the receptor monomers are not affected by agonist binding.

PFO-PAGE, a form of native gel electrophoresis, also provided evidence of dimer formation. The T43NTS1-eCFP protein migrated at approximately the same molecular weight (160 kDa) as the full length, uncleaved NTS1C protein. The molecular weight of NTS1C is 131 kDa and the molecular weight of a T43NTS1-eCFP dimer would be ~140 kDa. This suggests that the T43NTS1-eCFP protein forms a dimer in PFO detergent whilst the uncleaved NTS1C is monomeric, given that PFO electrophoresis has been shown to preserve physiological oligomeric interaction for membrane proteins (Ramjeesingh *et al.*, 1999).

Further variation of receptor density of the reconstitutions over a greater range would help to confirm this hypothesis if a constant FRET efficiency was observed. Another definitive experiment would be the addition of untagged NTS1 into the T43NTS1-eCFP/eYFP reconstitutions. One would expect the untagged receptor to compete with the fluorescent receptors for dimerisation, therefore causing a decrease in FRET efficiency. Such an experiment would also confirm whether any multimerisation is in fact caused by receptor-receptor interactions or whether it is an artificially induced interaction between eCFP and eYFP, since eCFP and eYFP have previously been shown to form weak dimers (Shaner *et al.*, 2005).

The reconstitution of purified T43NTS1-eCFP/eYFP into brain polar lipids appears to provide a useful minimal, *in vitro* experimental system for the study of NTS1 multimerisation. Increasing the complexity of the system through the addition of other signalling components could be envisaged in a quantitative, controlled manner.

In addition, single molecule FRET-based techniques, such as alternating-laser excitation (ALEX) spectroscopy (Kapanidis *et al.*, 2005), have yet to be applied to the GPCR field but have potential for the study of the mechanisms involved in receptor signalling and oligomerisation. Unlike the ensemble approaches, which yield data averaged over an entire population of molecules, single molecule methods such as ALEX allow the study of individual members of such populations (Zlatanova and van Holde, 2006). These methods can therefore yield extra information which is beyond the capabilities of population methods, such as intermolecular variations in a classically homogenous population of macromolecules ('static disorder') and fluctuations in the observable parameters of a single molecule over time ('dynamic disorder'). For example, quantification of the proportion of receptor in oligomeric verses monomeric state is problematic for ensemble techniques, as is differentiation between dimeric and higher order oligomeric forms. Single molecule approaches could yield such information. A single molecule study would be best applied to fluorescence-tagged GPCRs which have been incorporated into *in vitro* lipid-reconstituted systems, as has been achieved here. Therefore, indications are that this study represents a useful starting point for single molecule studies.

CHAPTER 6 - CONJUGATION OF NT WITH FLUORESCENT PROBES

SUMMARY

Fluorescently tagged NT derivatives will provide a useful tool for future fluorescence studies including alternating-laser excitation (ALEX) spectroscopy and single molecule tracking. In this chapter, NT_{2-13} was successfully produced by solid phase peptide synthesis with the fluorescent dye, carboxytetramethylrhodamine (TAMRA), attached at the N-terminus. Two alternative fluorescent peptides were produced, the first with the TAMRA dye directly conjugated to the peptide (TAMRA-NT_{2-13}), and the second with a PEG linker between the TAMRA and the N-terminus (TAMRA-linker-NT_{2-13}). Radioligand competition assays and fluorescence correlation spectroscopy (FCS) confirmed that the fluorescent peptides bound to purified NTS1 in specific competition with unlabelled NT. The fluorescent NT derivative which incorporated the PEG linker was found to bind the receptor with the higher affinity, although both peptides bound to NTS1 with considerably lower affinity than unlabelled NT.

6.1 - INTRODUCTION

6.1.1 - Fluorescence tagging of Peptide Ligands

The subject of fluorophore-tagging of GPCR ligands has recently been reviewed (Daly and McGrath, 2003; Middleton and Kellam, 2005). Peptide ligands, such as NT, are particularly amenable to labelling with fluorescent dyes since the fluorophore can be introduced using solid phase peptide synthesis techniques (Merrifield, 1963). Ideally, a fluorescent ligand should, as far as possible, retain the affinity and selectivity of the untagged agonist. In practice, however, the addition of a fluorescent moiety can often affect the binding affinity of the ligand. The degree of loss of affinity will usually be dependent on the site at which the fluorophore is attached to the ligand, but can also vary according to the particular fluorophore used. For example, the addition of the fluorophores fluorescein (FITC) or BODIPY to DTrp8-somatostatin (D-Trp8-SRIF) only slightly reduced the affinity of the ligand in brain membrane preparations, whereas the tagging of a Cy 3.5 fluorophore to the same molecule reduced its binding affinity by almost an order of magnitude (Beaudet *et al.*, 1998).

The synthesis of neurotensin (NT) peptide conjugated to fluorescent tags has been previously reported. The peptide has typically been successfully labelled at the N-terminus with little perturbation to binding affinity, likely because labelling at this position sites the fluorescent dye at a maximal distance from the six C-terminal amino acids required for receptor binding (section 1.5.1). For example, NT labelled at the N-terminus with Fluorescein isothiocyanate (FITC) was found to bind specifically to mouse brain membrane preparations with a K_i of 0.67 nM, a similar affinity to that observed for the unlabelled peptide (K_i = 0.55 nM) (Faure *et al.*, 1994). In a separate study, NT_{2-13} was N-terminally labelled with the fluorescent dye, Cy5 (Fang *et al.*, 2006). The authors reported a high affinity interaction of the fluorescent peptide with microarrays formed from membrane fractions containing NTS1 (K_d = 1.4 nM). However, analysis of the binding of NT_{2-13} which was N-terminally labelled with the fluorescent dye BODIPY (Nα-BODIPY-NT_{2-13}) to NTS2 receptor membrane preparations did reveal perturbation of binding (Sarret *et al.*, 2002). The fluorescence-tagged ligand bound with a 3-fold lower affinity than the unlabelled peptide.

6.1.2 - Fluorescence Correlation Spectroscopy

Fluorescence correlation spectroscopy (FCS) was first introduced to measure diffusion and chemical dynamics of DNA-drug intercalation (Magde *et al.*, 1972). It is an experimental technique which uses the statistical analysis of the fluctuations of fluorescence in a system to decipher dynamic molecular events, such as diffusion or conformational changes of biomolecules.

The sample fluorophore concentration is typically limited to the nanomolar (nM) range, and confocal microscopy, in which the incoming laser light is strongly focused by a high numerical aperature objective to a diffraction-limited spot, is used to generate a sub-femtolitre (10^{-15} l) observation volume (Schwille and Haustein, 2002). When the sample

concentration is around 1-10 nM, the average number of molecules in the excitation volume will then be of the order of one (Breusegem *et al.*, 2006). Diffusion will lead to constant entry and exit of fluorescent molecules from the excitation volume and will give rise to fluctuations in the fluorescent signal measured.

Fluctuations in the fluorescence signal are quantified by temporal autocorrelation analysis of the recorded intensity signal, in which the autocorrelation function (G(τ)) is calculated (Equation 6.1).

$$G(\tau) = 1 + \frac{\langle \delta I(t).\delta I(t+\tau) \rangle}{\langle I(t) \rangle^2}$$

Equation 6.1

Where <I(t)> is the average fluorescence intensity. In principle, this autocorrelation routine provides a measure for the self-similarity of a time signal and highlights characteristic time constants of underlying processes. Effectively, the method searches for recurring patterns when the measured signal is compared with itself at some later time.

Autocorrelation allows the diffusion times of molecular complexes (i.e. the average time it takes for the fluorescent molecules to diffuse through the confocal volume) to be readily measured using FCS. Consequently, molecular interactions can be monitored provided that the diffusion time of the unbound fluorescent binding partner is significantly different to that of the molecular complex formed (Schwille *et al.*, 1997). Binding of the fluorescently-labelled molecule to its binding partner to form a complex of higher molecular weight causes a change in the observed diffusion to a slower diffusion time (Figure 6.1).

In order to obtain a significant change in diffusion time, the mass ratio should be at least 8, preferably more than one order of magnitude, due to the approximate cube root

dependence of the diffusion coefficient on molecular mass (Equation 6.2, Stokes-Einstein Equation).

$$D = \frac{k.T}{6\pi.\eta_v.R_h}$$

Equation 6.2

Where D is the diffusion coefficient in aqueous solution, R_h is the hydrodynamic radius, T is the temperature, η_v is the viscosity of the solution and k is the Boltzmann constant (1.38×10^{-23} J/K).

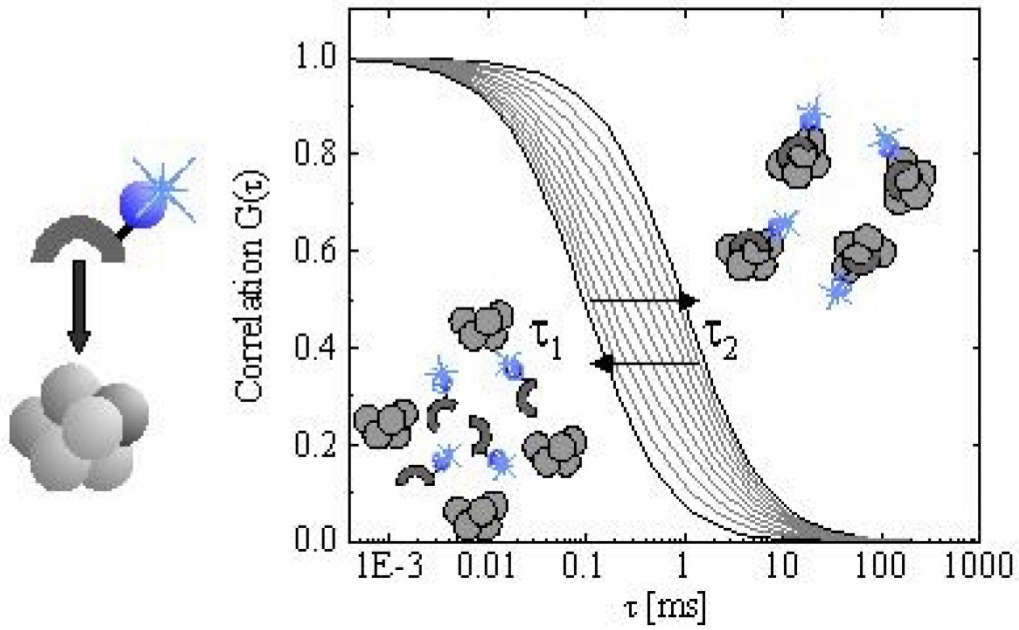

Figure 6.1 – Measurement of molecular interactions by FCS (Schwille and Haustein, 2002). A small molecule, labelled with a fluorophore, with a relatively fast diffusion time (τ_1) binds to a larger binding partner to form a complex of higher molecular weight and slower diffusion time (τ_2). Initially, the diffusion time of the small molecule is determined without the binding partner present. Curves obtained from samples which contain both binding partners can then be fitted using two diffusion components, fixing the diffusion time of the smaller component to the value determined previously (Schwille *et al.*, 1997).

6.1.3 - Aims

The aim of this chapter is to synthesise and purify fluorescently-labelled derivatives of NT. The binding affinity of the synthesised fluorescent peptides for NTS1 will be tested using radioligand competition assays and fluorescence correlation spectroscopy (FCS) in order to determine whether there are any perturbations to the ligand binding affinity arising from the conjugation to the fluorescent dye.

The synthesis and purification of a fluorescent NT-derivative will be a useful tool for future fluorescence studies including alternating-laser excitation (ALEX) spectroscopy, which incorporates single molecule FRET with fluorescence-aided molecule sorting (FAMS), and will be used to further probe the multimerisation state of the receptor (Kapanidis *et al.*, 2004; Doose *et al.*, 2007). In addition, a fluorescent NT derivative could be used for single molecule tracking experiments if bound to NTS1 expressed in tissue cells or cultured cell lines (Kusumi *et al.*, 2005; Garcia-Saez and Schwille, 2007).

6.2 - MATERIALS AND METHODS

6.2.1 - Synthesis of Fluorescent NT Derivatives

The following peptides were produced by solid phase peptide synthesis and purified by reversed phase HPLC (for detailed methods see Appendix A8):

TAMRA-NT_{2-13}	TAMRA- Leu-Tyr-Glu-Asn-Lys-Pro-Arg-Arg-Pro-Tyr-Ile-Leu
TAMRA-linker-NT_{2-13}	TAMRA-$(PEG)_2$- Leu-Tyr-Glu-Asn-Lys-Pro-Arg-Arg-Pro-Tyr-Ile-Leu

The 'linker' moiety is a PEG linker (Fmoc-NH-$(PEG)_2$-COOH (20 atoms)) obtained from Novabiochem (Merck). The TAMRA fluorophore was 5(6)-TAMRA (5(6)-Carboxytetramethylrhodamine) and was purchased from Anaspec.

6.2.2 - Radioligand Competition Assays

A radioligand binding assay was used to determine dissociation constants for the TAMRA-labelled NT peptides (section 6.2.1). The standard protocol (Appendix A3) was used with the following modifications. Detergent-solubilised NTS1Y (MBP-TeV-T43NTS1-eYFP-TeV-TrxA-His_{10}) was purified using the protocol described in section 3.3.2. ^{3}H-NT (final concentration of 1 nM) was incubated (1 h, 4 °C) with NTS1Y in assay buffer (50 mM Tris, pH 7.4, 0.1 % DDM (w/v), 0.01 % CHS (w/v), 1 mM EDTA, 0.1 mg/ml BSA) in the presence of varying concentration of TAMRA-labelled peptide. Receptor-bound ^{3}H-NT was separated from unbound ^{3}H-NT using P30 Tris microspin columns (BioRad). Competition curves were fitted to a one site competition model (Equation 6.3):

$$Y = A_2 + \left(\frac{A_1 - A_2}{1 + 10^{(X - \log IC_{50})}} \right)$$

Equation 6.3

Where A_2 is the bottom plateau of the competition curve, A_1 is the top plateau of the competition curve, X is the concentration of competitor, IC_{50} is the concentration of

competitor peptide at 50 % saturation and Y is the amount of specific binding. K_i, the equilibrium dissociation constant for the competitor peptide, was calculated from the IC_{50} using the following equation:

$$K_i = \frac{IC_{50}}{1 + \frac{[radioligand]}{K_d}}$$

Equation 6.4

Where [radioligand] is the concentration of tritiated NT used for the experiment (1 nM) and K_d is the equilibrium dissociation constant for unlabelled NT binding to NTS1 (0.9 nM, see section 3.3.5). Data was also fitted to the dose response (Hill) equation (Equation 6.5) to test for compliance for competition for a single class of binding site.

$$Y = A_2 + \left(\frac{A_1 - A_2}{1 + 10^{(X - \log IC_{50}) * p}} \right)$$

Equation 6.5

Where *p* is the Hill slope of the competition curve.

6.2.3 - Fluorescence Correlation Spectroscopy

Fluorescence correlation spectroscopy (FCS) was carried out using a custom setup (Kapanidis lab, OU Physics). A continuous-wave frequency-doubled NdYAG laser (WorldStarTech, Canada) emitting at 532 nm was coupled into the side-port of an inverted microscope (IX71, Olympus). The excitation light was focused into the sample solution through a water immersion objective (Olympus, 60x, NA = 1.2). Fluorescence emission was collected with the same objective and separated from excitation light using a dichroic beamsplitter (Semrock, USA). The objective was cooled to 6 °C using a recirculating chiller / cooling collar setup in order to maximise receptor sample stability. A 100 μm pinhole was mounted into the focal plane of the detection path to reduce scatter and background. Single photons were detected with an avalanche photodiode

(SPQR14, Perkin&Elmer, USA) using appropriate emission filters (585DF70 bandpass filter, Omega Optics, USA).

Varying amounts of purified, detergent-solubilised NTS1B were added to TAMRA-linker-NT peptide in FCS measurement buffer (50 mM Tris pH 7.4, 15 % glycerol (v/v), 0.1 % DDM (w/v), 0.01 % CHS (w/v), 1 mM EDTA) and equilibrated at 4 °C for 1 h. The final concentration of TAMRA-linker-NT was 10 nM and the final concentration of NTS1B was varied between 0 and 186 nM (as determined by radioligand binding assay (Appendix A3). Experiments were repeated in the presence of excess unlabelled NT (3.5 μM) as a control for non-specific binding. Autocorrelation analysis was performed using custom-written software in LabView v.7.1 (National Instruments). Origin v7.1 (Microcal Software) was used for curve fitting to the autocorrelation functions. In the case of a single diffusing fluorescent species, the autocorrelation function can be defined as:

$$G(\tau) = 1 + \left(\frac{1}{N}\right)\left(\frac{1}{1+\frac{\tau}{\tau_1}}\right) + base$$

Equation 6.6

Where τ_1 is the diffusion time of TAMRA-linker-NT, N is the total number of detected molecules in the effective detection volume. The *base* parameter is a constant offset that arises from the fact that two photons at time zero and time τ can originate from uncorrelated background or from different fluorescing molecules. In this case, the photons would not have any physical correlation which gives rise to the offset term that is completely independent of τ.

In the case of a small labelled probe (such as TAMRA-linker-NT) binding to a large labelled target (such as NTS1B), complex formation will change the rate of diffusion

while the fluorescence characteristics of the dye will be unaltered. Therefore, an extra diffusion term must be included and the process can be described by the following autocorrelation function:

$$G(\tau) = 1 + \left(\frac{1}{N}\right)\left(\frac{\theta}{1+\frac{\tau}{\tau_1}}\right) + \left(\frac{1-\theta}{1+\frac{\tau}{\tau_2}}\right) + base$$

Equation 6.7

Where θ is the fraction of TAMRA-linker-NT in the unbound state, τ_1 is the diffusion time of the TAMRA-linker-NT and τ_2 is the diffusion time of the TAMRA-linker-$NT_{2\text{-}13}$: NTS1B complex. The binding affinity for the TAMRA-linker-$NT_{2\text{-}13}$: NTS1B interaction was calculated by fitting the data to a single component binding isotherm (Equation 6.8)

$$Y = \frac{B_{\max} \cdot X}{X + K_d}$$

Equation 6.8

Where Y is the amount of specific binding, and in this case, B_{max} is the total amount of TAMRA-linker-$NT_{2\text{-}13}$ and X is the concentration of free NTS1B.

6.3 - RESULTS AND DISCUSSION

6.3.1 - Synthesis of Fluorescent Peptides

Two alternative carboxytetramethylrhodamine (TAMRA)-labelled neurotensin peptides were synthesised in order to determine the labelling strategy which was least perturbing to the peptide-receptor binding interaction:

TAMRA-NT_{2-13}	TAMRA- Leu-Tyr-Glu-Asn-Lys-Pro-Arg-Arg-Pro-Tyr-Ile-Leu
TAMRA-linker-NT_{2-13}	TAMRA-$(PEG)_2$- Leu-Tyr-Glu-Asn-Lys-Pro-Arg-Arg-Pro-Tyr-Ile-Leu

The TAMRA-NT_{2-13} peptide consisted of the NT peptide with the first residue (Glu) removed and replaced by the TAMRA fluorescent dye. This labelling position has been used to label NT with other fluorescent dyes (section 6.1.1). The TAMRA-linker-NT_{2-13} peptide was designed to increase the distance between the relatively bulky TAMRA moiety (Figure 6.2) and the ligand binding site by incorporating a 20 atom PEG linker between the N-terminus of NT_{2-13} and the TAMRA, and therefore help to alleviate possible steric inhibition to receptor binding.

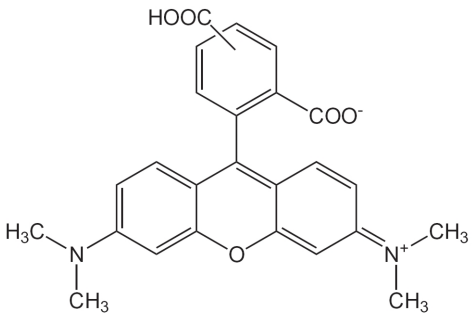

Figure 6.2 – Chemical structure of the rhodamine derivative, 5(6)-Carboxytetramethylrhodamine (5(6)-TAMRA). NT was conjugated with 5(6)-TAMRA using two different labelling schemes.

The peptides were synthesised by Fmoc-solid phase peptide synthesis. In each case, reversed phase HPLC purification yielded two major fluorescent peaks which were analysed by mass spectrometry (Figure 6.3 and Figure 6.4). Both fractions obtained from the purification of the TAMRA-NT_{2-13} synthesis were of the expected molecular

weight (1974 Da). The purification in two separate peaks is most likely caused by the use of a mixed 5,6-isomer form of TAMRA (5(6)-Carboxytetramethylrhodamine) for the synthesis (Figure 6.2). One peak for the purification of the TAMRA-linker-NT_{2-13} synthesis was of the correct molecular weight (2292 Da). The molecular weight of the second peak was 14 Da too large. The reason for this is unclear although it is possible that the peptide was methylated during the synthesis or cleavage reactions.

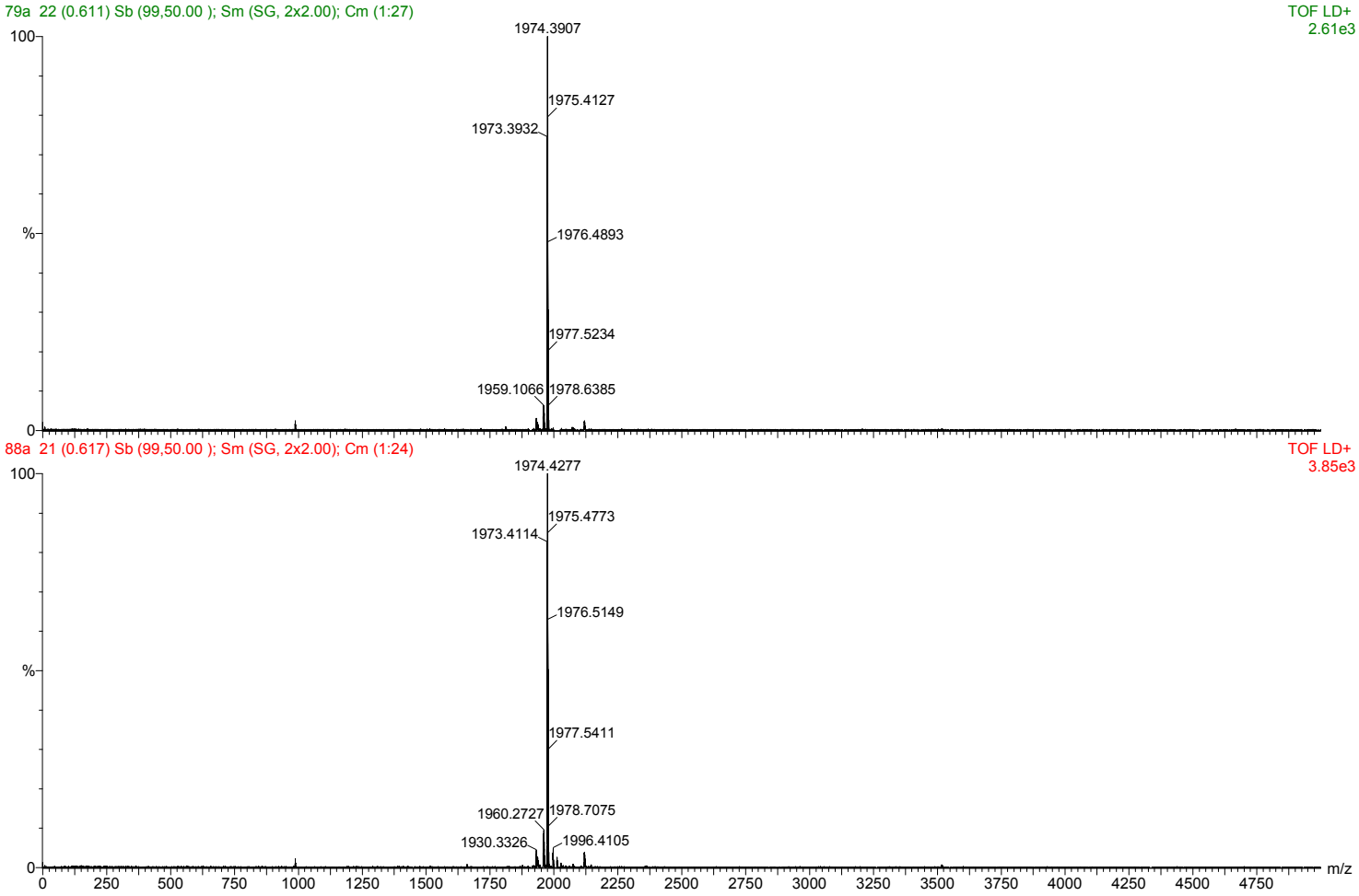

Figure 6.3 – MALDI-TOF mass spectrometry of the two major fractions obtained from reversed phase HPLC of the TAMRA-NT_{2-13} peptide synthesis (expected molecular weight (Mw) = 1974 Da). Both fractions contain fluorescent peptide of the desired Mw and are likely conjugates of NT_{2-13} to the 5- and 6-isomer forms of TAMRA.

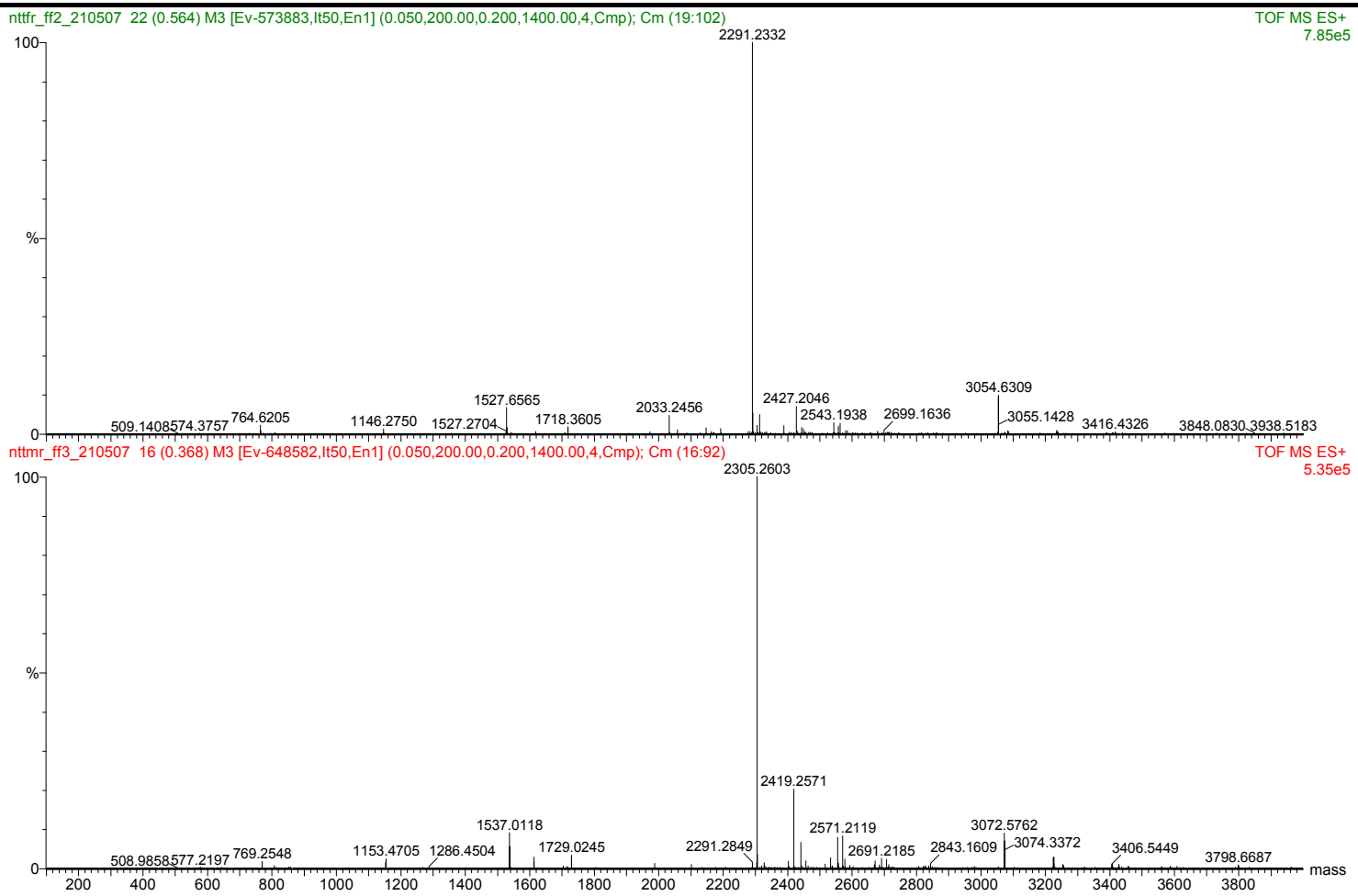

Figure 6.4 - ESI mass spectrometry of the two major fractions obtained from reversed phase HPLC of the TAMRA-linker-NT_{2-13} peptide synthesis (expected molecular weight (Mw) = 2292 Da). The first fraction appears to be the desired product. The second has a 14 Da adduct which is possibly a methylation product formed during the peptide synthesis or cleavage from the resin.

6.3.2 - Radioligand Competition Assay

A radioligand competition assay was carried out in order to determine the affinity of the TAMRA-labelled peptides for purified, detergent-solubilised NTS1Y (Figure 6.5). The fluorescent peptides were able to inhibit the binding of tritiated NT to NTS1Y and therefore demonstrated specific binding to the receptor. Fitting of a sigmoidal dose-response curve (Hill Equation, Equation 6.5) gave a Hill slope close to -1 (-1.04 for TAMRA-linker-$NT_{2\text{-}13}$ and -1.28 for TAMRA-$NT_{2\text{-}13}$). This suggested that the labelled peptides were competing with tritiated NT at a single class of receptor binding site. Fitting of the data to a single site competition model (Equation 6.3) yielded IC_{50} values of 158 ± 18 nM and 99 ± 12 nM for TAMRA-$NT_{2\text{-}13}$ and TAMRA-linker-$NT_{2\text{-}13}$ respectively. The equilibrium dissociation constants (K_i) for TAMRA-$NT_{2\text{-}13}$ (75 ± 9 nM) and TAMRA-linker-$NT_{2\text{-}13}$ (47 ± 6 nM) were calculated from these results using Equation 6.4.

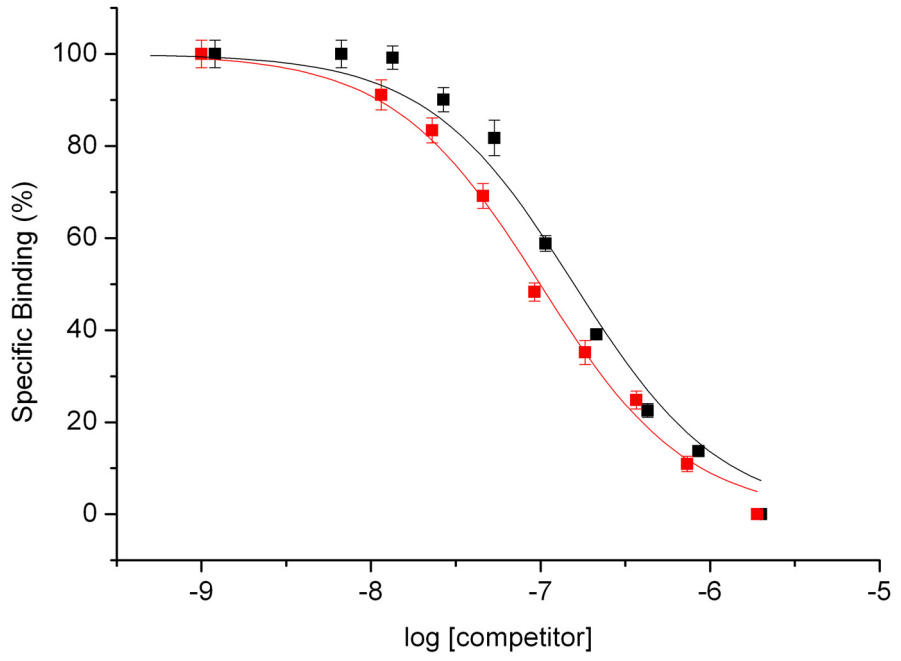

Figure 6.5 – Competition binding data for TAMRA-$NT_{2\text{-}13}$ and TAMRA-linker-$NT_{2\text{-}13}$. The concentration of tritiated NT was kept constant in the presence of varying concentrations of competitor (either TAMRA-$NT_{2\text{-}13}$ (black squares) or TAMRA-linker-$NT_{2\text{-}13}$ (red squares)). The data was fitted to a single site competition model (Equation 6.3) and the resulting fits are displayed as solid lines. The fits yielded IC_{50} values of 158 ± 18 nM and 99 ± 12 nM for TAMRA-$NT_{2\text{-}13}$ and TAMRA-linker-$NT_{2\text{-}13}$ respectively.

The calculated inhibition constants for the TAMRA-labelled NT peptides were higher than expected. The unlabelled peptide bound to the detergent-solubilised receptor with far higher affinity (K_d = 0.91 ± 0.08 nM, section 3.3.5). TAMRA, a relatively low molecular weight fluorescent probe (Mw = 430 Da), was conjugated to the N-terminus of the NT peptide. Given that the C-terminal six residues of the peptide (NT_{8-13}) have been implicated as the key residues required for binding to the NT receptors (section 1.5.1), it was surprising that labelling at this position was so perturbing to the binding affinity. Previously reported studies, in which other fluorescent probes have been conjugated to the N-terminus of NT, have only reported up to 3-fold lower affinity relative to unlabelled NT (section 6.1.1). The reason for the relatively low affinity is unclear. However, the affinity of other labelled GPCR peptide ligands has been reported to be fluorophore- as well as position-specific and, therefore, the low affinity could be a property of the TAMRA fluorophore itself (Beaudet *et al.*, 1998).

The competition results suggested that the TAMRA-linker-NT_{2-13} peptide bound to NTS1Y with significantly higher affinity than the peptide which did not contain the linker. A possible rationale for this observation is that the relatively large TAMRA molecule is moved further from the receptor NT binding site, which could help to alleviate inhibition of binding caused by steric effects. Alternatively, the introduction of the PEG linker could act to increase the solubility of the peptide-fluorophore conjugate.

6.3.3 - Fluorescence Correlation Spectroscopy

Fluorescence correlation spectroscopy (FCS) was carried out to confirm the affinity of the TAMRA-linker-NT_{2-13} peptide for NTS1. Samples were set up containing TAMRA-linker-NT_{2-13} at a constant concentration of 10 nM in the presence of purified, detergent-solubilised NTS1B (0 – 185 nM). Samples were incubated at 4 °C for 1 h to reach equilibrium before FCS measurement. The experiment was repeated in the

presence of an excess (3.5 μM) of unlabelled NT as a specificity control. Autocorrelation curves for both experiments are shown in Figure 6.6.

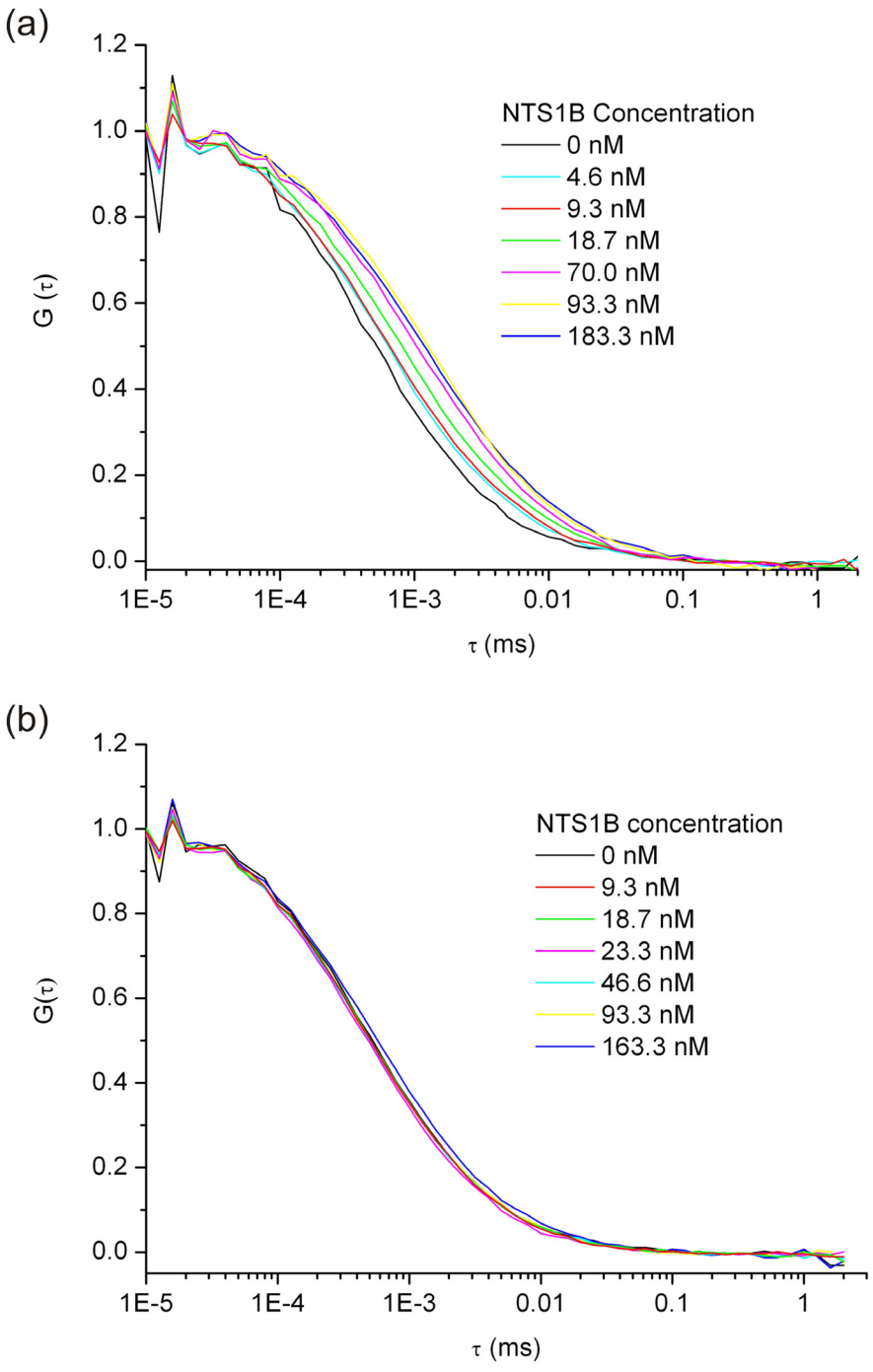

Figure 6.6 – Fluorescence correlation spectroscopy of TAMRA-linker-NT_{2-13} : NTS1B complexes. (a) The autocorrelation functions of samples containing TAMRA-linker-NT_{2-13} to a final concentration of 10 nM in the presence of varying concentrations of NTS1B. (b) Control for non-specific binding. Autocorrelation functions are shown for samples containing TAMRA-linker-NT_{2-13} to a final concentration of 10 nM and excess unlabelled NT (3.5 μM) in the presence of varying concentrations of NTS1B.

Figure 6.6a indicated a general shift in the autocorrelation curve to longer diffusion times at higher concentrations of NTS1B which is suggestive of the formation of the high molecular weight TAMRA-linker-NT_{2-13} : NTS1B complex. However, in the presence of an excess of unlabelled NT, little visible change in the autocorrelation function was observed in Figure 6.6b. This suggests that the observed interaction in Figure 6.6a was due to a specific interaction between the receptor and the fluorescent peptide.

The autocorrelation curve for the sample which contained the TAMRA-linker-NT_{2-13} peptide only (without NTS1B) was fitted using Equation 6.6, which describes the autocorrelation function for a single diffusing species, thus yielding the diffusion time for the peptide of 5.30×10^{-4} s. Likewise, the sample which contained the highest concentration of NTS1B (183.3 nM) (Figure 6.6a) was fitted to the same function. Assuming complete saturation of the TAMRA-linker-NT_{2-13} at this concentration of receptor, this yielded the diffusion time for the TAMRA-linker-NT_{2-13} : NTS1B complex (1.23×10^{-3} s). Given the molecular weights (Mw) of TAMRA-linker-NT_{2-13} (2292 Da) and NTS1B (100 kDa) and that the diffusion time is proportional to $(Mw)^{1/3}$ (Equation 6.2), complex formation would be expected to cause a 3.5-fold increase in the diffusion time. Therefore, the 2.3-fold increase observed does not appear unreasonable. Autocorrelation curves for the intermediate concentrations of NTS1B were subsequently fitted using Equation 6.7, which describes the autocorrelation function for two diffusing species. The diffusion times for the fast- and slow-diffusing components were kept constant using the values obtained from the single component fitting to the 0 nM and 183.3 nM samples respectively. The fits therefore yielded values for the fractional saturation term (θ) for each sample. Values for θ were also calculated in the same manner for the control samples, thus quantifying the degree of non-specific binding. Calculated values for total and non-specific binding are summarised in Figure

6.7. Fitting of the data to a single component binding isotherm yielded a K_d of 6.8 ± 2.7 nM for the TAMRA-linker-$NT_{2\text{-}13}$: NTS1B interaction. This affinity is approximately seven-fold higher than was measured using the radioligand competition assay and is closer to the K_d measured for unlabelled NT (0.91 ± 0.08 nM, section 3.3.5) and to the previously reported K_d values for NT which was N-terminally labelled with alternative fluorophores (section 6.1.1). A possible rationale for the discrepancy between the K_d obtained from the FCS measurements and radioligand competition assays (6.8 ± 2.7 nM and 47 ± 6 nM respectively) is non-specific binding of the TAMRA-functionalised NT peptides. If the fluorescent peptides had significant non-specific binding affinity for the receptor or the assay tube, it could considerably reduce the concentration of free fluorescent peptide during the course of the radioligand competition assays. Hence, in this case, the concentration of free fluorescent ligand available for competition with tritiated NT would be lower than expected.

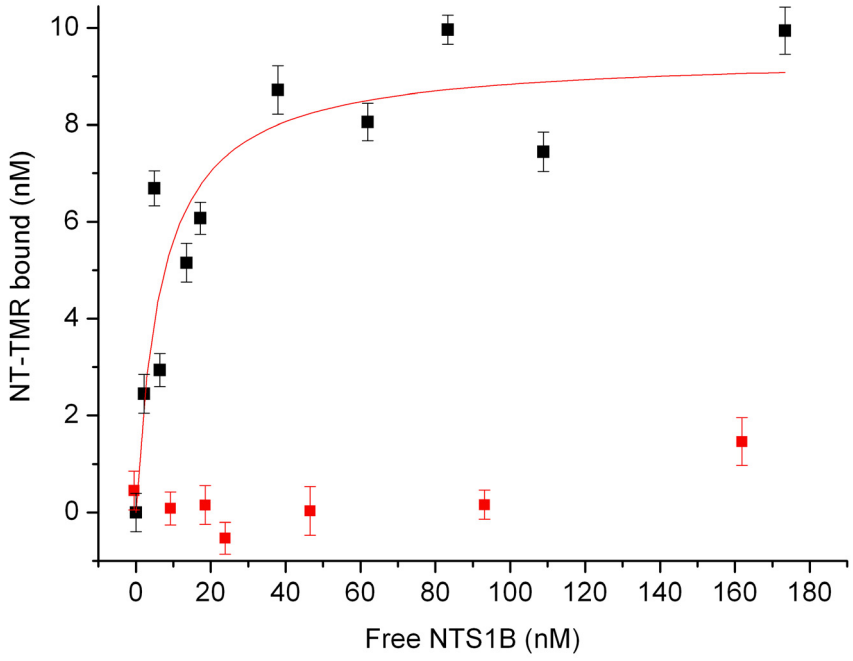

Figure 6.7 – Summary of total binding (black squares) and non-specific binding (red squares). The fraction of bound TAMRA-linker-$NT_{2\text{-}13}$ (θ) was used to calculate the concentration of TAMRA-linker-$NT_{2\text{-}13}$: NTS1B complex and the concentration of free NTS1B. The data was fitted to a single component binding isotherm (red line) which yielded a K_d of 6.8 ± 2.7 nM. Non-specific binding, determined in the presence of excess unlabelled NT, can be seen to be minimal.

6.4 - CONCLUSION

NT peptides conjugated with the fluorophore carboxytetramethylrhodamine (TAMRA) at two alternative N-terminal positions were successfully synthesised by solid phase peptide synthesis and purified by reversed phase HPLC. One peptide consisted of NT_{2-13} with TAMRA conjugated directly to the N-terminus while the other peptide consisted of NT_{2-13} with a 20 atom PEG linker conjugated to the N-terminus, which was in turn conjugated to TAMRA (thereby increasing the distance between the bulky TAMRA moiety and the receptor NT binding site). Both peptides were found to bind to NTS1Y via a specific interaction, as shown by the competition experiment with radiolabelled NT. The peptide which contained the PEG linker was found to bind to NTS1Y with the highest affinity. As discussed, this could be due to either the minimisation of steric effects between the receptor and the relatively large fluorophore or the decreased hydrophobicity conferred by the PEG linker. However, both peptides showed significantly lower affinity for NTS1Y than expected, with equilibrium dissociation constants (K_i) of 75 ± 9 nM and 47 ± 6 nM for TAMRA-NT_{2-13} and TAMRA-linker-NT_{2-13} respectively.

Fluorescence correlation spectroscopy (FCS) confirmed a specific interaction of TAMRA-linker-NT_{2-13} with NTS1B. As the concentration of NTS1B was raised, there was an increased contribution from a fluorescent species with a 2.3-fold slower diffusion time than was measured for the free peptide. This suggested that a complex between the fluorescent peptide and the receptor was being formed. The lack of the slow diffusing component in the presence of excess unlabelled NT confirmed that the interaction was specific. The K_d for the interaction obtained from the FCS measurements was 6.8 ± 2.7 nM, which is significantly higher affinity than was obtained from the radioligand competition experiments. The reason for the discrepancy is

unclear. However, the radioligand binding assay buffer and the FCS measurement buffer had the same composition, except the FCS buffer contained 15 % glycerol which may help to alleviate non-specific binding. As previously mentioned (section 6.3.3), a possible reason for the low apparent affinity in the radioligand competition experiments could be non-specific interactions of the fluorescent peptide with the assay tube or the receptor during the equilibration period. If this was the case, the concentration of free fluorescent peptide could be significantly lower than expected and therefore the use of alternative assay conditions could alleviate the problem. For example, the current assay buffer is of low ionic strength (the concentration of NaCl is kept low since the NT-NTS1 interaction is inhibited by sodium ions). Inclusion of KCl in the assay buffer would help to prevent non-specific binding. In addition, an alternative technique to confirm the affinity of the peptides would be desirable. For example a fluorescence-based binding assay involving the direct measurement of fluorescent peptide to the receptor could be carried out. The separation of bound from free fluorescent peptides could be achieved using microspin gel filtration columns in a similar protocol to that already used in the radioligand binding assay. The column flow-through could be assayed using fluorimetry to quantify the amount of TAMRA-labelled NT, which corresponds to the amount of fluorescent peptide which was complexed to receptor. This technique would therefore provide a direct measurement of the K_d for the interaction of the fluorescent peptide with the receptor, rather than a K_i value derived from competition measurements.

In conclusion, two alternative TAMRA-labelled NT peptides have been synthesised and purified, and have been demonstrated to specifically bind NTS1 at the NT binding site. However, single molecule fluorescence techniques typically require relatively low fluorophore concentrations. For example, ALEX experiments are usually performed

using fluorophore concentrations of the order of 100 pM (Kapanidis *et al.*, 2005; Doose *et al.*, 2007). Although complex formation can be promoted by the use of samples with higher fluorophore concentrations which can then be rapidly diluted directly prior to single molecule measurement, further investigation to produce fluorescent NT-derivatives with higher affinity for NTS1 would be advantageous.

CHAPTER 7 - SURFACE PLASMON RESONANCE ANALYSIS OF THE NTS1-NT INTERACTION

SUMMARY

Surface Plasmon Resonance (SPR) is an optical technique which allows biomolecular interactions to be monitored in real time. SPR was used to confirm the ligand binding activity of purified NTS1. A novel approach was utilised which involved the measurement of the binding of purified, detergent-solubilised NTS1 to immobilised, N-terminally biotinylated NT on the sensor surface. The use of a rigorous control surface, which consisted of immobilised, N-terminally biotinylated 'scrambled sequence' NT, demonstrated a specific interaction of the receptor with the NT peptide. Analysis of the kinetics revealed a multiphasic interaction with a K_d in the nanomolar range. The technique shows potential for application to the screening of inhibitor compounds and may be applicable to other suitable GPCRs.

7.1 - INTRODUCTION

7.1.1 - Surface Plasmon Resonance

Surface Plasmon resonance (SPR) is an optical technology that detects refractive index changes at the surface of a sensor chip which is lined with a thin gold film on the flat surface of a prism (Biacore, 2001). The refractive index is, in turn, dependent on the sample concentration at the interface, allowing binding interactions to be monitored in real time. Figure 7.1 shows a schematic of an SPR system.

When plane polarised light passing through the prism (a medium of high refractive index) strikes the gold film (a medium of low refractive index) at an angle greater than the critical angle, the light will be totally internally reflected (TIR). However, the TIR is not total since some of the energy is lost through interaction with oscillating plasma waves (termed 'surface plasmons') at the surface of the metal film. When the wave vector of the incident light matches the wavelength of the surface plasmons, the electrons resonate, resulting in a loss of energy and therefore a reduction in the intensity of the reflected light. Since the amplitude of the wave vector in the plane of the metallic film depends on the angle at which it strikes the interface, a surface plasmon resonance

angle (θ_{spr}) exists at which the energy loss is greatest. This can be viewed as a minimum or 'dip' in the intensity of TIR light and it is the changes in the angle of the dip that are measured by the SPR instrument (Figure 7.2).

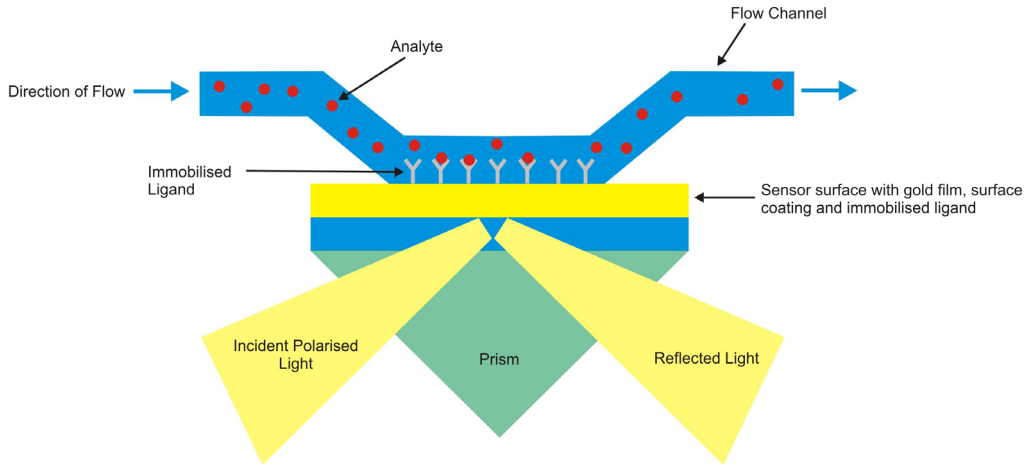

Figure 7.1: Schematic of a Biacore system. 'Ligand' is immobilised onto the SPR chip surface and its binding partner, the 'analyte', passed through the flow cell in solution. Binding of analyte to the ligand causes an increased sample concentration at the surface of the sensor chip. This causes a corresponding increase in the refractive index which alters the angle of incidence required to create the SPR phenomenon. Kinetics of binding interactions can therefore be measured in real time (adapted from Biacore technology note).

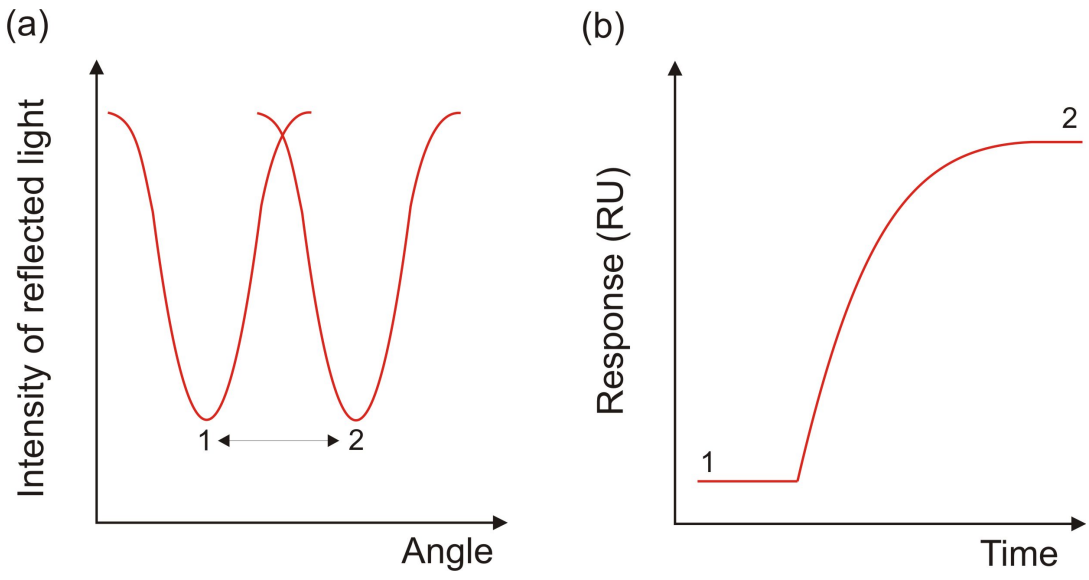

Figure 7.2 – SPR angle and the observed response. (a) An increase in the refractive index of the medium at the sensor surface causes an increase in angle of the reflected intensity dip (SPR angle, curve 1 to curve 2). (b) By monitoring the SPR angle as a function of time the kinetics of binding events at the surface are displayed as a sensorgram.

An evanescent (decaying) electrical field associated with the plasma wave travels for a short distance (approximately 300 nm) into the medium from the metallic film. Therefore, the resonant frequency of the surface plasma wave (and thus θ_{spr}) depends on the refractive index of this medium. If the surface is immersed in an aqueous buffer (refractive index of approximately 1.0), and protein (refractive index of approximately 1.33) binds to the surface, an increase in refractive index occurs which is detected by a shift in the θ_{spr}. The instrument uses a photo-detector array to measure very small changes in θ_{spr} which are quantified in resonance units or response units (RUs), with 1 RU equivalent to a shift of 10^{-4} degrees.

The sensor chip most commonly used ('Sensor CM5', Biacore AB) consists of a gold surface modified with a carboxymethylated dextran layer that forms a hydrophilic environment for the covalent attachment of ligands. Other sensor chips are also commercially available, for example, the 'Sensor SA' and the 'Sensor L1' (both Biacore AB). The former consists of a CM5 surface pre-modified by covalent attachment of streptavidin to allow the capture of biotinylated ligands, and the latter consists of carboxymethylated dextran with additional hydrophobic alkane groups (Cooper *et al.*, 2000) to allow the capture of lipid bilayers (www.biacore.com). The sensor chip forms the floor of small flow cells, each with an approximate volume of 20 nl. An aqueous solution ('running buffer') is pumped through the flow cells (Jonsson *et al.*, 1991) and small volumes (typically 5-300 μl) of sample containing the 'analyte' in aqueous solution ('sample buffer') are injected through the flow cells, in a continuous, pulse free and controlled flow.

7.1.2 - Application of SPR to GPCRs

Surface plasmon resonance (SPR) allows the sensitive detection of molecular interactions in real time, without the use of labels (Van der Merwe, 2000). The technique has proved to

be extremely versatile, permitting the study of analytes ranging in size from hundreds of daltons to whole cell binding (McDonnell, 2001). However, application to receptor-ligand interactions has, until recently, been largely limited to the study of soluble ligand-binding domains (Kroger *et al.*, 1999; De Crescenzo *et al.*, 2000; Rich *et al.*, 2002).

Application of SPR to the study of ligand-receptor interactions for GPCRs has proved challenging, partly due to problems encountered in attempts to achieve successful overexpression and purification of sufficient quantities of active GPCRs, which also tend to be relatively unstable when purified. Immobilisation of rhodopsin (a GPCR of high natural abundance) on the biosensor surface has been achieved, allowing the kinetics of transducin activation to be observed (Heyse *et al.*, 1998; Karlsson and Lofas, 2002). Immobilisation in this case involved covalent (amine) coupling of detergent-solubilised receptor to the sensor surface, followed by on-chip lipid reconstitution. When the work described in this chapter was carried out, only a single example of the study of ligand-receptor interactions for recombinantly-expressed GPCRs by SPR had been published (Stenlund *et al.*, 2003). This involved the study of the chemokine receptors CXCR4 and CCR5, using a similar receptor immobilisation technique to that described for rhodopsin. However, antibody capture, rather than covalent immobilisation, was used prior to on-chip reconstitution. Active ligand binding was demonstrated, although with lower affinity than had previously been published. More recently, further work has been published for these chemokine receptors involving antibody capture of detergent-solubilised GPCR (no on-chip reconstitution) and binding of ligands demonstrated (Navratilova *et al.*, 2005; Navratilova *et al.*, 2006) and a similar approach was also applied to the α2-adrenergic receptor (Sen *et al.*, 2005). SPR has not yet been applied to the study of NT with any of the NTS receptors.

7.1.3 - Aims

The aim is to study the interaction of neurotensin with the NTS1 receptor using SPR. Instead of immobilising the receptor on the sensor surface, an alternative approach will be used which involves the immobilisation of neurotensin (NT) peptide. The purified NTS1 will then be injected over the surface, as the analyte, and binding to the immobilised NT measured. This approach has potential advantages over the conventional examples discussed in the previous section:

(i) Responses observed in SPR are proportional to the molecular weight of bound analyte. Therefore, binding of the large receptor protein gives improved sensitivity when compared with analyses in the reverse orientation which measure the binding of the relatively small GPCR ligand.

(ii) The approach avoids the need to immobilise the receptor on the sensor surface. Therefore, the problems of receptor inactivation due to immobilisation and the potential instability of the immobilised receptor over multiple cycles are avoided.

7.2 - MATERIALS AND METHODS

7.2.1 - Expression and Purification

This study was carried out before the plasmid encoding the new NTS1B construct was available. Consequently, the plasmid encoding the fusion protein NTS1A was used which does not contain TeV protease sites (pRG/III-hs-MBP-T43NTR1-TrxA-H10) (Tucker and Grisshammer, 1996). The work was also carried out prior to the optimisation of the expression and purification of NTS1 (Chapter 2) and therefore the receptor was expressed and purified according to the method developed by Grisshammer *et al.* (Tucker and Grisshammer, 1996; Grisshammer *et al.*, 1999; Williamson *et al.*, 2001; White *et al.*, 2004).

NTS1A for SPR analysis was expressed in *E.coli* DH5α and was solubilised and purified on a large scale as described (White *et al.*, 2004) (Appendix A7). A two stage purification procedure, involving immobilised metal affinity chromatography (IMAC) followed by an NT affinity column, was carried out, with all steps at 4 °C unless otherwise stated. A 250 g bacterial pellet was resuspended and disrupted by ultrasonication. Functionally active receptors were solubilised using a CHAPS (0.5 % (w/v)) / DDM (1 % (w/v)) / CHS (0.1 % (w/v)) detergent mix. NTS1A was purified by IMAC using a 100 ml Ni-NTA column. This was followed by a 20 ml neurotensin affinity column, which comprised biotinylated-NT immobilised on streptavidin sepharose resin (GE Healthcare). NT affinity column eluate was stored at -80 °C in NTS1A storage buffer (50 mM Tris/HCl, pH 7.4, 30 % glycerol (v/v), 50 mM NaCl, 0.5 % CHAPS (w/v), 0.1 % CHS (w/v), 0.1 % DDM (w/v), 1 mM EDTA). The progress of the purifications was monitored by SDS-PAGE and radioligand binding assay (Appendix A3).

7.2.2 - Solid Phase Peptide Synthesis

N-terminally-biotinylated NT (biotin-Glu-Leu-Tyr-Glu-Asn-Lys-Pro-Arg-Arg-Pro-Tyr-Ile-Leu) and 'scrambled sequence' NT (biotin-Leu-Tyr-Asn-Arg-Pro-Arg-Pro-Tyr-Leu-Glu-Ile-Lys-Glu) peptide ligands were produced by Fmoc solid phase peptide synthesis and purified using reversed phase HPLC (for detailed methods see Appendix A8).

7.2.3 - Surface Plasmon Resonance

Surface Plasmon Resonance (SPR) analysis was carried out using a Biacore 3000 biosensor instrument (Biacore AB) at 25 °C. All buffers used were filtered and de-gassed though a 0.2 μm filter (Whatman). Biotinylated NT in HBS-EP buffer (Biacore AP) (10 mM HEPES pH 7.4 , 150 mM NaCl, 3 mM EDTA, 0.005 % polysorbate 20 (v/v)) was immobilised in two flow cells of a streptavidin-coated chip (Biosensor SA, Biacore) to immobilisation densities of 135 RU and 250 RU. 250 RU of 'scrambled sequence' biotinylated NT was immobilised in a third flow cell in the same manner and the fourth flow cell was left blank. Analyte used was purified, detergent-solubilised NTS1A, buffer-exchanged into a glycerol-free 'SPR' buffer to reduce bulk shift effects (50 mM Tris HCl, pH 7.4, 50 mM NaCl, 0.5 % CHAPS (w/v), 0.1 % CHS (w/v), 0.1 % DDM (w/v), 1 mM EDTA). Interaction experiments were carried out at a flow rate of 20 $\mu l.min^{-1}$, with sample racks maintained at a constant 4 °C throughout. Surface regeneration was achieved via two sequential 1 min injections of SPR buffer containing 1 M NaCl to dissociate bound receptor. Injection time was subsequently varied between 1 min and 7 min to test for compliance with the conformational change model. Mass transport control experiments were carried out by variation of flow rate between 15 μl/min and 75 μl/min.

7.2.4 - Kinetic analysis of the NTS1A-NT interaction

BiaEvaluation Software v4.1 (Biacore AB) and Origin v7.5 (Microcal Software) were used for data analysis and curve fitting. Differential rate equations were fitted iteratively by numerical integration, where response curves are calculated step by step using small time increments and the calculated data compared to the measured data. The models and the corresponding differential rate equations used in this study are presented in Table 7.1. Models were fitted globally; the association and dissociation phases were fitted simultaneously using only one set of rate constants.

Table 7.1 – Reaction schemes and corresponding differential equations used for the kinetic analysis of the NTS1A-NT interaction. Global analysis to the reaction schemes was carried out using Biaevaluation software v.4.1.1. Biaevaluation relies on the Marquardt-Levenberg algorithm, which optimises parameter values by minimising the sum of the squared residuals. The residuals are the difference between the calculated and experimental curve at each point. A baseline drift parameter was also included for each model.

Model	Reaction Scheme	Differential Rate Equations	Definition of terms
Langmuir (1:1)	$A + B \Leftrightarrow AB$	$\frac{dB}{dt} = -\left(k_{on}.A.B - k_{off}.AB\right)$ $\frac{dAB}{dt} = k_{on}.A.B - k_{off}.AB$	A = concentration of analyte B = concentration of ligand AB = concentration of molecular complex of A and B. Response generated by AB
Langmuir (1:1) with mass transfer	$A + B \Leftrightarrow AB$	$\frac{dA}{dt} = k_t.\left(A_{solution} - A\right) - \left(k_{on}.A.B - k_{off}.AB\right)$ $\frac{dB}{dt} = -\left(k_{on}.A.B - k_{off}.AB\right)$ $\frac{dAB}{dt} = k_{on}.A.B - k_{off}.AB$	A = concentration of analyte close to the surface (initially zero) $A_{solution}$ = concentration of analyte B = concentration of ligand AB = concentration of molecular complex of A and B. Response generated by AB
Two state reaction	$A + B \Leftrightarrow AB \Leftrightarrow AB*$	$\frac{dB}{dt} = -\left(k_{on}.A.B - k_{off}.AB\right)$ $\frac{dAB}{dt} = \left(k_{on}.A.B - k_{off}.AB\right) - \left(k_{on2}.AB - k_{off2}.AB*\right)$ $\frac{dAB*}{dt} = \left(k_{on2}.AB - k_{off2}.AB*\right)$	A = concentration of analyte B = concentration of ligand AB = concentration of molecular complex of A and B. AB* = concentration of alternative conformation state of the complex AB. Response generated by AB and AB*

Table continued on the following page.

Model	Reaction Scheme	Differential Rate Equations	Definition of terms
Hetergeneous analyte	$A_1 + B \Leftrightarrow A_1B$ $A_2 + B \Leftrightarrow A_2B$	$\frac{dB}{dt} = -\left(k_{on1}.A_1.B - k_{off1}.A_1B\right) - \left(k_{on2}.A_2.B - k_{off2}.A_2B\right)$ $\frac{dA_1B}{dt} = k_{on1}.A_1.B - k_{off1}.A_1B$ $\frac{dA_2B}{dt} = k_{on2}.A_2.B - k_{off2}.A_2B$	A_1 = concentration of analyte 1 A_2 = concentration of analyte 2 B = concentration of ligand A_1B = concentration of molecular complex of A_1 and B. A_2B = concentration of molecular complex of A_2 and B. Response generated by A_1B and A_2B (Assumes A_1 and A_2 have the same molecular weight)
Heterogeneous ligand	$A + B_1 \Leftrightarrow AB_1$ $A + B_2 \Leftrightarrow AB_2$	$\frac{dB_1}{dt} = -\left(k_{on1}.A.B_1 - k_{off1}.AB_1\right)$ $\frac{dB_2}{dt} = -\left(k_{on2}.A.B_2 - k_{off2}.AB_2\right)$ $\frac{dAB_1}{dt} = k_{on1}.A.B_1 - k_{off1}.AB_1$ $\frac{dAB_2}{dt} = k_{on2}.A.B_2 - k_{off2}.AB_2$	A = concentration of analyte B_1 = concentration of ligand 1 B_2 = concentration of ligand 2 AB_1 = concentration of molecular complex of A and B_1. AB_2 = concentration of molecular complex of A and B_2. Response generated by AB_1 and AB_2

Apparent values for the affinity constant (K_A) were calculated from the rate constants for the Langmuir (1:1) binding model (equation $K_A = k_{on} / k_{off}$), and for the two state reaction (equation $K_A = K_A1\ (1 + K_A2)$ where $K_A1 = k_{on}1 / k_{off}1$ and $K_A2 = k_{on}2 / k_{off}2$ (Lipschultz *et al.*, 2002))

7.3 - RESULTS AND DISCUSSION

7.3.1 - Experimental design

Functionally active rat NTS1 was expressed as the NTS1A fusion protein, which consists of an N-terminally truncated NTS1 with an *E.coli* maltose binding protein (MBP) attached to the N-terminus, and thioredoxin and a deca-His tag attached to the C-terminus (Tucker and Grisshammer, 1996; Grisshammer *et al.*, 1999; Williamson *et al.*, 2002). NTS1A for SPR analysis was solubilised and purified on a large scale using a two stage purification procedure, involving immobilised metal affinity chromatography (IMAC) followed by an NT affinity column (White *et al.*, 2004) and ligand-binding activity confirmed by radioligand binding assay. An N-terminally-biotinylated NT peptide ligand was produced by solid phase synthesis to facilitate immobilisation on streptavidin-functionalised SPR chips. As a control for binding, a biotinylated 'scrambled sequence' peptide, with the same 13 residues as NT, was synthesised to ensure the specificity of any interactions observed with NT (Figure 7.3). Successful synthesis and purification of the biotinylated peptides were confirmed by ESI mass spectrometry (Figure 7.4).

		N												C
		1	2	3	4	5	6	7	8	9	10	11	12	13
NT	Biotin	Glu	Leu	Tyr	Glu	Asn	Lys	Pro	Arg	Arg	Pro	Tyr	Ile	Leu
Control	Biotin	Leu	Tyr	Asn	Arg	Pro	Arg	Pro	Tyr	Leu	Glu	Ile	Lys	Glu

Figure 7.3 - Comparison of the sequences of biotinylated NT and 'scrambled' control peptide. The sequence of NT was randomly scrambled to generate the control peptide. Amino acids implicated to be involved in the binding to NTS-1 are highlighted in red (NT_{8-13}). Peptides were produced by solid phase peptide synthesis and purified by HPLC.

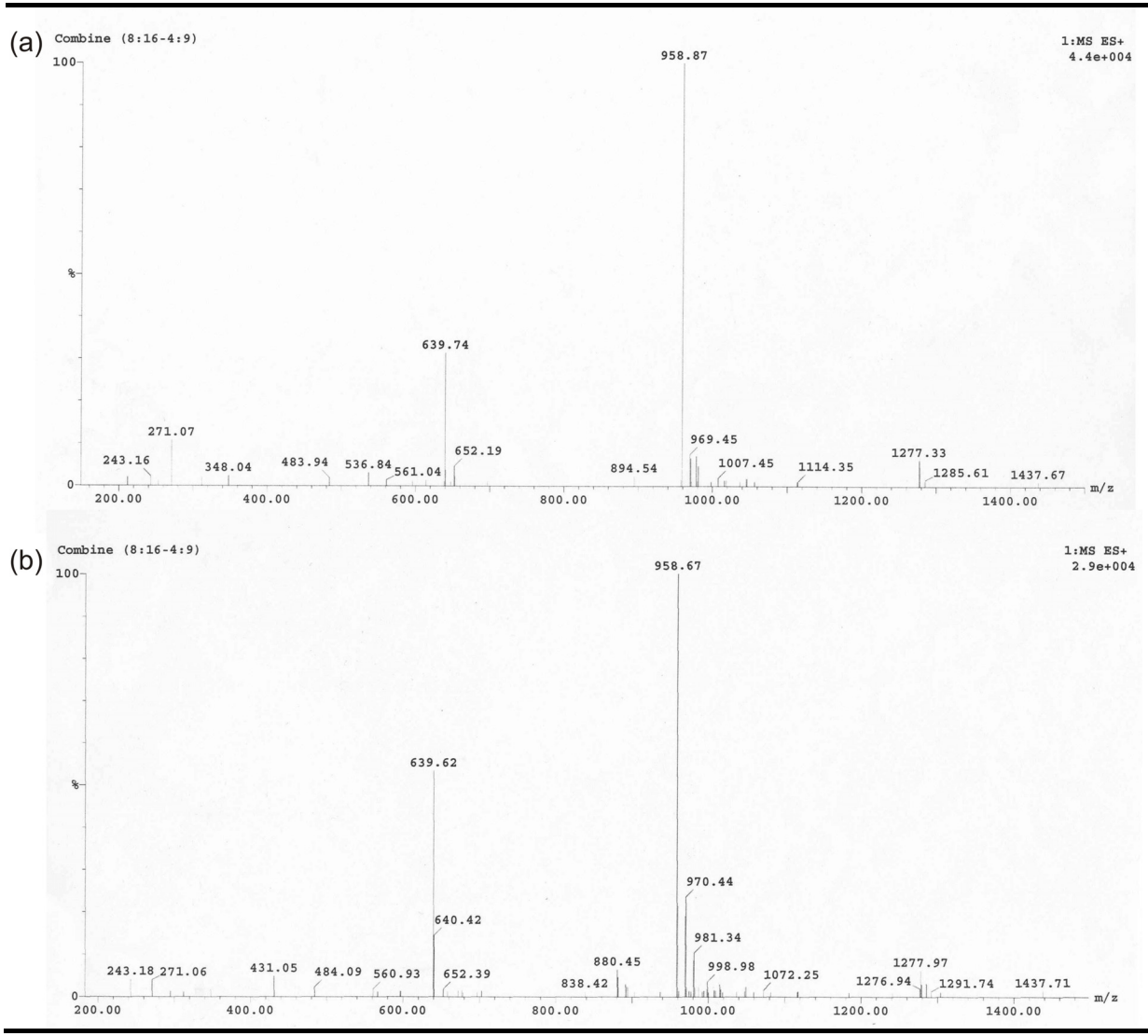

Figure 7.4 – ESI mass spectrometry of the biotinylated NT (a) and 'scrambled' biotinylated NT (b) peptides. In both cases, the peaks at m/z values of 639 and 958 correspond to the +3 and +2 charged ions respectively (molecular weight = 1916 Da).

Figure 7.5 shows a schematic of the interaction experiment performed using SPR. Previous applications of SPR to the study of GPCR-ligand interactions have involved the immobilisation of the receptor on the sensor surface, either through covalent coupling followed by on-chip lipid reconstitution or, more recently, through the covalent coupling of the receptor in detergent solution (section 7.1.2). As mentioned in section 7.1.3, performing the experiment in the alternative orientation as described here has a number of potential advantages, namely improved amplitude of response and the avoidance of receptor inactivation caused by either covalent coupling or the finite stability of the receptor on the sensor surface. The concept of the immobilisation of short peptides to the sensor surface and the measurement of binding of a large protein binding partner analyte has been widely used for soluble, globular proteins (Hassan *et al.*, 2006) but examples of this approach for purified membrane proteins have not been published.

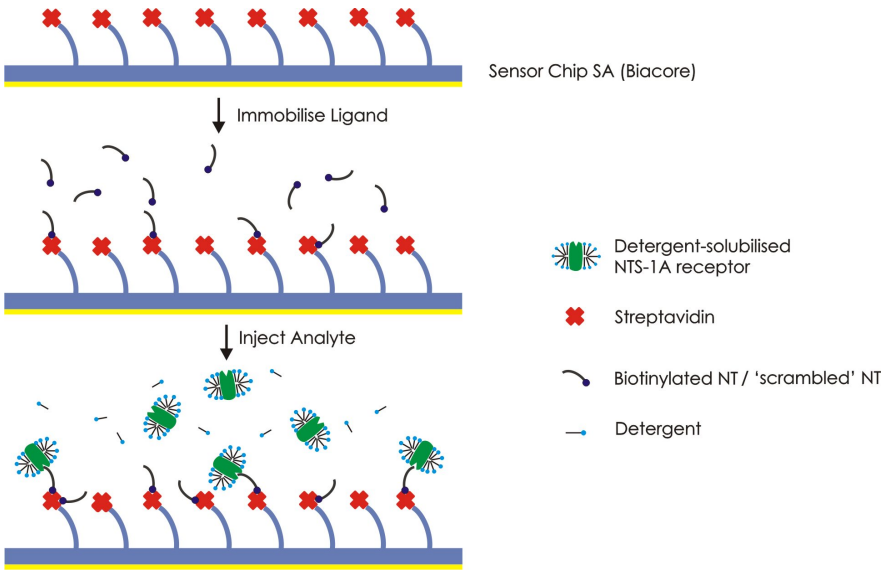

Figure 7.5 - Schematic depicting the detergent-solubilised NTS1A : biotinylated NT interaction experiment carried out using SPR. Biotinylated NT or scrambled NT control were immobilised on a strepatvidin coated surface (Sensor SA, Biacore AB). Purified, detergent-solubilised NTS1A was injected and binding to the surface measured by SPR.

The use of a rigorous control surface for non-specific binding of analyte is extremely important in SPR experiments. A control surface is also required for subtraction of 'matrix effects' which can occur as a consequence of the properties of the dextran matrix attached to the CM5 sensor chip. The matrix is a non-crosslinked and negatively charged hydrogel (Lofas and Johnsson, 1990). In water, the dextran polymer chains repel each other and the entire matrix expands. As a consequence of this expansion, the mass distribution is changed within the SPR evanescent field, resulting in a change in the observed SPR response. When buffers of differing composition (for example ionic strength) are injected over the surface, differences in SPR response can be caused not only by differences in the refractive index of the buffers in question, but also by 'matrix effects' which result from the described expansion and contraction of the dextran matrix. When protein is immobilized to the dextran polymers, attraction and/or repulsion between protein molecules and the dextran may give rise to similar effects. Importantly, it has been reported that matrix effects caused by changes in running buffer are dependent on the immobilisation level of the protein on the surface (Karlsson and Falt, 1997). Consequently, it is prudent to have a control surface, comprising a peptide or protein with similar physical characteristics, at a similar level of immobilisation to that used for the experimental surface. The use of the 'scrambled NT' control, which is composed of the same amino acids as NT but in a randomly scrambled sequence, immobilised to the same level as the NT surface, is a rigorous control to use in this case.

7.3.2 - Response Curves and Specificity

Subtraction of the control flow cell response from the flow cell containing immobilised NT yielded a specific binding response (Figure 7.6a). Responses observed for the flow cell with scrambled control peptide immobilised were not significantly different from a

blank flow cell (Figure 7.6b). Therefore, binding of NTS1A to the control peptide is insignificant, indicating a highly specific interaction between NTS1A and NT.

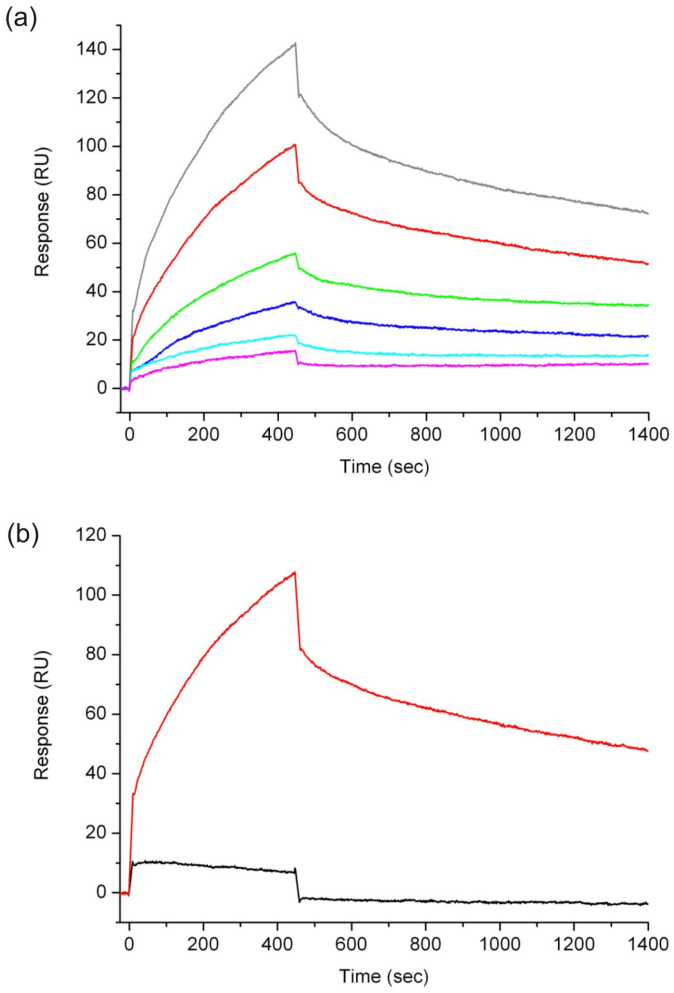

Figure 7.6 - SPR response curves for the interaction of NT peptide with detergent-solubilised NTS1A. (Harding *et al.*, 2006) (a) The interaction between detergent-solubilised NTS1A and biotinylated NT immobilised to the sensor surface. Various concentrations of NTS1A (5.8 nM (grey), 2.9 nM (red), 1.5 nM (green), 0.73 nM (blue), 0.36 nM (cyan), 0.18 nM (magenta)), were injected at 20 µl/min over 250 RU immobilised NT and control ligands. The control (scrambled peptide) response is subtracted and therefore only specific binding of NTS1A to immobilised NT is shown. (b) Binding of detergent-solubilised NTS-1A to the biotinylated NT (red) and control peptide (black) flow cells at a concentration of 2.9 nM. The response obtained for a blank Sensor Chip SA flow cell has been subtracted from both curves, revealing negligible non-specific binding to the control peptide surface. Receptor concentrations were determined by radioligand binding assay.

The amplitude of the observed response is lower than might be expected, given the immobilisation level (250 RU) and the mass of the analyte (100 kDa). It is possible that this is caused by occlusion of a proportion of the immobilised ligand, thereby preventing analyte binding. However, a systematic study of alternative sensor surfaces

which might address problems of ligand occlusion has not yet been carried out. Also, whilst the biotinylated NT used in this experiment already has seven residues between the point of immobilisation and the six C-terminal residues known to be involved in receptor binding, an increase in linker length might also relieve any ligand occlusion problems.

7.3.3 - Kinetic Analysis of the NT-NTS1A interaction

Response curves were initially fitted globally to the simple Langmuir 1 : 1 binding mechanism (Figure 7.7, Table 7.2). From the residual plots and the value obtained for χ^2 for the fit, it appears that the interaction does not comply with simple monophasic Langmuir kinetics. The interaction appears to be multiphasic which suggests that binding is occurring with at least two observable time constants.

Such deviation from first order kinetics can be caused by complex binding mechanisms, for example, conformational changes in the ligand or analyte upon binding. They can also be caused by experimental artefacts such as mass transfer limitations, and ligand or analyte heterogeneity (O'Shannessy and Winzor, 1996; Schuck, 1997). Therefore, response curves were fitted to a 1 : 1 Langmuir binding model which included mass transfer, a heterogeneous analyte model and a heterogeneous ligand model. These reaction schemes (discussed in section 7.2.3) were globally fitted to the experimental data. Fits and corresponding residuals are shown in Figure 7.7 and the fit parameters are shown in Table 7.2.

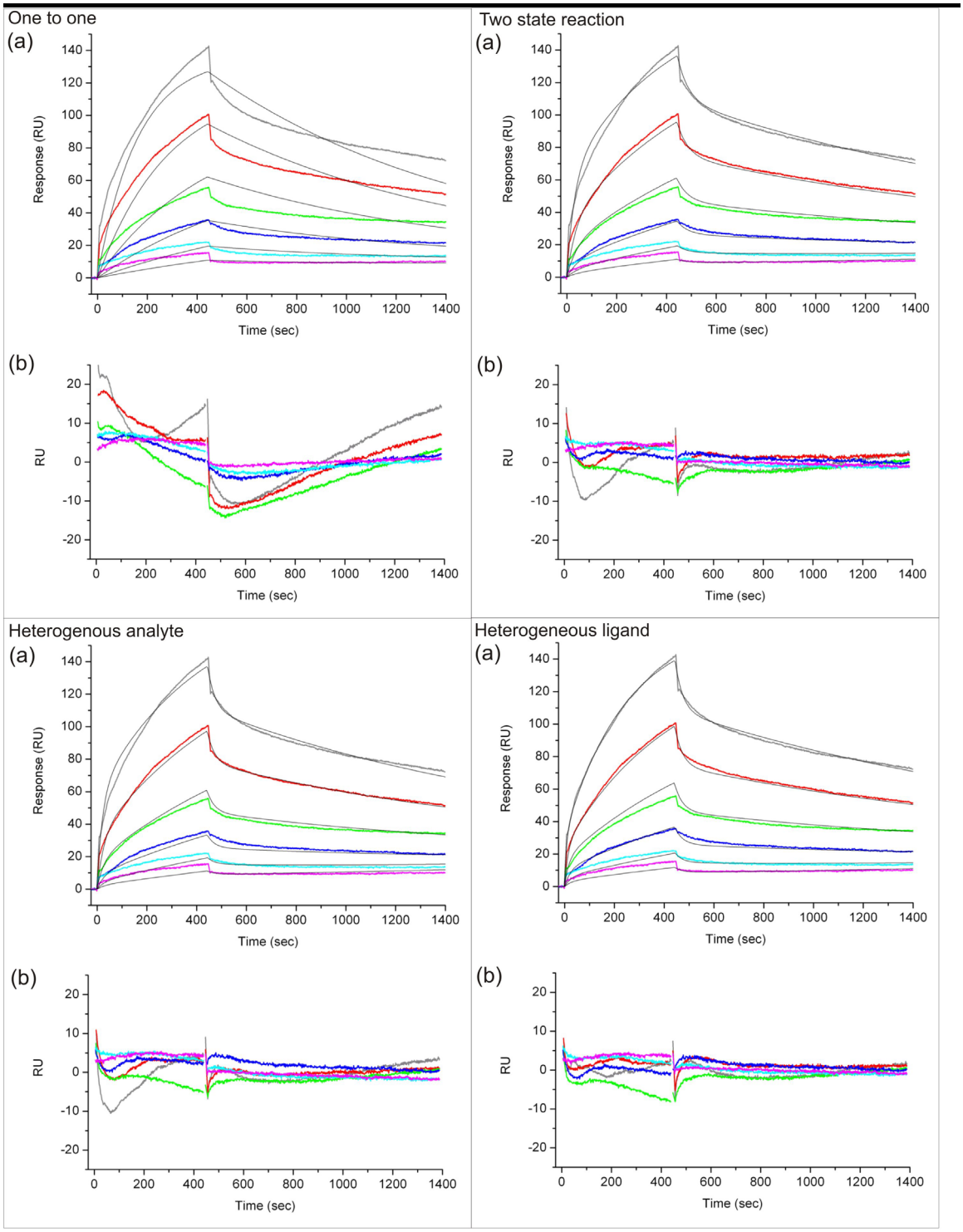

Figure 7.7 – Kinetic analysis of SPR data for the interaction of NTS1A with immobilised NT (250 RU). Global fits of one to one, two state, heterogeneous analyte and heterogeneous ligand binding schemes were made to the response curves (a). The fits are overlaid in black with the experimental data in each plot (5.8 nM (grey), 2.9 nM (red), 1.5 nM (green), 0.73 nM (blue), 0.36 nM (cyan), 0.18 nM (magenta). The residual plots, obtained by subtracting the calculated fits from the experimental data, are shown for each fit (b). The experiment was performed in duplicate by injecting low to high followed by high to low concentrations of NTS1A (only low-high are displayed for clarity).

Table 7.2 – Summary of the kinetic data obtained for the interaction of NTS1A with immobilised NT, as determined by surface plasmon resonance (High ligand density (250 RU), left; low ligand density (135 RU), right). Response curves were globally fitted to the binding models (see Table 7.1 for a description of the binding models and Figure 7.7 for graphical representation of the fits obtained). The experiment was performed in duplicate by injecting low to high followed by high to low concentrations of NTS1A. The kinetic constants are the resulting mean values (± SE).

	HIGH DENSITY (250 RU)					LOW DENSITY (135 RU)				
	1:1	1:1 and mass transfer	Two state	Heterogeneous analyte	Heterogeneous ligand	1:1	1:1 and mass transfer	Two state	Heterogeneous analyte	Heterogeneous ligand
k_{on1} ($M^{-1}s^{-1}$)	(9.4 ± 0.6) ×10^{5}	(9.4 ± 0.6) ×10^{5}	(1.8 ± 0.1) ×10^{6}	(3.2 ± 0.3) ×10^{6}	(1.7 ± 0.2) ×10^{7}	(1.5 ± 0.1) ×10^{6}	(1.5 ± 0.1) ×10^{6}	(3.1 ± 0.6) ×10^{6}	(3.3 ± 0.3) ×10^{6}	(1.3 ± 0.3) ×10^{7}
k_{off1} (s^{-1})	(9.6 ± 0.7) ×10^{-4}	(9.6 ± 0.7) ×10^{-4}	(1.5 ± 0.4) ×10^{-2}	(2.6 ± 0.4) ×10^{-2}	(3.3 ± 0.5) ×10^{-2}	(1.1 ± 0.2) ×10^{-3}	(1.1 ± 0.2) ×10^{-3}	(1.9 ± 0.9) ×10^{-2}	(2.3 ± 0.9) ×10^{-2}	(1.9 ± 0.9) ×10^{-2}
k_{on2} ($M^{-1}s^{-1}$)	na	na	†(4.7 ± 0.5) ×10^{-3}	(9.6 ± 1.0) ×10^{5}	(6.2 ± 0.7) ×10^{5}	na	na	†(4.4 ± 0.4) ×10^{-3}	(1.0 ± 0.5) ×10^{6}	(1.1 ± 0.2) ×10^{6}
k_{off2} (s^{-1})	na	na	(7.5 ± 0.7) ×10^{-4}	(6.1 ± 0.5) ×10^{-4}	(5.9 ± 0.6) ×10^{-4}	na	na	(7.7 ± 0.8) ×10^{-4}	(6.1 ± 1.1) ×10^{-4}	(6.0 ± 0.9) ×10^{-4}
χ^2	36	36	4.8	4.5	2.2	28	28	4.5	4.6	2.7
K_A (M^{-1})	(9.8 ± 0.9) ×10^{8}	(9.8 ± 0.9) ×10^{8}	(8.7 ± 2.5) ×10^{8}	na	na	(1.4 ± 0.3) ×10^{9}	(1.4 ± 0.3) ×10^{9}	(1.1 ± 0.6) ×10^{9}	na	na
K_D (M)	(1.0 ± 0.1) ×10^{-9}	(1.0 ± 0.1) ×10^{-9}	(1.2 ± 0.3) ×10^{-9}	na	na	(0.7 ± 0.2) ×10^{-9}	(0.7 ± 0.2) ×10^{-9}	(0.9 ± 0.5) ×10^{-9}	na	na
k_t ($RU.M^{-1}s^{-1}$)	na	3×10^{17} ± 6×10^{19}	na	na	na	na	8.0×10^{16} ± 3×10^{19}	na	na	na

† The units for this association rate constant are s^{-1}

Mass transfer limitations occur when the observed binding rate is limited by the rate of transfer of the analyte to the surface, rather than the kinetic association rate and/or when the observed dissociation rate is affected by rebinding of dissociated analyte to the surface. Fitting of the 1 : 1 Langmuir binding model which included mass transfer parameters gave exactly the same fit as the simple 1 : 1 model without mass transfer (Table 7.2). Also, the rate constant for mass transfer obtained from the fit was not biologically relevant (3×10^{17} RU.M^{-1}s^{-1}) and typical reported values of k_t for proteins of molecular weight 50 – 100 kDa are of the order of 10^8 RU.M^{-1}s^{-1} (Biacore, 2004). The error for this parameter in the fit was also extremely large (6×10^{19} RU.M^{-1}s^{-1}) suggesting that the mass transport contribution to the interaction was insignificant. The results obtained for binding of NTS1A to the flow cell which contained a lower ligand density (135 RU as opposed to 250 RU) also support the results obtained from the high density flow cell. Fitting of the models to the response curves obtained for the lower density flow cell gave kinetic constants which are not significantly different from those obtained for the higher density flow cell (Table 7.2, right hand side).

The χ^2 values for the fits show that all of the biphasic models give significantly better fits than the Langmuir 1 : 1 model and the parameters obtained all appear reasonable in a biological context. In addition, the relative quality of the fit for different kinetic models can be evaluated by taking into consideration the trends in the residuals. If a kinetic model adequately depicts the interaction, the difference between the fits and the experimental points will be small and the residuals will be normally distributed around a zero value. Systematic deviations between the experimental and fitted data indicate that the model is inappropriate for the experimental data. The residuals for the 1 : 1 model show far larger systematic deviations between the fit and the experimental data than any of the biphasic models (Figure 7.7). However, differentiating between the biphasic fits

is inconclusive since both the residuals and the χ^2 values for each fit are comparable. Such difficultly in differentiating between biphasic models by curve fitting alone has been reported previously for other interactions studied by SPR which failed to comply with monophasic behaviour (Karlsson and Falt, 1997; De Crescenzo *et al.*, 2000; Van der Merwe, 2000).

The contact time of the analyte was subsequently varied. A decrease in the observed dissociation rate when the sample injection time is increased is indicative of either a conformational change or heterogenous analyte, whereas no decrease in observed dissociation rate is indicative of heterogenous ligand. Control experiments carried out involving the variation of the sample injection time between 1 min and 7 min suggested just such a time dependence in the dissociation phase, supporting the conformational change or heterogenous analyte models rather than the heterogenous ligand possibility (Figure 7.8). This might be expected since, in addition to being purified by reversed phase HPLC, the biotinylated peptide ligand from solid phase synthesis has only one possible site of immobilisation. Therefore, there is only limited scope for ligand heterogeneity (apart from partial occlusion of the peptide on the surface, as discussed in section 7.3.2). However, this conclusion is by no means definitive and a more rigorous analysis of the variation of dissociation kinetics with contact time will need to be carried out.

Variation of analyte contact time cannot differentiate between a conformational change model and heterogeneity in the analyte. The fit of the heterogenous analyte model to the data does provide extra evidence for the conformational change model. The fit resulted in a high affinity and a low affinity component, both with k_{on} values of the same order of magnitude (3×10^6 and 1×10^6 $M^{-1}s^{-1}$ respectively, see Table 7.2). Whilst this cannot be used as definitive evidence for the conformational change model, a fit with

vastly differing k_{on} values for the two components would have provided an argument against the conformational change hypothesis.

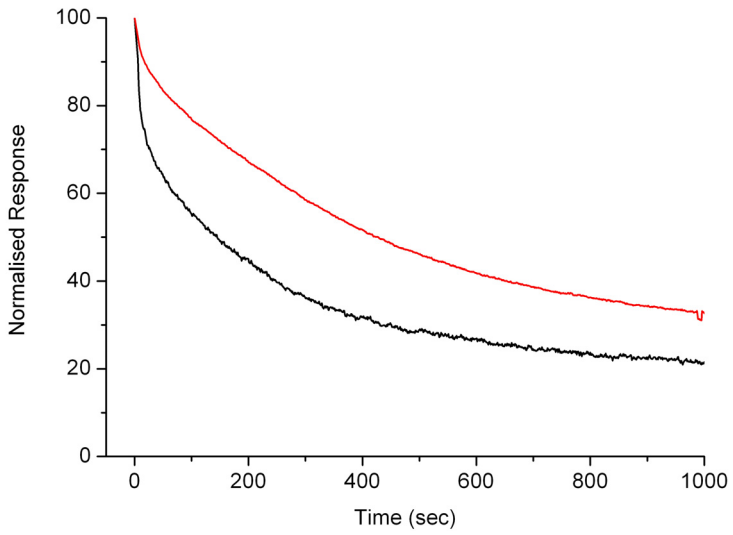

Figure 7.8 - Variation of dissociation phase kinetics with analyte contact time. NTS1A was injected for 1 min (black) and 7 min (red) and the dissociation phases normalised. An increased contribution from the fast dissociation component is evident at short injection time. This result supports the heterogeneous analyte and two state conformational change models rather than the heterogeneous ligand model.

A conformational change of the receptor upon ligand binding is to be expected, since this is fundamental to coupling ligand binding at the cell surface to downstream signalling inside the target cell. Indeed, such conformational changes are now widely accepted as an integral part of receptor signalling, and several multi-state models have been proposed (Figure 7.9) (Kenakin, 2002). Specifically, a change in conformation of the third intracellular loop (I3) or the C-terminus, which have been identified as key functional domains of NTS1 implicated in the coupling to the G proteins Gq and Gs / Gi/o respectively (Kitabgi, 2006), could be envisaged. Chimeric receptor studies (Cusack *et al.*, 1996) and site directed mutagenesis (SDM) analysis (Pang *et al.*, 1996; Barroso *et al.*, 2000) have revealed the location of the agonist-binding site. They suggest that the third extracellular loop (E3) and the sixth TM domain of the receptor are involved in the binding of the C-terminal region of NT. Given that TM6 is attached to

the I3 loop and that the E3 loop is linked to TM7 (and the C-terminus), a ligand-induced conformational change transmitted via TM6 and TM7 would seem to be a reasonable hypothesis.

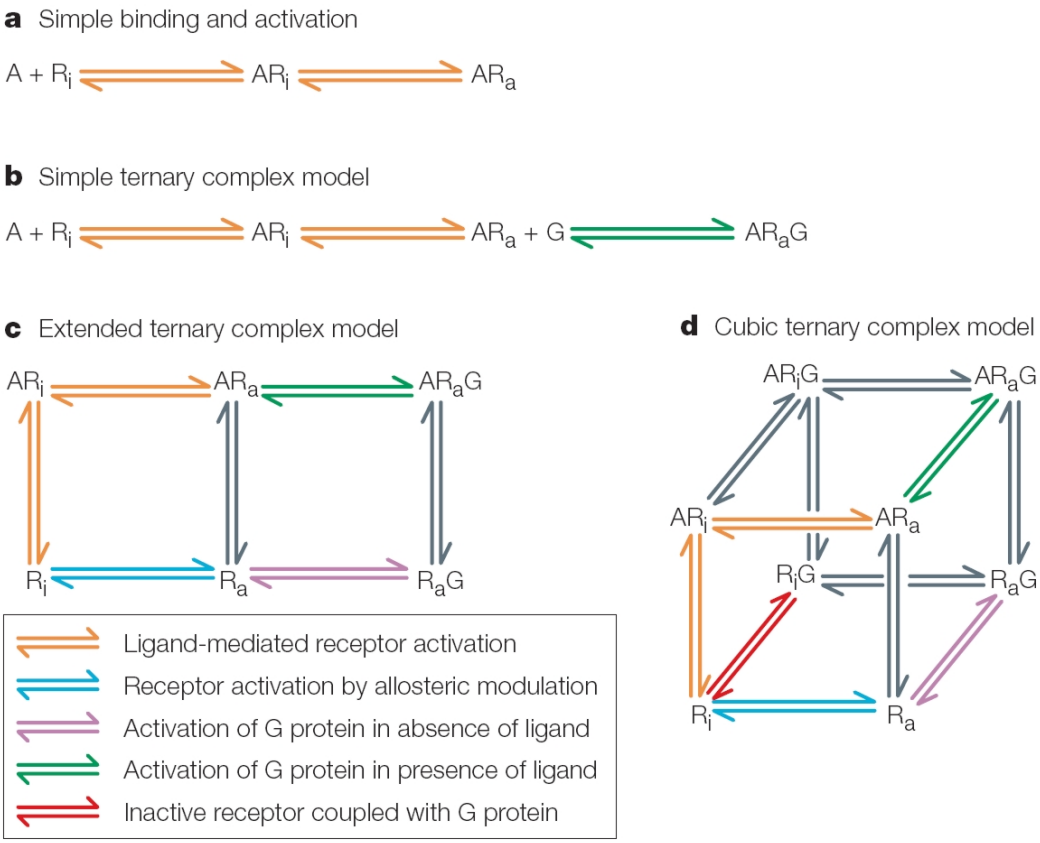

Figure 7.9 – Proposed Models of GPCR Activation (reproduced from Kenakin, (2002)). **(a) The simple binding and activation model of GPCR activation.** An agonist (A) binds to an inactive receptor (R_i) to form a complex (AR_i) which undergoes a conformational change to the active state (AR_a). Other multistate models of varying complexity have also been proposed. **(b) Simple ternary complex model.** Activation of the receptor is followed by topographically distinct binding of the active-state receptor to the G protein (G). Response then emanates from the ternary AR_aG complex. **(c) The extended ternary complex model** (Samama *et al.*, 1993). This allows for the spontaneous formation of an active-state receptor (R_a) independent of the presence of an agonist. R_a can then interact with, and activate, a G protein. **(d) The cubic ternary complex (CTC) model** (Weiss *et al.*, 1996a; Weiss *et al.*, 1996b) also allows the inactive-state receptor (R_i) to form a non-signalling complex with the G protein. Abbreviations: R_i = Receptor in the inactive state, R_a = Receptor in the active state, G = G proteins.

The 1 : 1 Langmuir fit and the two state conformation change fits both yielded an apparent K_D of approximately 1 nM (Table 7.2). This affinity compares well with affinities for the NT-NTS1 interaction reported previously from radioligand binding

studies, both for receptor expressed in *E.coli* (0.43 ± 0.11 nM) (Tucker and Grisshammer, 1996) and other systems, including synaptic membranes (0.9 nM) (Kitagbi *et al.*, 1977), *Xenopus* oocytes (0.19 ± 0.04 nM) (Tanaka *et al.*, 1990) and HT29 cells (0.56 ± 0.10 nM) (Vita *et al.*, 1993). The affinity is also in agreement with the radioligand binding data for detergent-solubilised, purified receptor obtained in this project, both for NTS1B (1.14 ± 0.15 nM) and fluorescently tagged receptor (K_d = 0.91 ± 0.17 nM) (Chapter 3).

7.4 - CONCLUSIONS

This preliminary SPR study has yielded the first SPR binding data for the interaction of detergent-solubilised NTS1 with its agonist, the NT peptide. In addition, this is the first time that a GPCR-ligand interaction has been studied by SPR in this orientation (i.e. with the ligand immobilised on the sensor surface and with the use of the receptor as the analyte). The use of a reference flow cell containing immobilised 'scrambled sequence' NT control peptide ensured that the response being measured was due to a specific interaction between NTS1A and immobilised NT.

The ability of SPR to resolve the separate kinetic processes involved in binding highlights an advantage of using this technique to study the interaction in real time. Analysis of the kinetics of the interaction was complicated by the multiphasic response observed, which can potentially be caused by a number of factors. Binding models corresponding to 1 : 1 binding, 1 : 1 binding with mass transfer, two state binding, heterogeneous ligand and heterogeneous analyte were fitted to the response curves. Poor fits to both 1 : 1 binding models suggested that mass transfer artefacts were not the cause of the multiphasic response. Distinguishing between the three biphasic models by curve fitting proved inconclusive, as has been reported previously for other interactions (Karlsson and Falt, 1997; Van der Merwe, 2000). However, variation of the dissociation kinetics with analyte contact time supported either the conformation change model or the heterogeneous analyte model, although a more rigorous variation of injection time will need to be carried out to confirm this. In addition, repetition of the experiment using receptor prepared by the optimised expression and purification method (Chapter 3) should be carried out. This protocol uses an expression strain which has been shown to express the receptor at a higher level and includes a size exclusion purification step which will likely lead to a more homogenous receptor

preparation. The negative stain electron micrographs of receptor purified using the optimised protocol suggest a monodisperse receptor population (section 2.3.4).

However, despite the complexity of the kinetics observed and consequently the inherent difficulty in identifying the underlying cause, the method has considerable potential as a competition assay that can be used for the identification of novel inhibitor compounds. Addition of an inhibitor to the analyte prior to injection should lead to a decrease in the observed SPR response. Furthermore, information regarding the mode of action of the inhibitor could potentially be obtained. The method gives improved sensitivity when compared with analyses in the reverse orientation and avoids potential problems caused by immobilisation of the receptor on the sensor surface (section 7.1.3). As discussed in section 7.3.2, the amplitude of the observed response is lower than might be expected, given the immobilisation level (250 RU) and the mass of the analyte (100 kDa). The synthesis of NT derivatives with a longer linker length on the N-terminus might improve the response by reducing any possible occlusion of binding sites on the sensor surface.

An interesting future experiment would involve the use of SPR to study reconstituted samples. An analyte consisting of NTS1 reconstituted into vesicles could be injected over NT peptide immobilised to the sensor surface. Alternatively, and with the likelihood of being more informative, biotinylated lipids could be incorporated into the reconstitutions. This would allow intact proteoliposomes, containing NTS1, to be immobilised to a streptavidin-coated sensor surface. The binding of NT peptide to the reconstituted receptor could therefore be measured. Whilst this approach would not gain the increased sensitivity afforded by using the receptor as the analyte, the approach would have a number of advantages over other studies of reconstituted, recombinant GPCRs. Previous studies with recombinant GPCRs have either involved

immobilisation of detergent-solubilised receptor (Navratilova *et al.*, 2005) or the 'on-chip reconstitution' of purified receptor on an 'L1' sensor surface (consists of carboxymethyl dextran with additional hydrophobic alkane groups) (Cooper *et al.*, 2000). On-chip reconstitution (Stenlund *et al.*, 2003) involves initial capture of purified, detergent-solubilised receptor followed by addition of lipid and removal of detergent to form lipid bilayers on the sensor surface. Since both methods involve the direct immobilisation of the receptor to the surface, they preclude receptor multimerisation which is likely to be a ligand-induced or constitutive property of many GPCRs (Chapter 6). A method such as the one proposed, which will allow diffusion of individual receptor molecules in the lipid bilayer and allow receptor multimerisation, is therefore likely to be advantageous.

CHAPTER 8 - CONCLUSIONS AND FUTURE WORK

Despite the remarkable diversity within the GPCR superfamily, and its pharmacological significance, only one GPCR, bovine rhodopsin, has been structurally described at high resolution (Palczewski *et al.*, 2000; Okada *et al.*, 2002; Li *et al.*, 2004; Okada *et al.*, 2004). This is largely because the successful overexpression and purification of GPCRs for structural studies has proved so challenging (Sarramegna *et al.*, 2006) and a high resolution structure of a ligand-binding GPCR is still awaited. NTS1 is of particular pharmacological relevance since NT signalling networks have been postulated to be linked with medical conditions such as Schizophrenia, Parkinson's Disease and drug addiction. Consequently, any structural information which can be obtained will be of use for the structure-based design of therapeutics to treat such conditions.

As discussed, overexpression and purification are typically limiting steps in the high resolution structure determination of GPCRs. These stages were optimised in this study (Chapter 2). The *E.coli* strain used for the overexpression of NTS1 was also successfully optimised. By using the BL21(DE3) or C41(DE3) expression strains rather than the DH5α strain used previously, a 2.5-fold improvement in the yield of ligand-binding NTS1 was obtained (section 2.3.1). Combined with the increase in purification yields achieved through the addition of the phospholipid POPC to the purification buffers (section 2.3.2), NTS1 is now being produced in sufficient quantities for it to be amenable to high resolution structural studies. Negative stain electron microscopy analysis of the cleaved NTS1 samples revealed a homogenous receptor population with no signs of aggregation (section 2.3.4). Therefore, the purified receptor is being produced in sufficient quantity (approximately 0.1 mg of purified receptor per litre of culture) and quality for use as starting material for 3D crystallisation trials and the future

application of x-ray crystallography. Preliminary 3D crystallisation trials are already underway. In addition, cryo-EM of NTS1 samples has already allowed the 3D reconstruction of a single receptor particle from a relatively small dataset (Figure 2.6). The continuation of this preliminary work will likely allow the elucidation of structural details of NTS1. Since this technique requires relatively little purified material in comparison to 3D crystallisation, it will be a useful complementary technique while the process of 3D crystallisation is being carried out. The labelling of proteins for both solution- and solid-state NMR studies requires expensive media which contain NMR-visible isotopes and therefore an optimal yield of protein per volume of culture is a priority (Marley *et al.*, 2001). Given the improved yields now possible, the production of NTS1 labelled with NMR-visible isotopes is now feasible.

Evidence accumulated over the past three decades suggests that many GPCRs can exist as dimers and/or higher order oligomers and the hypothesis that homo- or heterodimerisation of GPCRs is a constitutive or ligand-induced property of many receptor types is widely accepted (Milligan, 2004; Milligan, 2007). However, there have been no studies of NTS1 homodimerisation to date and the study of the multimerisation of purified GPCRs which have been reconstituted into *in vitro* lipid systems is yet to be carried out. With a view towards such studies, the existing NTS1 expression construct was successfully modified to contain the fluorescent proteins eCFP and eYFP fused to the C-terminus of the receptor (Chapter 3). The fluorescent fusion proteins were expressed and purified at a comparable level to the non-fluorescently-tagged receptor. Radioligand binding studies revealed that the addition of the C-terminal fluorescent tag did not perturb the affinity of the receptor for NT (K_d = 0.91 ± 0.08 nM).

The fluorescent tags will also offer the opportunity for further optimisation of the expression and purification of NTS1. As demonstrated in this study, in-gel fluorescence measurements can be readily applied to GPCRs, and in combination with radioligand binding assays, facilitate the direct comparison of the total receptor present with the proportion of receptor which is able to bind ligand.

Reconstitution trials using the fluorescence-tagged receptors were successful (Chapter 4). Receptor was reconstituted into brain polar lipid (BPL) liposomes in an active form which was both fluorescent and able to bind ligand with high affinity. In addition, the trials revealed that the maintenance of the native, ligand binding conformation of NTS1 appears to be highly dependent on the membrane phospholipid composition (section 4.3.2). While reconstitution into POPC-only bilayers was successful, as revealed by incorporation of fluorescent receptor into the liposomes, the inserted receptor showed no ligand binding activity. However, ligand binding activity was restored upon addition of BPL extract to the POPC in a 50 : 50 (w/w) ratio. It is hypothesised that high proportions of non-lamellar forming lipids, such as PE, or charged lipids, such as PS, which are major constituents of the BPL extract, are required to maintain ligand binding activity. A future systematic study of the effect of ligand binding activity on membrane phospholipid composition will be carried out to determine more precisely which components of the BPL extract are required to maintain the native receptor conformation. In addition, scale-up of the NTS1 reconstitutions will allow the structure of the receptor-bound NT peptide, labelled with NMR-visible isotopes, to be studied using solid state NMR (Williamson *et al.*, 2001; Luca *et al.*, 2003; Watts, 2005).

The lipid reconstitution of mixed samples of eCFP- and eYFP-tagged, purified, detergent-solubilised NTS1 allowed the multimerisation state of the receptor to be

analysed in lipid bilayers (Chapter 5). In a preliminary FRET study, FRET between eCFP and eYFP was observed (section 5.3.2). The FRET efficiency was comparable to that observed for a dimeric GPCR *in vivo* using the eCFP-eYFP FRET pair (Overton and Blumer, 2000; Floyd *et al.*, 2003). Variation of the receptor density had no effect on the observed FRET efficiency, which suggested the FRET observed was due to a true receptor-receptor interaction as opposed to random collisions ('bystander FRET') in the membrane. Further control experiments, including reconstitution of the eCFP- and eYFP-tagged receptors in the presence of untagged receptor, are required to confirm whether the observed FRET is due to multimer formation. In contrast, a similar experiment carried out on detergent-solubilised samples showed no FRET, which suggested that the receptor is monomeric in detergent solution (section 5.3.1). However, the cryo-EM of detergent-solubilised T43NTS1 (section 2.3.4) yielded a reconstruction of comparable dimensions to the putative rhodopsin dimers previously observed by EM and AFM (Fotiadis *et al.*, 2006). This suggests that the receptor can exist as a monomer or a dimer in detergent solution, depending on the particular experimental conditions used.

An *in vitro* system, which will be useful for the further study of GPCR multimerisation, has been successfully developed in this project. This will allow the fine control of the receptor environment through variation of parameters such as lipid composition and receptor density. It will also allow the complexity of the system to be systematically increased through the addition of further signalling components such as heterotrimeric G proteins. In addition, receptor deletion mutants lacking particular transmembrane domains could be produced. The relative abilities of the mutants to inhibit FRET between T43NTS1-eCFP/eYFP, when reconstituted into the *in vitro* system, could be used to identify domains of the receptor which mediate oligomerisation. Subsequently,

site-directed mutagenesis could be used to identify key individual residues within the domains.

Ensemble FRET studies, such as those described, cannot be used to determine the precise stoichiometry of any multimeric receptor complexes formed. Therefore, photobleaching studies combined with single particle analysis are planned in order to determine the exact stoichiometry. Subsequently, alternating-laser excitation (ALEX) spectroscopy, which incorporates single molecule FRET with fluorescence-aided molecule sorting (FAMS) (Kapanidis *et al.*, 2004; Doose *et al.*, 2007) will be used to further probe the multimerisation state.

Fluorescent derivatives of NT were successfully synthesised and purified (Chapter 6). Radioligand competition assays (section 6.3.2) and fluorescence correlation spectroscopy (section 6.3.3) confirmed that the fluorescent peptides bound to purified NTS1 in specific competition with unlabelled NT. However, the binding affinities were significantly lower than was observed for the unmodified NT peptide (7 – 50-fold) (section 3.3.5). Since single molecule fluorescence techniques typically require fluorophore concentrations of the order of 100 pM, further investigation of the optimal labelling position and fluorophore type are certainly required for application to these techniques.

Surface plasmon resonance (SPR) was used to confirm the ligand binding activity of purified NTS1 (Chapter 7). A novel approach, which involved the measurement of the binding of detergent-solubilised NTS1 to immobilised, N-terminally biotinylated NT on the sensor surface, was carried out (Harding *et al.*, 2006). The use of a rigorous control surface, which consisted of immobilised 'scrambled sequence' NT, demonstrated a specific interaction with the NT peptide. Analysis of the kinetics of the interaction revealed a poor fit to Langmuir 1:1 (monophasic) binding models (section 7.3.3). Whilst

the cause of the multiphasicity was hypothesised to be either heterogeneity in the receptor preparation or a conformation change upon ligand binding, further study is required for this hypothesis to be confirmed. This method shows potential for application to the screening of inhibitor compounds and may be applicable to other suitable GPCRs. In addition, future application of SPR to the measurement of NT-NTS1 binding in lipid-reconstituted systems will be investigated. A planned approach for such experiments involves the supplementation of phospholipid mixtures used for reconstitution with biotinylated phospholipids. This would therefore allow proteoliposomes containing reconstituted NTS1 to be immobilised on the SPR sensor surface. In a similar approach to the *in vitro* FRET measurements, this would facilitate study of the specificity of NTS1 for particular membrane lipid compositions and extra signalling components, such as heterotrimeric G proteins, could be included and their effects on receptor-ligand binding determined.

In this work, considerable progress in the study of NTS1 has been made. In particular, improvements in the expression and purification of the receptor, the generation of fluorescent constructs as useful tools in the study of receptor multimerisation and optimisation of lipid-reconstitution protocols has opened up several preliminary lines of study which show considerable potential for future research.

APPENDIX

APPENDIX A - GENERAL METHODS

A1 - Transformation by Heat Shock

DH5α and BL21(DE3) competent cells were obtained from Invitrogen. C41(DE3) and C43(DE3)pREP4 were donated by Prof. Daan van Aalten (University of Dundee) and Prof. Ben Berks (Biochemistry Dept., University of Oxford) respectively. A 50 µl aliquot of competent cells was thawed on ice, 1 µg of plasmid DNA stock added and the cells incubated on ice for 30 min. The cells were then subjected to heat shock (42 °C, 60 s) and placed on ice for a further 10 min. 450 µl of SOC media was added and the culture incubated for 1 h (37 °C, 200 rpm). The cells were then plated onto LB agar plates containing the appropriate antibiotic and incubated at 37 °C overnight.

A2 - Isolation of *E.coli* Membrane Fraction

All purification steps were carried out at 4 °C unless otherwise stated. *E.coli* cell pellet was resuspended in resuspension buffer 1 (50 mM Tris pH 8.0, 10 mM EDTA, protease inhibitors, 1 mg/ml lysozyme) at a concentration of 25 % (w/v) by hand homogenisation. The cell suspension was incubated at 4 °C with gentle stirring (30 min) followed by disruption by ultrasonication with the sample cooled on ice. Cell debris, unlysed cells and putative inclusion bodies were separated from membranes by centrifugation at 10,000 g, 4 °C, 20 min. The supernatant was centrifuged again at high speed (140,000 g, 4 °C, 90 min). The membrane pellet was resuspended in minimal resuspension buffer 2 (50 mM Tris pH 8.0, 10 % glycerol (v/v), 1 mM EDTA, protease inhibitors) and flash frozen in liquid nitrogen.

A3 - Ligand Binding Assay

A ^{3}H-NT (New England Nuclear) radioligand binding assay was used to quantify amounts of active receptor in reconstituted and resolubilised samples. Samples were

incubated in assay buffer (50 mM Tris pH 7.4, 0.1 % DDM (w/v), 0.01 % CHS (w/v), 1 mM EDTA, 0.1 mg/ml BSA) containing ^{3}H-NT to a final concentration of 5 nM (1 h, 4 °C). Detergent was omitted from the buffer for assay of the reconstituted samples. Non-specific binding was quantified in the presence of excess unlabelled NT (3.5 μM). Separation of bound from free ligand was achieved by gel filtration using P30 Tris spin columns (BioRad) for detergent solubilised samples and by filtration using Durapore PVDF membranes with a 0.2 μm MWCO (Millipore) for reconstituted samples. Filter membranes were added to 5 ml of scintillant (Wallac Optiphase HiSafe, Perkin Elmer) and incubated for 6 h and mixed by vortexing immediately prior to scintillation counting. Gel filtration eluate was added to 5 ml scintillant and counted immediately.

A4 - SDS PAGE

Proteins were separated by SDS-PAGE using an X-cell Surelock minicell and pre-cast Tris-Glycine gels (Invitrogen). For Coomassie staining, gels were incubated for 1-2 h with agitation in Coomassie Brilliant Blue staining solution (Coomassie Brilliant Blue R250 (0.25 % w/v), methanol (45 % v/v), MilliQ H_2O (45 % v/v), glacial acetic acid (10 % v/v)), followed by destain solution (methanol (45 % v/v), MilliQ H_2O (45 % v/v), glacial acetic acid (10 % v/v)). For Western blotting, proteins were transferred to nitrocellulose membrane (GE Healthcare) by semi-dry transfer (Biorad 'Transblot'). Membranes were probed with mouse anti-His antibody (Sigma) using WesternBreeze Chemiluminescent Western Blot Immunodetection Kit (Invitrogen).

A5 - Expression and Purification of TeV-His$_6$

An LB starter culture (5 ml) containing kanamycin (50 μg/ml) was inoculated with a single colony of TeV-His6-transformed (pETNIP vector, donated by Dr Huanting Liu and Prof. Jim Naismith, University of St. Andrews) BL21(DE3) and incubated overnight (16 h, 37 °C). LB (450 ml) containing 50 μg/ml kanamycin, in a 2 l baffled

conical flask was inoculated with starter culture (5 ml) and incubated (37 °C, 200 rpm) until the cells reached an OD_{600} of 0.3. The temperature was decreased to 20 °C and the cells grown at the new temperature for approximately 30 min until an OD_{600} of 0.5 was reached. Expression of the protease was induced using IPTG at a final concentration of 0.4 mM and expression continued overnight at 20 °C. The cells were harvested by centrifugation (6000 g, 4 °C, 15 min) and stored at -80 °C.

Cell pellet from 1 l of culture was thawed on ice and resuspended in 10 ml of sample buffer (1x PBS containing 0.3 M NaCl, 10 mM imidazole, 1 mM PMSF, 1 mM benzamadine) by hand homogenisation. Cells were disrupted by pulsed ultrasonication (10 sec pulses, 20 sec pauses for 5 min) on ice and cell debris removed by centrifugation at 20,000 g, 20 min, 4 °C. The supernatant was clarified by further centrifugation at 70,000 g, 30 min, 4 °C.

The supernatant was filtered (0.2 μm) and loaded onto a 5 ml HisTrap column (GE Healthcare) which was pre-equilibrated with sample buffer. The column was then washed with 20 CV of washing buffer (1x PBS with 0.3 M NaCl, 30 mM Imidazole, 1 mM PMSF, 1 mM benzamadine) and eluted with elution buffer (1x PBS with 0.3 M NaCl, 250 mM Imidazole and 1 mM PMSF). Eluate was diluted in 5 volumes of sample buffer (minus imidazole) and re-purified by IMAC using the same protocol.

Eluate from the second IMAC purification was concentrated to 2.5 ml using a centrifugal concentrator (VivaSpin 20, 10,000 MWCO, Vivascience) and loaded onto a Superdex 200 gel filtration column (XK16/100) pre-equilibrated with TeV GF buffer (1x PBS containing 0.3 M NaCl, 1 mM PMSF, 1 mM benzamadine) and purified at a flow rate of 0.25 ml/min. Fractions containing protease (as shown by SDS PAGE analysis) were pooled and buffer exchanged by dialysis, firstly against 50 mM Tris, 0.3 M NaCl, 1 mM PMSF and finally against 50 mM Tris, 0.3 M NaCl, 50 % glycerol (v/v).

A6 - TeV Trial Cleavage

Trial cleavage reactions with purified TeV-His_6 on IMAC-purified NTS1Y were carried out to determine cleavage efficiency of purified TeV-His_6. This was carried out individually for every batch of purified TeV. Aliquots (2 µg) of NTS1Y were incubated with increasing amounts of TeV-His_6 in a total volume of 0.5 ml cleavage buffer (50 mM Tris pH 7.4, 30 % glycerol (v/v), 0.5 M NaCl, 0.5 % CHAPS (w/v), 0.1 % DDM (w/v), 0.1 % CHS (w/v), 0.05 mg/ml POPC, 1 mM EDTA, 1 mM DTT) at 4 °C overnight. Analysis by western blotting typically revealed complete cleavage at TeV-His_6 concentrations greater than 4 µg TeV-His_6 per µg fusion protein (Figure A1).

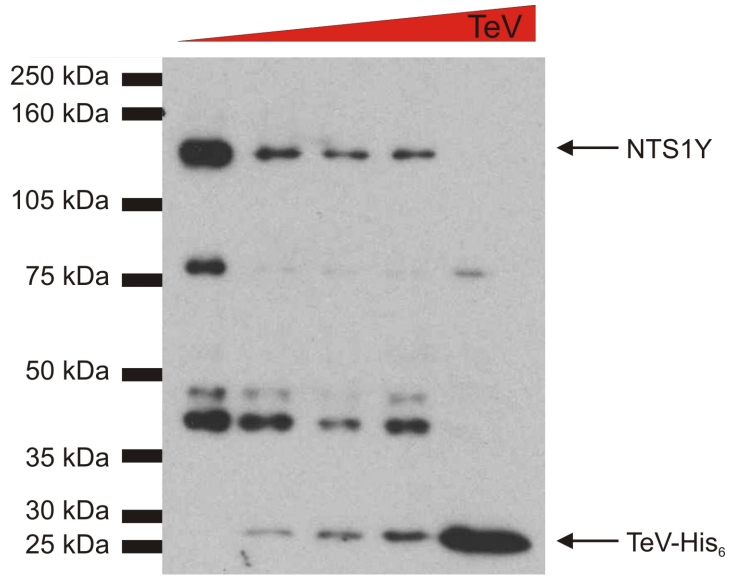

Figure A1 – Trial proteolytic cleavage with purified TeV-His_6. IMAC-purified NTS1Y was incubated with increasing amounts of TeV-His_6 at 4 °C overnight. Analysis by SDS-PAGE followed by immunoblotting (anti-His_6 antibody) revealed the concentration of TeV required for complete cleavage, which was typically 4 µg TeV-His_6 per µg fusion protein (as determined by radioligand binding assay).

A7 - Large Scale Purification of NTS1A

Prior to optimisation of NTS1 purification, purification of NTS1A was carried out using the following protocol which is based on that used by Grisshammer et al (White *et al.*, 2004). All steps were carried out at 4 °C unless otherwise stated. 250 g of cell pellet

from a DH5α culture transformed with pNTS1A was resuspended in 500 ml of 2x solubilisation buffer using a Waring Blender. 100 ml of each detergent stock (5 % CHAPS (w/v) / 1 % CHS (w/v) and 10 % DDM (w/v)) was added slowly whilst stirring on ice. MilliQ H_2O was added to give a total volume of 1 l. Cells were further disrupted by sonication on ice (10 sec pulses, 20 sec pauses for 5 min). The resulting suspension was clarified by centrifugation at 108,000 g, 60 mins, 4 °C (JA 30.5 rotor).

An Amersham Biosciences AKTA system with Frac 950 fraction collector was used for the column purification steps. A 100 ml Ni-NTA IMAC column (Qiagen) was equilibrated with 2 column volumes (CV) of NiA buffer and the clarified sample loaded at 5 ml/min. Non-specifically bound proteins were removed by washing with 4 CV of NiA buffer and protein eluted in 4 CV of NiB at 5 ml/min. Protein elution was monitored by absorbance at 280 nm.

Elution fractions were concentrated to 100 ml using an Amicon 350 ml stirred vessel, then diluted 5x in NT0 buffer (50 mM Tris/HCl, pH 7.4, 30 % glycerol (v/v), 0.5 % CHAPS (w/v), 0.1 % CHS (w/v), 0.1 % DDM (w/v), 1 mM EDTA), reducing the NaCl concentration to 50 mM. Diluted concentrate was loaded onto a 20 ml Neurotensin Affinity column (Biotinylated NT immobilised to streptavidin sepharose resin (GE Healthcare)) at a flow rate of 0.5 ml/min. The NT column was washed with 4 CV of NT0 and bound NT eluted in 4 CV of NT1 (NT0 plus 1 M NaCl) at 1 ml/min. Elution fractions were diluted 20x in NT0, concentrated to a volume of 10 ml using an Amicon stirred cell and stored at -80 °C.

A8 - Solid Phase Peptide Synthesis

Figure A2 gives a general overview of solid phase peptide synthesis using Fmoc (9-fluorenylmethoxycarbonyl) chemistry.

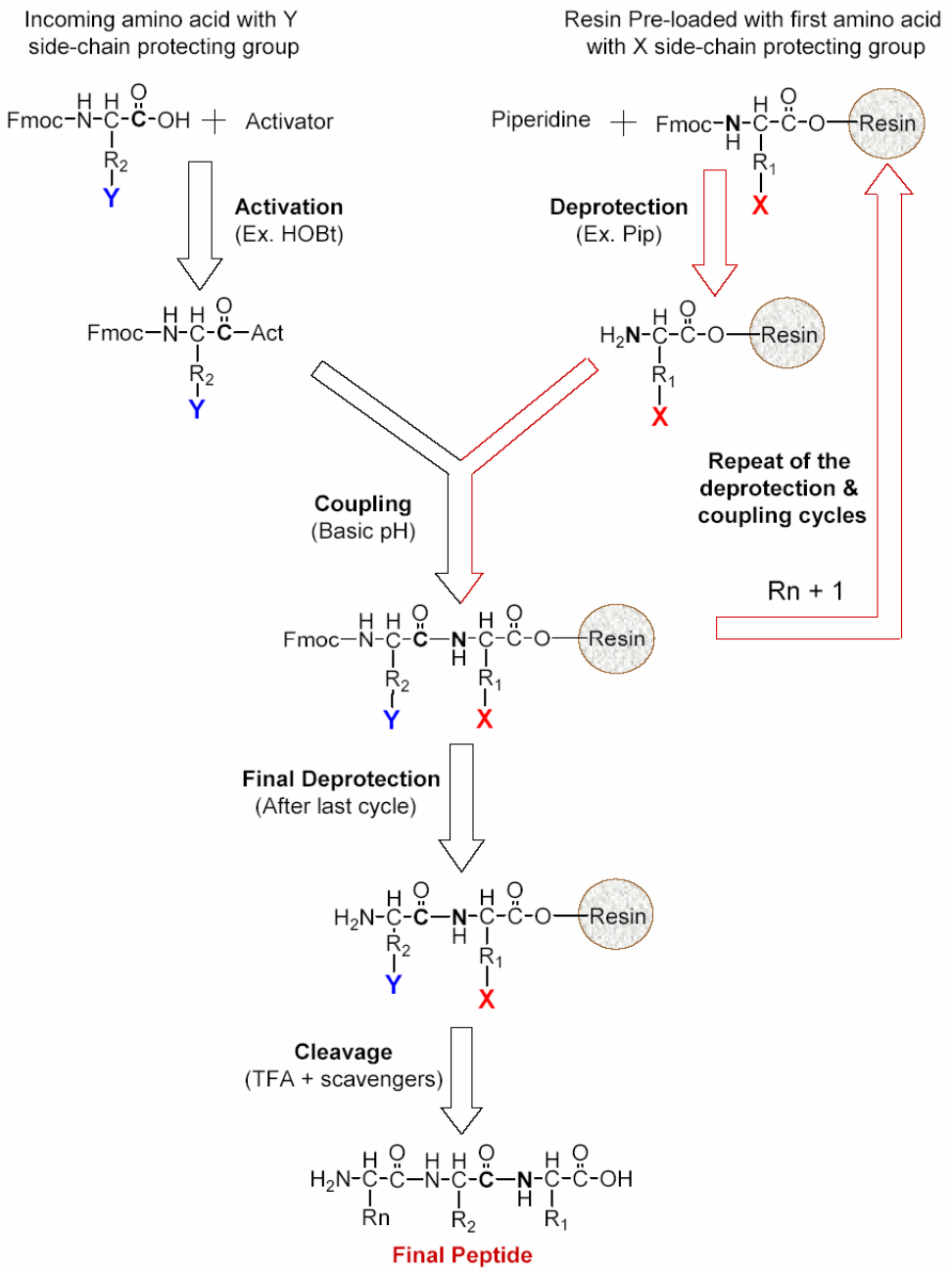

Figure A2 – General scheme for solid phase peptide synthesis using Fmoc chemistry. Initially, the first Fmoc amino acid is attached to an insoluble support resin via an acid labile linker. Deprotection of the Fmoc protecting group is accomplished by treatment of the resin with a base, typically piperidine. The second Fmoc protected amino acid is coupled utilising a preactivated species or in situ activation. After coupling, excess reagents are removed by washing the resin. This process is repeated until the desired peptide sequence is assembled. In the final step, the resin-bound peptide is deprotected and then detached from the solid support via trifluoroacetic acid (TFA) cleavage. (Adapted from Sigma Genosys technical bulletin).

The following peptides were produced by solid phase peptide synthesis:

Biotinylated NT	biotin-Glu-Leu-Tyr-Glu-Asn-Lys-Pro-Arg-Arg-Pro-Tyr-Ile-Leu
Biotinylated 'scrambled' NT	biotin-Leu-Tyr-Asn-Arg-Pro-Arg-Pro-Tyr-Leu-Glu-Ile-Lys-Glu
TAMRA-NT_{2-13}	TAMRA- Leu-Tyr-Glu-Asn-Lys-Pro-Arg-Arg-Pro-Tyr-Ile-Leu
TAMRA-linker-NT_{2-13}	TAMRA-$(PEG)_2$- Leu-Tyr-Glu-Asn-Lys-Pro-Arg-Arg-Pro-Tyr-Ile-Leu

Coupling reagents (N-Hydroxybenzotriazole (HOBt), 2-(H-Benzotriazole-1-yl)-1,1,3,3-tetramethyluronium hexafluorophosphate (HBTU), Benzotriazole-1-yl-oxy-tris-pyrrolidino-phosphonium hexafluorophosphate (PyBOP)), Fmoc-protected amino acids, biotinylation reagent (Biotin-OSu), PEG linker (Fmoc-NH-$(PEG)_2$-COOH (20 atoms)) and solid support (Novasyn TGR resin, loading 0.29 mmol/g) were obtained from Novabiochem (Merck). The fluorophore, 5(6)-Carboxytetramethylrhodamine (5(6)-TAMRA) was purchased from Anaspec.

In each case, the initial part of the synthesis, up to and including the N-terminal amino acid, was carried out using an automated peptide synthesiser (Pioneer, Perspective Biosystems). Coupling was carried out in DMF using a four-fold excess of coupling reagents and amino acids and a reaction time of 45 min. Deprotection of Fmoc groups was carried out in 20 % piperidine / 80 % DMF for 20 min. Each peptide-resin was subsequently removed from the synthesiser and the extra C-terminal constituents (biotin, linker and TAMRA) added manually to allow for more careful monitoring of successful coupling. Complete coupling and deprotection were confirmed using the ninhydrin test for primary amines.

Prior to peptide-resin cleavage, the resin was washed with DCM, methanol and diethyl ether and dried for 24 h in a dessicator under vacuum. The peptides were cleaved from the resin by agitation for 3 h in cleavage solution (trifluoroacetic acid (TFA) (95 %), triethylsilane (TES) (2.5 %) and water (2.5 %)). The resultant liquid was filtered and the

resin washed with 95 % TFA / 5 % water. Excess TFA was then evaporated off under a stream of nitrogen until approximately 1 ml remained. 40 ml of ice cold diethyl ether was added, followed by centrifugation at 5000 g, 4 °C, 15 min. The supernatant was discarded and the ether extraction was repeated twice on the peptide pellet.

Peptide was purified by reversed phase HPLC using a C18 Kromasil 150-10 12 ml semi-preparative column (Hichrom) by applying a gradient of acetonitrile containing 0.1 % TFA. The presence of desired product was confirmed using either MALDI or ESI mass spectrometry.

A9 - Expression and Purification of eCFP/eYFP-His_6

An LB starter culture (100 ml) containing ampicillin (75 μg/ml) was inoculated with a single colony of DH5α transformed with a pQE80 vector containing His_6-tagged eCFP/eYFP and incubated overnight (16 h, 37 °C). Double strength TY (450 ml, 75 μg/ml ampicillin) in a 2 l baffled conical flask was inoculated with starter culture (25 ml) and incubated (37 °C, 200 rpm) until the cells reached an OD_{600} of 0.6. The temperature was reduced to 18 °C and expression induced by adding IPTG (0.1 mM). The cells were harvested after 16 h of induction, and resuspended in 30 ml of GFP lysis buffer (50 mM Tris pH 8.0, 10 % glycerol (v/v), 150 mM NaCl, 10 mM imidazole, 1 mM DTT, protease inhibitors), frozen in liquid nitrogen and stored at -80 °C overnight.

Resuspended cells were thawed and sonicated (2 min at 100 % amplitude; 20 seconds on and 20 seconds off) and cell debris removed by centrifugation (40,000 g, 20 min, 4 °C). The supernatant was purified by IMAC using a 5 ml HisTrap HP column (GE Healthcare). After loading, the column was washed with 50 CV of GFP wash buffer (GFP lysis buffer plus 30 mM imidazole) and eluted using GFP elution buffer (GFP

lysis buffer plus 500 mM imidazole). Column eluate was flash frozen using liquid nitrogen and stored at -80 °C.

A10 - Functionalisation of Glass Coverslips with Anchor-TWW Oligonucleotide

Glass coverslips were initially immersed in saturated KOH solution for ~12 h, sonicated for ~1 h and then rinsed thoroughly with distilled water. They were then silanised by immersion in ethanol containing 0.02 % (v/v) acetic acid and 2 % (v/v) 3-mercaptopropyltrimethoxysilane (MPS) heated to ~70 °C, using a hot water bath, for ~2 h. Finally coverslips were washed thoroughly with distilled water and placed in an oven set to 120 °C for ~30 min.

MPS-decorated coverslip surfaces were reduced using 100 mM TCEP / 20 mM Tris·HCl pH 8.8 and a 5'-thiolated, 15-mer oligonucleotide (Anchor-TWW) reduced using 10 mM TCEP / 20 mM Tris·HCl pH 8.8. Both reactions were carried out at 20 °C for ~1 h. Reduced coverslips were then washed with distilled water and TCEP removed from the oligonucleotide solution using a P6 Microspin gel filtration column (Biorad).

Anchor-TWW was covalently attached to the coverslip surface through oxidation of DNA and coverslip thiol groups: 200 µM Anchor-TWW was applied to the reduced coverslip surface and incubated in 10 mM copper (II) nitrate / 20 mM Tris·HCl pH 8.8 at 20 °C for ~12 h.

APPENDIX B - BUFFER COMPOSITIONS

B1 - Growth Media

Luria-Bertani (LB)

Per Litre: 10 g bacto-tryptone, 5 g yeast extract, 10 g NaCl, adjusted to pH 7.0.

Luria-Bertani (LB) Agar

Per Litre: 10 g bacto-tryptone, 5 g yeast extract, 10 g NaCl, 15 g agar, adjusted to pH 7.0.

2x YT

Per Litre: 16 g bacto-tryptone, 10 g yeast extract, 5 g NaCl, adjusted to pH 7.0.

SOC medium

Per Litre: 20 g bacto-tryptone, 5 g yeast extract, 0.5 g NaCl, 2.5 mM KCl, 10 mM $MgCl_2$, 20 mM glucose, adjusted to pH 7.0.

B2 - NTS1 Purification Buffers

N.B. 'protease inhibitors' comprise Leupeptin, Pepstatin A, Aprotinin, all at a final concentration of 1 μg/ml.

2x solubilisation buffer

100 mM Tris/HCl, pH 7.4, 400 mM NaCl, 60 % glycerol (v/v), protease inhibitors.

NiA

50 mM Tris/HCl, pH 7.4, 200 mM NaCl, 30 % glycerol (v/v), 0.5 % CHAPS (w/v), 0.1 % DDM (w/v), 0.1 % CHS (w/v), 50 mM Imidazole, protease inhibitors.

NiB

NiA plus 350 mM imidazole.

Cleavage Buffer

50 mM Tris pH 7.4, 30 % glycerol (v/v), 0.5 M NaCl, 0.5 % CHAPS (w/v), 0.1 % DDM (w/v), 0.1 % CHS (w/v), 0.05 mg/ml POPC, 1 mM EDTA, 1 mM DTT.

GF buffer

50 mM Tris pH 7.4, 15 % glycerol (v/v), 500 mM NaCl, 0.1 % DDM (w/v), 0.01 % CHS (w/v), 0.05 mg/ml POPC, 1 mM EDTA, protease inhibitors.

B3 - Activity Assays

Assay buffer (detergent samples)

50 mM Tris pH 7.4, 0.1 % DDM (w/v), 0.01 % CHS (w/v), 1 mM EDTA, 0.1 mg/ml BSA.

Assay buffer (membrane samples)

50 mM Tris pH 7.4, 1 mM EDTA, 0.1 mg/ml BSA.

B4 - TeV-His_6 Purification buffers

TeV sample buffer

1x PBS containing 0.3 M NaCl, 10 mM imidazole, 1 mM PMSF, 1 mM benzamadine.

TeV IMAC Wash buffer

1x PBS with 0.3 M NaCl, 30 mM Imidazole, 1 mM PMSF, 1 mM benzamadine.

TeV IMAC Elution buffer

1x PBS with 0.3 M NaCl, 250 mM Imidazole and 1 mM PMSF.

TeV GF buffer

1x PBS with 0.3 M NaCl, 1 mM PMSF, 1 mM benzamadine.

TeV Storage buffer

50 mM Tris, 0.3 M NaCl, 50 % glycerol (v/v).

B5 - SDS PAGE

2x sample buffer

200 mM Tris-HCl (pH 8.8), 20 % glycerol (v/v), 5 mM EDTA, 0.02 % bromophenol blue (w/v). To a 700 µl aliquot, add 200 µl 20 % SDS (w/v) and 100 µl 0.5 M DTT before use.

Tris-Glycine SDS Running Buffer

25 mM Tris pH 8.3, 192 mM Glycine, 0.1 % SDS (w/v).

Tris-Glycine Transfer Buffer

12 mM Tris pH 8.3, 96 mM Glycine.

B6 - PFO PAGE

2x sample buffer

100 mM Tris-HCl (pH 8.0), 8 % PFO (w/v), 20 % glycerol (v/v), 0.005 % bromophenol blue (w/v).

PFO PAGE Running Buffer

25 mM Tris pH 8.5, 192 mM glycine, 0.5 % PFO (w/v).

B7 - Reconstitution

Buffer A

50 mM Tris pH 7.4, 200 mM NaCl, 1 mM EDTA.

Sucrose Gradient

0-35 % sucrose (w/v) in 50 mM Tris pH 7.4, 200 mM NaCl, 1 mM EDTA.

B8 - Measurement Buffers

FRET (detergent samples)

50 mM Tris pH 7.4, 15 % glycerol (v/v), 200 mM NaCl, 0.1 % DDM (w/v), 0.01 % CHS (w/v), 1 mM EDTA.

FRET (reconstituted samples)

50 mM Tris pH 7.4, 200 mM NaCl, 1 mM EDTA.

SPR Immobilisation Buffer (HBS-EP)

10 mM HEPES pH 7.4 , 150 mM NaCl, 3 mM EDTA, 0.005 % polysorbate 20 (v/v).

SPR Running Buffer

50 mM Tris/HCl, pH 7.4, 50 mM NaCl, 0.5 % CHAPS (w/v), 0.1 % CHS (w/v), 0.1 % DDM (w/v), 1 mM EDTA.

SPR Regeneration Buffer

50 mM Tris/HCl, pH 7.4, 1 M NaCl, 0.5 % CHAPS (w/v), 0.1 % CHS (w/v), 0.1 % DDM (w/v), 1 mM EDTA.

FCS Buffer

50 mM Tris pH 7.4, 15 % glycerol (v/v), 0.1 % DDM (w/v), 0.01 % CHS (w/v), 1 mM EDTA.

B9 - DNA Array Buffers

Array Buffer A

30 mM $MgCl_2$ / 20 mM Tris·HCl pH 8.8.

Array Buffer B

Array Buffer A plus 500 nM NTS1Y, BSA (1 mg/ml), 100 mM NaCl.

Array Buffer C

Array Buffer A plus 10 mM $NiCl_2$.

B10 - eCFP/eYFP-His6 Purification Buffers

GFP lysis buffer

50 mM Tris pH 8.0, 10 % glycerol (v/v), 150 mM NaCl, 10 mM imidazole, 1 mM DTT, protease inhibitors.

GFP Wash Buffer

GFP Lysis Buffer plus 30 mM Imidazole, protease inhibitors.

GFP Elution Buffer

GFP Lysis Buffer plus 500 mM Imidazole.

REFERENCES

Akermoun, M., Koglin, M., Zvalova-Iooss, D., Folschweiller, N., Dowell, S. J. and Gearing, K. L. (2005). "Characterization of 16 human G protein-coupled receptors expressed in baculovirus-infected insect cells." Protein Expression and Purification **44**(1): 65-74.

Alves, I. D., Salgado, G. F., Salamon, Z., Brown, M. F., Tollin, G. and Hruby, V. J. (2005). "Phosphatidylethanolamine enhances rhodopsin photoactivation and transducin binding in a solid supported lipid bilayer as determined using plasmon-waveguide resonance spectroscopy." Biophysical Journal **88**(1): 198-210.

Andersen, B. and Stevens, R. C. (1998). "The human D1A dopamine receptor: heterologous expression in Saccharomyces cerevisiae and purification of the functional receptor." Protein Expression and Purification **13**(1): 111-9.

Arechaga, I., Miroux, B., Karrasch, S., Huijbregts, R., de Kruijff, B., Runswick, M. J. and Walker, J. E. (2000). "Characterisation of new intracellular membranes in Escherichia coli accompanying large scale over-production of the b subunit of F(1)F(o) ATP synthase." FEBS Letters **482**(3): 215-9.

Babcock, G. J., Farzan, M. and Sodroski, J. (2003). "Ligand-independent dimerization of CXCR4, a principal HIV-1 coreceptor." Journal of Biological Chemistry **278**(5): 3378-85.

Baneres, J. L., Martin, A., Hullot, P., Girard, J. P., Rossi, J. C. and Parello, J. (2003). "Structure-based analysis of GPCR function: conformational adaptation of both agonist and receptor upon leukotriene B4 binding to recombinant BLT1." Journal of Molecular Biology **329**(4): 801-14.

Baneres, J. L. and Parello, J. (2003). "Structure-based analysis of GPCR function: evidence for a novel pentameric assembly between the dimeric leukotriene B4 receptor BLT1 and the G-protein." Journal of Molecular Biology **329**(4): 815-29.

Barber, E. J. (1966). "Calculation of density and viscosity of sucrose solutions as a function of concentration and temperature." National Cancer Institute Monograph **21**: 219-39.

Barroso, S., Richard, F., Nicolas-Eteve, D., Reversat, J.-L., Bernassau, J.-M., Kitabgi, P. and Labbe-Jullie, C. (2000). "Identification of Residues Involved in Neurotensin Binding and Modeling of the Agonist Binding Site in Neurotensin Receptor 1." The Journal of Biological Chemistry **275**(1): 328-336.

Barroso, S., Richard, F., Nicolas-Etheve, D., Kitabgi, P. and Labbe-Jullie, C. (2002). "Constitutive activation of the neurotensin receptor 1 by mutation of Phe(358) in Helix seven." British Journal of Pharmacology **135**(4): 997-1002.

Beaudet, A., Nouel, D., Stroh, T., Vandenbulcke, F., Dal-Farra, C. and Vincent, J. P. (1998). "Fluorescent ligands for studying neuropeptide receptors by confocal microscopy." Brazalian Journal of Medical and Biological Research **31**(11): 1479-89.

Biacore (2001). Technology Note 1 : Surface Plasmon Resonance, Biacore, AB.

Biacore (2004). BIAevaluation Software Handbook, version 4, Biacore AB.

Botelho, A. V., Gibson, N. J., Thurmond, R. L., Wang, Y. and Brown, M. F. (2002). "Conformational energetics of rhodopsin modulated by nonlamellar-forming lipids." Biochemistry **41**(20): 6354-68.

Brejc, K., Sixma, T. K., Kitts, P. A., Kain, S. R., Tsien, R. Y., Ormo, M. and Remington, S. J. (1997). "Structural basis for dual excitation and photoisomerization of the Aequorea victoria green fluorescent protein." Proceedings of the National Academy of Sciences U S A **94**(6): 2306-11.

Breusegem, S. Y., Levi, M. and Barry, N. P. (2006). "Fluorescence correlation spectroscopy and fluorescence lifetime imaging microscopy." Nephron Experimental Nephrology **103**(2): e41-9.

Breyton, C., Tribet, C., Olive, J., Dubacq, J. P. and Popot, J. L. (1997). "Dimer to monomer conversion of the cytochrome b6 f complex. Causes and consequences." Journal of Biological Chemistry **272**(35): 21892-900.

Brzostowski, J. A. and Kimmel, A. R. (2001). "Signaling at zero G: G-protein-independent functions for 7-TM receptors." Trends in Biochemical Sciences **26**(5): 291-7.

Caceda, R., Kinkead, B. and Nemeroff, C. B. (2006). "Neurotensin: Role in psychiatric and neurological diseases." Peptides.

Carraway, R. E. and Leeman, S. E. (1973). "Discovery of Neurotensin." Journal of Biological Chemistry **248**: 6854.

Chalon, P., Vita, N., Kaghad, M., Guillemot, M., Bonnin, J., Delpech, B., Le Fur, G., Ferrara, P. and Caput, D. (1996). "Molecular cloning of a levocabastine-sensitive neurotensin binding site." FEBS Letters **386**(2-3): 91-4.

Claing, A., Laporte, S. A., Caron, M. G. and Lefkowitz, R. J. (2002). "Endocytosis of G protein-coupled receptors: roles of G protein-coupled receptor kinases and beta-arrestin proteins." Progress in Neurobiology **66**(2): 61-79.

Clegg, R. M. (1992). "Fluorescence resonance energy transfer and nucleic acids." Methods in Enzymology **211**: 353-88.

Cohen, E., Goldshleger, R., Shainskaya, A., Tal, D. M., Ebel, C., le Maire, M. and Karlish, S. J. (2005). "Purification of Na+,K+-ATPase expressed in Pichia pastoris reveals an essential role of phospholipid-protein interactions." Journal of Biological Chemistry **280**(17): 16610-8.

Cohn, E. J. and Edsall, J. T. (1943). Proteins, Amino Acids and Peptides as Ions and Dipolar Ions. New York, Reinhold Publishing.

Cooper, M. A., Hansson, A., Lofas, S. and Williams, D. H. (2000). "A vesicle capture sensor chip for kinetic analysis of interactions with membrane-bound receptors." Analytical Biochemistry **277**(2): 196-205.

Cubitt, A. B., Woollenweber, L. A. and Heim, R. (1999). "Understanding structure-function relationships in the Aequorea victoria green fluorescent protein." Methods in Cell Biology **58**: 19-30.

Cusack, B., Groshan, K., McCormick, D. J., Pang, Y. P., Perry, R., Phung, C. T., Souder, T. and Richelson, E. (1996). "Chimeric rat/human neurotensin receptors localize a region of the receptor sensitive to binding of a novel, species-specific, picomolar affinity peptide." Journal of Biological Chemistry **271**(25): 15054-9.

Cvejic, S. and Devi, L. A. (1997). "Dimerization of the delta opioid receptor: implication for a role in receptor internalization." Journal of Biological Chemistry **272**(43): 26959-64.

Daly, C. J. and McGrath, J. C. (2003). "Fluorescent ligands, antibodies, and proteins for the study of receptors." Pharmacology and Therapeutics **100**(2): 101-18.

David, N. E., Gee, M., Andersen, B., Naider, F., Thorner, J. and Stevens, R. C. (1997). "Expression and purification of the Saccharomyces cerevisiae alpha-factor receptor (Ste2p), a 7-transmembrane-segment G protein-coupled receptor." Journal of Biological Chemistry **272**(24): 15553-61.

Davies, A., Gowen, B. E., Krebs, A. M., Schertler, G. F. and Saibil, H. R. (2001). "Three-dimensional structure of an invertebrate rhodopsin and basis for ordered alignment in the photoreceptor membrane." Journal of Molecular Biology **314**(3): 455-63.

De Crescenzo, G., Grothe, S., Lortie, R. and Debanne, M. (2000). "Real-Time Kinetic Studies on the Interaction of Transforming Growth Factor R with the Epidermal Growth Factor Receptor Extracellular Domain Reveal a Conformational Change Model." Biochemistry **39**: 9466-9476.

de Jong, L. A., Grunewald, S., Franke, J. P., Uges, D. R. and Bischoff, R. (2004). "Purification and characterization of the recombinant human dopamine D2S receptor from Pichia pastoris." Protein Expression and Purification **33**(2): 176-84.

de la Masa, A. and Parra, J. L. (1997). "Solubilising Effects Caused by the Nonionic Surfactant Dodecylmaltoside in Phosphatidylcholine Liposomes." Biophysical Journal **72**: 1668-1675.

Dean, M. K., Higgs, C., Smith, R. E., Bywater, R. P., Snell, C. R., Scott, P. D., Upton, G. J., Howe, T. J. and Reynolds, C. A. (2001). "Dimerization of G-protein-coupled receptors." Journal of Medicinal Chemistry **44**(26): 4595-614.

Dinger, M. C., Bader, J. E., Kobor, A. D., Kretzschmar, A. K. and Beck-Sickinger, A. G. (2003). "Homodimerization of neuropeptide y receptors investigated by fluorescence resonance energy transfer in living cells." Journal of Biological Chemistry **278**(12): 10562-71.

Dobner, P. R. (2005). "Multitasking with neurotensin in the central nervous system." Cellular and Molecular Life Sciences **62**(17): 1946-63.

Dobner, P. R., Barber, D. L., Villa-Komaroff, L. and McKiernan, C. (1987). "Cloning and sequence analysis of cDNA for the canine neurotensin/neuromedin N precursor." Proceedings of the National Academy of Sciences U S A **84**(10): 3516-20.

Doose, S., Heilemann, M., Michalet, X., Weiss, S. and Kapanidis, A. N. (2007). "Periodic acceptor excitation spectroscopy of single molecules." European Biophysical Journal.

dos Remedios, C. G. and Moens, P. D. (1995). "Fluorescence resonance energy transfer spectroscopy is a reliable "ruler" for measuring structural changes in proteins. Dispelling the problem of the unknown orientation factor." Journal of Structural Biology **115**(2): 175-85.

Drew, D., Lerch, M., Kunji, E., Slotboom, D. and de Gier, J. W. (2006). "Optimisation of membrane protein overexpression and purification using GFP fusions." Nature Methods **3**(4): 303-313.

Drew, D., von Heijne, G., Nordlund, P. and de Gier, J. W. (2001). "Green fluorescent protein as an indicator to monitor membrane protein overexpression in Escherichia coli." FEBS Letters **507**: 220-224.

Dubuc, I., Costentin, J., Terranova, J. P., Barnouin, M. C., Soubrie, P., Le Fur, G., Rostene, W. and Kitabgi, P. (1994). "The nonpeptide neurotensin antagonist, SR 48692, used as a tool to reveal putative neurotensin receptor subtypes." British Journal of Pharmacology **112**(2): 352-4.

Dumon-Seignovert, L., Cariot, G. and Vuillard, L. (2004). "The toxicity of recombinant proteins in Escherichia coli: a comparison of overexpression in BL21(DE3), C41(DE3), and C43(DE3)." Protein Expression and Purification **37**(1): 203-6.

Durchschlag, H. (1986). Thermodynamic Data for Biochemistry and Biotechnology. Berlin, Springer-Verlag.

Elde, R., Schalling, M., Ceccatelli, S., Nakanishi, S. and Hokfelt, T. (1990). "Localization of neuropeptide receptor mRNA in rat brain: initial observations using probes for neurotensin and substance P receptors." Neuroscience Letters **120**(1): 134-8.

Ellis, C. (2004). "The state of GPCR research in 2004." Nature Reviews Drug Discovery **3**(7): 575, 577-626.

Eytan, G. D. and Broza, R. (1978). "Role of charge and fluidity in the incorporation of cytochrome oxidase into liposomes." Journal of Biological Chemistry **253**(9): 3196-202.

Fang, Y., Peng, J., Ferrie, A. M. and Burkhalter, R. S. (2006). "Air-stable G protein-coupled receptor microarrays and ligand binding characteristics." Analytical Chemistry **78**(1): 149-55.

Faure, M. P., Gaudreau, P., Shaw, I., Cashman, N. R. and Beaudet, A. (1994). "Synthesis of a biologically active fluorescent probe for labeling neurotensin receptors." The Journal of Histochemistry and Cytochemistry **42**(6): 755-63.

Feilmeier, B. J., Iseminger, G., Schroeder, D., Webber, H. and Phillips, G. J. (2000). "Green fluorescent protein functions as a reporter for protein localization in Escherichia coli." Journal of Bacteriology **182**(14): 4068-76.

Ferguson, S. S. (2001). "Evolving concepts in G protein-coupled receptor endocytosis: the role in receptor desensitization and signaling." Pharmacological Reviews **53**(1): 1-24.

Findlay, H. E. and Booth, P. J. (2006). "The biological significance of lipid-protein interactions." Journal of Physics: Condensed Matter **18**: S1281-S1291.

Findlay, J. B. C. (1989). Protein Purification - A Practical Approach, IRL Press, Oxford.

Floyd, D. H., Geva, A., Bruinsma, S. P., Overton, M. C., Blumer, K. J. and Baranski, T. J. (2003). "C5a receptor oligomerization. II. Fluorescence resonance energy transfer studies of a human G protein-coupled receptor expressed in yeast." Journal of Biological Chemistry **278**(37): 35354-61.

Förster, T. (1948). "Zwischenmolekulare Energiwanderung und Fluoreszence [Intermolecular energy migration and fluorescence]." Ann. Phys. **2**: 55-75.

Fotiadis, D., Jastrzebska, B., Philippsen, A., Muller, D. J., Palczewski, K. and Engel, A. (2006). "Structure of the rhodopsin dimer: a working model for G-protein-coupled receptors." Current Opinion in Structural Biology **16**(2): 252-9.

Fraser, M. J. (1992). "The baculovirus-infected insect cell as a eukaryotic gene expression system." Current Topics in Microbiology and Immunology **158**: 131-72.

Garcia-Saez, A. J. and Schwille, P. (2007). "Single molecule techniques for the study of membrane proteins." Applied Microbiology and Biotechnology **online first**.

Gouldson, P. R., Dean, M. K., Snell, C. R., Bywater, R. P., Gkoutos, G. and Reynolds, C. A. (2001). "Lipid-facing correlated mutations and dimerization in G-protein coupled receptors." Protein Engineering **14**(10): 759-67.

Grisshammer, R., Averbeck, P. and Sohal, A. K. (1999). "Improved purification of a rat neurotensin receptor expressed in Escherichia coli." Biochemical Society **27**(5): 899-903.

Grisshammer, R., Duckworth, R. and Henderson, R. (1993). "Expression of a rat neurotensin receptor in Escherichia coli." Biochemical Journal **295**: 571-576.

Grisshammer, R., White, J. F., Trinh, L. B. and Shiloach, J. (2005). "Large-scale expression and purification of a G-protein-coupled receptor for structure determination -- an overview." Journal of Structural and Functional Genomics **6**(2-3): 159-63.

Gully, D., Canton, M., Boigegrain, R., Jeanjean, F., Molimard, J. C., Poncelet, M., Gueudet, C., Heaulme, M., Leyris, R., Brouard, A. and et al. (1993). "Biochemical and pharmacological profile of a potent and selective nonpeptide antagonist of the neurotensin receptor." Proceedings of the National Academy of Sciences U S A **90**(1): 65-9.

Guo, W., Shi, L., Filizola, M., Weinstein, H. and Javitch, J. A. (2005). "Crosstalk in G protein-coupled receptors: changes at the transmembrane homodimer interface determine activation." Proceedings of the National Academy of Sciences U S A **102**(48): 17495-500.

Haas, E., Wilchek, M., Katchalski-Katzir, E. and Steinberg, I. Z. (1975). "Distribution of end-to-end distances of oligopeptides in solution as estimated by energy transfer." Proceedings of the National Academy of Sciences U S A **72**(5): 1807-11.

Hampe, W., Voss, R. H., Haase, W., Boege, F., Michel, H. and Reilander, H. (2000). "Engineering of a proteolytically stable human beta 2-adrenergic receptor/maltose-binding protein fusion and production of the chimeric protein in Escherichia coli and baculovirus-infected insect cells." Journal of Biotechnology **77**(2-3): 219-34.

Harding, P. J., Hadingham, T. C., McDonnell, J. M. and Watts, A. (2006). "Direct analysis of a GPCR-agonist interaction by surface plasmon resonance." European Biophysical Journal **35**(8): 709-12.

Hassan, N. J., Simmonds, S. J., Clarkson, N. G., Hanrahan, S., Puklavec, M. J., Bomb, M., Barclay, A. N. and Brown, M. H. (2006). "CD6 regulates T-cell responses through activation-dependent recruitment of the positive regulator SLP-76." Molecular and Cellular Biology **26**(17): 6727-38.

Hayashi, M. K. and Haga, T. (1996). "Purification and functional reconstitution with GTP-binding regulatory proteins of hexahistidine-tagged muscarinic acetylcholine receptors (m2 subtype)." Journal of Biochemistry (Tokyo) **120**(6): 1232-8.

Hebert, T. E., Moffett, S., Morello, J. P., Loisel, T. P., Bichet, D. G., Barret, C. and Bouvier, M. (1996). "A peptide derived from a beta2-adrenergic receptor transmembrane domain inhibits both receptor dimerization and activation." Journal of Biological Chemistry **271**(27): 16384-92.

Heyse, S., Ernst, O. P., Dienes, Z., Hofmann, K. P. and Vogel, H. (1998). "Incorporation of Rhodopsin in Laterally Structured Supported Membranes: Observation of Transducin Activation with Spatially and Time-Resolved Surface Plasmon Resonance." Biochemistry **37**: 507-522.

Hill, S. J. (2006). "G-protein-coupled receptors: past, present and future." British Journal of Pharmacology **147**: S27-S37.

Israelachvili, J. N., Marcelja, S. and Horn, R. G. (1980). "Physical principles of membrane organization." Quarterly Review of Biophysics **13**(2): 121-200.

Iyengar, R., Hildebrandt, J. D. and eds (2002). "G-protein pathways." Methods in Enzymology **343, 344, 345**: Parts A, B and C.

Jacoby, E., Bouhelal, R., Gerspacher, M. and Seuwen, K. (2006). "The 7 TM G-protein-coupled receptor target family." ChemMedChem **1**(8): 761-82.

Jain, M. (1988). Introduction to Biological Membranes, Wiley Inter-science.

James, J. R., Oliveira, M. I., Carmo, A. M., Iaboni, A. and Davis, S. J. (2006). "A rigorous experimental framework for detecting protein oligomerization using bioluminescence resonance energy transfer." Nature Methods **3**(12): 1001-6.

Ji, T. H. and Ji, I. (1998). "G Protein-coupled receptors." The Journal of Biological Chemistry **28**(10): 17299-17302.

Jonsson, U., Fagerstam, L., Ivarsson, B., Johnsson, B., Karlsson, R., Lundh, K., Lofas, S., Persson, B., Roos, H., Ronnberg, I. and et al. (1991). "Real-time biospecific interaction analysis using surface plasmon resonance and a sensor chip technology." Biotechniques **11**(5): 620-7.

Kapanidis, A. N., Laurence, T. A., Lee, N. K., Margeat, E., Kong, X. and Weiss, S. (2005). "Alternating-Laser Excitation of Single Molecules." Accounts of Chemical Research **38**: 523-533.

Kapanidis, A. N., Lee, N. K., Laurence, T. A., Doose, S., Margeat, E. and Weiss, S. (2004). "Fluorescence-aided molecule sorting: analysis of structure and interactions by alternating-laser excitation of single molecules." Proceedings of the National Academy of Sciences U S A **101**(24): 8936-41.

Karlsson, O. P. and Lofas, S. (2002). "Flow-Mediated On-Surface Reconstitution of G-Protein Coupled Receptors for Applications in Surface Plasmon Resonance Biosensors." Analytical Biochemistry **300**: 132-138.

Karlsson, R. and Falt, A. (1997). "Experimental design for kinetic analysis of protein-protein interactions with surface plasmon resonance biosensors." Journal of Immunological Methods **200**: 121-133.

Kasahara, M. and Hinkle, P. C. (1977). "Reconstitution and purification of the D-glucose transporter from human erythrocytes." Journal of Biological Chemistry **252**(20): 7384-90.

Kenakin, T. (2002). "Efficacy at G-protein-coupled receptors." Nature Reviews Drug Discovery **1**(2): 103-10.

Kim, T. K., Zhang, R., Feng, W., Cai, J., Pierce, W. and Song, Z. H. (2005). "Expression and characterization of human CB1 cannabinoid receptor in methylotrophic yeast Pichia pastoris." Protein Expression and Purification **40**(1): 60-70.

Kitabgi, P. (2006). "Functional domains of the subtype 1 neurotensin receptor (NTS1)." Peptides **27**(10): 2461-8.

Kitabgi, P., Checler, F., Mazella, J. and Vincent, J. P. (1985). "Pharmacology and biochemistry of neurotensin receptors." Rev Clin Basic Pharm **5**(3-4): 397-486.

Kitagbi, P., Carraway, R. E., Rietschoten, J. V., Granier, C., Morgat, J. L., Menez, A., Leeman, S. E. and Freychet, P. (1977). "Neurotensin: Specific binding to synaptic membranes from rat brain." Proceedings of the National Academy of Sciences U S A **74**(5): 1846-1850.

Knol, J., Sjollema, K. and Poolman, B. (1998). "Detergent-mediated reconstitution of membrane proteins." Biochemistry **37**: 16410.

Kobilka, B. K. (1995). "Amino and carboxyl terminal modifications to facilitate the production and purification of a G protein-coupled receptor." Analytical Biochemistry **231**(1): 269-71.

Krepkiy, D., Wong, K., Gawrisch, K. and Yeliseev, A. (2006). "Bacterial expression of functional, biotinylated peripheral cannabinoid receptor CB2." Protein Expression and Purification **49**(1): 60-70.

Kroger, D., Hucho, F. and Vogel, H. (1999). "Ligand binding to Nicotinic Acetylcholine Receptor Investigated by Surface Plasmon Resonance." Analytical Chemistry **71**: 3157.

Kusumi, A., Ike, H., Nakada, C., Murase, K. and Fujiwara, T. (2005). "Single-molecule tracking of membrane molecules: plasma membrane compartmentalization and dynamic assembly of raft-philic signaling molecules." Semin Immunol **17**(1): 3-21.

Kwatra, M. M., Schwinn, D. A., Schreurs, J., Blank, J. L., Kim, C. M., Benovic, J. L., Krause, J. E., Caron, M. G. and Lefkowitz, R. J. (1993). "The substance P receptor, which couples to Gq/11, is a substrate of beta-adrenergic receptor kinase 1 and 2." Journal of Biological Chemistry **268**(13): 9161-4.

Labbe-Jullie, C., Barroso, S., Nicolas-Eteve, D., Reversat, J.-L., Botto, J.-M., Mazella, J., Bernassau, J.-M. and Kitabgi, P. (1998). "Mutagenesis and Modelling of the Neurotensin Receptor NTR1." The Journal of Biological Chemistry **273**(26): 16351-16357.

Lakowicz, J. R. (1999). Principles of Fluorescence Spectroscopy, Kluwer Academic / Plenum Publishers.

Lambert, O., Levy, D., Ranck, J. L., Leblanc, G. and Rigaud, J. L. (1998). "A New 'Gel-like' Phase in Dodecyl Maltoside-Lipid Mixtures: Implications in Solubilisation and Reconstitution Studies." Biophysical Journal **74**: 918-930.

Lee, C., Ji, I., Ryu, K., Song, Y., Conn, P. M. and Ji, T. H. (2002). "Two defective heterozygous luteinizing hormone receptors can rescue hormone action." Journal of Biological Chemistry **277**(18): 15795-800.

Levitzki, A. (1985). "Reconstitution of membrane receptor systems." Biochimica et Biophysica Acta **822**: 127-153.

Li, J., Edwards, P. C., Burghammer, M., Villa, C. and Schertler, G. F. (2004). "Structure of bovine rhodopsin in a trigonal crystal form." Journal of Molecular Biology **343**(5): 1409-38.

Liang, Y., Fotiadis, D., Filipek, S., Saperstein, D. A., Palczewski, K. and Engel, A. (2003). "Organization of the G protein-coupled receptors rhodopsin and opsin in native membranes." Journal of Biological Chemistry **278**(24): 21655-62.

Lichtenberg, D. (1985). "Characterization of the solubilization of lipid bilayers by surfactants." Biochimica et Biophysica Acta **821**(3): 470-8.

Lipschultz, C. A., Yee, A., Mohan, S., Li, Y. and Smith-Gill, S. J. (2002). "Temperature differentially affects encounter and docking thermodynamics of antibody-antigen association." Journal of Molecular Recognition **15**: 44-52.

Lofas, S. and Johnsson, B. (1990). "A novel hydrogel matrix on gold surfaces in surface plasmon resonance sensors for fast and efficient covalent immobilisation of ligands." Journal of the Chemical Society, Chemical Communications **21**: 1526-1528.

Lohse, M. J. (1992). "Stable overexpression of human beta 2-adrenergic receptors in mammalian cells." Naunyn Schmiedebergs Archives of Pharmacology **345**(4): 444-51.

Luca, S., White, J. F., Sohal, A. K., Filippov, D. V., van Boom, J. H., Grisshammer, R. and Baldus, M. (2003). "The conformation of neurotensin bound to its G protein-coupled receptor." Proceedings of the National Academy of Sciences U S A **100**(19): 10706-11.

Lundstrom, K. (2007). "Structural genomics and drug discovery." Journal of Cellular and Molecular Medicine **11**(2): 224-38.

MacDonald, R. C., MacDonald, R. I., Menco, B. P., Takeshita, K., Subbarao, N. K. and Hu, L. R. (1991). "Small-volume extrusion apparatus for preparation of large, unilamellar vesicles." Biochimica et Biophysica Acta **1061**(2): 297-303.

Magde, D., Webb, W. W. and Elson, E. (1972). "Thermodynamic Fluctuations in a Reacting System - Measurement by Fluorescence Correlation Spectroscopy." Physical Review Letters **29**(11): 705-&.

Maggio, R., Vogel, Z. and Wess, J. (1993). "Coexpression studies with mutant muscarinic/adrenergic receptors provide evidence for intermolecular "cross-talk" between G-protein-linked receptors." Proceedings of the National Academy of Sciences U S A **90**(7): 3103-7.

Malo, J., Mitchell, J. C., Venien-Bryan, C., Harris, J. R., Wille, H., Sherratt, D. J. and Turberfield, A. J. (2005). "Engineering a 2D protein-DNA crystal." Angew Chem Int Ed Engl **44**(20): 3057-61.

Mandal, A., Das, S., Chakraborti, T., Kar, P., Ghosh, B. and Chakraborti, S. (2006). "Solubilization, purification and reconstitution of Ca(2+)-ATPase from bovine pulmonary artery smooth muscle microsomes by different detergents: preservation of native structure and function of the enzyme by DHPC." Biochimica et Biophysica Acta **1760**(1): 20-31.

Marinissen, M. J. and Gutkind, J. S. (2001). "G-protein-coupled receptors and signaling networks: emerging paradigms." Trends in Pharmacological Sciences **22**(7): 368-76.

Marley, J., Lu, M. and Bracken, C. (2001). "A method for efficient isotopic labeling of recombinant proteins." Journal of Biomolecular NMR **20**(1): 71-5.

Martin, S., Navarro, V., Vincent, J. P. and Mazella, J. (2002). "Neurotensin receptor-1 and -3 complex modulates the cellular signaling of neurotensin in the HT29 cell line." Gastroenterology **123**(4): 1135-43.

Mathews, C. K. and van Holde, K. E. (1990). Biochemistry, Benjamin-Cummings Publishing Co.

Matz, M. V., Fradkov, A. F., Labas, Y. A., Savitsky, A. P., Zaraisky, A. G., Markelov, M. L. and Lukyanov, S. A. (1999). "Fluorescent proteins from nonbioluminescent Anthozoa species." Nature Biotechnology **17**(10): 969-73.

Mazella, J. and Vincent, J. P. (2006). "Functional roles of the NTS2 and NTS3 receptors." Peptides **27**(10): 2469-75.

Mazella, J., Zsurger, N., Navarro, V., Chabry, J., Kaghad, M., Caput, D., Ferrara, P., Vita, N., Gully, D., Maffrand, J. P. and Vincent, J. P. (1998). "The 100-kDa neurotensin receptor is gp95/sortilin, a non-G-protein-coupled receptor." Journal of Biological Chemistry **273**(41): 26273-6.

McDonnell, J. M. (2001). "Surface plasmon resonance: towards an understanding of the mechanisms of biological molecular recognition." Current Opinion in Chemical Biology **5**: 572-577.

Meier, C. A. and Turberfield, A. J. (2003). "DNA-Nanotechnological approaches to protein crystallisation and biological structure determination." Wellcome Rotation Project.

Mercier, J. F., Salahpour, A., Angers, S., Breit, A. and Bouvier, M. (2002). "Quantitative assessment of beta 1- and beta 2-adrenergic receptor homo- and heterodimerization by bioluminescence resonance energy transfer." Journal of Biological Chemistry **277**(47): 44925-31.

Merrifield, R. B. (1963). "Solid Phase Peptide Synthesis. I. The Synthesis of a Tetrapeptide." Journal of the American Chemical Soceity **85**(14): 2149-2154.

Michel, H. (2007). Membrane Proteins of Known 3D Structure (http://blanco.biomol.uci.edu/Membrane_Proteins_xtal.html).

Middleton, R. J. and Kellam, B. (2005). "Fluorophore-tagged GPCR ligands." Current Opinion in Chemical Biology **9**(5): 517-25.

Milligan, G. (2004). "G protein-coupled receptor dimerization: function and ligand pharmacology." Molecular Pharmacology **66**(1): 1-7.

Milligan, G. (2007). "G protein-coupled receptor dimerisation: Molecular basis and relevance to function." Biochimica et Biophysica Acta **1768**(4): 825-35.

Milligan, G. and Bouvier, M. (2005). "Methods to monitor the quaternary structure of G protein-coupled receptors." FEBS Journal **272**(12): 2914-25.

Milligan, G., Ramsay, D., Pascal, G. and Carrillo, J. J. (2003). "GPCR dimerisation." Life Sciences **74**(2-3): 181-8.

Miroux, B. and Walker, J. (1996). "Over-production of Proteins in Escherichia coli: Mutant Hosts that Allow Synthesis of some Membrane Proteins and Globular Proteins at High Levels." Journal of Molecular Biology **260**: 289-298.

Monnot, C., Bihoreau, C., Conchon, S., Curnow, K. M., Corvol, P. and Clauser, E. (1996). "Polar residues in the transmembrane domains of the type 1 angiotensin II receptor are required for binding and coupling. Reconstitution of the binding site by co-expression of two deficient mutants." Journal of Biological Chemistry **271**(3): 1507-13.

Mukhopadhyay, J., Kapanidis, A. N., Mekler, V., Kortkhonjia, E., Ebright, Y. W. and Ebright, R. H. (2001). "Translocation of sigma(70) with RNA polymerase during transcription: fluorescence resonance energy transfer assay for movement relative to DNA." Cell **106**(4): 453-63.

Navratilova, I., Dioszegi, M. and Myszka, D. G. (2006). "Analyzing ligand and small molecule binding activity of solubilized GPCRs using biosensor technology." Analytical Biochemistry **355**(1): 132-9.

Navratilova, I., Sodroski, J. and Myszka, D. G. (2005). "Solubilization, stabilization, and purification of chemokine receptors using biosensor technology." Analytical Biochemistry **339**(2): 271-81.

Nemoto, W. and Toh, H. (2005). "Prediction of interfaces for oligomerizations of G-protein coupled receptors." Proteins **58**(3): 644-60.

Noguchi, S. and Satow, Y. (2006). "Purification of human beta2-adrenergic receptor expressed in methylotrophic yeast Pichia pastoris." Journal of Biochemistry (Tokyo) **140**(6): 799-804.

Norton, W. T., Abe, T., Poduslo, S. E. and DeVries, G. H. (1975). "The lipid composition of isolated brain cells and axons." Journal of Neuroscience Research **1**(1): 57-75.

O'Shannessy, D. J. and Winzor, D. J. (1996). "Interpretation of Deviations from Pseudo-First-Order Kinetic Behaviour in the Characterisation of Ligand Binding by Biosensor Technology." Analytical Biochemistry **236**: 275-283.

Ohtaki, T., Ogi, K., Masuda, Y., Mitsuoka, K., Fujiyoshi, Y., Kitada, C., Sawada, H., Onda, H. and Fujino, M. (1998). "Expression, purification, and reconstitution of receptor for pituitary adenylate cyclase-activating polypeptide. large-scale purification of a functionally active G protein-coupled receptor produced in Sf9 insect cells." Journal of Biological Chemistry **273**(25): 15464-73.

Okada, T., Fujiyoshi, Y., Silow, M., Navarro, J., Landau, E. M. and Shichida, Y. (2002). "Functional role of internal water molecules in rhodopsin revealed by X-ray crystallography." Proceedings of the National Academy of Sciences U S A **99**(9): 5982-7.

Okada, T., Sugihara, M., Bondar, A. N., Elstner, M., Entel, P. and Buss, V. (2004). "The retinal conformation and its environment in rhodopsin in light of a new 2.2 A crystal structure." Journal of Molecular Biology **342**(2): 571-83.

Opekarova, M. and Tanner, W. (2003). "Specific lipid requirements of membrane proteins--a putative bottleneck in heterologous expression." Biochimica et Biophysica Acta **1610**(1): 11-22.

Ormo, M., Cubitt, A. B., Kallio, K., Gross, L. A., Tsien, R. Y. and Remington, S. J. (1996). "Crystal structure of the Aequorea victoria green fluorescent protein." Science **273**(5280): 1392-5.

Ostrom, R. S. and Insel, P. A. (2004). "The evolving role of lipid rafts and caveolae in G protein-coupled receptor signaling: implications for molecular pharmacology." British Journal of Pharmacology **143**(2): 235-45.

Overton, M. C. and Blumer, K. J. (2000). "G-protein-coupled receptors function as oligomers in vivo." Current Biology **10**(6): 341-4.

Overton, M. C. and Blumer, K. J. (2002a). "The extracellular N-terminal domain and transmembrane domains 1 and 2 mediate oligomerization of a yeast G protein-coupled receptor." Journal of Biological Chemistry **277**(44): 41463-72.

Overton, M. C. and Blumer, K. J. (2002b). "Use of fluorescence resonance energy transfer to analyze oligomerization of G-protein-coupled receptors expressed in yeast." Methods **27**(4): 324-32.

Palczewski, K., Kumasaka, T., Hori, T., Behnke, C. A., Motoshima, H., Fox, B. A., Le Trong, I., Teller, D. C., Okada, T., Stenkamp, R. E., Yamamoto, M. and Miyano, M. (2000). "Crystal structure of rhodopsin: A G protein-coupled receptor." Science **289**(5480): 739-45.

Pang, Y.-P., Cusack, B., Groshan, K. and Richelson, E. (1996). "Proposed Ligand Binding Site of the Transmembrane Receptor for Neurotensin(8-13)." The Journal of Biological Chemistry **271**(25): 15060-15068.

Parker, E. M., Kameyama, K., Higashijima, T. and Ross, E. M. (1991). "Reconstitutively active G protein-coupled receptors purified from baculovirus-infected insect cells." Journal of Biological Chemistry **266**(1): 519-27.

Paternostre, M. T., Roux, M. and Rigaud, J. L. (1988). "Mechanisms of membrane protein insertion into liposomes during reconstitution procedures involving the use of detergents. 1. Solubilization of large unilamellar liposomes (prepared by reverse-phase evaporation) by triton X-100, octyl glucoside, and sodium cholate." Biochemistry **27**(8): 2668-77.

Patterson, G., Day, R. N. and Piston, D. (2001). "Fluorescent protein spectra." Journal of Cell Science **114**(Pt 5): 837-8.

Pautsch, A. and Schulz, G. E. (1998). "Structure of the outer membrane protein A transmembrane domain." Nature Structural Biology **5**(11): 1013-7.

Perron, A., Sharif, N., Sarret, P., Stroh, T. and Beaudet, A. (2006). "NTS2 modulates the intracellular distribution and trafficking of NTS1 via heterodimerization." Biochemical and Biophysical Research Communications.

Peterson, G. L., Toumadje, A., Johnson, W. C., Jr. and Schimerlik, M. I. (1995). "Purification of recombinant porcine m2 muscarinic acetylcholine receptor from Chinese hamster ovary cells. Circular dichroism spectra and ligand binding properties." Journal of Biological Chemistry **270**(30): 17808-14.

Pettibone, D. J., Hess, J. F., Hey, P. J., Jacobson, M. A., Leviten, M., Lis, E. V., Mallorga, P. J., Pascarella, D. M., Snyder, M. A., Williams, J. B. and Zeng, Z. (2002). "The effects of deleting the mouse neurotensin receptor NTR1 on central and peripheral responses to neurotensin." The Journal of Pharmacology and Experimental Therpeutics **300**(1): 305-13.

Phillips, G. N., Jr. (1997). "Structure and dynamics of green fluorescent protein." Curr Opin Struct Biol **7**(6): 821-7.

Pierce, K. L., Premont, R. T. and Lefkowitz, R. J. (2002). "Seven-transmembrane receptors." Nature Reviews in Molecular Cell Biology **3**(9): 639-50.

Pitcher, J. A., Freedman, N. J. and Lefkowitz, R. J. (1998). "G protein-coupled receptor kinases." Annual Review of Biochemistry **67**: 653-92.

Pollok, B. A. and Heim, R. (1999). "Using GFP in FRET-based applications." Trends in Cell Biology **9**(2): 57-60.

Quinn, P. J., Tessier, C., Rainteau, D., Koumanov, K. S. and Wolf, C. (2005). "Structure and thermotropic phase behaviour of detergent-resistant membrane raft fractions isolated from human and ruminant erythrocytes." Biochimica et Biophysica Acta **1713**(1): 5-14.

Ramjeesingh, M., Huan, L. J., Garami, E. and Bear, C. E. (1999). "Novel method for evaluation of the oligomeric structure of membrane proteins." Biochemical Journal **342 (Pt 1)**: 119-23.

Ramjeesingh, M., Kidd, J. F., Huan, L. J., Wang, Y. and Bear, C. E. (2003). "Dimeric cystic fibrosis transmembrane conductance regulator exists in the plasma membrane." Biochemical Journal **374**(Pt 3): 793-7.

RCSB (2007). RCSB Protein Data Bank (www.rcsb.org).

Rich, R. L., Hoth, L. R., Geoghegan, K. F., Brown, T. A., LeMotte, P. K., Simons, S. P., Hensley, P. and Myszka, D. G. (2002). "Kinetic analysis of estrogen receptor / ligand interactions." Proceedings of the National Academy of Sciences U S A **99**(13): 8562-8567.

Rigaud, J. L., Bluzat, A. and Buschlen, S. (1983). "Incorporation of bacteriorhodopsin into large unilamellar liposomes by reverse phase evaporation." Biochemical Biophysical Research Communications **111**(2): 373-82.

Rigaud, J. L., Mosser, G., Lacapere, J. J., Olofsson, A., Levy, D. and Ranck, J. L. (1997). "Bio-Beads: An Efficient Strategy for Two-Dimensional Crystallisation of Membrane Proteins." Journal of Structural Biology **118**: 226-235.

Rigaud, J. L., Paternostre, M. T. and Bluzat, A. (1988). "Mechanisms of membrane protein insertion into liposomes during reconstitution procedures involving the use of detergents. 2. Incorporation of the light-driven proton pump bacteriorhodopsin." Biochemistry **27**(8): 2677-88.

Rigaud, J. L., Pitard, B. and Levy, D. (1995). "Reconstitution of membrane proteins into liposomes: application to energy-transducing membrane proteins." Biochimica et Biophysica Acta **1231**(3): 223-46.

Rizzo, M. A., Springer, G. H., Granada, B. and Piston, D. W. (2004). "An improved cyan fluorescent protein variant useful for FRET." Nature Biotechnology **22**(4): 445-9.

Sakaki, T., Zahringer, U., Warnecke, D. C., Fahl, A., Knogge, W. and Heinz, E. (2001). "Sterol glycosides and cerebrosides accumulate in Pichia pastoris, Rhynchosporium secalis and other fungi under normal conditions or under heat shock and ethanol stress." Yeast **18**(8): 679-95.

Samama, P., Cotecchia, S., Costa, T. and Lefkowitz, R. J. (1993). "A mutation-induced activated state of the beta 2-adrenergic receptor. Extending the ternary complex model." Journal of Biological Chemistry **268**(7): 4625-36.

Sarramegna, V., Muller, I., Milon, A. and Talmont, F. (2006). "Recombinant G protein-coupled receptors from expression to renaturation: a challenge towards structure." Cellular and Molecular Life Sciences **63**(10): 1149-1164.

Sarramegna, V., Muller, I., Mousseau, G., Froment, C., Monsarrat, B., Milon, A. and Talmont, F. (2005). "Solubilisation, purification, and mass spectrometry analysis of the human mu-opioid receptor expressed in Pichia pastoris." Protein Expression and Purification **43**: 85-93.

Sarramegna, V., Talmont, F., Demange, P. and Milon, A. (2003). "Heterologous expression of G-protein-coupled receptors: comparison of expression systems fron the standpoint of large-scale production and purification." Cellular and Molecular Life Sciences **60**(8): 1529-46.

Sarramegna, V., Talmont, F., Seree de Roch, M., Milon, A. and Demange, P. (2002). "Green fluorescent protein as a reporter of human u-opioid receptor overexpression and localisation in the methylotrophic yeast Pichia pastoris." Journal of Biotechnology **99**: 23-39.

Sarret, P., Gendron, L., Kilian, P., Nguyen, H. M., Gallo-Payet, N., Payet, M. D. and Beaudet, A. (2002). "Pharmacology and functional properties of NTS2 neurotensin receptors in cerebellar granule cells." Journal of Biological Chemistry **277**(39): 36233-43.

Schagger, H., Hagen, T., Roth, B., Brandt, U., Link, T. A. and von Jagow, G. (1990). "Phospholipid specificity of bovine heart bc1 complex." European Journal of Biochemistry **190**(1): 123-30.

Schagger, H. and von Jagow, G. (1991). "Blue native electrophoresis for isolation of membrane protein complexes in enzymatically active form." Analytical Biochemistry **199**(2): 223-31.

Schuck, P. (1997). "Use of surface plasmon resonance to probe the equilibrium and dynamic aspects of interactions between biological macromolecules." Annual Review of Biophysics and Biomolecular Structure **26**: 541-66.

Schwille, P., Bieschke, J. and Oehlenschlager, F. (1997). "Kinetic investigations by fluorescence correlation spectroscopy: the analytical and diagnostic potential of diffusion studies." Biophysical Chemistry **66**(2-3): 211-28.

Schwille, P. and Haustein, E. (2002). "Fluorescence Correlation Spectroscopy: A Tutorial for the Biophysics Textbook Online ".

Seddon, A. M., Curnow, P. and Booth, P. J. (2004). "Membrane proteins, lipids and detergents: not just a soap opera." Biochimica et Biophysica Acta **1666**: 105-117.

Seeman, N. C. (1999). "DNA engineering and its application to nanotechnology." Trends Biotechnol **17**(11): 437-43.

Selmi, D., Malo, J. and Turberfield, A. J. (2003). "DNA-Nanotechnological approaches to protein crystallisation and biological structure determination." DTC Rotation Project.

Sen, S., Jaakola, V., Pirila, P., Finel, M. and Goldman, A. (2005). "Functional studies with membrane-bound and detergent-solubilized a2-adrenergic receptors expressed in Sf 9 cells." Biochimica et Biophysica Acta **1712**: 62-70.

Shaner, N. C., Steinbach, P. A. and Tsien, R. Y. (2005). "A guide to choosing fluorescent proteins." Nature Methods **2**(12): 905-9.

Shi, C., Shin, Y. O., Hanson, J., Cass, B., Loewen, M. C. and Durocher, Y. (2005). "Purification and characterization of a recombinant G-protein-coupled receptor, Saccharomyces cerevisiae Ste2p, transiently expressed in HEK293 EBNA1 cells." Biochemistry **44**(48): 15705-14.

Shimada, M., Chen, X., Cvrk, T., Hilfiker, H., Parfenova, M. and Segre, G. V. (2002). "Purification and characterization of a receptor for human parathyroid hormone and parathyroid hormone-related peptide." Journal of Biological Chemistry **277**(35): 31774-80.

Shimomura, O., Johnson, F. H. and Saiga, Y. (1962). "Extraction, purification and properties of aequorin, a bioluminescent protein from the luminous hydromedusan, Aequorea." Journal of Cellular and Comparative Physiology **59**: 223-39.

Singer, S. J. and Nicolson, G. L. (1972). "The fluid mosaic model of the structure of cell membranes." Science **175**(23): 720-31.

Skrzydelski, D., Lhiaubet, A. M., Lebeau, A., Forgez, P., Yamada, M., Hermans, E., Rostene, W. and Pelaprat, D. (2003). "Differential involvement of intracellular domains of the rat NTS1 neurotensin receptor in coupling to G proteins: a molecular basis for agonist-directed trafficking of receptor stimulus." Molecular Pharmacology **64**(2): 421-9.

Small, D. M. (1967). "Phase equilibria and structure of dry and hydrated egg lecithin." Journal of Lipid Research **8**(6): 551-7.

Stenlund, P., Babcock, G. J., Sodroski, J. and Myszka, D. G. (2003). "Capture and reconstitution of G protein-coupled receptors on a biosensor surface." Analytical Biochemistry **316**(2): 243-50.

Stokes, G. G. (1852). "On the change of refrangibility of light." Phil. Trans. R. Soc. London **142**: 463-562.

Szoka, F., Olson, F., Heath, T., Vail, W., Mayhew, E. and Papahadjopoulos, D. (1980). "Preparation of unilamellar liposomes of intermediate size (0.1-0.2 mumol) by a combination of reverse phase evaporation and extrusion through polycarbonate membranes." Biochimica et Biophysica Acta **601**(3): 559-71.

Takanishi, C. L., Bykova, E. A., Cheng, W. and Zheng, J. (2006). "GFP-based FRET analysis in live cells." Brain Research **1091**(1): 132-9.

Tanaka, K., Masu, M. and Nakanishi, S. (1990). "Structure and Functional Expression of the Cloned Rat Neurotensin Receptor." Neuron **4**(6): 847-854.

Terstappen, G. C. and Reggiani, A. (2001). "In silico research in drug discovery." Trends in Pharmacological Sciences **22**: 23-26.

Thomas, J. D., Daniel, R. A., Errington, J. and Robinson, C. (2001). "Export of active green fluorescent protein to the periplasm by the twin-arginine translocase (Tat) pathway in Escherichia coli." Molecular Microbiology **39**(1): 47-53.

Toyoshima, C., Nakasako, M., Nomura, H. and Ogawa, H. (2000). "Crystal structure of the calcium pump of sarcoplasmic reticulum at 2.6 A resolution." Nature **405**(6787): 647-55.

Tsien, R. Y. (1998). "The green fluorescent protein." Annual Review of Biochemistry **67**: 509-44.

Tucker, J. and Grisshammer, R. (1996). "Purification of a rat neurotensin receptor expressed in Escherichia coli." Biochemical Journal **317**: 891-899.

Van der Merwe, P. A. (2000). Surface Plasmon Resonance in Protein-Ligand Interactions: A Practical Approach., Oxford University Press.

Vanti, W. B., Swaminathan, S., Blevins, R., Bonini, J. A., O'Dowd, B. F., George, S. R., Weinshank, R. L., Smith, K. E. and Bailey, W. J. (2001). "Patent status of the therapeutically important G-protein-coupled receptors." Expert Opinion on Therapeutic Patents **11**(12): 1861-1887.

Vassilatis, D. K., Hohmann, J. G., Zeng, H., Li, F., Ranchalis, J. E., Mortrud, M. T., Brown, A., Rodriguez, S. S., Weller, J. R., Wright, A. C., Bergmann, J. E. and Gaitanaris, G. A. (2003). "The G protein-coupled receptor repertoires of human and mouse." Proceedings of the National Academy of Sciences U S A **100**(8): 4903-8.

Vila-Coro, A. J., Rodriguez-Frade, J. M., Martin De Ana, A., Moreno-Ortiz, M. C., Martinez, A. C. and Mellado, M. (1999). "The chemokine SDF-1alpha triggers CXCR4 receptor dimerization and activates the JAK/STAT pathway." The FASEB Journal **13**(13): 1699-710.

Vincent, J.-P., Mazella, J. and Kitabgi, P. (1999). "Neurotensin and Neurotensin Receptors." Trends in Pharmacological Sciences **20**: 302-309.

Vita, N., Laurent, P., Lefort, S., Chalon, P., Dumont, X., Kaghad, M., Gully, D., Le Fur, G., GFerrara, P. and Caput, D. (1993). "Cloning and expression of a complementary DNA encoding a high affinity human neurotensin receptor." FEBS Letters **317**: 139-142.

Vogler, O., Casas, J., Capo, D., Nagy, T., Borchert, G., Martorell, G. and Escriba, P. V. (2004). "The Gbetagamma dimer drives the interaction of heterotrimeric Gi proteins with nonlamellar membrane structures." Journal of Biological Chemistry **279**(35): 36540-5.

Waldo, G. S., Standish, B. M., Berendzen, J. and Terwilliger, T. C. (1999). "Rapid protein-folding assay using green fluorescent protein." Nature Biotechnology **17**(7): 691-5.

Walker, N., Lepee-Lorgeoux, I., Fournier, J., Betancur, C., Rostene, W., Ferrara, P. and Caput, D. (1998). "Tissue distribution and cellular localization of the levocabastine-sensitive neurotensin receptor mRNA in adult rat brain." Molecular Brain Research **57**(2): 193-200.

Wallin, E. and von Heijne, G. (1998). "Genome-wide analysis of integral membrane proteins from eubacterial, archaean, and eukaryotic organisms." Protein Science **7**(4): 1029-38.

Watts, A. (1989). "Membrane structure and dynamics." Current Opinion in Cell Biology **1**(4): 691-700.

Watts, A. (2005). "Solid-state NMR in drug design and discovery for membrane-embedded targets." Nature Reviews Drug Discovery **4**(7): 555-68.

Weiss, H. M. and Grisshammer, R. (2002). "Purification and characterization of the human adenosine A(2a) receptor functionally expressed in Escherichia coli." European Journal of Biochemistry **269**(1): 82-92.

Weiss, J. M., Morgan, P. H., Lutz, M. W. and Kenakin, T. P. (1996a). "The Cubic Ternary Complex Receptor-Occupancy Model I. Model Description." Journal of Theoretical Biology **178**: 151-167.

Weiss, J. M., Morgan, P. H., Lutz, M. W. and Kenakin, T. P. (1996b). "The Cubic Ternary Complex Receptor Occupancy Model II. Understanding Apparent Affinity." Journal of Theoretical Biology **178**: 169-182.

White, J. F., Loc, T. B., Shiloach, J. and Grisshammer, R. (2004). "Automated large-scale purification of a G protein-coupled receptor for neurotensin." FEBS Letters **564**: 289-293.

Williamson, P. T. F., Bains, S., Chung, C., Cooke, R., Meier, B. and Watts, A. (2001). "Characterization and assignment of uniformly labeled NT(8-13) at the agonist binding site of the G-protein coupled neurotensin receptor." Focus on Structural Biology Vol. 1 Perspectives on Solid State NMR in Biology (Eds. S.R. Kühne & H.J.M. de Groot), Focus on Stuctural Biology, Kluwer Academic Publishers, Dordrecht: 191-202.

Williamson, P. T. F., Bains, S., Chung, C., Cooke, R. and Watts, A. (2002). "Probing the Environment of neurotensin whilst bound to the neurotensin receptor by solid state NMR." FEBS Letters **518**: 111-115.

Winfree, E., Liu, F., Wenzler, L. A. and Seeman, N. C. (1998). "Design and self-assembly of two-dimensional DNA crystals." Nature **394**(6693): 539-44.

Xu, Y., Piston, D. W. and Johnson, C. H. (1999). "A bioluminescence resonance energy transfer (BRET) system: application to interacting circadian clock proteins." Proceedings of the National Academy of Sciences U S A **96**(1): 151-6.

Yamada, M., Yamada, M., Watson, M. A. and Richelson, E. (1994). "Deletion mutation in the putative third intracellular loop of the rat neurotensin receptor abolishes polyphosphoinositide hydrolysis but not cyclic AMP formation in CHO-K1 cells." Molecular Pharmacology **46**(3): 470-6.

Yang, F., Moss, L. G. and Phillips, G. N., Jr. (1996). "The molecular structure of green fluorescent protein." Nature Biotechnology **14**(10): 1246-51.

Yang, Q., Alemany, R., Casas, J., Kitajka, K., Lanier, S. M. and Escriba, P. V. (2005). "Influence of the membrane lipid structure on signal processing via G protein-coupled receptors." Molecular Pharmacology **68**(1): 210-7.

Yeagle, P. (1993). The Membranes of Cells, Academic Press.

Yeliseev, A., Zoubak, L. and Gawrisch, K. (2007). "Use of dual affinity tags for expression and purification of functional peripheral cannabinoid receptor." Protein Expression and Purification **53**(1): 153-63.

Yeliseev, A. A., Wong, K. K., Soubias, O. and Gawrisch, K. (2005). "Expression of human peripheral cannabinoid receptor for structural studies." Protein Science **14**(10): 2638-53.

Zinser, E. and Daum, G. (1995). "Isolation and biochemical characterization of organelles from the yeast, Saccharomyces cerevisiae." Yeast **11**(6): 493-536.

Zlatanova, J. and van Holde, K. (2006). "Single-molecule biology: what is it and how does it work?" Molecular Cell **24**(3): 317-29.